Solar Photocatalytic Treatment of Oil Sands Process Water by Bismuth Tungstate Based Semiconductor Photocatalysts

by

Lingjun Meng

A thesis submitted in partial fulfillment of the requirements for the degree of

Doctor of Philosophy

in

Environmental Engineering

Department of Civil and Environmental Engineering
University of Alberta

ABSTRACT

Bitumen extraction in Alberta produces large quantities of oil sands process water (OSPW), which contains highly recalcitrant organics such as naphthenic acids (NAs). NAs are known to be the major contributors to the OSPW toxicity that need effective treatment before being released into the environment. Photocatalysis is a minimally invasive, sustainable, and economical approach to effectively treat wastewater by using renewable solar energy in a semi-passive treatment strategy. However, photocatalysts are limited by their bandgap and/or capability to separate the photoinduced charge carriers. Theoretically, photocatalytic activities are improved by the use of semiconductors with narrow bandgap and Z-scheme heterojunction systems. In this thesis, novel visible-light-driven bismuth tungstate (Bi_2WO_6) based semiconductor photocatalysts were prepared, and the application of the catalysts for the treatment of OSPW and the fundamentals in the treatment process were investigated.

Firstly, three different morphologies of Bi_2WO_6 photocatalysts were prepared by the hydrothermal method. The prepared catalysts were characterized to obtain their structural, textural, and chemical properties and tested for the degradation of model NAs and real OSPW under simulated solar irradiation. The flower-like structure exhibited the highest specific surface area and total pore volume. Accordingly, flower-like Bi_2WO_6 displayed the highest photocatalytic activity for the degradation of NAs, by achieving complete degradation of cyclohexanoic acid (CHA) at a fluence-based rate constant of 0.0929 cm^2/J. The effect of metallic ions on the degradation rates of S-containing and N-containing NAs varied, whereas heteroatom appeared as a main reactive site. The by-products of heteroatomic NAs were identified and the degradation pathways were reported for the first time. The concentration changes of each byproduct were

further estimated by mass balance.

Then, a novel photocatalyst Ag/NiO/Bi_2WO_6 with hierarchical flower-like Z-scheme heterojunction was synthesized. The photocatalyst exhibited excellent stability and activity over a wide light spectrum. The as-prepared composites were used in the remediation of OSPW, and a complete removal of aromatics, classical NAs, and heteroatomic NAs was observed after 6 h of the photocatalytic treatment. The acute toxicity of OSPW was completely eliminated after only 2 hours of treatment. In the photocatalytic system, h^+, $O_2^{\bullet-}$, and hydroxyl radical ($^{\bullet}OH$) were found to be the major oxidative species. The enhanced photocatalytic efficiency appeared to be the result of unique Z-scheme electron transfer among electron mediator Ag, NiO, and Bi_2WO_6 and the surface plasmon resonance effect near Ag, which was further supported by the Density Function Theory (DFT) calculations of the electronic properties of Ag/NiO/Bi_2WO_6 heterostructure.

OSPW inorganic fraction (IF) is a complex saline solution comprising inorganic ions and trace metals. These ions and metals are known to influence the remediation efficiency of NAs in OSPW. In this research, different photocatalytic performances were tested for six model NA compounds mixtures in buffer and OSPW-IF using Bi_2WO_6 and Bi_2WO_6/NiO/Ag. The distinct water matrices significantly affected the removal of model NA compounds. Further experimental analysis suggested that chloride and bicarbonate could commonly produce the inhibited effects for photocatalytic pollutant elimination. The addition of catalysts only accelerated the degradation rate of 1-adamantanecarboxylic acid (ACA) but did not change its degradation pathway. However, it reduced the chronic toxicity by generating lesser toxic byproducts as observed via ecological structure activity relationships. Additionally, the transformation products of 4,5-dihydronaphtho[1,2-b]thiophene-2-carboxylic acid (DTCA) were proposed for the photocatalytic system.

In recent years, oxidant-assisted photocatalysis has attracted extensive attention as it can overcome the shortcomings of traditional advanced oxidation and photocatalysis for the decontamination of organic pollutants. In this thesis, photocatalytic performances for hydrogen peroxide (H_2O_2), peroxymonosulfate (PMS), and potassium permanganate ($KMnO_4$) were compared for the treatment of OSPW using z-scheme photocatalyst Bi_2WO_6/NiO/Ag. Briefly, H_2O_2 and PMS assisted photocatalysis significantly promoted the degradation of aromatics in OSPW as compared to the control, while $KMnO_4$ assisted photocatalysis inhibited the degradation. Accordingly, the detoxification of OSPW was only observed for H_2O_2 and PMS assisted photocatalysis. The main reactive species were h^+, $O_2^{\bullet-}$, $^{\bullet}OH$ and electron (e^-) in H_2O_2 assisted photocatalysis; and sulphate radical ($SO_4^{\bullet-}$), h^+, $O_2^{\bullet-}$, $^{\bullet}OH$ in PMS assisted photocatalysis. Therefore, H_2O_2 and PMS displayed a dual role as an electron acceptor and radical precursor in the oxidant-assisted photocatalysis.

PREFACE

All the research completed in this thesis was designed and performed by me under the supervision of Dr. Mohamed Gamal El-Din in the Department of Civil and Environmental Engineering at the University of Alberta. I conducted all the experimental work as well as the data interpretation and the preparation of the manuscripts under the supervision of Dr. Mohamed Gamal El-Din. Some colleagues contributed to sample analysis or manuscript edits, and some of them were co-authors in the manuscripts. The contribution from the collaborators and the coauthors of the manuscripts are described below.

Chapter 2 has been published as "L. Meng, Z. T. How, S. O. Ganiyu and M. Gamal El-Din. Solar photocatalytic treatment of model and real oil sands process water naphthenic acids by bismuth tungstate: Effect of catalyst morphology and cations on the degradation kinetics and pathways. J. Hazard. Mater. 2021; 413: 125396". Dr. Mohamed Gamal El-Din contributed to the supervision, reviewing paper, funding acquisition. Dr. Zuo Tong How contributed the edit of the manuscript and the analysis of by-products. Dr. Soliu Ganiyu contributed the edit of the manuscript.

Chapter 3 has been submitted to Chemical Engineering Journal as "L. Meng, Z. T. How, P. Chelme-Ayala and M. Gamal El-Din. Z-scheme plasmonic Ag decorated NiO/Bi_2WO_6 hybrids for enhanced photocatalytic treatment of naphthenic acids in real oil sands process water under simulated solar irradiation". Dr. Mohamed Gamal El-Din contributed to the supervision, reviewing paper, funding acquisition. Dr. Zuo Tong How and Dr. Pamela Chelme-Ayala contributed the edit of the manuscript.

Chapter 4 will be submitted to the Journal of Hazardous Materials as "L. Meng, Z. T. How, P. Chelme-Ayala and M. Gamal El-Din. Solar photocatalytic degradation of model compounds

NAs mixtures: The effect of inorganic fraction of OSPW." Dr. Mohamed Gamal El-Din contributed to the supervision, reviewing paper, funding acquisition. Dr. Zuo Tong How contributed the edit of the manuscript and the analysis of by-products. Dr. Pamela Chelme-Ayala contributed the edit of the manuscript.

Chapter 5 will be submitted to the Science of total environment as "L. Meng, Z. T. How, P. Chelme-Ayala and M. Gamal El-Din. Comparison of different oxidant-assisted photocatalytic treatment of naphthenic acid in real OSPW: $KMnO_4$, H_2O_2 and PMS" Dr. Mohamed Gamal El-Din contributed to the supervision, reviewing paper, funding acquisition. Dr. Zuo Tong How and Dr. Pamela Chelme-Ayala contributed the edit of the manuscript.

All the work associated with this study was performed by me except for the contributions from the collaborators and co-authors described above.

ACKNOWLEDGEMENTS

First of all, I would like to express my sincere appreciation to my supervisor Dr. Mohamed Gamal El-Din for his academic guidance, supervision, and financial support to help me to complete this thesis successfully. He is good at teaching students in accordance with their aptitude and provided me with an excellent research platform for understanding many aspects within the wastewater treatment field. It was a fabulous experience to work with him, which improved my study and research capacity remarkably.

I would like to thank Dr. Pamela Chelme-Ayala, the program manager in Dr. Gamal El-Din's research group, who encourages me when I am upset, and she is very nice and kind to provide generous support to help me to conquer the difficulties in my study.

My sincere gratitude also goes to Dr. Zuo Tong How, who has spent lots of time giving me supervision and valuable suggestions on my research work. He revised my manuscripts and gave me good feedback. He often urged me to study and reminded me of the deadlines. Although we often stick to our own point of view, we always manage to come out with a solution. He is the most responsible person I have ever seen. He is also a trusted and reliable friend in life.

I also would like to thank Dr. Soliu Ganiyu, Dr. Muhammad Arslan and Dr. Lingling Yang who helped me revise my paper and thesis and analyze samples. I am grateful for the help and support from all the current and previous members in Dr. Gamal El-Din's research group including the postdoctoral fellows and students. Thanks to the staff in the Department of Civil and Environmental Engineering and NanoFab including the technical staff and academic advisors.

I highly appreciate the scholarship from the Chinese Scholarship Council. I also appreciate the financial support provided by the research grant from a Natural Sciences and Engineering

Research Council of Canada (NSERC) Senior Industrial Research Chair (IRC) in Oil Sands Tailings Water Treatment through the support of Syncrude Canada Ltd., Suncor Energy Inc., Canadian Natural Resources Ltd., Imperial Oil Resources, Teck Resources Limited., EPCOR Water Services, Alberta Innovates, and Alberta Environment and Parks. The financial support provided by the Future Energy Systems (FES) - Resilient Reclaimed Land and Water Systems Theme through the Canada First Research Excellence Fund is also well- appreciated.

DEDICATION

To my parents; Xiangmin & Guiqing

Tolerate my willfulness and shelter me from the wind and rain

To all my family and friends

To everyone who seeks the truth

TABLE OF CONTENTS

LIST OF TABLES

LIST OF FIGURES

CHAPTER 1 GENERAL INTRODUCTION AND RESEARCH OBJECTIVES

1.1 Background

1.1.1 Oil sands process water

Canada has the world's third largest proven oil reserves of 170 billion barrels. The oil and natural gas industries in Canada have invested ~$201 billion for bitumen extraction from oil sands (Poveda and Lipsett 2013). In northern Alberta, oil sands reserves are estimated to hold 166 billion barrels of crude oil, thus accounting for more than 95% of Canada's total reserves (NRC 2022a). The oil sands are water-wet which allows bitumen extraction feasible using warm water (Lo et al. 2006). More than 80% of the produced water is recovered while the remaining fraction is stored in the tailing ponds (NRC 2022b). The water injected during bitumen extraction is termed as oil sands process water (OSPW). It is a complex saline solution that contains suspended solids, heavy metals and ions, and organic compounds such as naphthenic acids (NAs), phenols, polycyclic aromatic hydrocarbons (PAHs), and BTEX (benzene, toluene, ethyl benzene, and xylenes). NAs are a group of alkyl-substituted acyclic, monocyclic, and polycyclic carboxylic acids with a general chemical formula of $C_nH_{2n+Z}O_x$, where n is the carbon number ($7 \leq n \leq 26$), Z is even integer that represents the hydrogen deficiency due to the formation of ring or double bond structure ($0 \leq -Z \leq 18$), and x indicates the oxygen number. In addition, the heteroatomic NAs are designated as $C_nH_{2n+z}SO_x$ and $C_nH_{2n+z}NO_x$. Previously, OSPW profiling revealed 23% abundance of sulfur-containing NAs (S-NAs), 8% of nitrogen-containing NAs (N-NAs), and 64% of classical and oxy-NAs ($C_nH_{2n+z}O_x$) (Nyakas et al. 2013). As per the guidelines of Natural Resources Canada, OSPW must be stored on-site in tailing ponds for subsequent remediation prior to the release in the environment concerning potential environmental, health and economic crisis (Pramanik 2016).

Some of the oldest tailing ponds have now been reclaimed by transforming them into end pit lakes or dry landscape capping. in which OSPW may be connected to natural water bodies through surface or groundwater flows (Sun et al. 2017). However, fresh OSPW stored in tailings ponds may also infiltrate into groundwater or surface water. It is argued that OSPW is likely present in two tributaries of the Athabasca River adjacent to tailings ponds, i.e., McLean Creek and Lower Beaver River (Fennell and Arciszewski 2019).

1.1.2 The toxicity of OSPW

OSPW has attracted increasing attention not only because of its potential appearance in natural water but also due to the adverse toxic effects on living organisms. Numerous studies have widely recognized NAs as most toxic and dominant fraction in OSPW with an average concentration of 20-80 mg/L in fresh tailing ponds (Leclair et al. 2015). In an ageing OSPW, indigenous microbial communities can potentially degrade NAs with low carbon number (C<22), but high carbon fraction stays longer. Therefore, the toxicity of OSPW is related to the exposure time (Biryukova et al. 2007, Clemente et al. 2004). OSPW causes acute, sub-chronic, and chronic toxicity to a variety of organisms. For examples, fresh OSPW from West-In-Pit settling basin displayed lethal effects on *Daphnia magna* (Zubot et al. 2012). Similarly, exposure of OSPW to the larvae of *Chironomus dilutus* decreased 64–77% of the population in comparison with the freshwater. OSPW could also cause a significant impairment of adult emergence and reproductive output, and enhanced susceptibility to predation because of behavioral changes for *Chironomus dilutes* (Anderson et al. 2012). In another study, 100% mortality of rainbow trout was observed upon 96 h of exposure to 50% OSPW (Rogers et al. 2007). Study on the acute toxicity of zebrafish larvae confirmed that the toxicity of OSPW depends on the structure and composition of NAs. Specifically, 96 h-LC_{50} were 13.1 mg/L and 8.1 mg/L for those exposed to OSPW fraction

containing classical NAs and aromatic NAs, respectively (Scarlett et al. 2013). Some aromatic NAs are structurally similar to estrogens (Rowland et al. 2011, Scarlett et al. 2012), thus can induce endocrine disruptive effects for fish (Wang et al. 2015). Moreover, esterifiable NAs possess the vitellogenin-inducing effects on zebrafish larvae (Reinardy et al. 2013). *In vitro* experiments of OSPW showed antiandrogenic and estrogenic effects on MDA-kb2 and T47D-kbluc cell lines, respectively (He et al. 2011). The ethoxyresorufin-*o*-deethylase activity, a well-used biomarker, was increased in tadpoles of *Lithobates sylvaticus or Bufo boreas* being exposed to OSPW, thus indicated an enhanced concentration of the contaminants (Hersikorn and Smits 2011, Pollet and Bendell-Young 2000, Whyte et al. 2000). The limited reproductive performance and elevated mortality of nestlings of tree swallows *Tachycineta bicolor* were observed during cold and rainy weather. While the mortality rates were low during less challenging environmental conditions, nestlings inhabiting OSPW-impacted wetlands were smaller and showed higher hepatic ethoxyresorufin-*o*-deethylase activity (Gentes et al. 2006). It was recorded that diverse bone marrow-derived macrophage functions and the expression of many pro-inflammatory cytokine and chemokine genes in the liver of mice could be affected by the dissolved organics in OSPW (Garcia-Garcia et al. 2011).

In addition to NAs, other components in OSPW may also be responsible for toxic effects on aquatic life. PAHs concentration in OSPW is often 100 μg/L which is significantly higher than the environmental quality standards, i.e., 0.01–0.06 μg/L (Allen 2008, Parajulee and Wania 2014). When Japanese medaka was exposed to organic chemicals extracted from fresh OSPW, accumulation of PAHs was increased due to the inhibition of multidrug-resistance protein activity which is essential for excretion of PAHs and their metabolites (Alharbi et al. 2016). The high salinity of OSPW could influence osmotic stress and ionic imbalances in fish. Previously, OSPW

salinity decreased the reproduction ability of *Ceriodaphnia* (Zubot et al. 2012). Metals in OSPW are non-biodegradable and may bioaccumulate, resulting in potential toxicity to living organisms. The concentrations of arsenic, cadmium, lead, copper, chromium in OSPW have already exceeded the maximum concentrations of water quality guidelines of the Canadian Council of Ministers of the Environment (CCME). It has been reported that some metals in OSPW pose acute and chronic toxicity to *Chironomus dilutes* (Anderson et al. 2012). Further, OSPW toxicity may also be attributed to the synergistic or antagonistic chemical effects due to the complexity of OSPW components. For instance, Nero *et al.* (2006) reported that the addition of salts decreased the gill surface area of yellow perch, leading to less toxicity induced by NAs due to the decreased NAs entry. However, simultaneous effect on the exchange of respiratory gases was also recorded.

1.1.3 Treatment methods of OSPW

Novel treatment methods are needed for the safe release of OSPW into the environment due to its potential harmful impacts on living species as well as deterioration of surface and groundwater quality. Adsorption is the most common physical method proposed for the treatment of OSPW. Previously, many adsorbents such as petroleum-coke (Gamal El-Din et al. 2011), granular activated carbon (Islam et al. 2015), and carbon xerogel were used to remove dissolved organics in OSPW. For example, total acid-extractable organics (AEF) was decreased from 63 mg/L to 5.7 mg/L after adsorption by petroleum-coke (Gamal El-Din et al. 2011). Accordingly, chemical oxygen demand (COD) removal was around 40% by granular activated carbon adsorption (Islam et al. 2015). Likewise, 6% of AEF and 88.8% of classical NAs were removed by carbon xerogel adsorption in 24 h (Benally et al. 2019).

Meanwhile, many advanced oxidation processes (AOPs) have also been tested for the removal of NAs from OSPW. For example, ozonation was highly effective for the degradation of

NAs with multiple rings and alkyl branching whereas NA degradation rate was further increased with an increase in pH (Pérez-Estrada et al. 2011). Ozonation also successfully attenuated the developmental toxicity toward embryos of fathead minnow (He et al. 2012). Accordingly, ferrate oxidation achieved 64.0% and 78.4% removal of NAs at the dose of 200 and 400 mg/L of Fe (VI) respectively, while NAs with high carbon number and ring number were removed preferentially (Wang et al. 2016). In addition, 90% of total NAs fraction was removed within 6 days of exposure at 20 °C in zerovalent iron/ $S_2O_8^{2-}$ system (Drzewicz et al. 2012). In addition to the direct use of oxidants, UV based AOPs are also widely proposed for the treatment of OSPW, including UV/H_2O_2, UV/$S_2O_8^{2-}$, UV/OCl^- and UV-Fenton. For example, UV−Fenton process was successfully applied at natural pH in the presence of chelating agents (nitrilotriacetic acid), while the removal rates for classical NAs, mono-oxidized and di-oxidized NAs were 98.4%, 86.0%, and 81.0%, respectively (Zhang et al. 2016). Electrochemical advanced oxidation processes have also showed potential to be used for the OSPW treatment. The degradation rate of model NAs, cyclohexane carboxylic acid, was 0.01 min^{-1} at 20 mA/cm^2 using graphite anodic oxidation (Abdalrhman et al. 2019).

Biological treatment methods have been widely studied for the remediation of OSPW because they offer low-cost and minimally invasive treatment solutions. For example, a modified Ludzack-Ettinger membrane bioreactor with a submerged ceramic membrane was continuously operated to evaluate its feasibility on OSPW treatment. The system was able to remove 24.7% of NAs in 361 days of operation (Xue et al. 2016). Similarly, in an anoxic stabilization pond amended with nitrate continuous stirred tank reactor, NA removal rate was 105.3 mg L^{-1} h^{-1} at NA loading rate of 157.8 mg L^{-1} h^{-1} (Gunawan et al. 2014). Notably, the bioremediation effects on the OSPW can be improved significantly through the combination of physical, chemical, and biological

processes. For example, after 11 months of operation, 12.1% of acid-extractable fraction and 43.1% of NAs were removed from the raw OSPW in integrated fixed-film activated sludge (IFAS) reactors. However, removal rates of AEF and NAs was increased up to 42.0% and 80.2% in the IFAS for pre-ozonated OSPW (Huang et al. 2015).

1.1.4 Photocatalytic treatment of OSPW

Photocatalysis has been regarded as a green, economical, and effective method as it uses renewable solar energy and environment-friendly materials. To this end, titanium dioxide (TiO_2) and its composites have been tested for the treatment of OSPW at the bench-scale. AEF and acute toxicity toward *Vibrio fischeri* were significantly decreased by TiO_2 photocatalysis (Leshuk et al. 2016b). TiO_2-graphene composites exhibited better photocatalytic performance than pure TiO_2. 80–90% of NAs were removed by using TiO_2-graphene composites after 80 min of UV illumination (Liu et al. 2016a). It was also reported that TiO_2-zeolite composites have the ability to decrease 31% of the total acidity values of stock NAs being exposed to UV illumination using titration (Kalebaila and Fairbridge 2014). Furthermore, application of fixed-film TiO_2 resulted in >92% removal of NAs after 4h treatment, with an average removal rate of 15.5 mg/L/h of NA (McQueen et al. 2016). The buoyant photocatalysts, which were synthesized by coating TiO_2 nanoparticles on hollow glass microspheres using mesoporous silica as a binder, exhibited successful removal of AEF in OSPW (Leshuk et al. 2018).

1.1.4.1 The mechanism of semiconductor photocatalysis

The photocatalytic reactions are initiated when particle is irradiated by photons with energies larger than that of its band gap energy (E_g) (Fig. 1.1 I). In this way, photoinduced electron is excited from the valence band (VB) to the conduction band (CB), forming a positive hole (h_{VB}^+) and electron (e_{CB}^-) on the surface of the particle. The photoexcited electron could recombine with

the valence band hole with simultaneous dissipation of heat or light energy, leading to the decreased efficiency of photocatalysis (Fig. 1.1 II). The h_{vb}^{+} and e_{cb}^{-} can act as oxidant and reductant (Fig. 1.1 III, IV) to react with electron acceptors (A) and electron donors (D) adsorbed on the surface of semiconductor. The presence of oxygen as electron scavengers prolongs the recombination of electron-hole pair while forming the $O_2^{\bullet -}$ (Eq. 1.1). The reaction of h_{vb}^{+} with OH^{-} (Eq. 1.2) may leads to the formation of $^{\bullet}OH$. The $^{\bullet}OH$ is an extremely strong, non-selective oxidant (E_0=3.06 V) which leads to the partial or complete mineralization of organics (Eq. 1.4). Moreover, high oxidative potential of the hole in the photocatalyst also permits the direct oxidation of organic matter to reactive intermediates as shown in Eq. 1.3.

$$e_{CB}^{-} + O_2 \rightarrow O_2^{-\cdot} \qquad (1.1)$$

$$h_{VB}^{+} + OH^{-} \rightarrow {}^{\bullet}OH \qquad (1.2)$$

$$h_{VB}^{+} + R \rightarrow R^{+\cdot} \rightarrow intermidiates \qquad (1.3)$$

$${}^{\bullet}OH + R - H \rightarrow R^{+\cdot} + H_2O \qquad (1.4)$$

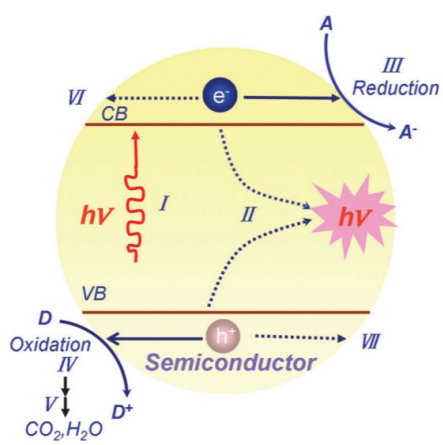

Fig. 5.1 Fundamental principles of semiconductor photocatalysts (Wang et al. 2014).

1.1.4.2 Strategies to improve Bi_2WO_6 photocatalysis efficiency

Bi_2WO_6 is a simple member of the Aurivillius family with orthorhombic structures which are constructed by alternating $(Bi_2O_2)_n^{2n+}$ layers and perovskite-like $(WO_4)_n^{2n-}$ layers. Bi_2WO_6 was selected in this thesis due to its narrow bandgap, easy synthesis, morphology adjustability. The photocatalytic performance of Bi_2WO_6 could be limited owing to the poor capability for separating the photoinduced charge carriers. Numerous efforts have been done to improve Bi_2WO_6 photocatalysis efficiency such as ion doping, metal deposition, and heterojunction fabrication. The heterojunction photocatalysts were the focus of this thesis whose details are provided below.

The heterojunction photocatalysts that combine at least two functional materials in one system have gained more interests in the past decades. It is one of the most effective strategies to broaden the visible light adsorption and potentially act to avoid the recombination of charge carriers. As shown in Fig. 1.2, when two semiconductors are in contact, they form a junction with a space-charge region at the interfaces because of the diffusion of e^- and h^+. Hence, a built-in electrical potential is created and then guide the e^- and h^+ to migrate to the opposite direction. When the p-n heterojunction absorbs photons with energy greater than or equal to the band gap of photocatalyst from the illumination, the e^- and h^+ can be separated rapidly by the built-in electric field. Driven by electric field, h^+ are transferred to VB of p-type semiconductor and e^- are transferred to CB of n-type semiconductor. Therefore, the charge carrier is successfully separated (Ge et al. 2011).

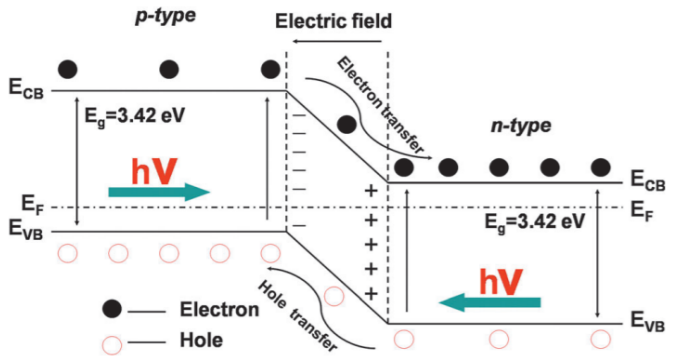

Fig. 1.6 Schematic diagram showing the energy band structure and electron-hole pair separation in the p–n heterojunction (Ge et al. 2011).

Various Bi_2WO_6 based p-n heterojunction structures have been reported such as MoS_2 quantum dots-interspersed Bi_2WO_6 (Meng et al. 2017b), CuS-Bi_2WO_6 (Lv et al. 2020), and Bi_2O_3-Bi_2WO_6 (Ge et al. 2011). The electron-hole separation rate is greatly improved via the built-in electric field of p-n heterostructure and the MoS_2 quantum dots interspersed on the surface of Bi_2WO_6. The enhanced photocatalytic activities are confirmed through the degradation of RhB and the temporal course of inactivation of *Escherichia coli.* The CuS/Bi_2WO_6 heterojunctions displayed higher degradation rate of glyphosate than pure CuS and Bi_2WO_6 (Lv et al. 2020). The improved photocatalytic performance of CuS-Bi_2WO_6 can be attributed to strong visible light absorption and enhanced separation of photogenerated charge carriers by the internal electric field near the interface of the p-n junction.

The traditional p-n semiconductor heterojunction can effectively improve the separation efficiency of photo-generated carriers, but the directional migration of charge carriers will reduce the reduction and oxidation potential of the original photo-generated electrons and holes. Therefore, Z-scheme photocatalysts appears to be a good choice. There are three types of Z-scheme photocatalysts: (1) redox-mediator Z-scheme, (2) all-solid-state Z-scheme, and (3) direct Z-

scheme charge transfer. Among them, the most common case is all-solid-state Z-scheme. For redox-mediator Z-scheme, introduction of redox mediator such as Fe^{3+}/Fe^{2+} and IO_3^-/I^- in the liquid phase increase the photocatalytic performance. However, pH of solution, changes in concentration ratio, and longer distance of electron migration makes redox-mediator Z-scheme can only work in liquid phase, thus limiting the application in many settings.

$Bi_2Fe_4O_9/Bi_2WO_6$ heterojunction displayed higher catalytic activity for RhB photodegradation compared to the pure $Bi_2Fe_4O_9$ and Bi_2WO_6 (Li et al. 2018). The authors explored the possible mechanism toward carrier migration, where two assumptions are proposed: p-n heterojunction (Fig. 1.3a) and Z-scheme heterojunction (Fig. 1.3b). Although $^{\bullet}OH$ and $O_2^{\bullet-}$ are determined in this system by electron spin resonance spin-trap technique; theoretically, VB hole cannot oxidize H_2O to generate $^{\bullet}OH$, $O_2^{\bullet-}$ due to the oxidation and reduction potential. The $VB_{Bi2Fe4O9}$ +1.19 eV < $OH^-/^{\bullet}OH$ +2.40 eV; $O_2/^{\bullet}O_2^-$ −0.33 eV < CB_{Bi2WO6} potential +0.53 eV. Thus, p-n heterojunction cannot be used to explain the mechanism of photocatalytic activity. The photogenerated electron migrates from CB of Bi_2WO_6 to VB of $Bi_2Fe_4O_9$, which can combine with photoexcited hole generated from VB of $Bi_2Fe_4O_9$. Meanwhile, the hole originated in VB of Bi_2WO_6 can easily oxidize H_2O to $^{\bullet}OH$ and the electron generated in CB of $Bi_2Fe_4O_9$ reduces O_2 to $^{\bullet}O_2^-$. Subsequently, the formed $^{\bullet}OH$, h^+ and $^{\bullet}O_2^-$ participate in the RhB photodegradation system. Therefore, the increased photoinduced carrier separation as well as the broadened photoabsorption range enhance the photocatalytic performance of $Bi_2Fe_4O_9/Bi_2WO_6$ due to direct Z-scheme.

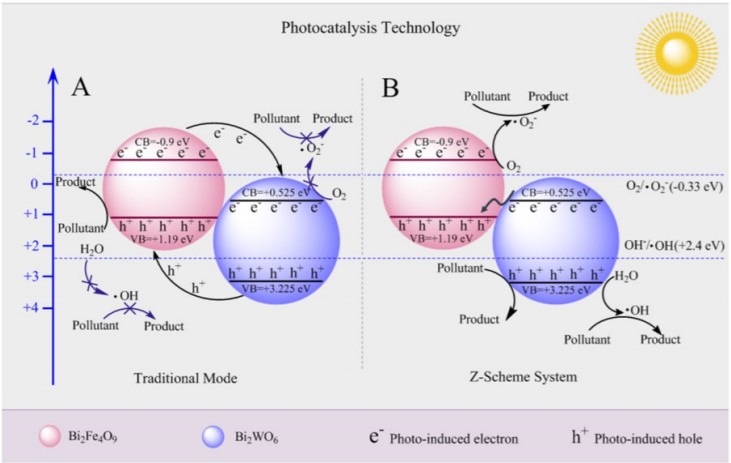

Fig. 1.7 Schematic diagram of possible mechanism toward carrier migration and photocatalytic reaction of $Bi_2Fe_4O_9/Bi_2WO_6$: (a) p-n heterojunction and (b) Z-scheme heterojunction system (Li et al. 2018).

Bi_2WO_6 (BWO), g-C_3N_4 (CN) and reduced graphene oxide (RGO) were combined with a 2D/2D/2D configuration to generate solar fuels (Fig. 1.4) (Jo et al. 2018). The improved photocatalytic activity was because of the all-solid-state Z-scheme heterojunction structures. Both CN and BWO could be excited by visible light to generate e^- and h^+. Then, the generated e^- at BWO CB transferred to the VB of CN through redox mediator RGO and finally combine with h^+ at CN VB. The h^+ stayed in the VB of BWO and e^- in the CB of CN participated in the reduction and oxidation reactions, respectively. The electrons retained in the CB of CN then migrated to the RGO due to the exceptional storage capacity and electron conductivity of RGO. The electrons could be trapped by CO_2 to generate $CO_2^{\bullet-}$. After that, CO, H_2 and CH_4 were generated. Meanwhile, H_2O could be reacted with the h^+ which stayed in the VB of BWO to produce e^- and O_2. Therefore, efficient separation of photoinduced charge carriers due to the all-solid-state Z-scheme heterojunction structure, together with higher optical absorption significantly improved the catalytic activity.

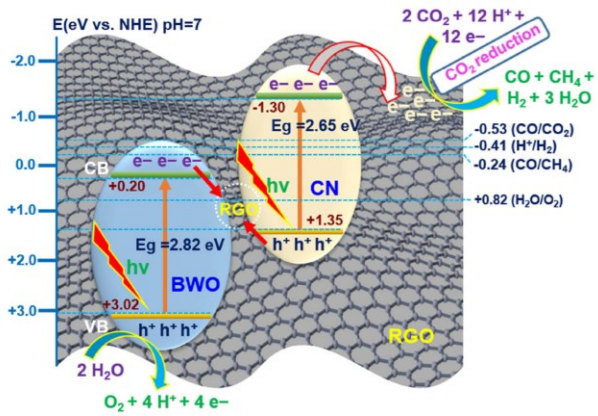

Fig. 1.8 Schematic illustration of the proposed mechanism for CO_2 photoreduction in the BWO/RGO/CN 2D/2D/2D hybrid heterojunctions (Jo et al. 2018).

Metals which can induce localized surface plasmon resonance (SPR), like silver and gold, have also gained wide attention as promising photocatalyst candidates. The formation of SPR can absorb visible light and convert it to the formation of free energetic electrons, and also enhance the formation rate of electron–hole pair driven by the electromagnetic field formed nearby the semiconductor. For instance, a series of Ag@AgX (X = Cl, Br, I) plasmonic photocatalysts were prepared, which exhibited an increase in photo-oxidation capability and were stable under visible light illumination (Wang et al. 2010a, Wang et al. 2010b). The photocatalytic activity of Ag doped Bi_2WO_6 for inactivation of pathogenic bacteria was promoted due to the following mechanisms: Firstly, the SPR effects of Ag nanoparticles under visible light illumination improve the photocatalytic activity of Bi_2WO_6; Secondly, Ag could facilitate the separation of photogenerated charge carriers due to the role of electron traps and enhance interfacial electron transfer process (Ren et al. 2009).

1.1.5 Advanced oxidation processes (AOPs)

During the past decades, incredible research confirmed the great potential of the AOPs in the field of wastewater treatment. AOPs are characterized with an *in-situ* production of reactive

oxygen species (ROS) such as $^{\bullet}OH$, $O_2^{\bullet-}$, $SO_4^{\cdot-}$, O_3 and H_2O_2; and achieving high removal rates and mineralization of target pollutants to CO_2, H_2O and inorganic acids or ions. So far, different kinds of AOPs have been regarded as effective approaches for the degradation of various recalcitrant organics in wastewater treatment, such as ozonation (Wang et al. 2011, Zhao et al. 2017b), $KMnO_4$ oxidation (Jiang et al. 2009, Tian et al. 2019), Fenton, photo-Fenton (Michael et al. 2012, Trovó et al. 2011), UV based AOPs (Meng et al. 2017a, Tang et al. 2020), photocatalysis (Meng et al. 2021, Xu et al. 2021), electrochemical oxidation (García-Espinoza et al. 2018, Loos et al. 2018), radiation (Liu et al. 2016b, Wang and Wang 2018) and sonolysis (Güyer and Ince 2011, Serna-Galvis et al. 2016). Since NAs could hardly be degraded by conventional physical and biological treatment, AOPs provide a viable attenuation option of NAs degradation (Miklos et al. 2018).

1.1.5.1 Hydroxyl radical-based advanced oxidation processes

Hydrogen peroxide cleaves into two $^{\bullet}OH$ after adsorbing photo energy. The $^{\bullet}OH$ is an extremely powerful oxidant with a high oxidation potential (E_0 = 2.8 V), and capable of oxidizing organic compounds through electron transfer, electrophilic addition and hydrogen abstraction (Legrini et al. 1993). However, the molar absorption coefficient (ε=18.6 $M^{-1}cm^{-1}$) of H_2O_2 is relatively low at 254 nm. Thus, the turnover of H_2O_2 is below 10%. Generally, the oxidation ability is increasing with the increased concentration of H_2O_2. However, excessive H_2O_2 hindered the generation of $^{\bullet}OH$ based on the following equation. For example, Afzal *et al.* reported that the degradation rate of model NAs such as cyclohexanoic acid (CHA) was not increased at high concentration of H_2O_2 (80 mg/L) (Afzal et al. 2012).

$H_2O_2 + {}^{\bullet}OH \rightarrow HO_2^{\bullet} + H_2O$; $k_{\cdot OH,H2O2} = 2.7\times10^7\ M^{-1}s^{-1}$ (Buxton et al. 1988)

1.1.5.2 Sulfate radical-based advanced oxidation processes

Sulfate radical-based AOPs (SR-AOPs) is regarded as an interesting alternative to hydroxyl radical-based AOPs (HR-AOPs) for wastewater treatment. Traditionally, sulfate radical is generated through activation of peroxydisulfate (PDS) or peroxymonosulfate (PMS), which are among the strongest oxidants and have gained increasing attention in recent years (Ganiyu et al. 2022). PDS and PMS are stable in both solid and water at a wide range of pH. As the p*K*a of PMS is 9.4, the protonated form (HSO_5^-) of PMS is the major form below pH 9.4 and the unprotonated form (SO_5^{2-}) is above pH 9.4. While, in aqueous solution, PDS exists as $S_2O_8^{2-}$ (Bouchard et al. 1998, Liu et al. 2015). In comparation to the price of H_2O_2 of 0.05 USD/mol, PDS and PMS are more expensive with 0.18 USD/mol for $Na_2S_2O_8$ and 1.36 USD/mol for Oxone® salt ($2KHSO_5 \cdot KHSO_4 \cdot K_2SO_4$). However, the molar absorption coefficient of $S_2O_8^{2-}$ (22 $M^{-1}cm^{-1}$) is larger than H_2O_2. The quantum yield for $S_2O_8^{2-}$ is 1.4 compared to 1 for H_2O_2, leading to higher productivity of radicals in UV radiation system (Legrini et al. 1993, Lutze 2013, Nawaz and Sengupta 2021, Xiao et al. 2016). Under UV radiation at pH 7, $^{\bullet}OH$ and $SO_4^{\bullet-}$ were generated by HSO_5^- with a quantum yield equal to 0.52 (Guan et al. 2011). Compared to non-selective $^{\bullet}OH$, $SO_4^{\bullet-}$ is known as an electron transfer oxidant and has a comparable oxidizing ability with $^{\bullet}OH$ (E_0 = 2.5–3.1 V). It can exist in a wide pH range and has longer half-time ($t_{1/2}$ = 30-40 μs) than $^{\bullet}OH$ ($t_{1/2}$ = 10 ns) in aquatic systems (Oh et al. 2016). From their second-order rate constant, dissolved organic matter (DOM) has less influence on $SO_4^{\bullet-}$ than $^{\bullet}OH$ where the rate constant is $k_{\cdot OH\ DOM}$=1.4×10^4 $mgC^{-1}s^{-1}$ and $k_{SO4\cdot-\ DOM}$=6.8×10^3 $mgC^{-1}s^{-1}$, respectively (Lutze et al. 2015). In addition, higher mineralization rate can be achieved in SR-AOPs than HR-AOPs (Sánchez-Polo et al. 2013). Halogenated disinfection byproducts (HDBPs) yields through the reaction of $SO_4^{\bullet-}$ with Cl^- and Br^-, while negligible HDBPs were detected in HR-SOPs (Lutze et al. 2014, Redpath

and Willson 1975, von Gunten 2003, von Gunten and Oliveras 1998). After activation, PDS typically decays into $SO_4^{\bullet-}$, but the conversion of $SO_4^{\bullet-}$ to $^{\bullet}OH$ could be possible in alkaline environment. For PMS, it decomposes into both $SO_4^{\bullet-}$ and $^{\bullet}OH$ after activation (Guan et al. 2011, Luo et al. 2015). The activation method of PDS and PMS have been extensively studied, including heat (Anipsitakis and Dionysiou 2004, Ghauch et al. 2012), UV radiation (Ghauch et al. 2017, Guan et al. 2011), metal or non-metal catalysts (Peng et al. 2013, Rastogi et al. 2009, Sun et al. 2014, Zhao et al. 2014), alkaline pH (Furman et al. 2010, Qi et al. 2016), electrolysis (Govindan et al. 2014, Yuan et al. 2014), radiolysis (Criquet and Karpel Vel Leitner 2011).

1.1.5.2.1 Application of SR-AOPs for petrochemical wastewater treatment

Petrochemical wastewater (PWW) is toxic whereas the components depend on its source. Typically, it is a complex mixture containing suspend solids, heavy metals, polyaromatic hydrocarbons (PAHs), phenolic compounds and BTEX (benzene, toluene, ethyl benzene, xylene). OSPW is one specific type of petrochemical wastewater, which is produced through bitumen extraction from oil sands, and the major toxic organics is NAs. UV radiation is one of the most commonly used activation methods of PDS and PMS for PWW treatment. For example, 950 mg/L COD of PWW was reduced by 66% and 74% after 60 min of irradiation at pH 7 through the addition of 15 mM PDS in UV/PDS and UV/PDS/Fe^{2+} systems, respectively. In addition, the initial biodegradability of the PWW was 0.2, which was elevated to 0.3 and 0.45 after treatment by UV/PDS and UV/PDS/Fe^{2+}, respectively (Babaei and Ghanbari 2016). The initial concentration of 5 mg/L NAs was successfully removed in UV/PDS system using 20 mM PDS at pH 10, however, residual SO_4^{2-} was detected at the end of the experiment (Liang et al. 2011). SR-AOPs have also been highly effective in detoxification of PWW. For instance, the acute toxicity of *Vibrio fischeri* was reduced by both UV/PDS and UV/H_2O_2, but higher removal efficiency of NAs was found

with UV/PDS compared to UV/H_2O_2 (Fang et al. 2019). For PWW, PMS/MnO_2/UV could reduce 46% of TOC, 54% of COD, 42% of BOD_5 and 40% of toxicity after 2h of irradiation at pH 7 using 1 mM PMS and 0.25 g/L MnO_2 (Eslami et al. 2018). Alternatively, ultrasound is also an efficient activation method used for PWW treatment. For example, 1025 mg/L of COD and 275 mg/L of TOC of PWW were removed by 60% and 47% using ultrasound/PMS/nanoscale ZVI at 1.25 mM PMS, 0.4 g/L nanoscale zerovalent iron (ZVI), at pH 3, 90 min reaction time and 200 W ultrasound power. Meanwhile, biodegradability was increased from 0.24 to 0.4 (Barzegar et al. 2018). The optimum condition for Sonoelectro/PDS was pH 3, 20 mM PDS and 60 °C. The removal efficiency was increased with increasing ultrasonic frequency, ultrasonic power intensity, and electrode potential (Yousefi et al. 2019). Transition metals have also been considered by researchers to investigate the performance for the PWW treatment. For example, degradation of model compound CHA, and real NAs from OSPW were studied in presence of PDS and ZVI. Approximately 90% of NAs were removed in OSPW under the condition of 100 mg/L PDS and 20 g ZVI, at 20 °C and 6-day reaction time (Drzewicz et al. 2012, Liang et al. 2011). Biochar-La/ultrasonic/PDS has been introduced for the treatment of PWW. COD, BOD and phenol of the PWW were eliminated 88.4%, 88.7% and near 100% respectively at pH 3, 63 min of reaction time with 86 mg/L PDS, and 43 mg/L catalyst. Different from traditional Fenton reaction, the H_2O_2/PDS/Fe^{2+} process optimum pH was 11, and the mineralization degree of PWW was higher than 86% (Takdastan et al. 2019). In recent years, photocatalysts were used as a novel activation method for SR-AOPs. He *et al*. reported the activation of PDS using photocatalyst Co-TiO_2/zeolite (He et al. 2019). COD removal rate was up to 93.4% at the presence of 2.03 g/L PDS and 250 g/L catalyst under UV irradiation and aeration. The authors concluded that PDS was working as electron acceptor during photocatalysis process. However, the high amount of used catalyst was

not able to provide a clear oxidation removal efficiency as the organics could be adsorbed by catalysts rather than oxidized. Photocatalytic fuel cell with self-bias photoanode consisting of a WO_3 photoanode and a Si photovoltaic cell photocathode was established for the treatment of sulfate rich PWW, which could accelerate the separation of electrons and holes (Tan et al. 2019). This indicated that SO_4^{2-} could be oxidized by the holes to produce $SO_4^{\cdot -}$.

1.1.5.3 $KMnO_4$ oxidation

Initially, $KMnO_4$ is mainly used to remove dissolved iron and manganese, taste and odor from water and to inhibit the growth of microorganisms. The potential of removing organic pollutants from water by $KMnO_4$ oxidation is gradually becoming a key research area because of the diversity of active species during oxidation processes and the complexity of reaction mechanisms (Li et al. 2019, Peng et al. 2021, Zhu et al. 2019b). There are various valence states of transition metal Mn, including Mn(II), Mn(III), Mn(IV), Mn(V), Mn(VI), Mn(VII). Generally, Mn(II) and Mn(IV) (MnO_2) are stable in the water. Mn (III) is easy to transfer to Mn (II) and MnO_2 by disproportionation. The addition of H^+ and chelating agent could inhibit this disproportionation. Recently, it was found that the main form is complex of Mn (III) and humic acids rather than Mn (II) and MnO_2 in natural water. Mn (V) and Mn (VI) are also unstable and easy to disproportionate. Similar as Mn (III), Mn (V) is stable in the presence of chelating agent and extreme acid environment, while Mn (VI) is stable in the presence of chelating agent and extreme alkaline environment. $KMnO_4$ prefers to react with organics containing electron-rich moieties such as olefins, phenols and anilines. It was found that $KMnO_4$ oxidizes alkene organic compounds containing double bonds mainly through the addition reaction. For example, $KMnO_4$ initially attacked the C = C double bond of carbamazepine to form an organometallic complex. This complex then undergone a series of self-decomposition and hydrolysis to produce corresponding

products (Hu et al. 2009). $KMnO_4$ oxidizes amine organics mainly through electron transfer. In the initial stage of the reaction, $KMnO_4$ attacks the tertiary aromatic amine on piperazine of ciprofloxacin, making it lose an electron to produce enamine, which is unstable and generates corresponding products through a series of hydrolysis and oxidation reactions (Hu et al. 2010, Hu et al. 2011). $KMnO_4$ also oxidizes phenols mainly through electron transfer. Firstly, the phenolic hydroxyl is attacked to lose an electron and form unstable phenolic oxygen radical. Then, the phenolic oxygen radical coupling reaction takes place to form a series of byproducts (Jiang et al. 2014).

Potassium permanganate can react with a variety of inorganic substances including SO_3^{2-}, NO_2^-, Br^-, I^-. In the initial step of the reaction between $KMnO_4$ and SO_3^{2-}, Br^-, I^-, potassium permanganate forms a Lewis acid base complex with inorganic anions. The formation of the intermediate complex is a reversible and rapid process. The rate control step is a subsequent oxygen transfer process (Ernst et al. 1992, Kirschenbaum and Sutter 1966, Lawani and Sutter 1973). Reaction rate constants for oxidation of Br^- and I^- by $KMnO_4$ $k_{Mn(VII)+H+}$ are 149 (Lawani and Sutter 1973) and 1.7×10^7 (Kirschenbaum and Sutter 1966) M^{-2} s^{-1}, respectively. The degradation of halogenated organics by $KMnO_4$ oxidation is accompanied with dehalogenation, as well as generation of disinfection byproducts (DBPs) (Zhao et al. 2016a). Considering that Cl^- and Br^- do not react with $KMnO_4$, Zhao *et al.* reported the kinetic and mechanistic studies of the reactions of iodide (I^-) and hypoiodous acid (HOI) with $KMnO_4$ (Zhao et al. 2016b). In general, iodide ion could be transformed to iodate (IO_3^-) and reactive iodine species (HOI/I_2) by $KMnO_4$, HOI/I_2 could be further oxidized to IO_3^- or react with natural organic matter (NOM) to form iodinated-DBPs (I-DBPs). Iodide oxidation and iodate (IO_3^-) formation were faster at lower pH. As pH continued to rise, the oxidation rate of iodide and the formation of HOI/I_2 were decreased.

The concentration of HOI/I_2 reached to a highest state at pH 7. Meanwhile, the oxidation of HOI by $KMnO_4$ oxidation is also fast at acidic pH. $KMnO_4$ works as catalyst rather than an oxidant to accelerate the disproportionation of HOI to produce IO_3^- at pH ≥ 8. Based on the conclusion mentioned above, when applied $KMnO_4$ to iodide-containing waters, the formation of I-DBPs was highest at pH 7.0−8.0 due to the long lifetime of HOI. Specifically, HOI/I_2 was quickly oxidized by $KMnO_4$ to IO_3^- at pH < 6.0, whereas HOI/OI^- undergone a rapid $KMnO_4$-mediated disproportionation for pH ≥ 8.0. Ye *et al.* proposed that the I-DBPs (iodoform, iodoacetic acid and triiodoacetic acid) were produced during $KMnO_4$ oxidation in iodide containing water, of which the main I-DBPs was iodoform. The iodide was further oxidized to I_2, HOI and I_3^- (Ye et al. 2013, Ye et al. 2012, Zhang et al. 2015b). Zhao *et al.* investigated the kinetics of HOI with phenols, 3-oxopentanedioic acid (3-OPA) and flavone (Zhao et al. 2017a). In comparation to the HOI/3-OPA system, enhanced concentration of iodoform was observed in $KMnO_4$/HOI/3-OPA and $KMnO_4$/iodide/3-OPA system at pH < 8.0. Whereas decreased iodoform concentration and increased iodate were found in the presence of $KMnO_4$ at pH > 8.0. This could be explained by a faster disproportionation of HOI to IO_3^- to the iodination process.

1.1.5.3.1 Approaches to enhance $KMnO_4$ oxidation

1.1.5.3.1.1 $KMnO_4$ /MnO_2

One approach to enhance $KMnO_4$ oxidation is through the addition of MnO_2. It was found that the addition of MnO_2 could accelerate the oxidation of 4-nitrophenol (4-NP) by $KMnO_4$ (Jiang et al. 2009). Since 4-NP oxidized by MnO_2 is negligible, MnO_2 was involved in the degradation of 4-NP as a catalyst rather than an oxidant. However, addition of reducing agent in $KMnO_4$ oxidation system to generate MnO_2 had no effect on the degradation of 4-NP. Since MnO_2 could not oxidize 4-NP, the degradation of 4-NP was not accelerated. However, MnO_2 is also considered

an oxidant (Sun et al. 2013), therefore, it is hard to clarify the reason why MnO_2 enhances the oxidative degradation of organic compounds by $KMnO_4$ only from the perspective of kinetics. $KMnO_4$ reacts with triclosan (TCS) and its analogue 2-phenoxyphenol, mainly producing ether bond cleavage byproducts, while MnO_2 oxidized them to hydroxylated and quinone-like products as well as dimers. MnO_2 significantly enhanced the degradation rate of these compounds but insignificantly affected the degradation pathways by $KMnO_4$ oxidation, which clearly showed the catalytic effect of MnO_2 (Jiang et al. 2015).

1.1.5.3.1.2 $KMnO_4$ /ligands

Another approach to improve $KMnO_4$ oxidation is by the use of ligands. Gao *et al.* explored the byproducts of TCS oxidized by ligand-stabilized Mn(III) ($Mn(III)_L$). The authors concluded that major products were hydroxylated, quinone-like products, and dimers. However, 2,4-dichlorophenol (DCP) was main product produced by $KMnO_4$ (Gao et al. 2018). The addition of ligands, including pyrophosphate, nitrilotriacetate, and humic acid greatly accelerated the reaction rate of TCS by $KMnO_4$ oxidation, but the yield of DCP was not increased. Thus, there are some other reactive species such as Mn(V) and Mn(VI) that are potentially responsible for the high yield of DCP.

1.1.5.3.1.3 $KMnO_4$ /$NaHSO_3$

The combination of sodium bisulfite ($NaHSO_3$) with $KMnO_4$ had also been explored to improve $KMnO_4$ oxidation. Potassium permanganate activated by sodium bisulfite could oxidize organic pollutants in milliseconds (Sun et al. 2015). This process oxidized methyl blue, phenol and ciprofloxacin at pH 5.0 with 5 to 6 orders of magnitude rate higher than those determined for $KMnO_4$ alone, and 5 to 7 orders of magnitude rate higher than the conventional AOPs for water treatment. In this process, non-complexed Mn(III), which was produced *in-situ* by $KMnO_4/HSO_3^-$

rather than $SO_4^{\bullet-}$ and $^{\bullet}OH$, showed excellent oxidation activity for pollutants. When there were no organic pollutants in the solution, Mn(III) was prone to disproportionation to form Mn(II) and MnO_2. The disproportionation was easier in basic pH, as a result, the utilization rate of Mn(III) and the pollutant removal rate were low under alkaline conditions (Sun et al. 2016, Sun et al. 2018b). Moreover, HSO_3^- did not only reduce $KMnO_4$ to Mn(III) but also formed reactive Mn(III)-sulfur complexes (Gao et al. 2017). Oxygen could have also played an important role in this process. Particularly, HSO_3^- could be oxidized by $KMnO_4$ to $SO_3^{\bullet-}$, which likely competed Mn(III) with the pollutants. Oxygen could oxidize $SO_3^{\bullet-}$ to $SO_5^{\bullet-}$, leading to higher utilization of Mn(III) (Sun et al. 2018a). However, the main reactive species involved in $KMnO_4$ /$NaHSO_3$ was controversial. It was reported that $SO_5^{\bullet-}$ could react with HSO_3^- to produce $SO_4^{\bullet-}$, which could be further transformed to $^{\bullet}OH$ through reaction with water in acidic aquatic environment (Connick and Zhang 1996). Chen *et al.* reported that the contributions of reactive species depend on the type of contaminants. The main reactive species shifted from reactive manganese species to free radicals with increasing pH and [S(IV)]/[Mn(VII)] (Chen et al. 2020). In addition to Mn(III), Mn(V) and Mn(VI) were also involved in the oxidation system (Gao et al. 2018). Despite the disputation of mechanisms, the efficient performance of $KMnO_4$ /$NaHSO_3$ system is confirmed and is successfully applied in a pilot-scale tests as a pretreatment process for drinking water treatment (Chen et al. 2021).

1.1.5.3.1.4 $KMnO_4$ / catalysts

Catalyst has also been used to enhance $KMnO_4$ oxidation efficiency. The enhanced oxidation of $KMnO_4$ was found in the presence of carbon materials. For example, degradation rates of various phenols and anilines by $KMnO_4$ were increased in the presence of carbon nanotubes with significant dehalogenation. This could be attributed to the reduction of $KMnO_4$ by carbon

nanotubes to produce MnO_2, which could work as catalyst during the oxidation process (Zhao et al. 2016a). Ruthenium (Ru) is another commonly used catalyst for enhanced $KMnO_4$ oxidation. For example, molecular sieve supported Ru nanoparticles increased the degradation rate of sulfamethoxazole by 30–1140 times (Zhang et al. 2015a). 1g/L TiO_2 supported Ru nanoparticles increased the oxidation rate of various emerging pollutants at pH 7.0 by 0.3-120 times (Zhang et al. 2014). 1 g/L CeO_2 supported Ru nanoparticles increased degradation rate of butylparaben by $KMnO_4$ at pH 4-8 by 3-96 times (Zhang et al. 2013). During these processes, Ru(III) was oxidized by $KMnO_4$ to Ru(VI) and Ru(VII), which are co-oxidants for target pollutants. After that, Ru(VI) and Ru(VII) were reduced by pollutants to initial Ru(III).

1.1.5.3.1.5 Electro-activated $KMnO_4$

Novel activation method such as electrochemical activation and solar activation of KMnO4 has also been used to improve $KMnO_4$ oxidation process. A significant amount of pollutants could be efficiently removed in electrolysis + $KMnO_4$ + Mn^{2+} system. Mn(II) is important as promoter and Mn(III) stabilizer to generate increasing concentration of Mn(III) (Zhu et al. 2019a). Up to 90% diclofenac was degraded in 5 min by electro-activated $KMnO_4$ process using activated carbon fiber as cathode (Zhu et al. 2019c). These studies demonstrated that electro-activated $KMnO_4$ is an efficient water treatment approach.

1.1.5.3.1.6 Solar/ $KMnO_4$

Guo *et al.* (2018) indicated that terephthalic acid, benzoic acid, p-chlorobenzoic acid, nitrobenzene, and two micropollutants namely nalidixic acid and gemfibrozil, which were resistant to $KMnO_4$ degradation, could be significant oxidized by UV/$KMnO_4$ due to the formation of $^{\bullet}OH$ and Mn(V) peroxide with degradation rates ranging from 0.065-0.678 min^{-1}. Recently, the removal of organoarsenic compounds of p-arsanilic acid and roxarsone in UV/ $KMnO_4$ system was

investigated. The reaction rate of roxarsone was 0.0375 min^{-1} under the condition of 100 μM $KMnO_4$ and pH 7.0. The C−As bond of roxarsone was initially attacked by $^{\bullet}OH$, leading to the release of As(V). Then *in-situ* generated MnO_2 adsorbed As(V) and removed it from the aqueous phase (Wei et al. 2021). $KMnO_4$ could also be activated by visible light in the presence of biochar. The removal of sulfamethoxazole significantly increased to 97% in 30 min by the addition of biochar powder, and simultaneous removal of the total organic carbon was more than 58%. The increased removal was attributed to the generation of intermediate reactive manganese species, and the adsorption of biochar (Tian et al. 2019).

1.2 Research significance and hypotheses

A huge amount of toxic OSPW is stored in tailing ponds which imparts harmful effects on the ecosystem, environment, and economy. Thus, the detoxification and treatment of OSPW are necessary before its release into the environment. Efforts have been implemented by the oil and natural gas industry, the Government of Alberta and collaborating researchers for the development of novel treatment approaches, among which, *in-situ* treatment methods are encouraged. Photocatalysis has been studied for the degradation of a variety of refractory organic pollutants. It seems to be an achievable process for the degradation of NAs in OSPW by using solar energy. Nowadays, studies on the photocatalytic treatment of OSPW have mainly focused on the TiO_2. However, weak visible light absorption has been one of the critical limitations of TiO_2 against its application in the field of wastewater treatment. The technology gaps could be filled by the application of visible-light driven catalysts to the treatment of OSPW.

Bi_2WO_6 is the most commonly used visible-light driven catalyst. However, photocatalytic performance of Bi_2WO_6 still needs to be improved owing to the poor capability of Bi_2WO_6 for separating the electron-hole pairs. The novel z-scheme semiconductor heterojunction can not only

effectively increase the separation rate of electrons and holes, but also remain the oxidation and reduction potential of the original photoinduced carriers. NAs in OSPW contain classical NAs, oxidized NAs, S-containing NAs, and N-containing NAs. Recently, extraction and analytical technologies further confirmed the existence of heteroatomic NAs in the OSPW. However, knowledge on the degradation kinetics and pathways of heteroatomic NAs is still limited. Therefore, in this research, novel catalysts with enhanced photocatalytic performance such as high specific surface area, strong light absorption, rapid separation and transfer rate of photo-generated charge carriers, were developed for the degradation of NAs in OSPW. The following hypotheses were tested in this research:

(1) The effects of three different morphologies of Bi_2WO_6 on NAs degradation

Hypothesis: Compared to the nanoplate (NP) and swirl-like Bi_2WO_6 (SL), flower-like Bi_2WO_6 (FL) will show higher photocatalytic efficiency due to higher specific surface area, and larger pore volume.

(2) Structure-relative degradation of NAs

Hypothesis: The degradation rates of heteroatomic NAs will be higher than those of classical and oxidized NAs due to more reactive site at N and S.

(3) Reactive species in photocatalytic systems

Hypothesis: the main reactive species in photocatalytic system will be $O_2^{\bullet-}$ and $^{\bullet}OH$

(4) Degradation of heteroatomic NAs

Hypothesis: S-NAs and N-NAs will show different degradation behaviors in the presence of cations.

(5) The effects of inorganic parts of OSPW

Hypothesis: Cl^- and HCO_3^- in OSPW inorganic part will decrease the degradation rate of NAs, while NO_3^- will increase.

(6) Z-scheme heterojunction Bi_2WO_6 /NiO/Ag

Hypothesis: The constructed Bi_2WO_6 /NiO/Ag Z-scheme structure will separate electrons and holes efficiently, leading to an increased removal of OSPW.

(7) Enhanced treatment of OSPW by the addition of oxidants

Hypothesis: The addition of $KMnO_4$, H_2O_2 and PMS will improve the treatment efficiency of Bi_2WO_6 /NiO/Ag under solar light irradiation.

1.3 Research objectives

The aim of this research was to develop novel visible light driven photocatalysts with enhanced photocatalytic ability for the degradation of NAs. Different types of Bi_2WO_6 based catalyst were evaluated for their performance to degrade NAs in OSPW treatment. To achieve the aim of the project, four sub-objectives were developed and listed below:

Specific objective 1: Solar photocatalytic treatment of model and real oil sands process water naphthenic acids by Bi_2WO_6

(1) To prepare three different morphologies (NP, SL and FL structure) of Bi_2WO_6 semiconductor catalysts by hydrothermal method

(2) To study the structural, textural, and chemical properties of Bi_2WO_6 by SEM, XRD, XPS, BET

(3) To investigate the effect of catalyst morphology on the degradation of model compound CHA under simulated solar irradiation

(4) To evaluate the structure relativity of classical NAs, oxidized NAs, S-containing NAs, and N-containing NAs for model compounds and real OSPW

(5) To determine the reactive species in photocatalytic system through scavenger experiments

(6) To explore the effect of cations on the degradation kinetics and mechanisms of S-NAs and N-NAs

(7) To determine the underlying degradation pathways and mechanisms of S-NAs and N-NAs model compounds

Specific objective 2: Solar photocatalytic treatment of model and real oil sands process water NAs by Bi_2WO_6 /NiO/Ag

(1) To prepare heterojunction photocatalyst Bi_2WO_6 /NiO/Ag

(2) To explore the structural, textural, chemical, and optical properties of Bi_2WO_6/NiO/Ag semiconductor catalyst

(3) To study the degradation of NAs in OSPW under simulated solar irradiation by SFS, TOFMS and IMS.

(4) To determine the reactive species in photocatalytic system through electron paramagnetic resonance (EPR)

(5) To investigate the underlying photocatalytic mechanisms of Bi_2WO_6/NiO/Ag

Specific objective 3: Effect of inorganic fraction of OSPW on solar photocatalytic degradation of model compounds NAs mixtures

(1) To prepare OSPW containing inorganic fraction only

(2) To prepare structure-relative model compounds NAs mixtures in both buffer and inorganic fraction

(3) To compare kinetics of NAs mixtures in buffer and inorganic fraction

(4) To study the degradation mechanisms of NAs

Specific objective 4: Enhanced treatment of OSPW by catalyst through the addition of oxidants

(1) To compare the removal efficiency of NAs in OSPW in the presence or absence oxidants

(2) To evaluate the toxicity of treated OSPW with H_2O_2, PMS and $KMnO_4$

(3) To explore the mechanisms in different oxidation system

1.4 Thesis organization

The thesis consists of six chapters that were logically organized according to the research objectives presented above.

Chapter 1 contains a general introduction to the research background, significance, and objectives. It covers a brief review of OSPW, OSPW toxicity, previously investigated treatment approaches for OSPW, photocatalysis fundamentals as well as AOPs fundamentals.

Chapter 2 presents the degradation of model and real oil sands process water NAs by Bi_2WO_6. Three different morphologies (NP, SL, and FL) of Bi_2WO_6 were prepared by hydrothermal method and the structural, textural, and chemical properties of Bi_2WO_6 were characterized through

scanning electron microscopy (SEM), X-ray diffraction spectroscopy (XRD), X-ray photoelectron spectroscopy (XPS) and Brunauer–Emmett–Teller (BET) adsorption. Structure relative model compounds were selected including: cyclohexanecarboxylic acid (CHA), tetrahydropyran-4-carboxylic acid (T4CA), tetrahydro-2H-thiopyran-4-carboxylic acid (T-2H-T4CA), isonipecotic acid (IA) and 5-Hexyl-2-thiophenecarboxylic acid (5H-2THCA). CHA was used to explore the photocatalytic performance of three types Bi_2WO_6 and optimize the experimental conditions. T-2H-T4CA, IA and 5H-2THCA were selected to explore the effect of cations on the degradation kinetics and mechanisms. The reactive species in photocatalytic system were determined through scavenger experiments. The underlying degradation pathways and mechanisms of S-NAs and N-NAs were revealed with the assistant of density functional theory (DFT) calculation.

Chapter 3 illustrates the results of treatment of OSPW using Bi_2WO_6/NiO/Ag under sunlight irradiation. Bi_2WO_6/NiO/Ag was prepared and characterized by SEM, XRD, XPS, bright-field scanning transmission electron microscopy (BF-STEM) and high-angle annular dark-field (HAADF)-STEM, high resolution transmission electron microscopy (HRTEM), fluorescence emission spectra, transient photocurrent responses, UV–vis diffuses reflectance spectra. The degradations of NAs in OSPW under simulated solar irradiation were detected by Synchronous fluorescence spectra (SFS), time of flight mass spectra (TOFMS) and the ion-mobility spectrometry (IMS). The reactive species in photocatalytic system were detected through electron paramagnetic resonance (EPR). The underlying photocatalytic mechanisms of Bi_2WO_6/NiO/Ag were investigated. The acute toxicity of OSPW before and after treatment was evaluated using *Vibrio fischeri* toxicity screening test.

Chapter 4 presents the findings of the effect of inorganic fraction of OSPW on the degradation of NAs mixtures. NAs mixtures were dissolved in buffer or OSPW containing inorganic fraction.

The kinetics of NAs mixtures in buffer and inorganic fraction were compared. The degradation mechanisms of NAs were investigated with the aid of DFT calculation.

Chapter 5 describes the treatment of OSPW by adding oxidants such as $KMnO_4$, PMS and H_2O_2. The degradation of NAs in OSPW under simulated solar irradiation were detected by SFS and TOFMS. The acute toxicity of OSPW treated with $KMnO_4$, PMS and H_2O_2 at different concentrations was evaluated using *Vibrio fischeri*. The mechanisms in different oxidant assisted photocatalytic system were studied through quenching experiments and EPR.

Chapter 6 summarizes the major findings and conclusions of the thesis. It outlines the objectives that were met and provides recommendations for future work.

1.5 References

Abdalrhman, A.S., Ganiyu, S.O. and Gamal El-Din, M. (2019) Degradation kinetics and structure-reactivity relation of naphthenic acids during anodic oxidation on graphite electrodes. Chemical Engineering Journal 370, 997-1007.

Afzal, A., Drzewicz, P., Martin, J.W. and Gamal El-Din, M. (2012) Decomposition of cyclohexanoic acid by the UV/H2O2 process under various conditions. Science of the Total Environment 426, 387-392.

Alharbi, H.A., Saunders, D.M.V., Al-Mousa, A., Alcorn, J., Pereira, A.S., Martin, J.W., Giesy, J.P. and Wiseman, S.B. (2016) Inhibition of ABC transport proteins by oil sands process affected water. Aquatic Toxicology 170, 81-88.

Allen, E.W.A.W. (2008) Process water treatment in Canada's oil sands industry: I. Target pollutants and treatment objectives. 7(2), 123-138.

Anderson, J., Wiseman, S.B., Moustafa, A., Gamal El-Din, M., Liber, K. and Giesy, J.P. (2012) Effects of exposure to oil sands process-affected water from experimental reclamation ponds on Chironomus dilutus. Water Research 46(6), 1662-1672.

Anipsitakis, G.P. and Dionysiou, D.D. (2004) Transition metal/UV-based advanced oxidation technologies for water decontamination. Applied Catalysis B: Environmental 54(3), 155-163.

Babaei, A.A. and Ghanbari, F. (2016) COD removal from petrochemical wastewater by UV/hydrogen peroxide, UV/persulfate and UV/percarbonate: biodegradability improvement and cost evaluation. Journal of Water Reuse and Desalination 6(4), 484-494.

Barzegar, G., Jorfi, S., Zarezade, V., Khatebasreh, M., Mehdipour, F. and Ghanbari, F. (2018) 4-Chlorophenol degradation using ultrasound/peroxymonosulfate/nanoscale zero valent iron: Reusability, identification of degradation intermediates and potential application for real wastewater. Chemosphere 201, 370-379.

Benally, C., Messele, S.A. and Gamal El-Din, M. (2019) Adsorption of organic matter in oil sands process water (OSPW) by carbon xerogel. Water Research 154, 402-411.

Biryukova, O.V., Fedorak, P.M. and Quideau, S.A. (2007) Biodegradation of naphthenic acids by rhizosphere microorganisms. Chemosphere 67(10), 2058-2064.

Bouchard, J., Maine, C., Argyropoulos, D. and Berry, R. (1998) Kraft pulp bleaching using in-situ dimethyldioxirane: mechanism and reactivity of the oxidants.

Buxton, G.V., Greenstock, C.L., Helman, W.P. and Ross, A.B. (1988) Critical Review of rate constants for reactions of hydrated electrons, hydrogen atoms and hydroxyl radicals (·OH/·O− in Aqueous Solution. 17(2), 513-886.

Chen, J., Ling, J., Sun, B., Wang, J., Zhou, B., Guan, X. and Sun, Y. (2021) Trace organic contaminants abatement by permanganate/bisulfite pretreatment coupled with conventional water treatment processes: Lab- and pilot-scale tests. Journal of Hazardous Materials 401, 123380.

Chen, J., Rao, D., Dong, H., Sun, B., Shao, B., Cao, G. and Guan, X. (2020) The role of active manganese species and free radicals in permanganate/bisulfite process. Journal of Hazardous Materials 388, 121735.

Clemente, J.S., MacKinnon, M.D. and Fedorak, P.M. (2004) Aerobic Biodegradation of Two Commercial Naphthenic Acids Preparations. Environmental Science & Technology 38(4), 1009-1016.

Connick, R.E. and Zhang, Y.-X. (1996) Kinetics and Mechanism of the Oxidation of HSO3- by O2. 2. The Manganese(II)-Catalyzed Reaction. Inorganic Chemistry 35(16), 4613-4621.

Criquet, J. and Karpel Vel Leitner, N. (2011) Electron beam irradiation of aqueous solution of persulfate ions. Chemical Engineering Journal 169(1), 258-262.

Drzewicz, P., Perez-Estrada, L., Alpatova, A., Martin, J.W. and Gamal El-Din, M. (2012) Impact of Peroxydisulfate in the Presence of Zero Valent Iron on the Oxidation of Cyclohexanoic Acid and Naphthenic Acids from Oil Sands Process-Affected Water. Environmental Science & Technology 46(16), 8984-8991.

Ernst, T., Cyfert, M. and Wilgocki, M. (1992) Kinetics and mechanism of sulfite oxidation by permanganate in basic medium. 24(10), 903-908.

Eslami, A., Hashemi, M. and Ghanbari, F. (2018) Degradation of 4-chlorophenol using catalyzed peroxymonosulfate with nano-MnO2/UV irradiation: Toxicity assessment and evaluation for industrial wastewater treatment. Journal of Cleaner Production 195, 1389-1397.

Fang, Z., Huang, R., Chelme-Ayala, P., Shi, Q., Xu, C. and Gamal El-Din, M. (2019) Comparison of UV/Persulfate and UV/H2O2 for the removal of naphthenic acids and acute toxicity towards Vibrio fischeri from petroleum production process water. Science of The Total Environment 694, 133686.

Fennell, J. and Arciszewski, T.J. (2019) Current knowledge of seepage from oil sands tailings ponds and its environmental influence in northeastern Alberta. Science of the Total Environment 686, 968-985.

Furman, O.S., Teel, A.L. and Watts, R.J. (2010) Mechanism of Base Activation of Persulfate. Environmental Science & Technology 44(16), 6423-6428.

Gamal El-Din, M., Fu, H., Wang, N., Chelme-Ayala, P., Pérez-Estrada, L., Drzewicz, P., Martin, J.W., Zubot, W. and Smith, D.W. (2011) Naphthenic acids speciation and removal during petroleum-coke adsorption and ozonation of oil sands process-affected water. Science of The Total Environment 409(23), 5119-5125.

Ganiyu, S. O., Arslan, M., El-Din, M. G. (2022). Combined solar activated sulfate radical-based advanced oxidation processes (SR-AOPs) and biofiltration for the remediation of dissolved organics in oil sands produced water. Chemical Engineering Journal, 134579.

Gao, Y., Jiang, J., Zhou, Y., Pang, S.-Y., Jiang, C., Guo, Q. and Duan, J.-B. (2018) Does Soluble Mn(III) Oxidant Formed in Situ Account for Enhanced Transformation of Triclosan by Mn(VII) in the Presence of Ligands? Environmental Science & Technology 52(8), 4785-4793.

Gao, Y., Jiang, J., Zhou, Y., Pang, S.-Y., Ma, J., Jiang, C., Wang, Z., Wang, P.-X., Wang, L.-H. and Li, J. (2017) Unrecognized role of bisulfite as Mn(III) stabilizing agent in activating

permanganate (Mn(VII)) for enhanced degradation of organic contaminants. Chemical Engineering Journal 327, 418-422.

García-Espinoza, J.D., Mijaylova-Nacheva, P. and Avilés-Flores, M. (2018) Electrochemical carbamazepine degradation: Effect of the generated active chlorine, transformation pathways and toxicity. Chemosphere 192, 142-151.

Garcia-Garcia, E., Ge, J.Q., Oladiran, A., Montgomery, B., El-Din, M.G., Perez-Estrada, L.C., Stafford, J.L., Martin, J.W. and Belosevic, M. (2011) Ozone treatment ameliorates oil sands process water toxicity to the mammalian immune system. Water Research 45(18), 5849-5857.

Ge, M., Li, Y., Liu, L., Zhou, Z. and Chen, W. (2011) Bi2O3−Bi2WO6 Composite Microspheres: Hydrothermal Synthesis and Photocatalytic Performances. The Journal of Physical Chemistry C 115(13), 5220-5225.

Gentes, M.-L., Waldner, C., Papp, Z. and Smits, J.E.G. (2006) Effects of oil sands tailings compounds and harsh weather on mortality rates, growth and detoxification efforts in nestling tree swallows (Tachycineta bicolor). Environmental Pollution 142(1), 24-33.

Ghauch, A., Baalbaki, A., Amasha, M., El Asmar, R. and Tantawi, O. (2017) Contribution of persulfate in UV-254nm activated systems for complete degradation of chloramphenicol antibiotic in water. Chemical Engineering Journal 317, 1012-1025.

Ghauch, A., Tuqan, A.M. and Kibbi, N. (2012) Ibuprofen removal by heated persulfate in aqueous solution: A kinetics study. Chemical Engineering Journal 197, 483-492.

Govindan, K., Raja, M., Noel, M. and James, E.J. (2014) Degradation of pentachlorophenol by hydroxyl radicals and sulfate radicals using electrochemical activation of

peroxomonosulfate, peroxodisulfate and hydrogen peroxide. Journal of Hazardous Materials 272, 42-51.

Guan, Y.-H., Ma, J., Li, X.-C., Fang, J.-Y. and Chen, L.-W. (2011) Influence of pH on the Formation of Sulfate and Hydroxyl Radicals in the UV/Peroxymonosulfate System. Environmental Science & Technology 45(21), 9308-9314.

Gunawan, Y., Nemati, M. and Dalai, A. (2014) Biodegradation of a surrogate naphthenic acid under denitrifying conditions. Water Research 51, 11-24.

Guo, K., Zhang, J., Li, A., Xie, R., Liang, Z., Wang, A., Ling, L., Li, X., Li, C. and Fang, J. (2018) Ultraviolet Irradiation of Permanganate Enhanced the Oxidation of Micropollutants by Producing HO• and Reactive Manganese Species. Environmental Science & Technology Letters 5(12), 750-756.

Güyer, G.T. and Ince, N.H. (2011) Degradation of diclofenac in water by homogeneous and heterogeneous sonolysis. Ultrasonics Sonochemistry 18(1), 114-119.

He, Q., Si, S., Song, L., Yan, H., Yao, Y., Zhao, D. and Cai, Q. (2019) Refractory petrochemical wastewater treatment by K2S2O8 assisted photocatalysis. Saudi Journal of Biological Sciences 26(4), 849-853.

He, Y., Patterson, S., Wang, N., Hecker, M., Martin, J.W., El-Din, M.G., Giesy, J.P. and Wiseman, S.B. (2012) Toxicity of untreated and ozone-treated oil sands process-affected water (OSPW) to early life stages of the fathead minnow (Pimephales promelas). Water Research 46(19), 6359-6368.

He, Y., Wiseman, S.B., Hecker, M., Zhang, X., Wang, N., Perez, L.A., Jones, P.D., Gamal El-Din, M., Martin, J.W. and Giesy, J.P. (2011) Effect of Ozonation on the Estrogenicity and

Androgenicity of Oil Sands Process-Affected Water. Environmental Science & Technology 45(15), 6268-6274.

Hersikorn, B.D. and Smits, J.E.G. (2011) Compromised metamorphosis and thyroid hormone changes in wood frogs (Lithobates sylvaticus) raised on reclaimed wetlands on the Athabasca oil sands. Environmental Pollution 159(2), 596-601.

Hu, L., Martin, H.M., Arce-Bulted, O., Sugihara, M.N., Keating, K.A. and Strathmann, T.J. (2009) Oxidation of Carbamazepine by Mn(VII) and Fe(VI): Reaction Kinetics and Mechanism. Environmental Science & Technology 43(2), 509-515.

Hu, L., Martin, H.M. and Strathmann, T.J. (2010) Oxidation Kinetics of Antibiotics during Water Treatment with Potassium Permanganate. Environmental Science & Technology 44(16), 6416-6422.

Hu, L., Stemig, A.M., Wammer, K.H. and Strathmann, T.J. (2011) Oxidation of Antibiotics during Water Treatment with Potassium Permanganate: Reaction Pathways and Deactivation. Environmental Science & Technology 45(8), 3635-3642.

Huang, C., Shi, Y., Gamal El-Din, M. and Liu, Y. (2015) Treatment of oil sands process-affected water (OSPW) using ozonation combined with integrated fixed-film activated sludge (IFAS). Water Research 85, 167-176.

Islam, M.S., Zhang, Y., McPhedran, K.N., Liu, Y. and Gamal El-Din, M. (2015) Granular activated carbon for simultaneous adsorption and biodegradation of toxic oil sands process-affected water organic compounds. Journal of Environmental Management 152, 49-57.

Jiang, J., Gao, Y., Pang, S.-Y., Lu, X.-T., Zhou, Y., Ma, J. and Wang, Q. (2015) Understanding the Role of Manganese Dioxide in the Oxidation of Phenolic Compounds by Aqueous Permanganate. Environmental Science & Technology 49(1), 520-528.

Jiang, J., Gao, Y., Pang, S.-Y., Wang, Q., Huangfu, X., Liu, Y. and Ma, J. (2014) Oxidation of Bromophenols and Formation of Brominated Polymeric Products of Concern during Water Treatment with Potassium Permanganate. Environmental Science & Technology 48(18), 10850-10858.

Jiang, J., Pang, S.-Y. and Ma, J. (2009) Oxidation of Triclosan by Permanganate (Mn(VII)): Importance of Ligands and In Situ Formed Manganese Oxides. Environmental Science & Technology 43(21), 8326-8331.

Jo, W.-K., Kumar, S., Eslava, S. and Tonda, S. (2018) Construction of Bi2WO6/RGO/g-C3N4 2D/2D/2D hybrid Z-scheme heterojunctions with large interfacial contact area for efficient charge separation and high-performance photoreduction of CO2 and H2O into solar fuels. Applied Catalysis B: Environmental 239, 586-598.

Kalebaila, K.K. and Fairbridge, C. (2014) UV Photocatalytic Degradation of Commercial Naphthenic Acid Using TiO₂-Zeolite Composites %J Journal of Water Resource and Protection. Vol.06No.12, 9.

Kirschenbaum, L.J. and Sutter, J.R. (1966) Kinetic Studies of Permanganate Oxidation Reactions. I. Reaction with Iodide Ion. The Journal of Physical Chemistry 70(12), 3863-3866.

Lawani, S.A. and Sutter, J.R. (1973) Kinetic studies of permanganate oxidation reactions. IV. Reaction with bromide ion. The Journal of Physical Chemistry 77(12), 1547-1551.

Leclair, L.A., Pohler, L., Wiseman, S.B., He, Y., Arens, C.J., Giesy, J.P., Scully, S., Wagner, B.D., van den Heuvel, M.R. and Hogan, N.S. (2015) In Vitro Assessment of Endocrine Disrupting Potential of Naphthenic Acid Fractions Derived from Oil Sands-Influenced Water. Environmental Science & Technology 49(9), 5743-5752.

Legrini, O., Oliveros, E. and Braun, A.M. (1993) Photochemical processes for water treatment. Chemical Reviews 93(2), 671-698.

Leshuk, T., de Oliveira Livera, D., Peru, K.M., Headley, J.V., Vijayaraghavan, S., Wong, T. and Gu, F. (2016a) Photocatalytic degradation kinetics of naphthenic acids in oil sands process-affected water: Multifactorial determination of significant factors. Chemosphere 165, 10-17.

Leshuk, T., Peru, K.M., de Oliveira Livera, D., Tripp, A., Bardo, P., Headley, J.V. and Gu, F. (2018) Petroleomic analysis of the treatment of naphthenic organics in oil sands process-affected water with buoyant photocatalysts. Water Research 141, 297-306.

Leshuk, T., Wong, T., Linley, S., Peru, K.M., Headley, J.V. and Gu, F. (2016b) Solar photocatalytic degradation of naphthenic acids in oil sands process-affected water. Chemosphere 144, 1854-1861.

Li, B., Lai, C., Zeng, G., Qin, L., Yi, H., Huang, D., Zhou, C., Liu, X., Cheng, M., Xu, P., Zhang, C., Huang, F. and Liu, S. (2018) Facile Hydrothermal Synthesis of Z-Scheme Bi2Fe4O9/Bi2WO6 Heterojunction Photocatalyst with Enhanced Visible Light Photocatalytic Activity. ACS Applied Materials & Interfaces 10(22), 18824-18836.

Li, B., Yang, Q., Peng, Y., Chen, J., Deng, L., Wang, D., Hong, X. and Li, J. (2019) Enhanced low-temperature activity of LaMnO3 for toluene oxidation: The effect of treatment with an acidic KMnO4. Chemical Engineering Journal 366, 92-99.

Liang, X., Zhu, X. and Butler, E.C. (2011) Comparison of four advanced oxidation processes for the removal of naphthenic acids from model oil sands process water. Journal of Hazardous Materials 190(1), 168-176.

Liu, J., Wang, L., Tang, J. and Ma, J. (2016a) Photocatalytic degradation of commercially sourced naphthenic acids by TiO2-graphene composite nanomaterial. Chemosphere 149, 328-335.

Liu, J., Zhao, Z., Shao, P. and Cui, F. (2015) Activation of peroxymonosulfate with magnetic Fe3O4–MnO2 core–shell nanocomposites for 4-chlorophenol degradation. Chemical Engineering Journal 262, 854-861.

Liu, N., Lei, Z.-D., Wang, T., Wang, J.-J., Zhang, X.-D., Xu, G. and Tang, L. (2016b) Radiolysis of carbamazepine aqueous solution using electron beam irradiation combining with hydrogen peroxide: Efficiency and mechanism. Chemical Engineering Journal 295, 484-493.

Lo, C.C., Brownlee, B.G. and Bunce, N.J. (2006) Mass spectrometric and toxicological assays of Athabasca oil sands naphthenic acids. Water Research 40(4), 655-664.

Loos, G., Scheers, T., Van Eyck, K., Van Schepdael, A., Adams, E., Van der Bruggen, B., Cabooter, D. and Dewil, R. (2018) Electrochemical oxidation of key pharmaceuticals using a boron doped diamond electrode. Separation and Purification Technology 195, 184-191.

Luo, C., Ma, J., Jiang, J., Liu, Y., Song, Y., Yang, Y., Guan, Y. and Wu, D. (2015) Simulation and comparative study on the oxidation kinetics of atrazine by UV/H2O2, UV/HSO5− and UV/S2O82−. Water Research 80, 99-108.

Lutze, H. (2013) Sulfate radical based oxidation in water treatment, Universität Duisburg-Essen.

Lutze, H.V., Bakkour, R., Kerlin, N., von Sonntag, C. and Schmidt, T.C. (2014) Formation of bromate in sulfate radical based oxidation: Mechanistic aspects and suppression by dissolved organic matter. Water Research 53, 370-377.

Lutze, H.V., Bircher, S., Rapp, I., Kerlin, N., Bakkour, R., Geisler, M., von Sonntag, C. and Schmidt, T.C. (2015) Degradation of Chlorotriazine Pesticides by Sulfate Radicals and the Influence of Organic Matter. Environmental Science & Technology 49(3), 1673-1680.

Lv, Y.-R., He, R.-K., Chen, Z.-Y., Li, X. and Xu, Y.-H. (2020) Fabrication of hierarchical copper sulfide/bismuth tungstate p-n heterojunction with two-dimensional (2D) interfacial coupling for enhanced visible-light photocatalytic degradation of glyphosate. Journal of Colloid and Interface Science 560, 293-302.

McQueen, A.D., Kinley, C.M., Kiekhaefer, R.L., Calomeni, A.J., Rodgers, J.H. and Castle, J.W. (2016) Photocatalysis of a Commercial Naphthenic Acid in Water Using Fixed-Film TiO2. Water, Air, & Soil Pollution 227(5), 132.

Meng, L., How, Z.T., Ganiyu, S.O. and Gamal El-Din, M. (2021) Solar photocatalytic treatment of model and real oil sands process water naphthenic acids by bismuth tungstate: Effect of catalyst morphology and cations on the degradation kinetics and pathways. Journal of Hazardous Materials 413, 125396.

Meng, L., Yang, S., Sun, C., He, H., Xian, Q., Li, S., Wang, G., Zhang, L. and Jiang, D. (2017a) A novel method for photo-oxidative degradation of diatrizoate in water via electromagnetic induction electrodeless lamp. Journal of Hazardous Materials 337, 34-46.

Meng, X., Li, Z., Zeng, H., Chen, J. and Zhang, Z. (2017b) MoS2 quantum dots-interspersed Bi2WO6 heterostructures for visible light-induced detoxification and disinfection. Applied Catalysis B: Environmental 210, 160-172.

Michael, I., Hapeshi, E., Michael, C., Varela, A.R., Kyriakou, S., Manaia, C.M. and Fatta-Kassinos, D. (2012) Solar photo-Fenton process on the abatement of antibiotics at a pilot scale:

Degradation kinetics, ecotoxicity and phytotoxicity assessment and removal of antibiotic resistant enterococci. Water Research 46(17), 5621-5634.

Miklos, D.B., Remy, C., Jekel, M., Linden, K.G., Drewes, J.E. and Hübner, U. (2018) Evaluation of advanced oxidation processes for water and wastewater treatment – A critical review. Water Research 139, 118-131.

Nawaz, T. and Sengupta, S. (2021) Handbook of Water Purity and Quality (Second Edition). Ahuja, S. (ed), pp. 293-337, Academic Press, Amsterdam.

Nero, V., Farwell, A., Lee, L.E.J., Van Meer, T., MacKinnon, M.D. and Dixon, D.G. (2006) The effects of salinity on naphthenic acid toxicity to yellow perch: Gill and liver histopathology. Ecotoxicology and Environmental Safety 65(2), 252-264.

NRC (2022a) Oil Resources, Natural Resource Canada, Canada.

NRC (2022b) Water Management in oil sands, Natural Resource Canada, Canada.

Nyakas, A., Han, J., Peru, K.M., Headley, J.V. and Borchers, C.H. (2013) Comprehensive Analysis of Oil Sands Processed Water by Direct-Infusion Fourier-Transform Ion Cyclotron Resonance Mass Spectrometry with and without Offline UHPLC Sample Prefractionation. Environmental Science & Technology 47(9), 4471-4479.

Oh, W.-D., Dong, Z. and Lim, T.-T. (2016) Generation of sulfate radical through heterogeneous catalysis for organic contaminants removal: Current development, challenges and prospects. Applied Catalysis B: Environmental 194, 169-201.

Parajulee, A. and Wania, F. (2014) Evaluating officially reported polycyclic aromatic hydrocarbon emissions in the Athabasca oil sands region with a multimedia fate model. 111(9), 3344-3349.

Peng, J., Zhou, P., Zhou, H., Liu, W., Zhang, H., Zhou, C., Lai, L., Ao, Z., Su, S. and Lai, B. (2021) Insights into the Electron-Transfer Mechanism of Permanganate Activation by Graphite for Enhanced Oxidation of Sulfamethoxazole. Environmental Science & Technology 55(13), 9189-9198.

Peng, W., Liu, S., Sun, H., Yao, Y., Zhi, L. and Wang, S. (2013) Synthesis of porous reduced graphene oxide as metal-free carbon for adsorption and catalytic oxidation of organics in water. Journal of Materials Chemistry A 1(19), 5854-5859.

Pérez-Estrada, L.A., Han, X., Drzewicz, P., Gamal El-Din, M., Fedorak, P.M. and Martin, J.W. (2011) Structure–Reactivity of Naphthenic Acids in the Ozonation Process. Environmental Science & Technology 45(17), 7431-7437.

Pollet, I. and Bendell-Young, L.I. (2000) Amphibians as indicators of wetland quality in wetlands formed from oil sands effluent. 19(10), 2589-2597.

Poveda, C. and Lipsett, M. (2013) The Canadian oil sands: environmental, economic, social, health, and other impacts. WIT Transactions on Ecology and the Environment 173, 575-587.

Pramanik, S. (2016) Review of biological processes in oil sands: a feasible solution for tailings water treatment. 24(3), 274-284.

Qi, C., Liu, X., Ma, J., Lin, C., Li, X. and Zhang, H. (2016) Activation of peroxymonosulfate by base: Implications for the degradation of organic pollutants. Chemosphere 151, 280-288.

Rastogi, A., Al-Abed, S.R. and Dionysiou, D.D. (2009) Sulfate radical-based ferrous–peroxymonosulfate oxidative system for PCBs degradation in aqueous and sediment systems. Applied Catalysis B: Environmental 85(3), 171-179.

Redpath, J.L. and Willson, R.L. (1975) Chain Reactions and Radiosensitization: Model Enzyme Studies. International Journal of Radiation Biology and Related Studies in Physics, Chemistry and Medicine 27(4), 389-398.

Reinardy, H.C., Scarlett, A.G., Henry, T.B., West, C.E., Hewitt, L.M., Frank, R.A. and Rowland, S.J. (2013) Aromatic Naphthenic Acids in Oil Sands Process-Affected Water, Resolved by GCxGC-MS, Only Weakly Induce the Gene for Vitellogenin Production in Zebrafish (Danio rerio) Larvae. Environmental Science & Technology 47(12), 6614-6620.

Ren, J., Wang, W., Sun, S., Zhang, L. and Chang, J. (2009) Enhanced photocatalytic activity of Bi2WO6 loaded with Ag nanoparticles under visible light irradiation. Applied Catalysis B: Environmental 92(1), 50-55.

Rogers, V., MacKinnon, M. and Brownlee, B. (2007) Analytical approaches to characterising fish tainting potential of oil sands process waters. Water Science and Technology 55(5), 311-318.

Rowland, S.J., West, C.E., Jones, D., Scarlett, A.G., Frank, R.A. and Hewitt, L.M. (2011) Steroidal Aromatic 'Naphthenic Acids' in Oil Sands Process-Affected Water: Structural Comparisons with Environmental Estrogens. Environmental Science & Technology 45(22), 9806-9815.

Sánchez-Polo, M., Abdel daiem, M.M., Ocampo-Pérez, R., Rivera-Utrilla, J. and Mota, A.J. (2013) Comparative study of the photodegradation of bisphenol A by HO, SO4− and CO3−/HCO3 radicals in aqueous phase. Science of the Total Environment 463-464, 423-431.

Scarlett, A.G., Reinardy, H.C., Henry, T.B., West, C.E., Frank, R.A., Hewitt, L.M. and Rowland, S.J. (2013) Acute toxicity of aromatic and non-aromatic fractions of naphthenic acids

extracted from oil sands process-affected water to larval zebrafish. Chemosphere 93(2), 415-420.

Scarlett, A.G., West, C.E., Jones, D., Galloway, T.S. and Rowland, S.J. (2012) Predicted toxicity of naphthenic acids present in oil sands process-affected waters to a range of environmental and human endpoints. Science of the Total Environment 425, 119-127.

Serna-Galvis, E.A., Silva-Agredo, J., Giraldo-Aguirre, A.L., Flórez-Acosta, O.A. and Torres-Palma, R.A. (2016) High frequency ultrasound as a selective advanced oxidation process to remove penicillinic antibiotics and eliminate its antimicrobial activity from water. Ultrasonics Sonochemistry 31, 276-283.

Sun, B., Bao, Q. and Guan, X. (2018a) Critical role of oxygen for rapid degradation of organic contaminants in permanganate/bisulfite process. Journal of Hazardous Materials 352, 157-164.

Sun, B., Dong, H., He, D., Rao, D. and Guan, X. (2016) Modeling the Kinetics of Contaminants Oxidation and the Generation of Manganese(III) in the Permanganate/Bisulfite Process. Environmental Science & Technology 50(3), 1473-1482.

Sun, B., Guan, X., Fang, J. and Tratnyek, P.G. (2015) Activation of Manganese Oxidants with Bisulfite for Enhanced Oxidation of Organic Contaminants: The Involvement of Mn(III). Environmental Science & Technology 49(20), 12414-12421.

Sun, B., Li, D., Linghu, W. and Guan, X. (2018b) Degradation of ciprofloxacin by manganese(III) intermediate: Insight into the potential application of permanganate/bisulfite process. Chemical Engineering Journal 339, 144-152.

Sun, B., Zhang, J., Du, J., Qiao, J. and Guan, X. (2013) Reinvestigation of the Role of Humic Acid in the Oxidation of Phenols by Permanganate. Environmental Science & Technology 47(24), 14332-14340.

Sun, C., Shotyk, W., Cuss, C.W., Donner, M.W., Fennell, J., Javed, M., Noernberg, T., Poesch, M., Pelletier, R., Sinnatamby, N., Siddique, T. and Martin, J.W. (2017) Characterization of Naphthenic Acids and Other Dissolved Organics in Natural Water from the Athabasca Oil Sands Region, Canada. Environmental Science & Technology 51(17), 9524-9532.

Sun, H., Kwan, C., Suvorova, A., Ang, H.M., Tadé, M.O. and Wang, S. (2014) Catalytic oxidation of organic pollutants on pristine and surface nitrogen-modified carbon nanotubes with sulfate radicals. Applied Catalysis B: Environmental 154-155, 134-141.

Takdastan, A., Ravanbakhsh, M., Hazrati, M. and Safapour, S. (2019) Removal of dinitrotoluene from petrochemical wastewater by Fenton oxidation, kinetics and the optimum experiment conditions. SN Applied Sciences 1(7), 794.

Tan, X., Bai, J., Zheng, J., Zhang, Y., Li, J., Zhou, T., Xia, L., Xu, Q. and Zhou, B. (2019) Photocatalytic fuel cell based on sulfate radicals converted from sulfates in situ for wastewater treatment and chemical energy utilization. Catalysis Today 335, 485-491.

Tang, S., Tang, J., Yuan, D., Wang, Z., Zhang, Y. and Rao, Y. (2020) Elimination of humic acid in water: comparison of UV/PDS and UV/PMS. RSC Advances 10(30), 17627-17634.

Tian, S.-Q., Wang, L., Liu, Y.-L., Yang, T., Huang, Z.-S., Wang, X.-S., He, H.-Y., Jiang, J. and Ma, J. (2019) Enhanced Permanganate Oxidation of Sulfamethoxazole and Removal of Dissolved Organics with Biochar: Formation of Highly Oxidative Manganese Intermediate Species and in Situ Activation of Biochar. Environmental Science & Technology 53(9), 5282-5291.

Trovó, A.G., Pupo Nogueira, R.F., Agüera, A., Fernandez-Alba, A.R. and Malato, S. (2011) Degradation of the antibiotic amoxicillin by photo-Fenton process – Chemical and toxicological assessment. Water Research 45(3), 1394-1402.

von Gunten, U. (2003) Ozonation of drinking water: Part II. Disinfection and by-product formation in presence of bromide, iodide or chlorine. Water Research 37(7), 1469-1487.

von Gunten, U. and Oliveras, Y. (1998) Advanced Oxidation of Bromide-Containing Waters: Bromate Formation Mechanisms. Environmental Science & Technology 32(1), 63-70.

Wang, C., Klamerth, N., Huang, R., Elnakar, H. and Gamal El-Din, M. (2016) Oxidation of Oil Sands Process-Affected Water by Potassium Ferrate(VI). Environmental Science & Technology 50(8), 4238-4247.

Wang, H., Zhang, L., Chen, Z., Hu, J., Li, S., Wang, Z., Liu, J. and Wang, X. (2014) Semiconductor heterojunction photocatalysts: design, construction, and photocatalytic performances. Chemical Society reviews 43(15), 5234-5244.

Wang, J., Cao, X., Huang, Y. and Tang, X. (2015) Developmental toxicity and endocrine disruption of naphthenic acids on the early life stage of zebrafish (Danio rerio). 35(12), 1493-1501.

Wang, P., Huang, B., Lou, Z., Zhang, X., Qin, X., Dai, Y., Zheng, Z. and Wang, X. (2010a) Synthesis of Highly Efficient Ag@AgCl Plasmonic Photocatalysts with Various Structures. 16(2), 538-544.

Wang, P., Huang, B., Zhang, Q., Zhang, X., Qin, X., Dai, Y., Zhan, J., Yu, J., Liu, H. and Lou, Z. (2010b) Highly Efficient Visible Light Plasmonic Photocatalyst Ag@Ag(Br,I). 16(33), 10042-10047.

Wang, S. and Wang, J. (2018) Degradation of carbamazepine by radiation-induced activation of peroxymonosulfate. Chemical Engineering Journal 336, 595-601.

Wang, Y., Zhang, H., Zhang, J., Lu, C., Huang, Q., Wu, J. and Liu, F. (2011) Degradation of tetracycline in aqueous media by ozonation in an internal loop-lift reactor. Journal of Hazardous Materials 192(1), 35-43.

Wei, W., Guo, K., Kang, X., Zhang, J., Li, C. and Fang, J. (2021) Complete Removal of Organoarsenic by the UV/Permanganate Process via HO• Oxidation and in Situ-Formed Manganese Dioxide Adsorption. ACS ES&T Engineering 1(4), 794-803.

Whyte, J.J., Jung, R.E., Schmitt, C.J. and Tillitt, D.E. (2000) Ethoxyresorufin-O-deethylase (EROD) Activity in Fish as a Biomarker of Chemical Exposure. Critical Reviews in Toxicology 30(4), 347-570.

Xiao, Y., Zhang, L., Zhang, W., Lim, K.-Y., Webster, R.D. and Lim, T.-T. (2016) Comparative evaluation of iodoacids removal by UV/persulfate and UV/H2O2 processes. Water Research 102, 629-639.

Xu, X., Meng, L., Luo, J., Zhang, M., Wang, Y., Dai, Y., Sun, C., Wang, Z., Yang, S., He, H. and Wang, S. (2021) Self-assembled ultrathin CoO/Bi quantum dots/defective Bi2MoO6 hollow Z-scheme heterojunction for visible light-driven degradation of diazinon in water matrix: Intermediate toxicity and photocatalytic mechanism. Applied Catalysis B: Environmental 293, 120231.

Xue, J., Zhang, Y., Liu, Y. and Gamal El-Din, M. (2016) Treatment of oil sands process-affected water (OSPW) using a membrane bioreactor with a submerged flat-sheet ceramic microfiltration membrane. Water Research 88, 1-11.

Ye, T., Xu, B., Lin, Y.-L., Hu, C.-Y., Lin, L., Zhang, T.-Y. and Gao, N.-Y. (2013) Formation of iodinated disinfection by-products during oxidation of iodide-containing waters with chlorine dioxide. Water Research 47(9), 3006-3014.

Ye, T., Xu, B., Lin, Y.-L., Hu, C.-Y., Xia, S.-J., Lin, L., Mwakagenda, S.A. and Gao, N.-Y. (2012) Formation of iodinated disinfection by-products during oxidation of iodide-containing water with potassium permanganate. Journal of Hazardous Materials 241-242, 348-354.

Yousefi, N., Pourfadakari, S., Esmaeili, S. and Babaei, A.A. (2019) Mineralization of high saline petrochemical wastewater using Sonoelectro-activated persulfate: Degradation mechanisms and reaction kinetics. Microchemical Journal 147, 1075-1082.

Yuan, S., Liao, P. and Alshawabkeh, A.N. (2014) Electrolytic Manipulation of Persulfate Reactivity by Iron Electrodes for Trichloroethylene Degradation in Groundwater. Environmental Science & Technology 48(1), 656-663.

Zhang, J., Sun, B., Guan, X., Wang, H., Bao, H., Huang, Y., Qiao, J. and Zhou, G. (2013) Ruthenium Nanoparticles Supported on CeO2 for Catalytic Permanganate Oxidation of Butylparaben. Environmental Science & Technology 47(22), 13011-13019.

Zhang, J., Sun, B., Huang, Y. and Guan, X. (2015a) Catalyzing the oxidation of sulfamethoxazole by permanganate using molecular sieves supported ruthenium nanoparticles. Chemosphere 141, 154-161.

Zhang, J., Sun, B., Xiong, X., Gao, N., Song, W., Du, E., Guan, X. and Zhou, G. (2014) Removal of emerging pollutants by Ru/TiO2-catalyzed permanganate oxidation. Water Research 63, 262-270.

Zhang, T.-Y., Xu, B., Hu, C.-Y., Lin, Y.-L., Lin, L., Ye, T. and Tian, F.-X. (2015b) A comparison of iodinated trihalomethane formation from chlorine, chlorine dioxide and potassium permanganate oxidation processes. Water Research 68, 394-403.

Zhang, Y., Klamerth, N., Chelme-Ayala, P. and Gamal El-Din, M. (2016) Comparison of Nitrilotriacetic Acid and [S,S]-Ethylenediamine-N,N′-disuccinic Acid in UV–Fenton for the Treatment of Oil Sands Process-Affected Water at Natural pH. Environmental Science & Technology 50(19), 10535-10544.

Zhao, L., Hou, H., Fujii, A., Hosomi, M. and Li, F. (2014) Degradation of 1,4-dioxane in water with heat- and Fe2+-activated persulfate oxidation. Environmental Science and Pollution Research 21(12), 7457-7465.

Zhao, X., Ma, J., Jiang, J., Bao, Y. and Liu, H. (2016a) Phenols and anilines degradation by permanganate in the absence/presence of carbon nanotubes: Oxidation and dehalogenation. Separation and Purification Technology 170, 344-352.

Zhao, X., Ma, J. and von Gunten, U. (2017a) Reactions of hypoiodous acid with model compounds and the formation of iodoform in absence/presence of permanganate. Water Research 119, 126-135.

Zhao, X., Salhi, E., Liu, H., Ma, J. and von Gunten, U. (2016b) Kinetic and Mechanistic Aspects of the Reactions of Iodide and Hypoiodous Acid with Permanganate: Oxidation and Disproportionation. Environmental Science & Technology 50(8), 4358-4365.

Zhao, Y., Kuang, J., Zhang, S., Li, X., Wang, B., Huang, J., Deng, S., Wang, Y. and Yu, G. (2017b) Ozonation of indomethacin: Kinetics, mechanisms and toxicity. Journal of Hazardous Materials 323, 460-470.

Zhu, Y., Wang, X., Zhang, J., Ding, L., Li, J., Zheng, H. and Zhao, C. (2019a) Generation of Active Mn(III)aq by a Novel Heterogeneous Electro-permanganate Process with Manganese(II) as Promoter and Stabilizer. Environmental Science & Technology 53(15), 9063-9072.

Zhu, Y., Yang, X., Qiao, J., Zhang, X. and Guan, X. (2019b) Effects of KMnO4/NaHSO3 pre-oxidation on the formation potential of disinfection by-products during subsequent chlorination. Chemical Engineering Journal 372, 825-835.

Zhu, Y., Zhao, C., Liang, J., Shang, R., Zhu, X., Ding, L., Deng, H., Zheng, H. and Strathmann, T.J. (2019c) Rapid removal of diclofenac in aqueous solution by soluble Mn(III) (aq) generated in a novel Electro-activated carbon fiber-permanganate (E-ACF-PM) process. Water Research 165, 114975.

Zubot, W., MacKinnon, M.D., Chelme-Ayala, P., Smith, D.W. and Gamal El-Din, M. (2012) Petroleum coke adsorption as a water management option for oil sands process-affected water. Science of the Total Environment 427-428, 364-372.

CHAPTER 2 SOLAR PHOTOCATALYTIC TREATMENT OF MODEL AND REAL OIL SANDS PROCESS WATER NAPHTHENIC ACIDS BY BISMUTH TUNGSTATE: EFFECT OF CATALYST MORPHOLOGY AND CATIONS ON THE DEGRADATION KINETICS AND PATHWAYS

2.1 Introduction

Canada has the world's third largest oil reserves, with more than 166 billion barrels of crude oil located in oil sands of northern Alberta (NRCAN 2019). Recovering of bitumen (also known as asphalt) from oil sands is currently conducted by either surface mining or *in-situ* extraction, both requiring water. It takes about 7 to 10 m^3 of water to extract 1 m^3 bitumen from the oil sands. For the mining sector, nearly ¾ of the water is recovered and the remaining water is retained in the tailings ponds, which is termed as oil sands process water (OSPW) (NRCAN 2019). OSPW is a complex brackish solution that contains suspended solids, inorganic compounds, dissolved organic compounds such as naphthenic acids (NAs) and trace metals. Some of the oldest tailing's ponds have now been reclaimed through conversion to end pit lakes or dry landscape capping, in which OSPW may be connected to natural water bodies through surface or groundwater flows (Sun et al. 2017).

OSPW has attracted increasing attention due to its potential adverse effects to living species. It might cause acute toxicity to bacteria and fish (Sun et al. 2014), algae (Debenest et al. 2012), chronic toxicity to invertebrates (Anderson et al. 2012), amphibians (Hersikorn et al. 2010) and mammals (Li et al. 2019, Wang et al. 2013). Numerous studies have attributed the organic fraction, particularly NAs, the dominant class of organic compounds present at mg/L concentrations, to be responsible for OSPW toxicity (Gagné et al. 2017, Leclair et al. 2015, Qin et al. 2019b). NAs are

a group of alkyl-substituted acyclic, monocyclic and polycyclic carboxylic acids with a general chemical formula of $C_nH_{2n+Z}O_x$, where n is the carbon number ($7 \leq n \leq 26$), Z is the even integer represents the hydrogen deficiency due to the formation of ring or double bond structure ($0 \leq -Z \leq 18$), and x indicates the oxygen number. Specifically, the heteroatomic NAs are designated as $C_nH_{2n+z}SO_x$ and $C_nH_{2n+z}NO_x$ (Huang et al. 2018). With the development of improved lab methods for extraction and analysis, more and more heteroatomic NAs are detected. For examples, Nyakas's study found that when 2.5 mL of OSPW extract was analyzed by FTICR-MS, sulfur-containing and nitrogen containing NAs account for 23% and 8% of identified compounds, respectively, while classical ($C_nH_{2n+z}O_2$) and oxy-NAs ($C_nH_{2n+z}O_x$) represented 64% (Nyakas et al. 2013). In recent years, most studies focused on the degradation kinetics and pathways of classical and oxy-NAs. However, seldom studies have been conducted on the degradation mechanisms of heteroatomic NAs which are indispensable part in OSPW.

Several physical, chemical and biological treatment methods have been studied for the treatment of OSPW, including adsorption such as petroleum-coke (Gamal El-Din et al. 2011), granular activated carbon (Islam et al. 2015) and carbon xerogel (Benally et al. 2019). Advanced oxidation processes (AOPs): ozonation (Pérez-Estrada et al. 2011), ferrate (VI) oxidation (Wang et al. 2016a) and zero valent iron/ $S_2O_8^{2-}$ oxidation (Drzewicz et al. 2012). UV based AOPs including UV-Fenton (Zhang et al. 2016a), UV/H_2O_2, UV/chlorine, and UV/persulfate (Fang et al. 2020). Aerobic and anaerobic biodegradation (Xue et al. 2016, Zhang et al. 2018). Among them, AOPs are widely used and shown to be effective for NAs removal and toxicity reduction (Sohrabi et al. 2013, Wang et al. 2016a, Wang et al. 2016b). However, the main disadvantages of traditional AOPs are their high cost due to high energy and consumable chemicals. Utilization of solar energy and recyclable materials are the benefits of photocatalytic AOPs technology (Xu et al. 2020) and

can be seen as a green alternative to the traditional AOPs. Research on photocatalytic treatment of OSPW are mainly conducted using TiO_2 at bench-scale. For example, acid extractable organics from raw OSPW and inhibition effect toward *Vibrio fischeri* were decreased by TiO_2 photocatalytic treatment (Leshuk et al. 2016b). In this system, degradation rates of NAs were decreased by the addition of Fe^{3+} and HCO_3^- due to hydroxyl ($^{\bullet}OH$) radical scavenging (Leshuk et al. 2016a). TiO_2-graphene composites exhibited higher photocatalytic activity than pure TiO_2 and the NA removal rate was 80–90% by using TiO_2-graphene composites after 80 min of UV irradiation (Liu et al. 2016). However, the weak visible light absorption has been one of the critical limitations of TiO_2 photocatalysis against application in the field of water treatment as UV light is only 3-5% in whole solar spectrum. Therefore, it is much more meaningful to explore the application of photocatalysts that can be stimulated by visible light. Bi_2WO_6 is one of the most commonly used visible-light catalyst with band gap of 2.75 eV and good photostability. Bi_2WO_6 has the simplest structure of Aurivillius family, the layer structures and unique properties offer great ability for the decomposition of organic compounds (Dong et al. 2017, Fu et al. 2006). In this work, three morphologies *vis-à-vis* nanoplate, flower-like and swirl-like structures of Bi_2WO_6 were prepared by hydrothermal methods and applied for the degradation of NAs. The photocatalytic performance of the different morphologies of Bi_2WO_6 was assessed by degradation of CHA. Structure relative reactivities were evaluated through both model compounds and real OSPW. Due to the limited information on environmental fate of heteroatomic NAs, it was selected to study the effects of environmental factors such as presence of metallic ions and pH of the solution. The degradation by-products and oxidation pathways of heteroatomic NAs were proposed for the first time. The study will demonstrate potential of solar light-driven photocatalysis as a passive treatment for the remediation of OSPW and provide valuable information for the design of engineered passive solar-

based treatment approaches.

2.2 Materials and methods

2.2.1 Materials

OSPW samples were collected from an active oil sands tailings pond in Fort McMurray, Alberta, Canada, stored at 4 °C and filtered by 0.45 μm nylon membranes prior to use. Properties, major ions and organic composition of raw OSPW were illustrated in Table 2.1. $Bi(NO_3)_3 \cdot 5H_2O$, $Na_2WO_4 \cdot 2H_2O$, sodium dodecyl sulfate (SDS), isopropanol (IPA), ammonium oxalate (AO), 4-hydroxy2, 2, 6, 6-tetramethylpiperidinyloxy (TEMPOL) and model NA compounds - cyclohexanecarboxylic acid (CHA), tetrahydropyran-4-carboxylic acid (T4CA), tetrahydro-2H-thiopyran-4-carboxylic acid (T-2H-T4CA), isonipecotic acid (IA) and 5-Hexyl-2-thiophenecarboxylic acid (5H-2THCA) were purchased from Sigma Aldrich. These 5 surrogate organic acids and their structures details were listed in Table 2.2. All chemicals were of analytical grade and used as received without any further purification. All solutions were prepared with ultra-pure water ($R \geq 18.2$ MΩ) obtained from Millipore Milli-Q system.

Table 2.1 Properties, major ions and organic composition of raw OSPW.

Parameter	Value
pH	8.6 ± 0.2
Alkalinity (mg L^{-1} as $CaCO_3$)	550 ± 10
Conductivity (mS cm^{-1})	3.1 ± 0.2
Total suspended solids (mg L^{-1})	62.5 ± 5
Ions (mg L^{-1})	
Cl^-	900±20
SO_4^{2-}	650±11.5
CO_3^{2-}	1500 ± 33.3
NO_3^-	18±2.3
Organic parameters (mg L^{-1})	
Dissolved organic carbon (mg L^{-1} as C)	73.8 ± 5.2
Classical NAs (O_2-NAs)	48.1 ± 2.1
O_3-NAs	20.5 ± 0.8
O_4-NAs	17.4 ± 0.6
O_5-NAs	4.3 ± 0.2
O_6-NAs	1.1 ±0.2

Table 2.2 Name, formula, molecular weight, and structure of selected NAs

Structure	Abbreviation	Name	Formula	M.W.
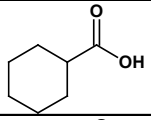	CHA	cyclohexanecarboxylic acid	$C_7H_{12}O_2$	128.17
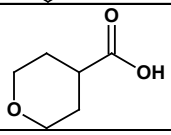	T4CA	tetrahydropyran-4-carboxylic acid	$C_6H_{10}O_3$	130.14
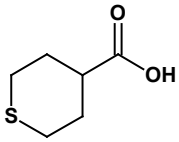	T-2H-T4CA	tetrahydro-2H-thiopyran-4-carboxylic acid	$C_6H_{10}O_2S$	146.21
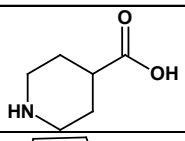	IA	isonipecotic acid	$C_6H_{11}O_2N$	129.16
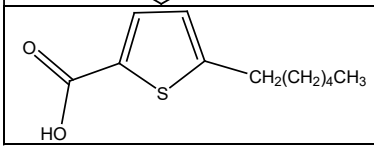	5H-2THCA	5-Hexyl-2-thiophenecarboxylic acid	$C_{11}H_{16}O_2S$	212.31

2.2.2 Preparation of three morphologies of Bi_2WO_6

The underlying Bi_2WO_6 were synthesized by hydrothermal method. For the preparation of nanoplate (NP) Bi_2WO_6: 1 mmol $Bi(NO_3)_3 \cdot 5H_2O$ was ultrasonically dissolved in 80 mL water. Then 0.5 mmol $Na_2WO_4 \cdot 2H_2O$ was added to this solution. Afterwards, the mixture was stirred for 30 min and transferred to a Teflon-lined stainless-steel autoclave, which was placed in an oven at 180 °C for 24 h. Finally allowed to cool to room temperature. For the preparation of swirl-like (SL) Bi_2WO_6: 2 mmol $Bi(NO_3)_3 \cdot 5H_2O$ and 1 mmol $Na_2WO_4 \cdot 2H_2O$ were dissolved separately in 60 mL of water under stirring. Thereafter, $Na_2WO_4 \cdot 2H_2O$ solution was added dropwise into $Bi(NO_3)_3 \cdot 5H_2O$ solution with constant stirring. After thorough mixing of the two solutions, 0.3 g SDS was added into the mixture and stirred for 30 min. The resulting solution was transferred into a Teflon-lined stainless-steel autoclave, which was treated at 150 °C for 12 h in an oven. For the preparation of flower-like (FL)Bi_2WO_6: 2 mmol $Bi(NO_3)_3 \cdot 5H_2O$ was dissolved in 10 mL glacial acetic acid under stirring until solution became transparent. 1 mmol $Na_2WO_4 \cdot 2H_2O$ in 70 mL water was added dropwise into $Bi(NO_3)_3 \cdot 5H_2O$ solution. The mixture was stirred for 1 h and transferred into a Teflon-lined stainless-steel autoclave, heated to 160 °C for 12 h. The final products for all three syntheses were centrifuged, washed with ultrapure water and ethanol for three times, and dried at 60 °C for 6 h.

2.2.3 Characterization

The scanning electron microscopy (SEM) was conducted using Zeiss EVO M10 SEM-imaging. The Brunauer-Emmett-Teller (BET) surface areas were investigated by adsorption of nitrogen onto samples at 77 K by Autosorb Quanthachrome 1MP. The crystallinity of the as-prepared materials was carried out at room temperature on Rigaku X-ray diffraction spectroscopy (XRD) Ultima IV with standard stage (Cu kα radiation, λ = 0.15406 nm). The surface chemical

composition and chemical states were characterized by X-ray photoelectron spectroscopy (XPS, Kratos AXIS 165, Kratos Analytical).

2.2.4 Photocatalytic experiments

The photocatalytic experiments were performed using a solar simulator (66485-300XF-R1, Newport) equipped with a 300 W Xenon ozone-free arc lamp as the light source to simulate the solar light (Fig. B1 in appendix B). An Air Mass 1.5 Global Filter was used to simulate the effect of the earth atmosphere. The sunlight irradiance (Fig. 2.1) was measured by a black-comet-sr spectroradiometer with a CR2 UV-VIS-NIR cosine receptor and the software program SpectraWiz® (StellarNet Inc.). The irradiance of effective wavelengths (200-500 nm) was set at 6.541 mW/cm^2 (Table 2.3) for all experiment. In a typical experiment, 1 g/L catalyst was dispersed in a 50 mL of solution in an open reactor containing the targeted pollutant, which was placed on a magnetic stirrer under the direct irradiation of the simulated solar rays. Samples (3 mL) are taken at regular intervals and the suspended solids were filtered from the solution using a 0.2 µm Nylon filter (Thermo Scientific). 2mM scavenger was used in this study based on previous studies (Mavinakere Ramesh and Shivanna 2018; Wei et al. 2019). The sunlight fluence was calculated according to the method proposed by Bolton and Linden (Bolton and Linden 2003). The spreadsheets were listed in Appendix A-1.

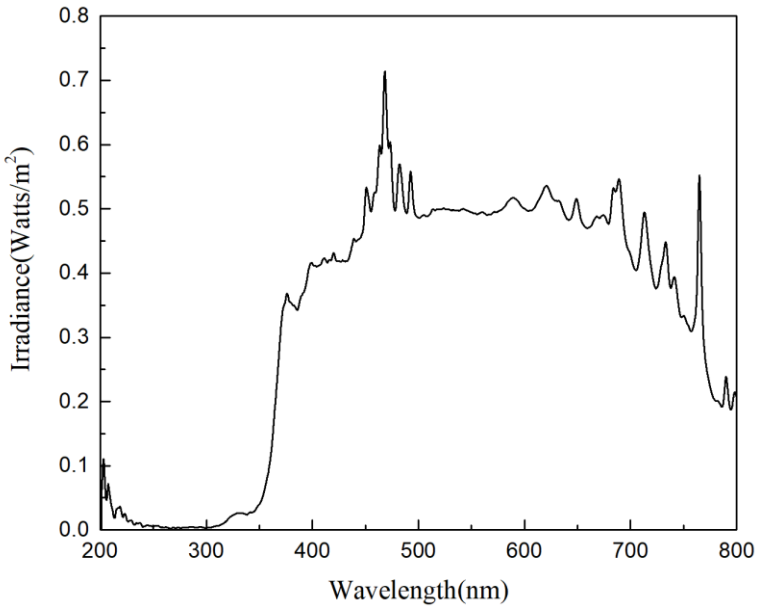

Fig. 2.16 Spectrum of solar simulator.

Table 2.3 The irradiance of different wavelength range

Wavelength (nm)	UVa (320-420)	UVb (275-320)	UVc (200-275)	400-500	Total
Irradiance (Watts/m^2)	14.26	0.256	2.198	48.69	65.404

2.2.5 Analytical procedure

The concentration of the model NAs was measured by an ultra-performance liquid chromatography coupled with a single quadrupole mass spectrometry (UPLC-MS) (SQ Detector 2, Water). The intermediate by-products formed during the photocatalytic degradation of heteroatomic NAs were identified by ultraperformance liquid chromatography coupled with time-of-flight mass spectrometry (UPLC-TOF-MS) (Synapt G2, Waters). The chromatographic separation was achieved by a method developed in our previous reports for the separation of NAs (Huang et al. 2015). In brief, the chromatographic separation was achieved by a Waters BEH Phenyl column with 2 mM ammonia acetate buffer in both water (A) and 50/50

methanol/acetonitrile (B). The chromatographic method was the same for both NAs and by-products analysis. TOF-MS operated at ESI negative mode using MS scan over the mass range of 50-1200 Da in high resolution mode (mass resolution = 40000 FWHM at 1431 *m/z*). Leucine enkephalin (*m/z*=554.2611) was used as lock mass for the mass correction and was continuously infused via the lock spray ESI. The data were acquired by MassLynx (Waters) and processed by TargetLynx (Waters).

The ion-mobility spectrometry (IMS) was determined using a Tri-Wave® ion-mobility cell of 15 cm long and nitrogen is the drift gas (Wang et al. 2013). The IMS consisted of a transfer cell that collected certain number of ions and a helium gate that released the ions into the ion mobility cell. The number of ions was known and the difference in the number ions had a threshold of 5%. Ions were separated using an electric field (T-wave) that moved the ions in one direction and a gas flow in the counter direction, which drifted the ions based on the cross-collision section (CCS). DriftScope were used to control. One raw OSPW sample has been used as the quality control sample to ensure the method stability.

2.2.6 Calculation of frontier electron densities (FEDs) of 5H-2THCA

The frontier electron densities (FEDs) theory is commonly used to evaluate the degradation of organics (Meng et al. 2017). Molecular orbital calculations were conducted using the Gaussian 03 program. The hybrid density functional B3LYP method with the 6-31G(d,p) basis set were used. The FEDs of the highest occupied molecular orbital (HOMO) and the lowest unoccupied molecular orbital (LUMO) were obtained from the Gaussian output files. The values of $2FED^2_{HOMO}$ were calculated to predict the initial reaction sites of 5H-2THCA for electrophilic reaction.

2.3 Results and discussion

2.3.1 Catalyst characterization

Three different morphologies of Bi_2WO_6 were prepared through hydrothermal processes. The SEM images illustrated in Fig. 2.2 clearly show NP (Fig. 2.2a), SL (Fig. 2.2b) and FL (Fig. 2.2c) structures of Bi_2WO_6. Different morphologies could be formed by tuning the experimental parameters (e.g., reaction time, temperature, pH, solvent or surfactant). The possible formation mechanisms of three Bi_2WO_6 are simplified as follows. The formation of NP structure was an Ostwald ripening process and amorphous nanoparticles are the precursor. In the initial stage, tiny crystalline nuclei were formed in a supersaturated medium. Then these tiny crystalline nuclei grew into lager particles at the cost of smaller particles according to the Gibbs–Thomson law. With prolonged hydrothermal treatment, based on the high anisotropy characteristics, Bi_2WO_6 grew along (001) plane parallel to the intrinsic a × b layer. The larger NP structure are finally formed (Zhang and Zhu 2005). As for FL Bi_2WO_6, the same as the formation of NP, amorphous nanoparticles act as the precursor to form crystallized Bi_2WO_6. During the hydrothermal processes, nanoparticles self-aggregate into microparticles. In a further crystallization process, these microparticles prefer to grow into NP structure through the anisotropic growth and dissolution–recrystallization process termed as Ostwald ripening. As the reaction continued, the flower-like structure could be formed by self-organization of these nanoplates (Zhang et al. 2007a). pH is an essential parameter which could influence the formation of Bi_2WO_6. When the pH value is ≤7, the chemical reactions is illustrated as follows (Tian et al. 2011):

$$Na_2WO_4 \cdot 2H_2O + 2H^+ \rightarrow H_2WO_4 \downarrow + 2Na^+ + 2H_2O \quad (2.1)$$

$$Bi(NO_3)_3 + H_2O \leftrightarrow BiONO_3 + 2HNO_3 \quad (2.2)$$

$$BiONO_3 + H_2O \leftrightarrow Bi_2O_2(OH)NO_3 + HNO_3 \quad (2.3)$$

$$Bi_2O_2(OH)NO_3 + H_2WO_4 \rightarrow Bi_2WO_6 + HNO_3 + H_2O \qquad (2.4)$$

If the pH of precursor solution is > 8, the reaction is shown as below:

$$7Bi_2O_2(OH)NO_3 + 2WO_4^{2-} + 3OH^- \rightarrow Bi_{14}W_2O_{27} + 7NO_3^- + 5H_2O \qquad (2.5)$$

In acidic conditions, the slightly soluble H_2WO_4 are formed richly in the solution, causing the rapid hydrolysis of $Bi(NO_3)_3$ as illustrated in Eq. (2.2-2.3), which further increases the substantially nucleation. Then self-organization of Bi_2WO_6. nanoplates occurred due to lattice tension or surface interaction in the edge areas of the sheets. When the pH value increases, the generation of H_2WO_4 decreased, the nucleation rates decrease and the diffusion free path increases, the self-organization of Bi_2WO_6. nanoplates was inhibited and prefers to form two-dimensional structures. Under the base condition, H_2WO_4 precipitate dissolved and the impurity $Bi_{14}W_2O_{27}$ was generated. Therefore, the change of pH (adjust using acetic acid) will greatly impact the morphology of Bi_2WO_6. The addition of surfactant (SDS) during the preparation of SL structure could selectively adsorb onto specific surfaces and change the chemical potential of facets, resulting the suppress the intrinsic anisotropic growth of Bi_2WO_6. Therefore, the nanoparticles prefer to grow into nanobricks rather than nanoplates. The orthorhombic structure of Bi_2WO_6 consists of alternating $(Bi_2O_2)_n^{2+}$ layers and $(WO_4)_n^{2-}$ octahedral layers. Because of the electrostatic effects, these nanobricks with polar charges on the top and bottom surfaces may stack or connect to each other. Eventually, the SL structure can be formed based on orientation of SDS (Zhang et al. 2007b).

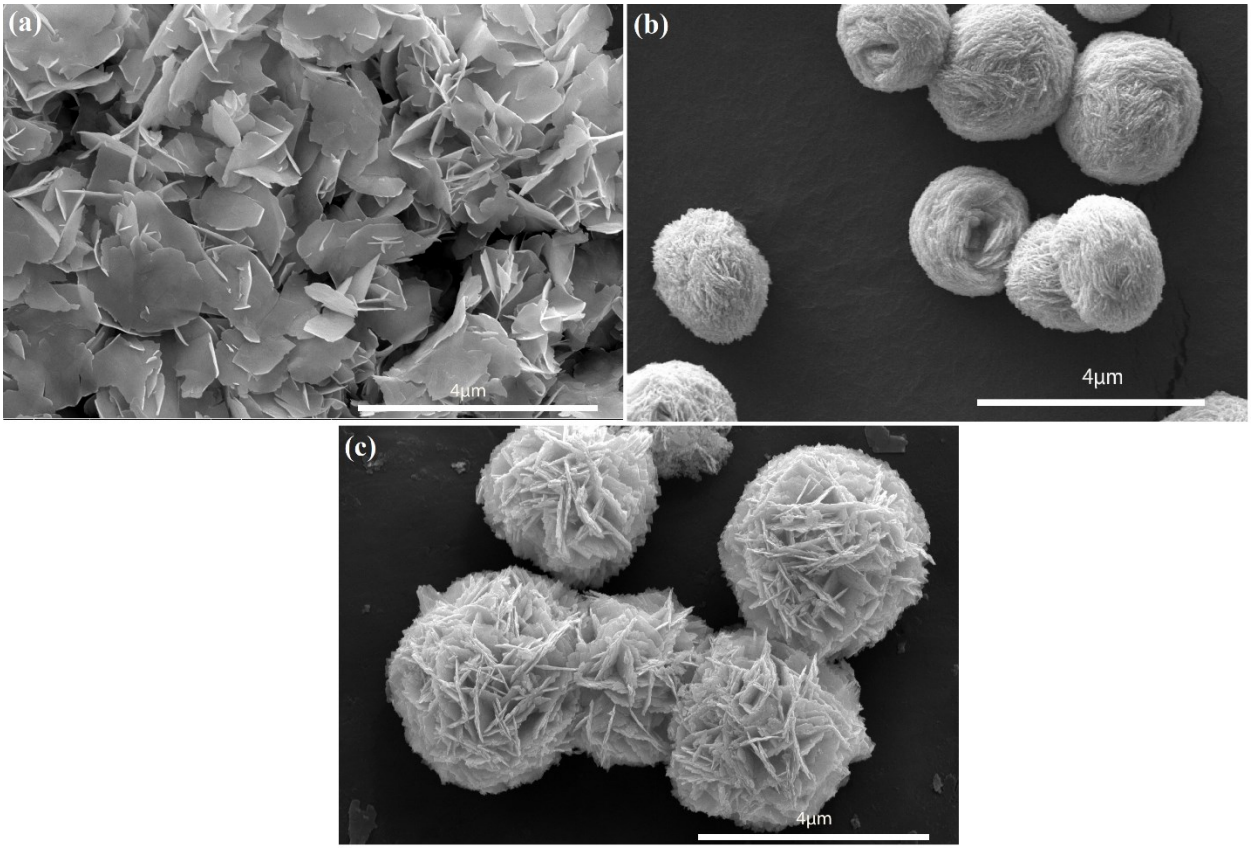

Fig. 17.2 SEM images of the three morphologies of Bi_2WO_6: (a) nanoplate (NP) (b) swirl-like (SL) (c) flower-like (FL) structures.

The crystal phase structures of the as-synthesized samples were characterized by XRD. The XRD patterns of NP, SL and FL structures of Bi_2WO_6 are presented in Fig. 2.3a. The diffraction peaks of all samples were readily indexed to the orthorhombic Bi_2WO_6 phase with lattice parameters (JCPDS card no. 73-1126, a = 5.457, b = 5.436 and c = 16.427 Å). No impurity peaks are observed, indicating that all the samples are of a high purity and a single phase. The surface elements and their valence status of NP, SL and FL Bi_2WO_6 were analyzed by XPS. As expected, the XPS survey scan spectrum (Fig. 2.4a) shows obvious binding energy peaks attribute to Bi 4p, O 1s, Bi 4d, W 4d, Bi 4f, W 4f, respectively. Fig. 2.4b-d depicts the high-resolution XPS spectra of Bi 4f, W 4f and O 1s, which further demonstrate the chemical states. The binding energy peaks

of Bi 4f 7/2 and Bi 4f 5/2 are located at 158.9 and 164.2 eV for FL, 159 and 164.3 eV for SL, 159.2 and 164.5 eV for NP, which corresponding to Bi^{3+} in the sample. As illustrated in Fig 2.4c, two peaks at 37.3 eV and 35.2 eV for FL, 37.5 eV and 35.3 eV for SL, 37.6 eV and 35.4 eV for NP are associated with W 4f 5/2 and W 4f 7/2, respectively, implying the oxidation state of W atoms is +6 (Li et al. 2016). Fig. 2.4d exhibits that the peak of the O 1s of FL could be de-convoluted into three peaks at 531.0, 530.4 and 529.8 eV, which are ascribed to surface O─H bonds, O─Bi bonds and O─W bands of the lattice oxygen, respectively (Hu et al. 2016, Zhou et al. 2019). For NP and SL, the O 1s spectra are also deconvoluted into three peaks at 531.3, 530.5, 530.0 eV and 531.3, 530.5, 530.0 eV, respectively. Compared with NP and SL, these characteristic peaks shift to lower binding energy, which results in the increasing electron density and a subdued binding energy of FL (Yang et al. 2017). The lower binding energy of FL makes the electron easier to be activated and exhibits a higher photocatalytic activity. The results of XRD and XPS analysis indicated the successful preparation of pure orthorhombic Bi_2WO_6.

The specific surface area is regarded as one of the critical parameters which could influence the photocatalytic efficiency of photocatalysts. Generally, for defect-free photocatalyst, larger surface area could supply more active sites for the reaction of radicals and target pollutants. N_2 adsorption–desorption isotherms and their corresponding BJH pore size distribution of Bi_2WO_6 structures are illustrated in Fig. 2.3 b and c. The isotherm curves of the three Bi_2WO_6 structures belong to type IV with H3 hysteresis loops, which indicated the presence of mesopores. This is coincided well with pore size distribution of Bi_2WO_6 shown in Fig. 2.3c, from which, the pore size of three morphologies mainly lies in the range of 2–10 nm. The pore size distribution of FL is narrowest, suggesting that the crystals are the most monodisperse, with respect to the other samples. From Table 2.4, the specific surface area of NP, SL, FL are calculated to be 15.32, 28.23 and 34.56

m^2/g, respectively. The total pore volume of Bi_2WO_6 structures is 0.067, 0.115 and 0.134 cm^3/g for NP, SL and FL respectively. Obviously, it can be seen that FL structure have higher specific surface area due to larger total pore volume.

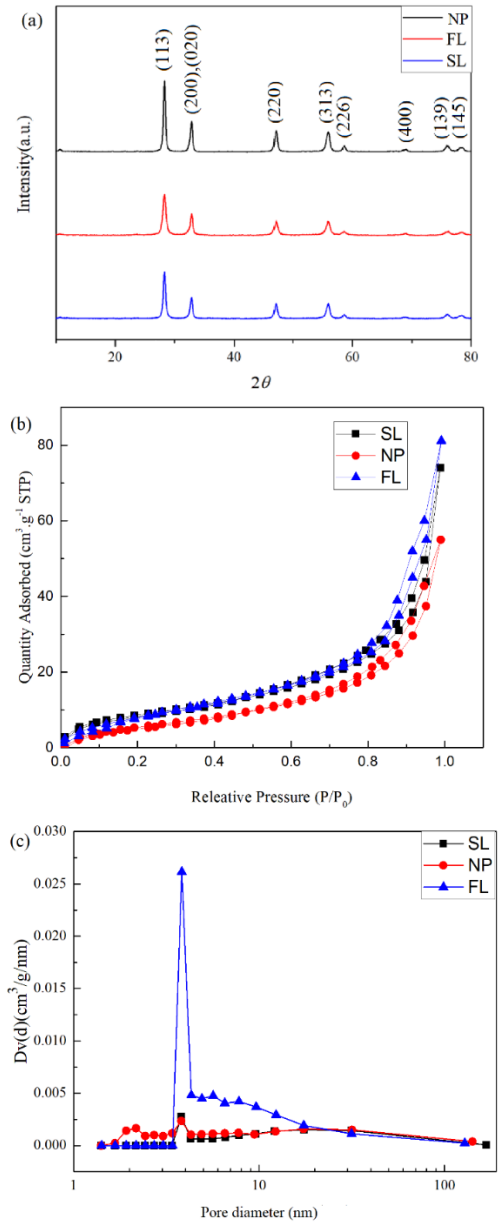

Fig. 2.18 (a) XRD patterns, (b) N_2 adsorption–desorption isotherms and (c) BJH pore size distribution of three as-prepared Bi_2WO_6 structures.

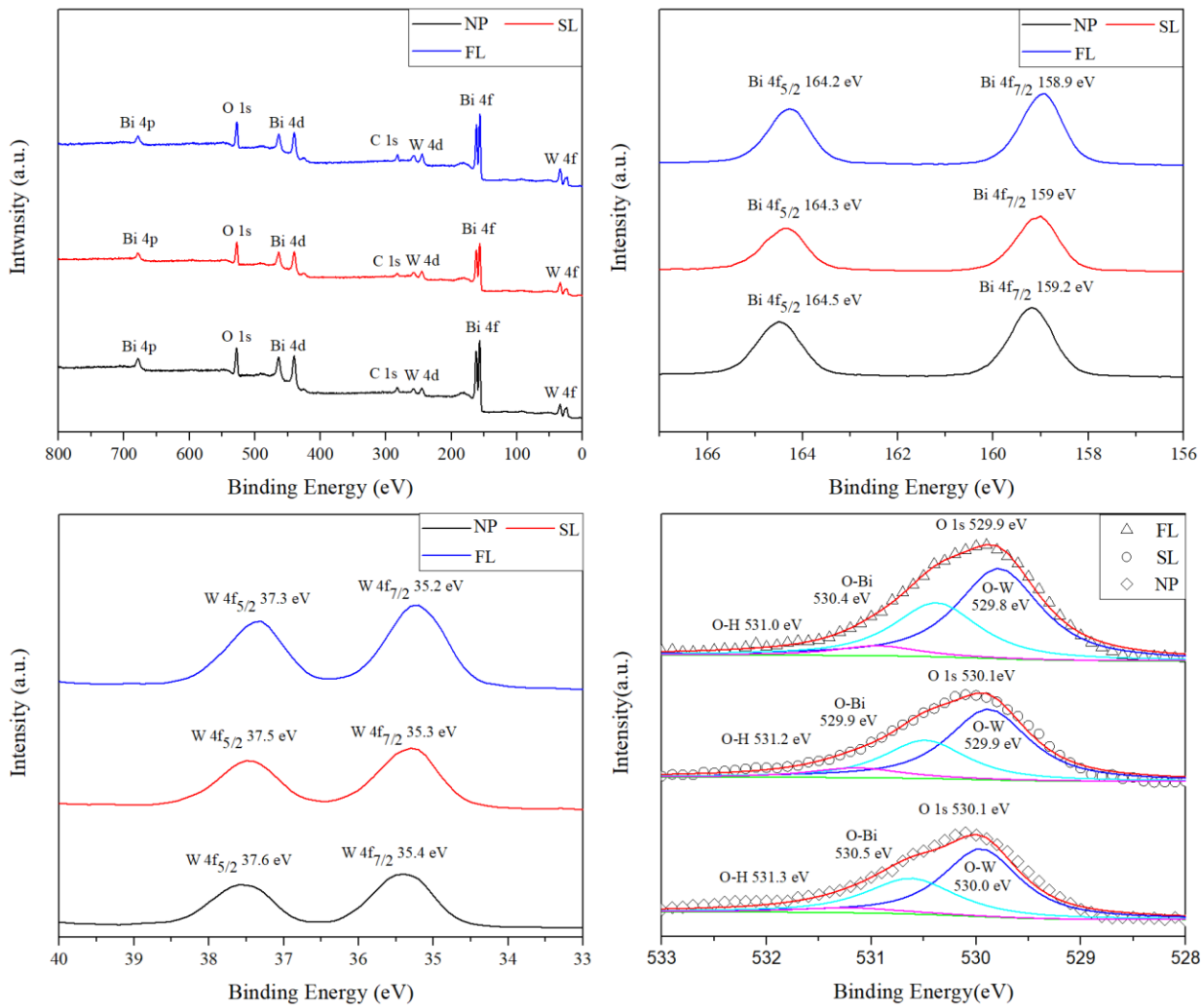

Fig. 2.19 (a) XPS survey scan spectrum and high-resolution XPS spectra of (b) Bi 4f, (c) W 4f and (d) O 1s for Bi_2WO_6.

Table 2.4 BET specific surface area and total pore volume of NP, FL and SL structures of as-prepared Bi_2WO_6

	BET specific surface area (m^2/g)	Total pore volume (cm^3/g)
NP	15.32	0.067 (at P/P_0 0.993)
SL	28.23	0.115 (at P/P_0 0.992)
FL	34.56	0.134 (at P/P_0 0.991)

2.3.2 Photocatalytic activity of Bi_2WO_6

CHA, a cyclic aliphatic carboxylic acid (Table. 2.2), is one of typical classical NAs and widely used in the study of degradation of NAs (Zhang et al. 2016b). Therefore, it was selected to evaluate the photocatalytic activity of Bi_2WO_6. 25 mg/L CHA was dissolved in carbonate buffer and pH was adjusted to 8.5 to simulate real pH of OSPW. Before irradiation, CHA suspension was allowed to stir in dark for 60 min to achieve adsorption equilibrium. Also, photolysis alone (without catalyst) was conducted, and the results (Fig. B2) showed that CHA could not be degraded under 4 h illumination without catalyst. The effect of different morphology of Bi_2WO_6 on the photocatalytic degradation of CHA is shown in Fig. 2.5a. The photocatalytic degradation of CHA followed a pseudo first order kinetic model with fluence-based rate constants of 0.0283, 0.0534 and 0.0929 cm^2/J obtained for NP, SL and FL structures of Bi_2WO_6, respectively. Compared to those of NP and SL structures, the highest removal rate of CHA by FL Bi_2WO_6 are attributed to the relative larger surface area and total pore volume of FL Bi_2WO_6. It was reported that the larger total pore volume the more transport paths, through which the reaction molecules could move in and out so that they are more accessible to get to the reactive sites, and the more likely the chemical reaction occurs (Zhang et al. 2007b). Therefore, FL Bi_2WO_6 was chosen to conduct the rest of the experiments. The effect of different concentrations of FL is presented in Fig. 2.5b. As clear depicted in Fig. 2.5b, the fluence-based rate constants were increased with increasing concentration of FL Bi_2WO_6 and were individually determined as 0.0162, 0.0599, 0.0929 and 0.1131 cm^2/J for 0.1, 0.5, 1.0 and 5.0 g/L FL Bi_2WO_6 dosage, respectively. The increase in CHA degradation rate with increased Bi_2WO_6 dosage is expected and can be attributed to the increase in photocatalytic active sites with increases in Bi_2WO_6 concentration. The higher number of photoactive sites ensures the generation of more reactive species/oxidants which can quickly

oxidize CHA and its intermediate products.

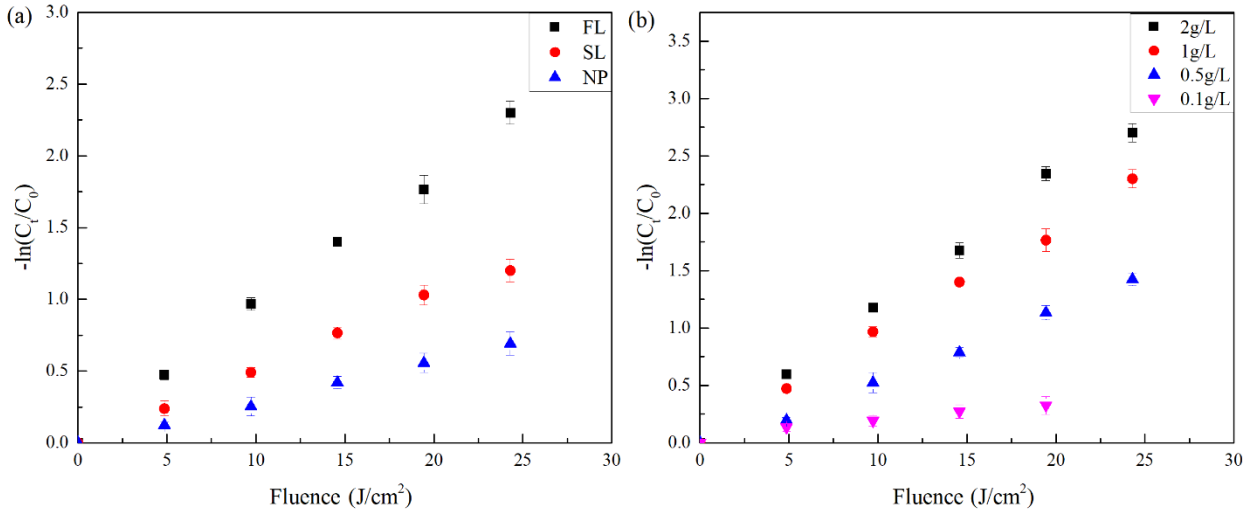

Fig. 2.20 (a) Effect of different morphology of Bi_2WO_6 on the photocatalytic degradation of CHA: [CHA] = 25 mg/L, [Bi_2WO_6] = 1 g/L, [HCO_3^-] = 5 mM, pH = 8.5; (b) Effect of different dosages of FL Bi_2WO_6: [CHA] = 25 mg/L, [HCO_3^-] = 5 mM, pH = 8.5 (1 h dark adsorption, 3 h illumination).

To investigate the photocatalytic mechanism of Bi_2WO_6, trapping measurements with different scavengers were conducted to identify the main reactive species in this system. IPA, AO and TEMPOL were used as the scavengers for hydroxyl radicals ($^{\bullet}OH$), holes (h^+) and superoxide radicals ($O_2^{\bullet-}$), respectively. The second-order rate constant of IPA with $^{\bullet}OH$ is 1.6×10^9 M^{-1} s^{-1} (Kormali et al. 2006), TEMPOL with $O_2^{\bullet-}$ is 6.5×10^4 M^{-1} s^{-1} (Samuni et al. 1990). Moreover, AO is commonly used in quenching experiments for h^+ (Dai et al. 2015, Mao et al. 2017). Generally, the degradation rates will be decreased as a result of quenching. With the addition of scavengers, the lower the degradation rates, the more important role the corresponding active species play in the photocatalytic system. Fig. 2.6 displays the degradation rates of CHA in the presence of different scavengers. The comparative test with no quencher was also conducted under the same

condition. As illustrated in Fig. 2.6, the degradation of CHA was slightly affected by introducing IPA. On the contrary, the addition of TEMPOL and AO almost terminated the photocatalytic degradation of CHA, indicating $O_2^{\bullet-}$ and h^+ are the main reactive species in the photocatalytic system. These reactive species were generated through reaction in Eq. (2.6–2.9). Bi_2WO_6 adsorbed the photon and electron was activated from valence band (VB) to conduction band (CB), forming h^+ and electron. The formation of $O_2^{\bullet-}$ is through reaction between electron and oxygen. Both h^+ and $O_2^{\bullet-}$ could oxidize NAs to intermediates. The oxidation details of NAs with these active species were discussed later.

$$Bi_2WO_6 + h\nu \rightarrow h^+ + e^- \quad (2.6)$$

$$O_2 + e^- \rightarrow O_2^{\bullet-} \quad (2.7)$$

$$h^+ + \text{pollutant} \rightarrow \text{pollutant}^{+\bullet} \rightarrow \text{Intermediates} \quad (2.8)$$

$$O_2^{\bullet-} + \text{pollutant} \rightarrow \text{pollutant}^{-\bullet} \rightarrow \text{Intermediates} \quad (2.9)$$

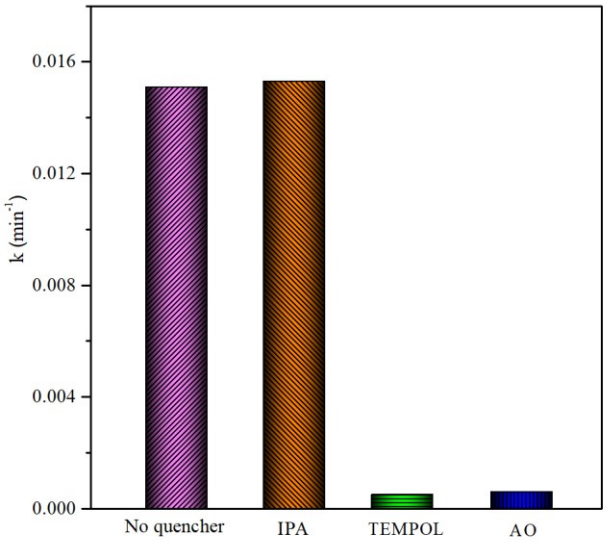

Fig. 2.21 Trapping measurement with different scavengers (IPA → $^{\bullet}OH$, AO → h^+, TEMPOL → $^{\bullet}O_2^-$) for photocatalytic degradation of CHA (1 h dark adsorption, 3 h illumination, [CHA]=25mg/L, [Scavenger]=2mM).

2.3.3. Application for the degradation of NAs

4 model compounds - CHA, T4CA, T-2H-T4CA, and IA, which are typical representative of classical, oxidized, sulfur and nitrogen containing NAs (Table 2.2), were selected to explore the effect of molecular structure on the relative reactivity in the photocatalytic oxidation system. These chosen compounds are good analogues of NAs from OSPW. Generally, adsorption and degradation are co-existence in the photocatalytic processes. To assure that the photocatalytic degradation of NAs occurred mostly in the presence of both the catalyst and solar light, the photodegradation and dark adsorption control were conducted for all NAs. The duration of photodegradation and dark adsorption of CHA, T4CA and IA is 4 h, and 2 h for T-2H-T4CA (fully degrade in 2 h with photocatalytic degradation). In addition, the pH was adjusted to 8.5 with 5 mM $NaHCO_3$ buffer to simulate the pH condition of real OSPW (Qin et al. 2019a). No degradations of all NAs were founded without catalyst (Fig. B2). Under dark conditions, the adsorption of CHA, T4CA, T-2H-T4CA and IA was approximately 20.8%, 5.7%, 11% and 8.2%, respectively (Fig. B3). The photocatalytic degradation of these four NAs is illustrated in Fig. 2.7. The fluence-based rate constants of CHA, IA, T4CA and T-2H-T4CA are 0.0929, 0.0059, 0.0034 and 0.2511 cm^2/J, respectively. This indicate that NAs were mainly oxidized by radicals such as $^{\bullet}O_2^-$ and h^+ in the presence of both solar light and photocatalysts. The preferential removal of T-2H-T4CA can be attributed presence of the non-bonding electrons of S atoms, which is a highly reactive site for the initiation of degradation process. Similar results were also found in other investigations. For example, de Oliveira Livera et al. (2018) used 0.5 g/L TiO_2 to study the structure-reactivity relationship of NAs in the photocatalytic degradation process. The reaction rate of T-2H-T4CA is 2.7 times of that of CHA. In essence, the degradation rate for the four studied model NAs decreased in the following order: T-2H-T4CA > CHA > IA > T4CA.

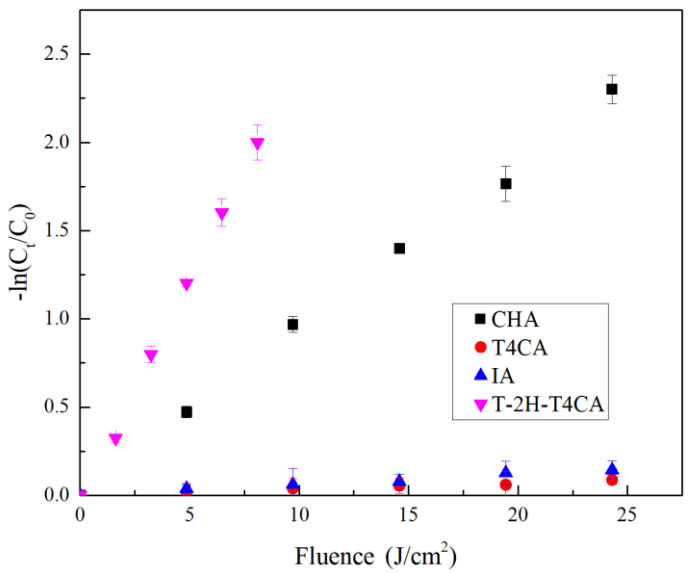

Fig. 2.22 Photocatalytic degradation of four different NAs as a function of fluence ([NAs] = 25 mg/L, [Bi_2WO_6] = 1g/L, [HCO_3^-] = 5 mM, pH = 8.5) (1 h dark adsorption, 3 h illumination).

Photocatalytic treatment of OSPW using Bi_2WO_6 were divided into 6 conditions (Fig. 7) to explore the effects of photolysis without catalyst, dark adsorption and photocatalytic degradation of NAs. The profiles of ion mobility separation spectra for different OSPW samples are shown in Fig. 2.8. The spectra could be divided into 3 different clusters based on retention and drift time, including classical NAs, oxy-NAs, and S-NAs (Xue et al. 2016, Zhang et al. 2018). High intensities of all three clusters could be observed in raw OSPW, control, Ad-0.1 and Ad-1(Fig. 2.8a, b, c and d). Although model compounds of NAs dissolved in $NaHCO_3$ buffer could be adsorbed by Bi_2WO_6, NAs in real OSPW could be hardly removed by merely adsorption as depicted by the spectra in Fig. 2.8c and d. OSPW is a complex saline solution contains inorganic compounds such as Cl^-, SO_4^{2-}, HCO_3^-, NO_3^-, Na^{2+}, K^+, Ca^{2+}, Mg^{2+} Fe^{3+} and Mn^{2+}, dissolved organic compounds and trace metals. The competitive adsorption of these ions is inevitable, leading to the decreased adsorption of NAs. Compared with raw OSPW (Fig. 2.8a), NAs couldn't be degraded by merely photolysis alone (Fig. 2.8b). In contrast, NAs were significantly reduced during photocatalytic treatment

using Bi_2WO_6. This could be explained by the generation of reactive species such as h^+, electron and other free radicals when Bi_2WO_6 absorbed photon, which can oxidize the NAs and other organic contents of the OSPW. As shown in Fig. 2.8e and f, photocatalytic treatment with 0.1 and 1 g/L Bi_2WO_6 significantly reduced the S-NAs. As expected, higher Bi_2WO_6 dosage showed greater NAs degradation (Fig. 2.8f) where S-NAs were completely degraded, and classical NAs significantly oxidized during photocatalytic treatment of OSPW with 1 g/L Bi_2WO_6. In contrast, partial degradation of S-NAs and negligible reduction in classical NAs spectra was observed at lower Bi_2WO_6 dosage (0.1 g/L) (Fig. 2.8e). It is hypothesized that the electron-rich S atom could be easily oxidized by generated reactive species, thus explaining the faster/complete degradation of S-NAs in OSPW during the photocatalytic treatment with Bi_2WO_6. Notably, no obvious removal of oxy-NAs was found. It was reported that the oxy-NAs are more recalcitrant to oxidation compared to other NAs and could be produced during the oxidation of classical NAs (Xue et al. 2016, Zhang et al. 2018). The result was also in agreement with what was obtained during photocatalytic treatment of model compounds, where we found that T4CA, an analogue compound for oxy-NAs have the lowest degradation rate. Therefore, the limited decrease of oxy-NAs might be due to the generation of new oxy-NAs from degradation of classical NAs or due to the low degradability of the oxy-NAs.

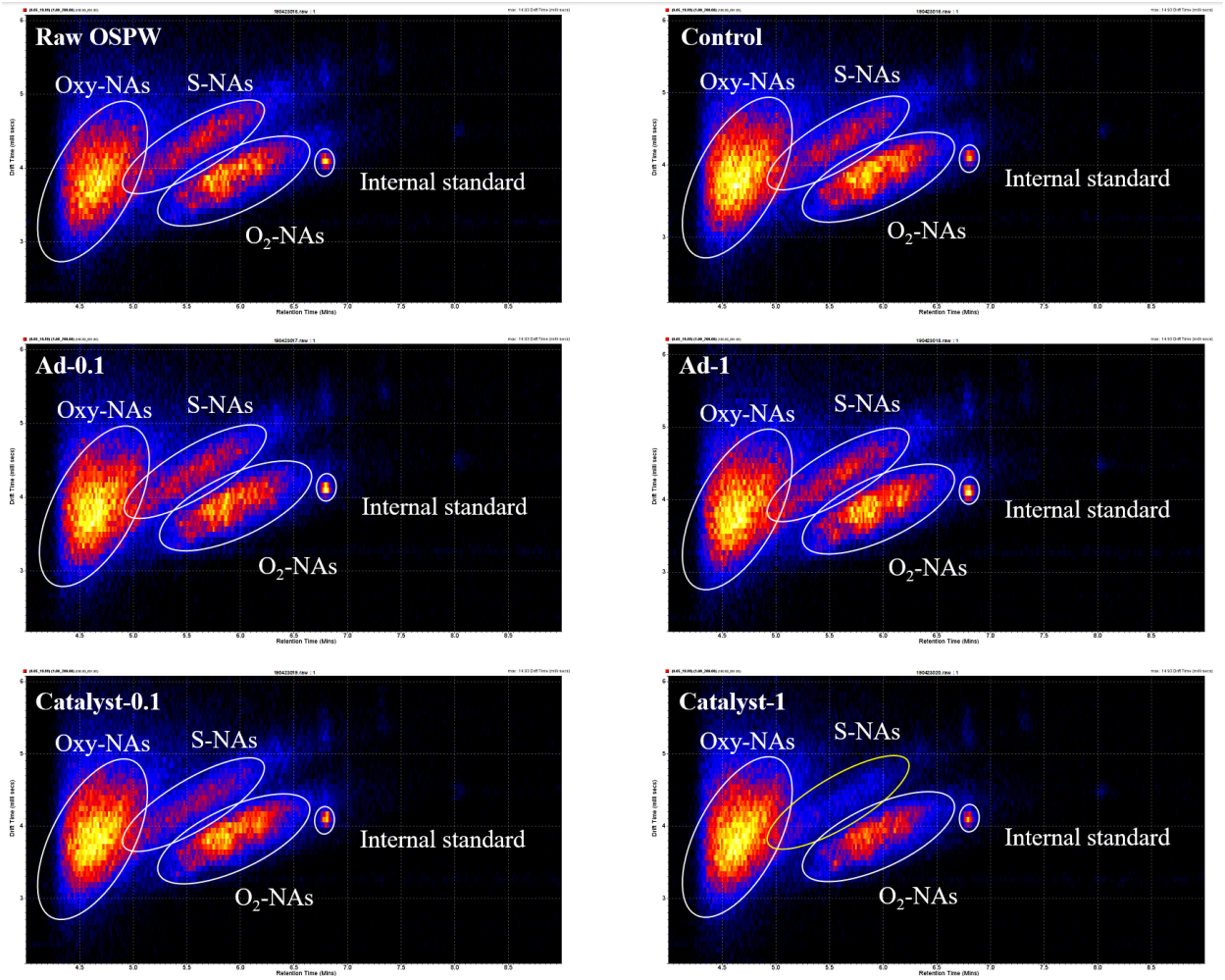

Fig. 2.23 Profiles of ion mobility separation spectra for the untreated and treated OSPW samples. (a) Raw OSPW, (b) photolysis treated OSPW (12 h illumination without catalyst), (c) Ad-0.1(12 h dark adsorption with 0.1 g/L Catalyst), (d) Ad-1(12 h dark adsorption with 1 g/L Catalyst), (e) Catalyst-0.1 (12 h illumination with 0.1 g/L Catalyst) (f) Catalyst-1 (12 h illumination with 1 g/L Catalyst).

2.3.4. Effect of cations on photocatalytic degradation of heteroatomic NAs

The effects of Mn^{2+} and Fe^{3+} on the photocatalytic degradation of T-2H-T4CA, 5H-2THCA and IA were illustrated in Fig. 2.9. Two different S-containing NAs were used to investigate the possible difference in the degradation of the two possible S-containing heterocyclic group, namely

thiopyran (T-2H-T4CA) and thiophene (5H-2THCA). Metallic ions are commonly encounter in different surface and ground water owing to industrial, geochemical and biological action in environment. The presence of these ions can positively or otherwise affect the treatment of organic pollutants in wastewater owing to their redox potential and inhibition/scavenging effect. In this case, Mn^{2+} and Fe^{3+} inhibited the photocatalytic degradation of S-NAs: T-2H-T4CA and 5H-2THCA (Fig. 2.9a and b). Two reasons were hypothesized to be responsible for the inhibition. Firstly, the electrostatic effects between Mn^{2+} and Fe^{3+} with target NAs. At pH 8.5, both target pollutants are negatively charged. Secondly, non-bonding S atom could form complex with Mn^{2+} and Fe^{3+}, thus decreased the possibility of reaction between the NAs and photogenerated free reactive species. In contrast, different behavior was observed for the degradation of IA in the presence of 2.5 mM Mn^{2+} or Fe^{3+} (Fig. 2.9c). Mn^{2+} and Fe^{3+} have no effects on the degradation of IA. However, another interesting phenomenon was observed. The reaction/degradation of IA continues even after the solar light was turned off, demonstrating spontaneous oxidation of the IA in the absence of the photogenerated reactive species (h^+ and $O_2^{\bullet-}$). The samples were quenched by $Na_2S_2O_3$ to allow quantification of the IA. This phenomenon can be explained as follow: under the solar irradiation, IA could be activated to aminyl radicals in an alkaline environment, which could act as a reactive species for its degradation. In essence, the aminyl radicals initiate the spontaneous, chain and continuous degradation of the IA. Similar phenomenon has been reported in other studies. For example, Svejstrup et al. (2017), found that protonated electron-poor O-aryl hydroxylamines produce aminium radicals under catalysis of $Ru(bpy)_3Cl_2$. These highly electrophilic species undergo high yield and selectivity of polarized radical addition to aromatics. Moreover, aminyl radicals (basic condition) have lower reactive than aminium radicals (acidic condition). This result coincides well with our result. As illustrated in Fig. 2.10, The removal rates

of IA were decreased with increasing solution pH values. Introduction of cations into suspension could change the pH. Thus, we estimated that the synergistic effect of pH and electrostatic effects are key points during the degradation of IA.

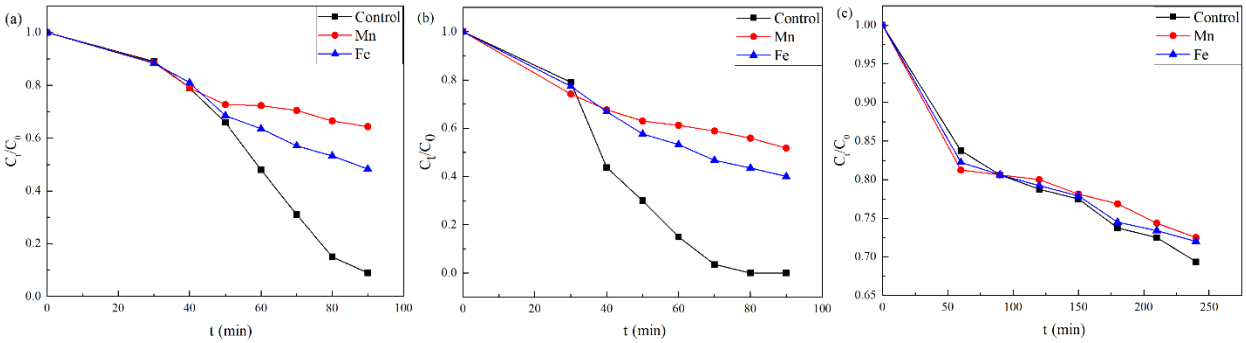

Fig. 2.24 Effects of Mn^{2+} and Fe^{3+} on the photocatalytic degradation of (a) T-2H-T4CA, (b) 5H-2THCA and (c) IA ([NAs] = 25 mg/L, [catalyst] = 1 g/L, $[Mn^{2+}] = [Fe^{3+}]$ = 2.5 mM, $[HCO_3^-]$ = 5 mM, pH = 8.5).

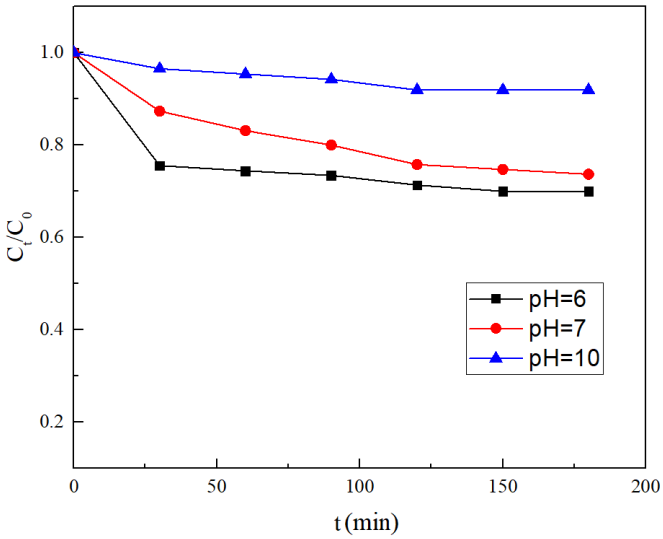

Fig. 2.25 Effect of pH on the photocatalytic degradation of IA ([pollutants] = 25 mg/L, [catalyst] = 1 g/L).

2.3.5 The transformation mechanisms of heteroatomic NAs

The reaction pathways of heteroatomic NAs T-2H-T4CA, IA and 5H-2THCA were reported for the first time in this study. The proposed products were separated and identified to elucidate the transformation mechanisms of heteroatomic NAs in photocatalytic system by UPLC-TOF-MS. The structure, theoretical and measured mass of the by-products are presented in Table B1 in appendix B. Fig. 2.11 illustrated the possible transformation pathways of photocatalytic degradation of T-2H-T4CA and IA. Total of four by-products were identified and a reaction scheme was proposed for each compound respectively. For T-2H-T4CA, two oxygen atoms were sequentially added at S heteroatom of the compound by $O_2^{\bullet-}$ attack due to the electron-rich of the S-site. This result confirmed the hypothesis in Section 2.3.4 that Mn^{2+} and Fe^{3+} may form complexes with –S thus blocking the addition of O, leading to the decreased reaction rates. For IA, it could be excited to form aminyl radicals which resulted in the hydroxyl addition and subsequently resulted in the ring opening.

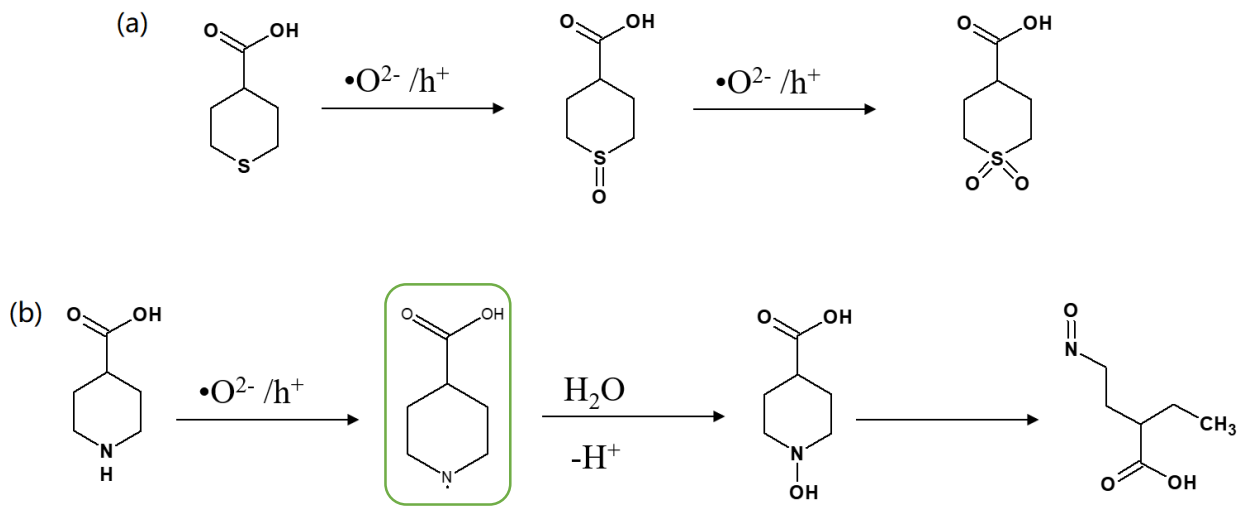

Fig. 2.26 Possible transformation pathway of photocatalytic degradation of (a) T-2H-T4CA and (b) IA

Six by-products were identified (Fig. 2.12) and four schemes (Fig. 2.13) were proposed for 5H-2THCA. 2 initial reaction sites of 5H-2THCA are suggested, which are the addition of oxygen at S atom or the heterocyclic ring via electrophilic addition of the $O_2^{\bullet-}$ and h^+ resulting in the formation of peroxyl radical intermediate which would then rearrange to generate transformation by-products P1, P2 and P3 (Scheme 1, 2 and 3). P4 was generated from P3 through decarboxylation reaction. P1, P2 and P4 were then oxidized to P5, also through the electrophilic addition of $O_2^{\bullet-}$. Subsequently, P5 was oxidized by $O_2^{\bullet-}$ to form an organic peroxide intermediate which was finally oxidized to form P6 (Scheme 4). To support our proposed pathways, molecular orbital calculations were conducted for 5H-2THCA using the Gaussian 09 program. The $2FED^2_{HOMO}$ values of each atom and the isosurface of the highest occupied molecular orbital (HOMO) are displayed in Fig. 2.14a and b. The highest $2FED^2_{HOMO}$ value of 5H-2THCA molecule was observed to be localized at 8O in the carboxyl, second to which is another oxygen in the carboxyl 7O, followed by 5S and 1C (Fig. 2.14a). The higher the $2FED^2_{HOMO}$ value indicated higher reactivity toward radical reaction. These calculations once again confirm that the oxidation of the thiol moiety is crucial part in the degradation of 5H-2THCA. These calculations indicated that the carboxyl could be oxidized to CO_2 (P4), and the oxidation of S (P3, P4 and P5). The HOMO isosurface in Fig. 2.14b also shows that the orbital is distributed over the oxygen in the carboxyl, then at the 1C, 2C, 3C, and 4C atoms and at 9C atom. As h^+ is electron deficit and unstable, it could extract electron from these electron rich atoms resulting in the alkenation and decarboxylation observed in the formation of P2 and P4. Furthermore, mass balance of 5H-2THCA was established and two unknown by-products were estimated. Fig. 2.15 displays the concentration of 5H-2THCA and by-products during 120 min photocatalytic degradation. 0.118 mol/L 5H-2THCA was decreased to 0.005 mol/L

during 60 min illumination and 96% of 5H-2THCA was transferred to byproducts. As exhibited in Fig. 2.15, P2, P4 and U1 are the dominant by-products. Meanwhile, trace amount (<0.003 mol/L) of P1, P3, P5 and U2 were generated through the degradation of 5H-2THCA. P2 increased to 0.081 mol/L at 60 min and with prolonged photocatalytic degradation decreased to 0.067 mol/L at 120min. P4 increased to 0.014 mol/L in the first 30 min then started to degrade and decreased to 0.005 mol/L at 120 min. Different from the formation of P2 and P4, which generated at the initial of the reaction, U1 formation started at 30 min and increased to 0.042 mol/L as the reaction proceed. Both P2 and P4 could transform to P5, but the concentration of P5 did not increase over time, which suggested that the reaction rate of 5H-2THCA to P2 was faster than that of P2 to P5. Since P4 started to decrease at 30 min but the concentration of P5 did not increase as expected, U1 was considered as a by-product from the transformation of P4. U2 was predicted to be the unidentified intermediate product between P5 and P6.

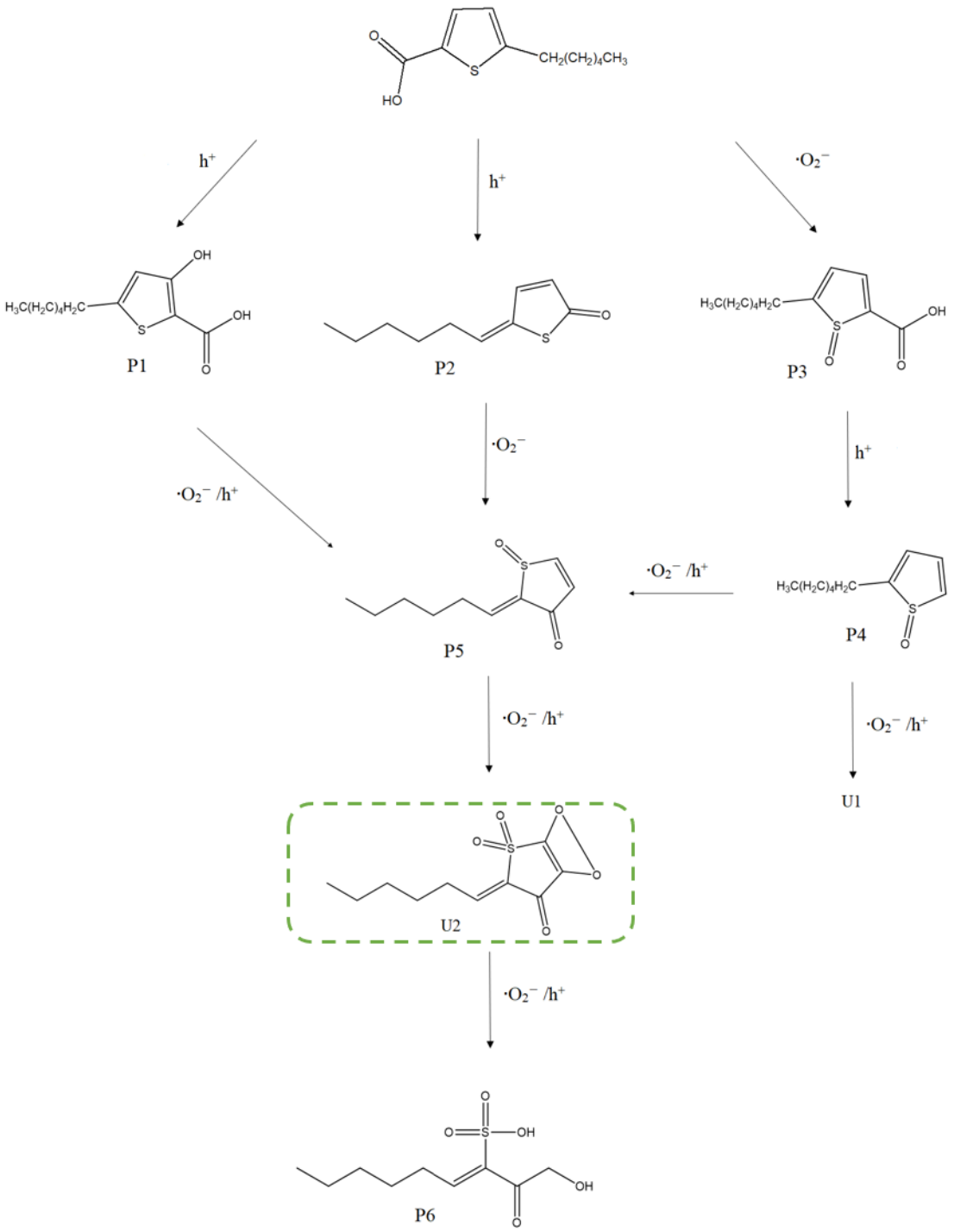

Fig. 2.27 Possible transformation pathway of photocatalytic degradation of 5H-2THCA.

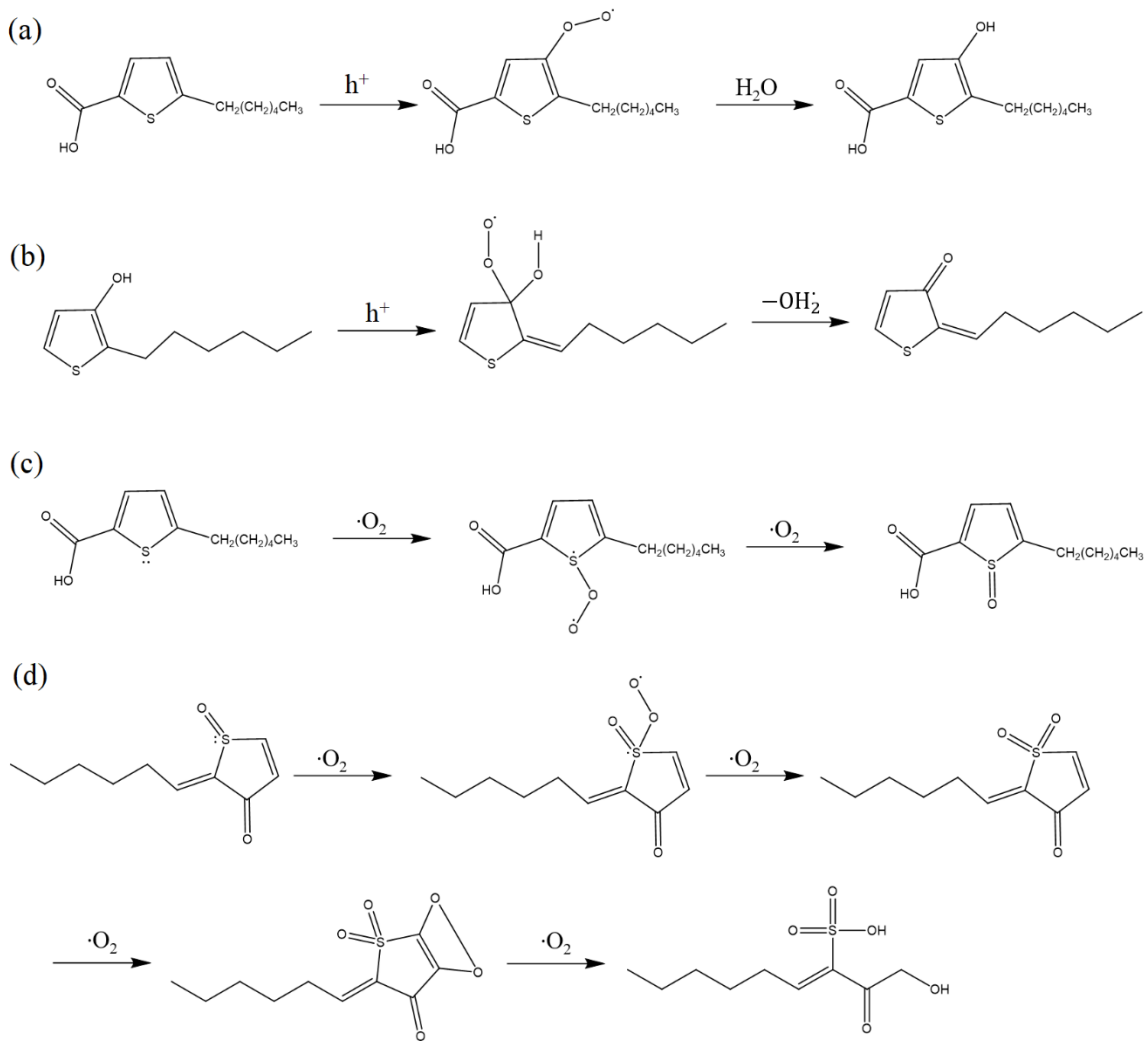

Fig. 2.28 (a) scheme 1 the formation of P1 (b) scheme 2 the formation of P2 (c) scheme 3 the formation of P3 (d) scheme 4 the formation of P6

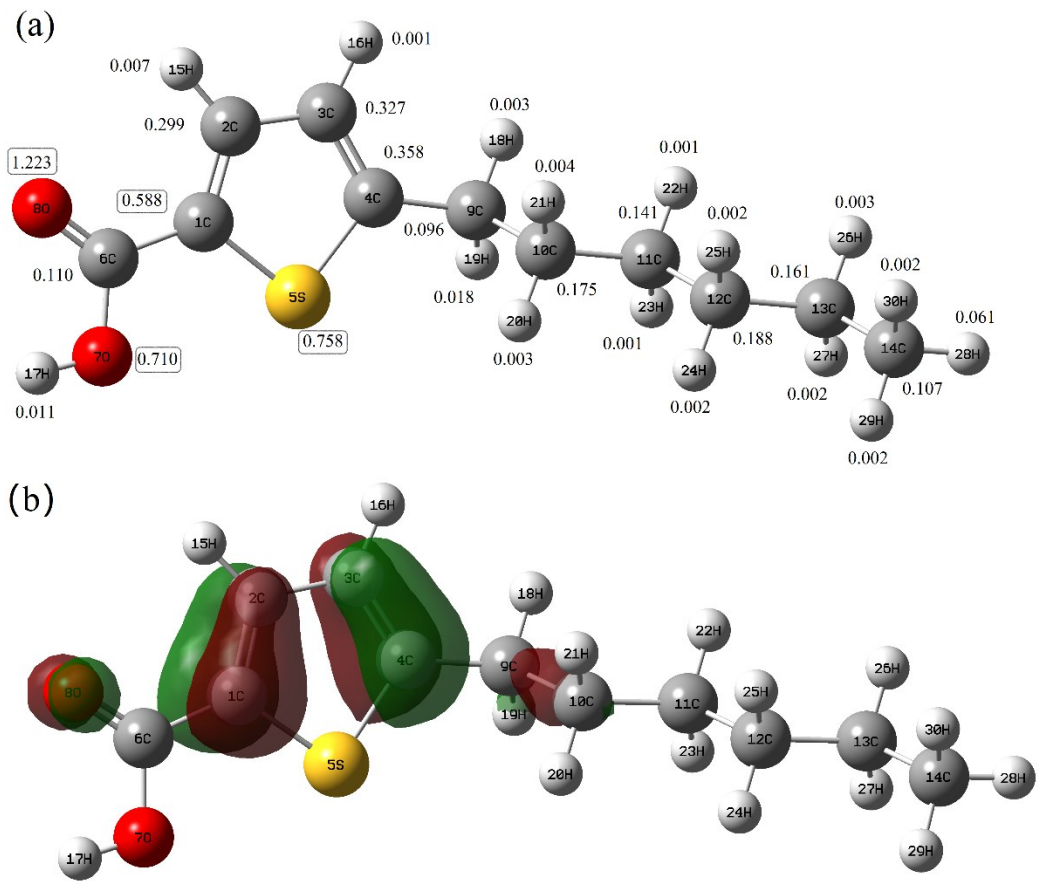

Fig. 2.29 (a) $2FED^2_{HOMO}$ data of each atom, (b) isodensity surfaces of HOMO with an isovalue of 0.05

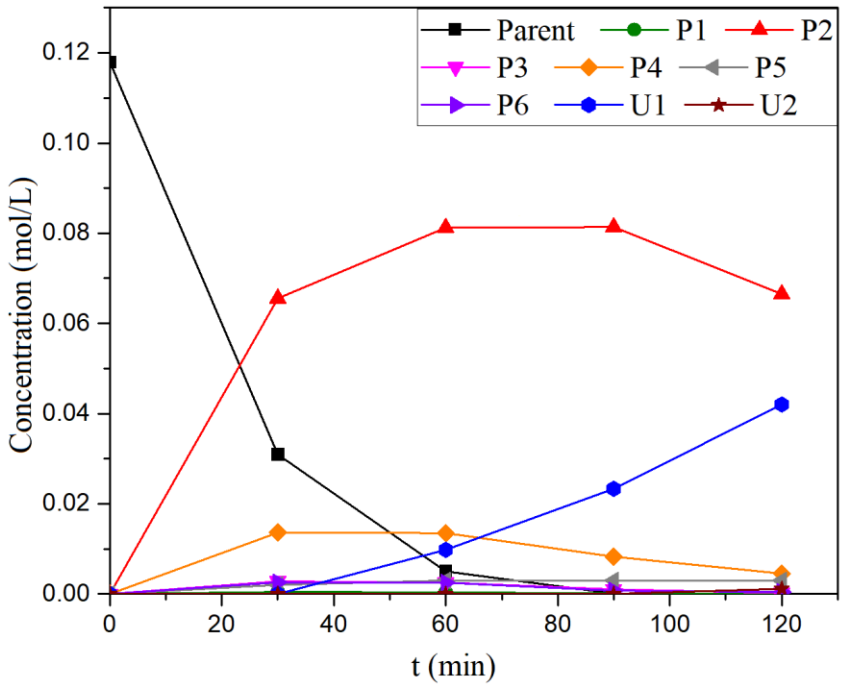

Fig. 2.30 Semi-quantification of 5H-2THCA and by-products during 120 min photocatalytic degradation.

2.4 Conclusion

This study has demonstrated that NAs in OSPW could be efficiently degraded by solar photocatalytic treatment using Bi_2WO_6. Different morphologies of Bi_2WO_6 such as FL, NP and SL structures were obtained by changing experimental parameters during the process of crystal growth. Among the three different morphologies synthesized, FL Bi_2WO_6 structure has better physicochemical properties such as larger surface area and pore volume and showed faster degradation of NAs compared to other structures. $O_2^{\bullet-}$ and h^+ are the main reactive species participating in the degradation of NAs during the photocatalytic treatment using Bi_2WO_6. The photocatalytic degradation rates were decreased in the order T-2H-T4CA > CHA > IA > T4CA. Solar photocatalytic treatment using Bi_2WO_6 were also efficient for the treatment of real OSPW

with S-NAs completely removed, classical NAs significantly reduced, and O-NAs produced from the oxidation of classical NAs. The presence of cations (Mn^{2+} and Fe^{3+}) in water matrix decreased the efficiency of S-NAs, T-2H-T4CA and 5H-2THCA due to complexation of the NAs with the cations. However, no effects were found on the degradation of IA (N-NAs). The proposed pathways for the oxidation of heteroatomic NAs were supported by identification of 12 by-products and by quantum chemical calculations and was found that the S or N atom in the structure play a crucial role in their degradation. This work has presented an effective method for the remediation of OSPW and elucidated the transformation mechanisms of heteroatomic NAs, which are valuable for the environmental fate of NAs in OSPW.

2.5 References

Anderson, J., Wiseman, S.B., Moustafa, A., Gamal El-Din, M., Liber, K. and Giesy, J.P. (2012) Effects of exposure to oil sands process-affected water from experimental reclamation ponds on Chironomus dilutus. Water Research 46(6), 1662-1672.

Benally, C., Messele, S.A. and Gamal El-Din, M. (2019) Adsorption of organic matter in oil sands process water (OSPW) by carbon xerogel. Water Research 154, 402-411.

Bolton, J.R. and Linden, K.G. (2003) Standardization of Methods for Fluence (UV Dose) Determination in Bench-Scale UV Experiments. Journal of Environmental Engineering 129(3), 209-215.

Dai, Z., Qin, F., Zhao, H., Tian, F., Liu, Y. and Chen, R. (2015) Time-dependent evolution of the Bi3.64Mo0.36O6.55/Bi2MoO6 heterostructure for enhanced photocatalytic activity via the interfacial hole migration. Nanoscale 7(28), 11991-11999.

de Oliveira Livera, D., Leshuk, T., Peru, K.M., Headley, J.V. and Gu, F. (2018) Structure-reactivity

relationship of naphthenic acids in the photocatalytic degradation process. Chemosphere 200, 180-190.

Debenest, T., Turcotte, P., Gagné, F., Gagnon, C. and Blaise, C. (2012) Ecotoxicological impacts of effluents generated by oil sands bitumen extraction and oil sands lixiviation on Pseudokirchneriella subcapitata. Aquatic Toxicology 112-113, 83-91.

Dong, S., Ding, X., Guo, T., Yue, X., Han, X. and Sun, J. (2017) Self-assembled hollow sphere shaped Bi2WO6/RGO composites for efficient sunlight-driven photocatalytic degradation of organic pollutants. Chemical Engineering Journal 316, 778-789.

Drzewicz, P., Perez-Estrada, L., Alpatova, A., Martin, J.W. and Gamal El-Din, M. (2012) Impact of Peroxydisulfate in the Presence of Zero Valent Iron on the Oxidation of Cyclohexanoic Acid and Naphthenic Acids from Oil Sands Process-Affected Water. Environmental Science & Technology 46(16), 8984-8991.

Fang, Z., Huang, R., How, Z.T., Jiang, B., Chelme-Ayala, P., Shi, Q., Xu, C. and Gamal El-Din, M. (2020) Molecular transformation of dissolved organic matter in process water from oil and gas operation during UV/H2O2, UV/chlorine, and UV/persulfate processes. Science of The Total Environment 730, 139072.

Fu, H., Zhang, L., Yao, W. and Zhu, Y. (2006) Photocatalytic properties of nanosized Bi2WO6 catalysts synthesized via a hydrothermal process. Applied Catalysis B: Environmental 66(1), 100-110.

Gagné, F., Bruneau, A., Turcotte, P., Gagnon, C. and Lacaze, E. (2017) An investigation of the immunotoxicity of oil sands processed water and leachates in trout leukocytes. Ecotoxicology and Environmental Safety 141, 43-51.

Gamal El-Din, M., Fu, H., Wang, N., Chelme-Ayala, P., Pérez-Estrada, L., Drzewicz, P., Martin,

J.W., Zubot, W. and Smith, D.W. (2011) Naphthenic acids speciation and removal during petroleum-coke adsorption and ozonation of oil sands process-affected water. Science of The Total Environment 409(23), 5119-5125.

Hersikorn, B.D., Ciborowski, J.J.C. and Smits, J.E.G. (2010) The effects of oil sands wetlands on wood frogs (Rana sylvatica). Toxicological & Environmental Chemistry 92(8), 1513-1527.

Hu, T., Li, H., Zhang, R., Du, N. and Hou, W. (2016) Thickness-determined photocatalytic performance of bismuth tungstate nanosheets. RSC Advances 6(38), 31744-31750.

Huang, R., Chen, Y., Meshref, M.N.A., Chelme-Ayala, P., Dong, S., Ibrahim, M.D., Wang, C., Klamerth, N., Hughes, S.A., Headley, J.V., Peru, K.M., Brown, C., Mahaffey, A. and Gamal El-Din, M. (2018) Characterization and determination of naphthenic acids species in oil sands process-affected water and groundwater from oil sands development area of Alberta, Canada. Water Research 128, 129-137.

Huang, R., Sun, N., Chelme-Ayala, P., McPhedran, K.N., Changalov, M. and Gamal El-Din, M. (2015) Fractionation of oil sands-process affected water using pH-dependent extractions: A study of dissociation constants for naphthenic acids species. Chemosphere 127, 291-296.

Islam, M.S., Zhang, Y., McPhedran, K.N., Liu, Y. and Gamal El-Din, M. (2015) Granular activated carbon for simultaneous adsorption and biodegradation of toxic oil sands process-affected water organic compounds. Journal of Environmental Management 152, 49-57.

Kormali, P., Triantis, T., Dimotikali, D., Hiskia, A. and Papaconstantinou, E. (2006) On the photooxidative behavior of TiO2 and PW12O403−: OH radicals versus holes. Applied Catalysis B: Environmental 68(3), 139-146.

Leclair, L.A., Pohler, L., Wiseman, S.B., He, Y., Arens, C.J., Giesy, J.P., Scully, S., Wagner, B.D., van den Heuvel, M.R. and Hogan, N.S. (2015) In Vitro Assessment of Endocrine

Disrupting Potential of Naphthenic Acid Fractions Derived from Oil Sands-Influenced Water. Environmental Science & Technology 49(9), 5743-5752.

Leshuk, T., de Oliveira Livera, D., Peru, K.M., Headley, J.V., Vijayaraghavan, S., Wong, T. and Gu, F. (2016a) Photocatalytic degradation kinetics of naphthenic acids in oil sands process-affected water: Multifactorial determination of significant factors. Chemosphere 165, 10-17.

Leshuk, T., Wong, T., Linley, S., Peru, K.M., Headley, J.V. and Gu, F. (2016b) Solar photocatalytic degradation of naphthenic acids in oil sands process-affected water. Chemosphere 144, 1854-1861.

Li, C., Chen, G., Sun, J., Rao, J., Han, Z., Hu, Y., Xing, W. and Zhang, C. (2016) Doping effect of phosphate in Bi2WO6 and universal improved photocatalytic activity for removing various pollutants in water. Applied Catalysis B: Environmental 188, 39-47.

Li, C., Fu, L., Lillico, D.M.E., Belosevic, M., Stafford, J.L. and Gamal El-Din, M. (2019) Exposure to Organic Fraction Extracted from Oil Sands Process-Affected Water Has Negligible Impact on Pregnancy and Lactation of Mice. Environmental Science & Technology 53(12), 7083-7094.

Liu, J., Wang, L., Tang, J. and Ma, J. (2016) Photocatalytic degradation of commercially sourced naphthenic acids by TiO2-graphene composite nanomaterial. Chemosphere 149, 328-335.

Mao, D., Ding, S., Meng, L., Dai, Y., Sun, C., Yang, S. and He, H. (2017) One-pot microemulsion-mediated synthesis of Bi-rich Bi4O5Br2 with controllable morphologies and excellent visible-light photocatalytic removal of pollutants. Applied Catalysis B: Environmental 207, 153-165.

Mavinakere Ramesh, A., Shivanna, S. (2018) Visible light assisted photocatalytic degradation of

chromium (VI) by using nanoporous Fe_2O_3. Journal of Materials, 2018.

Meng, L., Yang, S., Sun, C., He, H., Xian, Q., Li, S., Wang, G., Zhang, L. and Jiang, D. (2017) A novel method for photo-oxidative degradation of diatrizoate in water via electromagnetic induction electrodeless lamp. Journal of Hazardous Materials 337, 34-46.

Nyakas, A., Han, J., Peru, K.M., Headley, J.V. and Borchers, C.H. (2013) Comprehensive Analysis of Oil Sands Processed Water by Direct-Infusion Fourier-Transform Ion Cyclotron Resonance Mass Spectrometry with and without Offline UHPLC Sample Prefractionation. Environmental Science & Technology 47(9), 4471-4479.

Pérez-Estrada, L.A., Han, X., Drzewicz, P., Gamal El-Din, M., Fedorak, P.M. and Martin, J.W. (2011) Structure–Reactivity of Naphthenic Acids in the Ozonation Process. Environmental Science & Technology 45(17), 7431-7437.

Qin, R., How, Z.T. and Gamal El-Din, M. (2019a) Photodegradation of naphthenic acids induced by natural photosensitizer in oil sands process water. Water Research 164, 114913.

Qin, R., Lillico, D., How, Z.T., Huang, R., Belosevic, M., Stafford, J. and Gamal El-Din, M. (2019b) Separation of oil sands process water organics and inorganics and examination of their acute toxicity using standard in-vitro bioassays. Science of the Total Environment 695, 133532.

Samuni, A., Krishna, C.M., Mitchell, J.B., Collins, C.R. and Russo, A. (1990) Superoxide reaction with nitroxides. Free Radic Res Commun 9(3-6), 241-249.

Sohrabi, V., Ross, M.S., Martin, J.W. and Barker, J.F. (2013) Potential for in situ chemical oxidation of acid extractable organics in oil sands process affected groundwater. Chemosphere 93(11), 2698-2703.

Sun, C., Shotyk, W., Cuss, C.W., Donner, M.W., Fennell, J., Javed, M., Noernberg, T., Poesch, M.,

Pelletier, R., Sinnatamby, N., Siddique, T. and Martin, J.W. (2017) Characterization of Naphthenic Acids and Other Dissolved Organics in Natural Water from the Athabasca Oil Sands Region, Canada. Environmental Science & Technology 51(17), 9524-9532.

Sun, N., Chelme-Ayala, P., Klamerth, N., McPhedran, K.N., Islam, M.S., Perez-Estrada, L., Drzewicz, P., Blunt, B.J., Reichert, M., Hagen, M., Tierney, K.B., Belosevic, M. and Gamal El-Din, M. (2014) Advanced Analytical Mass Spectrometric Techniques and Bioassays to Characterize Untreated and Ozonated Oil Sands Process-Affected Water. Environmental Science & Technology 48(19), 11090-11099.

Svejstrup, T.D., Ruffoni, A., Juliá, F., Aubert, V.M. and Leonori, D. (2017) Synthesis of Arylamines via Aminium Radicals. Angewandte Chemie International Edition 56(47), 14948-14952.

Wang, C., Klamerth, N., Huang, R., Elnakar, H. and Gamal El-Din, M. (2016a) Oxidation of Oil Sands Process-Affected Water by Potassium Ferrate(VI). Environmental Science & Technology 50(8), 4238-4247.

Wang, C., Klamerth, N., Messele, S.A., Singh, A., Belosevic, M. and Gamal El-Din, M. (2016b) Comparison of UV/hydrogen peroxide, potassium ferrate(VI), and ozone in oxidizing the organic fraction of oil sands process-affected water (OSPW). Water Research 100, 476-485.

Wang, N., Chelme-Ayala, P., Perez-Estrada, L., Garcia-Garcia, E., Pun, J., Martin, J.W., Belosevic, M. and Gamal El-Din, M. (2013) Impact of Ozonation on Naphthenic Acids Speciation and Toxicity of Oil Sands Process-Affected Water to Vibrio fischeri and Mammalian Immune System. Environmental Science & Technology 47(12), 6518-6526.

Wei, T. T., Wu, T., Lin, Y. W. (2019) Controlled synthesis of Ag_3PO_4 microparticles with different

morphologies and their photocatalytic degradation of rhodamine B under white light-emitting diode irradiation. Micro & Nano Letters, 14(4), 363-366.

Xu, X., Meng, L., Dai, Y., Zhang, M., Sun, C., Yang, S., He, H., Wang, S. and Li, H. (2020) Bi spheres SPR-coupled Cu2O/Bi2MoO6 with hollow spheres forming Z-scheme Cu2O/Bi/Bi2MoO6 heterostructure for simultaneous photocatalytic decontamination of sulfadiazine and Ni(II). Journal of Hazardous Materials 381, 120953.

Xue, J., Zhang, Y., Liu, Y. and Gamal El-Din, M. (2016) Treatment of oil sands process-affected water (OSPW) using a membrane bioreactor with a submerged flat-sheet ceramic microfiltration membrane. Water Research 88, 1-11.

Yang, A.-M., Han, Y., Li, S.-S., Xing, H.-W., Pan, Y.-H. and Liu, W.-X. (2017) Synthesis and comparison of photocatalytic properties for Bi2WO6 nanofibers and hierarchical microspheres. Journal of Alloys and Compounds 695, 915-921.

Zhang, C. and Zhu, Y. (2005) Synthesis of Square Bi2WO6 Nanoplates as High-Activity Visible-Light-Driven Photocatalysts. Chemistry of Materials 17(13), 3537-3545.

Zhang, L., Wang, W., Chen, Z., Zhou, L., Xu, H. and Zhu, W. (2007a) Fabrication of flower-like Bi2WO6 superstructures as high performance visible-light driven photocatalysts. Journal of Materials Chemistry 17(24), 2526-2532.

Zhang, L., Wang, W., Zhou, L. and Xu, H. (2007b) Bi2WO6 Nano- and Microstructures: Shape Control and Associated Visible-Light-Driven Photocatalytic Activities. Small 3(9), 1618-1625.

Zhang, L., Zhang, Y. and Gamal El-Din, M. (2018) Degradation of recalcitrant naphthenic acids from raw and ozonated oil sands process-affected waters by a semi-passive biofiltration process. Water Research 133, 310-318.

Zhang, Y., Klamerth, N., Chelme-Ayala, P. and Gamal El-Din, M. (2016a) Comparison of Nitrilotriacetic Acid and [S,S]-Ethylenediamine-N,N′-disuccinic Acid in UV–Fenton for the Treatment of Oil Sands Process-Affected Water at Natural pH. Environmental Science & Technology 50(19), 10535-10544.

Zhang, Y., Klamerth, N. and Gamal El-Din, M. (2016b) Degradation of a model naphthenic acid by nitrilotriacetic acid – modified Fenton process. Chemical Engineering Journal 292, 340-347.

Zhou, H., Wen, Z., Liu, J., Ke, J., Duan, X. and Wang, S. (2019) Z-scheme plasmonic Ag decorated WO3/Bi2WO6 hybrids for enhanced photocatalytic abatement of chlorinated-VOCs under solar light irradiation. Applied Catalysis B: Environmental 242, 76-84.

CHAPTER 3 Z-SCHEME PLASMONIC AG DECORATED NIO/BI_2WO_6 HYBRIDS FOR ENHANCED PHOTOCATALYTIC TREATMENT OF NAPHTHENIC ACIDS IN REAL OIL SANDS PROCESS WATER UNDER SIMULATED SOLAR IRRADIATION

3.1 Introduction

The oil sands in northern region in Alberta, Canada, are one of the largest crude oil reserves on earth. Bitumen extraction from oil sands using hot caustic water extraction method produces a large volume of oil sands process water (OSPW) (Ganiyu and Gamal El-Din 2020). Despite that around 80% of the water are reused, the freshwater intake is still 2–3 m^3 to extract one m^3 of bitumen (Masliyah et al. 2004). OSPW is a saline solution that contains water, trace metals, inorganics, organics, and suspended solids. It has been reported that OSPW could induce acute and chronic toxicity to both prokaryotes and eukaryotes, such as bacteria (Sun et al. 2014), birds (Gentes et al. 2006), amphibians (Hersikorn and Smits 2011), fishes (Hagen et al. 2013), and others. Organic compounds, especially naphthenic acids (NAs), are believed to be the dominant contribution factors for toxicity resulted from OSPW (Li et al. 2017). Therefore, the removal of NAs is considered to be one of the most critical steps to safely discharge OSPW into environment. NAs are generally divided into classical NAs (O_2-NAs), oxidized NAs (Oxy-NAs), sulfur containing NAs (S-NAs) and nitrogen containing NAs (N-NAs) (Qin et al. 2019).

Visible light driven catalysts such as bismuth tungstate (Bi_2WO_6), have been widely applied in the field of CO_2 reduction (Cao et al. 2018), NO oxidation (Huo et al. 2019), water splitting (Wu et al. 2020), disinfection (Meng et al. 2017) and contaminants removal in water (Lv et al. 2019) owing to the high physicochemical stability, low toxicity and cost-effectiveness (Zhang et al. 2021). The superior photocatalytic performance of Bi_2WO_6 on the degradation of various

organic pollutants in water are confirmed in previous research (Zhu and Zhou 2020). However, in the majority of these studies, experiments were usually conducted using commercial chemicals (target pollutants) dissolved in ultrapure water at neutral pH and at concentrations higher than the environmentally relevant concentrations. Seldom of these studies focused on the application of Bi_2WO_6 for the real industrial wastewater remediation due to the diversity and challenges of treating real industrial wastewater. The range of physicochemical characteristic values of industrial wastewater are wide; the concentration of organics can be as high as thousands of mg/L, with wide pH value, solids and high ionic charge. For example, OSPW is characterized by high alkalinity (pH ~ 8.5) and salinity ($\sigma \geq 3.0$ mS cm^{-1}) as well as complex composition (Abdalrhman and Gamal El-Din 2020). Therefore, it is inevitable to explore the photocatalytic degradation behavior of complex organic wastewaters.

The photocatalytic performance of Bi_2WO_6 could be limited, owing to the poor capability for separating the photoinduced charge carriers. Therefore, many attempts have been taken to increase the photocatalytic activity of Bi_2WO_6, namely (1) anionic and cationic dopants (Cao et al. 2015, Shang et al. 2010); (2) noble metal deposition (Ren et al. 2009, Wang et al. 2014); and (3) heterojunction photocatalysts (Jo et al. 2018, Meng et al. 2017). Among numerous semiconductors, nickel oxide (NiO) is a p-type semiconductor with a band gap around 3.6 eV, and it is widely used as gas sensor (Hotovy et al. 1999), solar cells (Chen et al. 2018), electrochemical supercapacitors (Yao et al. 2018) and hydrogenation (Lin et al. 2018). NiO and Bi_2WO_6 could form p-n heterojunction catalyst. Nevertheless, the photocatalytic activities of p-n heterojunction may be restricted due to the reduced redox ability of original electrons and holes. Therefore, Z-scheme systems were employed to avoid the decrease of redox potential, meanwhile keeping the capability to separate photo-generated electron-hole pairs effectively. However, the directional migration of

traditional charge carriers usually competes with that in two phase Z-scheme heterojunction. In this case, an electron mediator is introduced to enhance Z-scheme charge transfer based on the difference of electrical resistances between different phases. Noble metals such as gold and silver, which could induce surface plasmon resonance (SPR), are employed as electron mediator in Z-scheme systems.

Herein, self-assembled 3D flower like Bi_2WO_6 was fabricated via hydrothermal methods followed by the deposition of 0D Ag nanoparticles and 2D NiO nanoplates using *in-situ* light reduction and hydrothermal methods, forming Ag/NiO/Bi_2WO_6 Z-scheme heterojunction. The as-obtained samples were firstly prepared and applied for real OSPW remediation. These catalysts were carefully characterized by different kinds of analytical methods. The photocatalytic performance was evaluated through the removal efficiency of NAs in real OSPW. The OSPW was characterized using mass spectrometry, ion mobility spectrometry (IMS) and synchronous fluorescence spectra (SFS). Through this study, a novel and efficient NA photocatalytic degradation process was investigated and a passive treatment approach for OSPW remediation through solar light-driven photocatalysis was developed.

3.2 Experimental

3.2.1 Chemicals and materials

Raw OSPW was obtained from an active oil sands tailings pond in Fort McMurray, Alberta, Canada, and was stored at 4 °C in the dark until use. OSPW samples were allowed to reach room temperature (23 ± 2 °C) and particulates were removed by 0.45 μm nylon membranes filter before the experiments. Table 3.1 lists the properties, major ions and organic composition of the raw OSPW. $Bi(NO_3)_3 \cdot 5H_2O$, $Na_2WO_4 \cdot 2H_2O$, $Ni(NO_3)_2 \cdot 6H_2O$, ammonium oxalate (AO), urea, isopropanol (IPA), NH_4F, 4-hydroxy2, 2, 6, 6-tetramethylpiperidinyloxy (TEMPOL) and model

NA compound, 1-adamantanecarboxylic acid (ACA) were purchased from Sigma Aldrich. The spin-trapping agent 5,5-dimethyl-1-pyrroline-N-oxide (DMPO) was obtained from Dojindo Molecular Technologies Inc.

Table 3.4 Properties, major ions and organic composition of raw OSPW.

Parameter	Value
pH	8.7 ± 0.2
Alkalinity (mg L^{-1} as $CaCO_3$)	550 ± 10
Conductivity (mS cm^{-1})	3.2 ± 0.2
Total suspended solids (mg L^{-1})	41 ± 4
Ions (mg L^{-1})	
K	41.56±0.702
Na	1,182±8.306
S	51.69±0.661
Cl^-	615.3760±5.312
SO_4^{2-}	93.4347±5.0320
CO_3^{2-}	1478.3530 ± 30
NO_3^-	19.5539±0.910
Organic parameters (mg L^{-1})	
Dissolved organic carbon (mg L^{-1} as C)	52.8 ± 5.2
Classical NAs (O_2-NAs)	29.46 ± 2.1
O_3-NAs	18.5 ± 0.8
O_4-NAs	15.4 ± 0.6
O_5-NAs	6.3 ± 0.2
O_6-NAs	1.4 ±0.2

3.2.2 Preparation of photocatalysts

For the preparation of Bi_2WO_6, $Bi(NO_3)_3{\cdot}5H_2O$ (2 mmol) was added into 10 mL glacial acetic acid under magnetic stirring until it became a clear solution (solution A). 1 mmol of $Na_2WO_4{\cdot}2H_2O$ was dissolved in 70 mL water to form solution B. Next, solution B was added dropwise into solution A. The mixture was stirred for 1 h and then treated with a hydrothermal method at 140 °C for 12 h. The obtained products were centrifuged, washed with ultrapure water and ethanol three times, and dried at 60 °C for 6 h.

The NiO/Bi_2WO_6 heterojunction composites were obtained by the following process: 0.4 g Bi_2WO_6 was added in 60 mL water under magnetic stirring for 30 min. After that, urea (1g), NH_4F

(0.2g) and appropriate amounts of $Ni(NO_3)_2 \cdot 6H_2O$ were added into the solution and stirred vigorously for 30 min. Then, the solution was transferred into a Teflon-lined stainless-steel autoclave, which was heated at 160 °C for 12 h. The resulted composites were washed with ultrapure water and ethanol and dried at 60 °C. Subsequently, the NiO/Bi_2WO_6 composites with a dark-green color were obtained by calcining in air at 380 °C for 2 h. The pure NiO was obtained by the same method but without the addition of Bi_2WO_6.

The $Ag/NiO/Bi_2WO_6$ plasmonic composites were prepared by a photoinduced method as follows: certain amounts of $AgNO_3$ and oxalic acid were added into 20 mL deionized water and then stirred vigorously until the chemicals were completely dissolved in the dark. After that, the as-prepared NiO/Bi_2WO_6 composites were dispersed into the above solution and irradiated for 3 h with a 300 W Xe lamp under magnetic stirring. The final $Ag/NiO/Bi_2WO_6$ products were collected, washed and dried at 60 ºC.

3.2.3 Characterization of materials

The phase purities and crystallinity of the samples were conducted at room temperature on Rigaku X-ray diffraction spectroscopy (XRD) Ultima IV with standard stage (Cu kα radiation, λ = 0.15406 nm). The scanning electron microscopy (SEM) image were taken with a Zeiss EVO M10 SEM-imaging. Transmission electron microscopy (TEM) was carried out using a JEOL JEM-ARM200CF S/TEM electron microscope at an accelerating voltage of 200 kV. The high-resolution transmission electron microscopy (HRTEM) images were processed by Gatan Digital Micrograph software (Version 3.4.1). The chemical composition was explored by energy-dispersive X-ray spectroscopy (EDX). The chemical states and surface chemical composition were characterized by X-ray photoelectron spectroscopy (XPS, Kratos AXIS 165, Kratos Analytical). Fluorescence emission spectra were recorded over a wavelength range of 200–800 nm on a Horiba Fluorolog 3–

22 type fluorescence spectrophotometer with excitation wavelength of 365 nm. The photoelectrochemical characterization was carried out on an electrochemical workstation with a standard three-electrode system. The as-prepared samples were uniformly coated on the FTO glass as the working electrode. Pt electrode and Ag/AgCl electrode were used as the counter and reference electrodes, respectively. The electrolyte was 0.2 M Na_2SO_4 aqueous solution. A 300 W xenon lamp was applied to provide light source.

3.2.4 Photocatalytic experiments

A solar simulator (Newport, 66485-300XF-R1, USA) was used to perform the photocatalytic experiments. Xenon arc lamp (300W) was employed with its irradiance being measured using a spectroradiometer with a CR2 UV-VIS-NIR cosine receptor. Data was acquired by the software program SpectraWiz® (StellarNet Inc.). The irradiance was set and maintained as 18.18 mW cm^{-2}, the detailed composition of the light spectra is listed in Table 3.2. The experiments were carried out in a 100ml cylindrical reactor, in which 50 mg as-prepared samples were added to 50 mL solution to form 1g L^{-1} suspension. A magnetic stirrer was employed with speed at 420 rpm. 3 mL samples were sampled at predetermined intervals and the catalysts were immediately filtered with 0.2 μm Nylon filter and stored at 4 °C till analysis.

Table 3.5 The irradiance of different wavelength range.

Wavelength (nm)	400-500	500-600	600-700	700-800	Total
Irradiance (Watts/m^2)	48.69	49.68	49.63	33.81	181.8

3.2.5 Analytical methods

Synchronous fluorescence spectra (SFS) of the filtered water were recorded with Varian Cary Eclipse fluorescence spectrometer. Excitation wavelengths ranged from 200 to 600 nm, and emission wavelengths were recorded from 218 to 618 nm. Scanning speed was 600 nm/min and the photomultiplier (PMT) voltage was 800 mV. SFS of OSPW provides specific information on fluorescing compounds: peak I at 267 nm is assigned to one ring aromatics, while peak II at 310 nm and peak III at 330 nm are assigned to aromatics with two and three fused rings, respectively.

The concentration of model NA compound was measured by an ultra-performance liquid chromatography (UPLC) coupled with a single quadrupole mass spectrometry (SQ Detector 2, Waters). Chromatographic separation was performed at a flow rate of 400 $\mu L \cdot min^{-1}$ by a BEH C18 column (2.1 mm × 100 mm × 1.7 μm, Waters) maintained at 40 °C. The mobile phase was 0.1% formic acid in water (A) and methanol (B). The MS was operated in a negative ion mode using an ESI source in single ion monitoring mode. For OSPW samples, 1 mL of each water sample was centrifuged at 10000 RPM for 10 min. The injection solution was prepared with 500 μL of the supernatant, 100 μL of 4.0 mg L^{-1} internal standard (ISTD) compound (Myristic acid-1-^{13}C) in methanol, and 400 μL methanol to reach a final sample volume of 1 mL. The samples were analyzed using UPLC-TOF-MS in high-resolution mode (mass resolution = 40000 FWHM at 1431 m/z) at mass range of 100-600 (m/z). The electrospray ionization source was operated in the negative mode to measure NAs in the samples. Data acquisition was controlled using MassLynx (Waters) and data analysis was performed using TargetLynx (Waters). One raw OSPW sample was used as the quality control sample to ensure the method stability. This method was developed previously for semi-quantification of NAs based on the signal of a compound versus the signal of

spiked ISTD. The chromatographic separation was achieved by a method developed in our previous reports for the separation of NAs (Wang et al. 2013).

The ion-mobility spectrometry (IMS) was conducted in a Tri-Wave® ion-mobility cell of 15 cm long, using nitrogen (purity > 99%) as the drift gas. The IMS consisted of a transfer cell that collected certain number of ions and a helium gate that released the ions into the ion mobility cell. The number of ions was known and the difference in the number ions had a threshold of 5%. Ions were separated using an electric field (T-wave) that moved the ions in one direction and a gas flow in the counter direction, which drifted the ions based on the cross-collision section (CCS). Drift-Scope ver. was used to control the mobility separation. One raw OSPW sample was used as the quality control sample to ensure the method stability.

Active species of photocatalysis in aqueous solution were determined by electron paramagnetic resonance (EPR) with an ELEXSYS – II EPR spectrometer (Bruker E–500, Billerica). The running parameters were as follows: The center field of the spectrometer was 3897 G and resonance frequency (empty) of 9.81 GHz. The EPR spectra were detected with a 100 kHz magnetic field modulation with amplitude of 1.0 G at microwave power of 20 mW and 60 s sweep time. DMPO was used as superoxide radical ($O_2^{\bullet-}$) and hydroxyl radical ($^{\bullet}OH$) spin-trapping agent.

3.2.6 Toxicity towards *Vibrio fischeri*

The toxicity of the raw and photocatalytic treated OSPW was measured by the inhibition of the bacteria (*Vibrio fischeri,* also known as *Aliivibrio fischeri*) luminescence. Reagent phenol was used as a positive control. After 15 min of exposure to the OSPW at 15°C, the data of luminescence was recorded using microplate reader after 5 and 15 min, respectively.

3.3 Results and discussion

3.3.1 Optimization and reusability

ACA is a typical classical naphthenic acid (NA) and widely used to explore the degradation kinetics and mechanisms of NAs (Qin et al. 2019). Therefore, it was selected to evaluate the photocatalytic activity of the prepared catalysts. Fig. 3.1a shows the photocatalytic degradation curve of ACA as a function of time. A dark adsorption experiment was conducted for 30 min before the solar irradiation to achieve adsorption equilibrium. It is clear that the heterojunction catalysts were all more efficient than the pure Bi_2WO_6. With the increase in NiO and Ag content in the nanohybrid, the photocatalytic activity of the composite initially increased and then decreased. Specifically, 5% of NiO and 2% of Ag exhibited the best ACA photodegradation efficiency with reaction rates of 0.0301 and 0.0684 min^{-1}, respectively. The appropriate amount NiO and Ag anchored on the surface of Bi_2WO_6 could improve the transfer of photoexcited charges and restrain the recombination of photogenerated electron-hole pairs. However, the high composition of NiO and Ag deposited on the Bi_2WO_6 might reduce the number of exposed active sites and inhibit the transfer of photogenerated charge carriers, thus decreasing the photodegradation efficiency of the ACA. The photocatalytic degradation experiments were repeated three more times to assess the reusability and stability of the catalysts (Fig. 3.1b). The cycling experiment indicates that Ag/NiO/Bi_2WO_6 still retained its efficient photocatalytic properties after multiple runs. The slightly reduced catalytic efficiency was ascribed to the small mass loss during the inevitably incomplete photocatalyst collection and decreased adsorption capacity. Therefore, the results of characterization and degradation in this chapter were conducted using 2% Ag/5% NiO/Bi_2WO_6 unless otherwise specified.

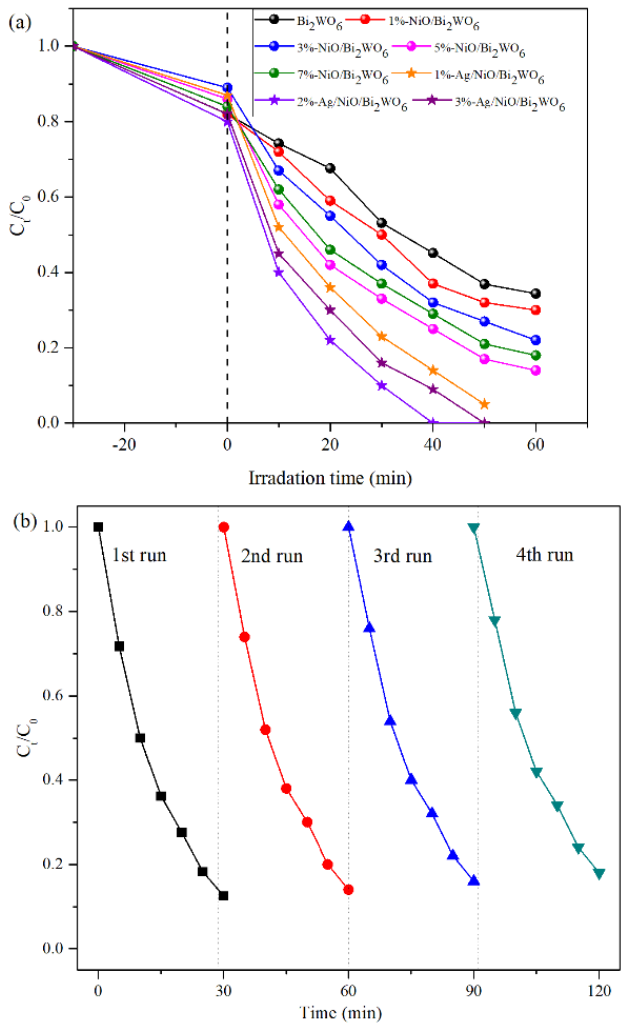

Fig. 3.8 (a) The photocatalytic degradation of ACA using the as-prepared catalysts; (b) cycle experiment of Ag/NiO/Bi_2WO_6 for ACA photocatalytic degradation.

3.3.2 Phase structure and composition

XRD was conducted to determine the phase purities and crystallographic structures of the as-prepared materials. The diffraction peaks of pure Bi_2WO_6 in Fig. 3.2 were well matched to the orthorhombic Bi_2WO_6 (JCPDS card No. 73–1126). The major diffraction peaks of NiO at 62.9°, 43.31° and 37.31° were ascribed to (2 2 0), (2 0 0) and (1 1 1) reflections of cubic NiO (JCPDS

card No. 47–1049), respectively. It can be seen that the NiO/Bi_2WO_6 composites retained the crystalline structure of the pristine Bi_2WO_6, which indicated that the crystal structure could not be changed by thermal treatment process. The diffraction peak at 38.1° recorded in the XRD pattern of Ag/Bi_2WO_6 composites was in accordance with the cubic Ag (1 1 1) phase (JCPDS card No. 04-0783). Furthermore, compared with the pure Bi_2WO_6 and NiO, there were no new impurity diffraction peak in the heterojunction materials. The XRD results confirmed the formation of a highly pure ternary crystal structure.

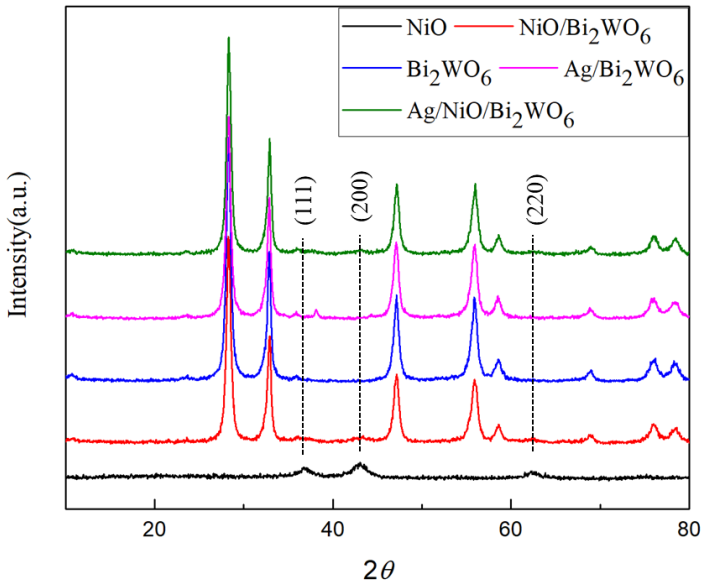

Fig. 3.9 XRD patterns of NiO, Bi_2WO_6, NiO/Bi_2WO_6, Ag/Bi_2WO_6 and Ag/NiO/Bi_2WO_6.

3.3.3 Morphology structure analyses

SEM and TEM were conducted to explore the comprehensive information on the microstructures and morphology of the photocatalysts. As depicted in Fig. 3.3a, pure Bi_2WO_6 exhibited a flower-like spherical superstructure with a diameter around 4 μm, which was assembled by plenty of nanoplates, forming interspace of different sizes, resulting in the increased specific surface area. Meanwhile, the removal rate of target pollutant increased with increasing

surface area. Although the surface of Ag/NiO/Bi_2WO_6 (Fig. 3.3b) was rougher than pure Bi_2WO_6 (Fig. 3.3a), their size and shape remained the same. Bright-field scanning transmission electron microscopy (BF-STEM) (Fig. 3.3c) and high-angle annular dark-field (HAADF)-STEM (Fig. 3.3d) also conformed the spherical superstructure of Ag/NiO/Bi_2WO_6. The enlarged image of Ag/NiO/Bi_2WO_6 is shown in Fig. 3.3e, f, g, which indicates that Ag nanoparticles were successfully and tightly decorated on the Bi_2WO_6. HAADF-STEM elemental mapping (Fig. 3.3h) further confirmed that Bi, W, Ni and O were evenly distributed throughout the material, whereas Ag was distributed as nanoparticles. HRTEM images (Fig. 3.3i-l) also revealed the coexistence of Ag, NiO and Bi_2WO_6. However, due to the different heights of the sample, the lattice fringes in different regions could not be clearly observed at the same time. Therefore, Fig. 3.3j-l present lattice fringes focused on different parts of catalyst, corresponding to Bi_2WO_6 (1 1 3), Ag (1 1 1) and NiO (2 0 0), respectively. These results proved the formation of intimate interfaces between the Ag, NiO and Bi_2WO_6 rather than simple physical mixing, which could avoid the recombination of photoinduced charge carriers at the tight heterojunction interface of Ag/NiO/Bi_2WO_6.

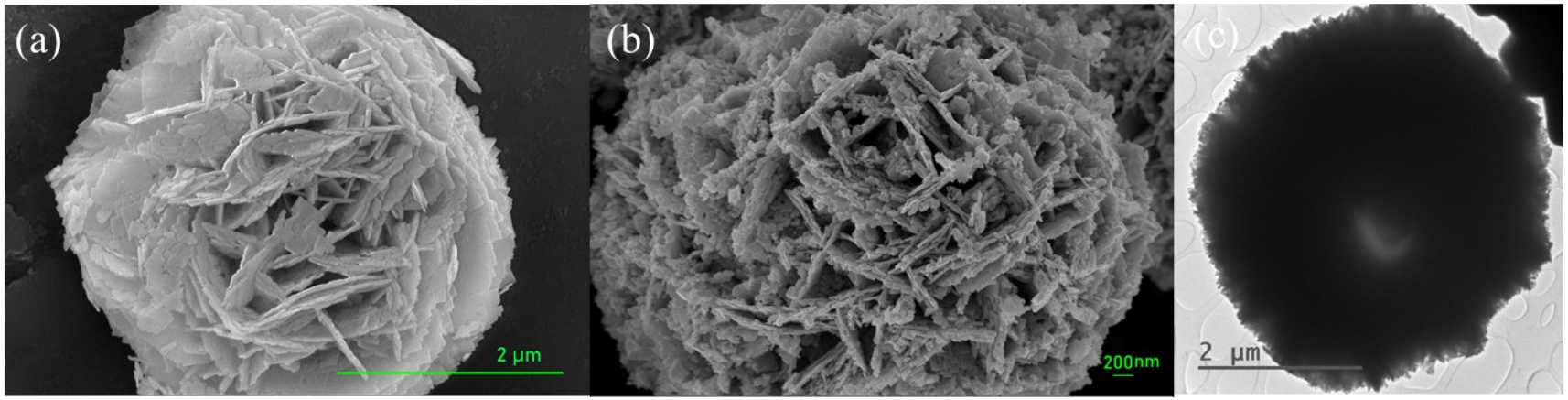
(a)
2 μm
(b)
200nm
(c)
2 μm

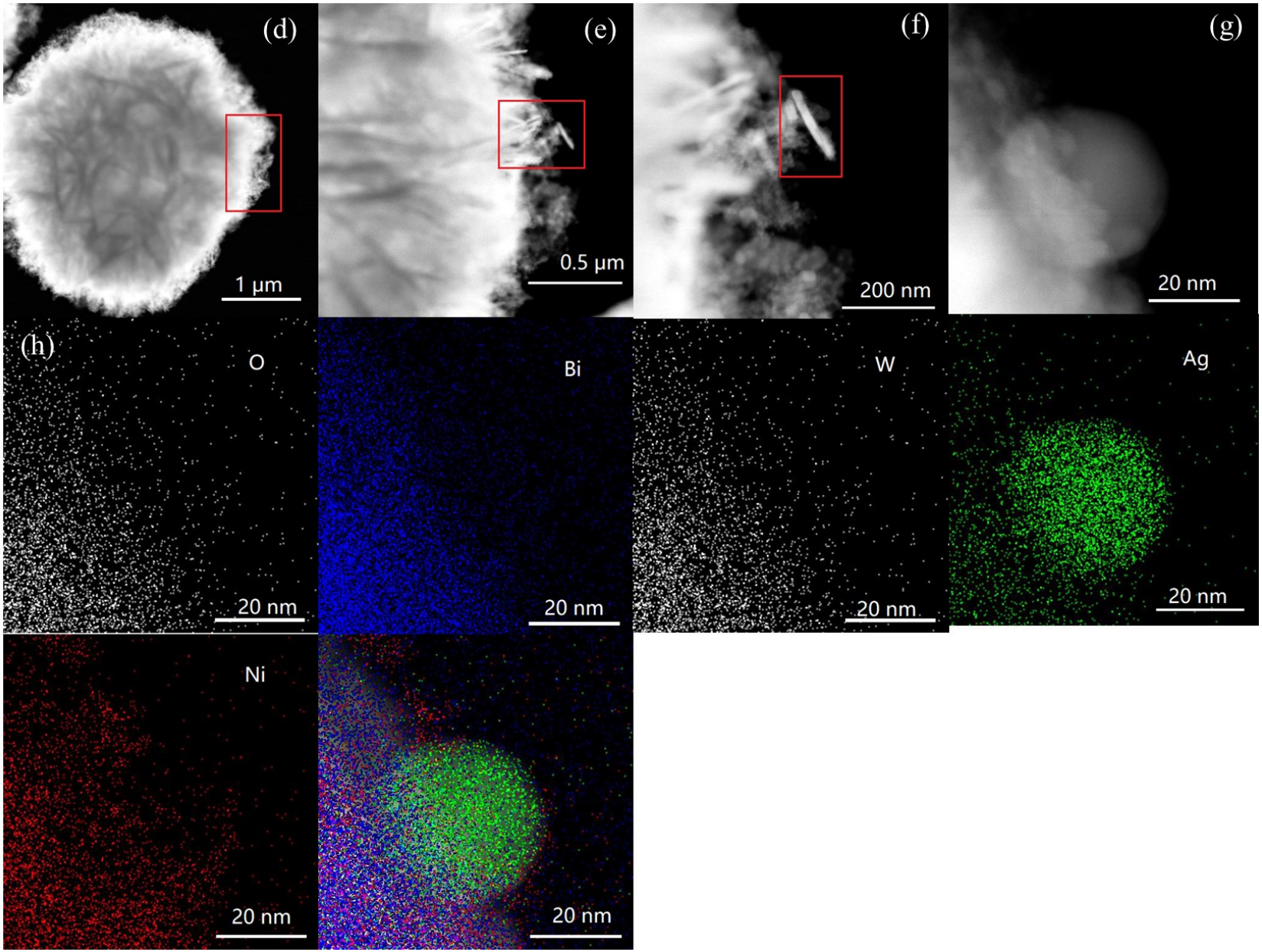
(d)
1 μm
(e)
0.5 μm
(f)
200 nm
(g)
20 nm
(h)
O
20 nm
Bi
20 nm
W
20 nm
Ag
20 nm
Ni
20 nm
20 nm

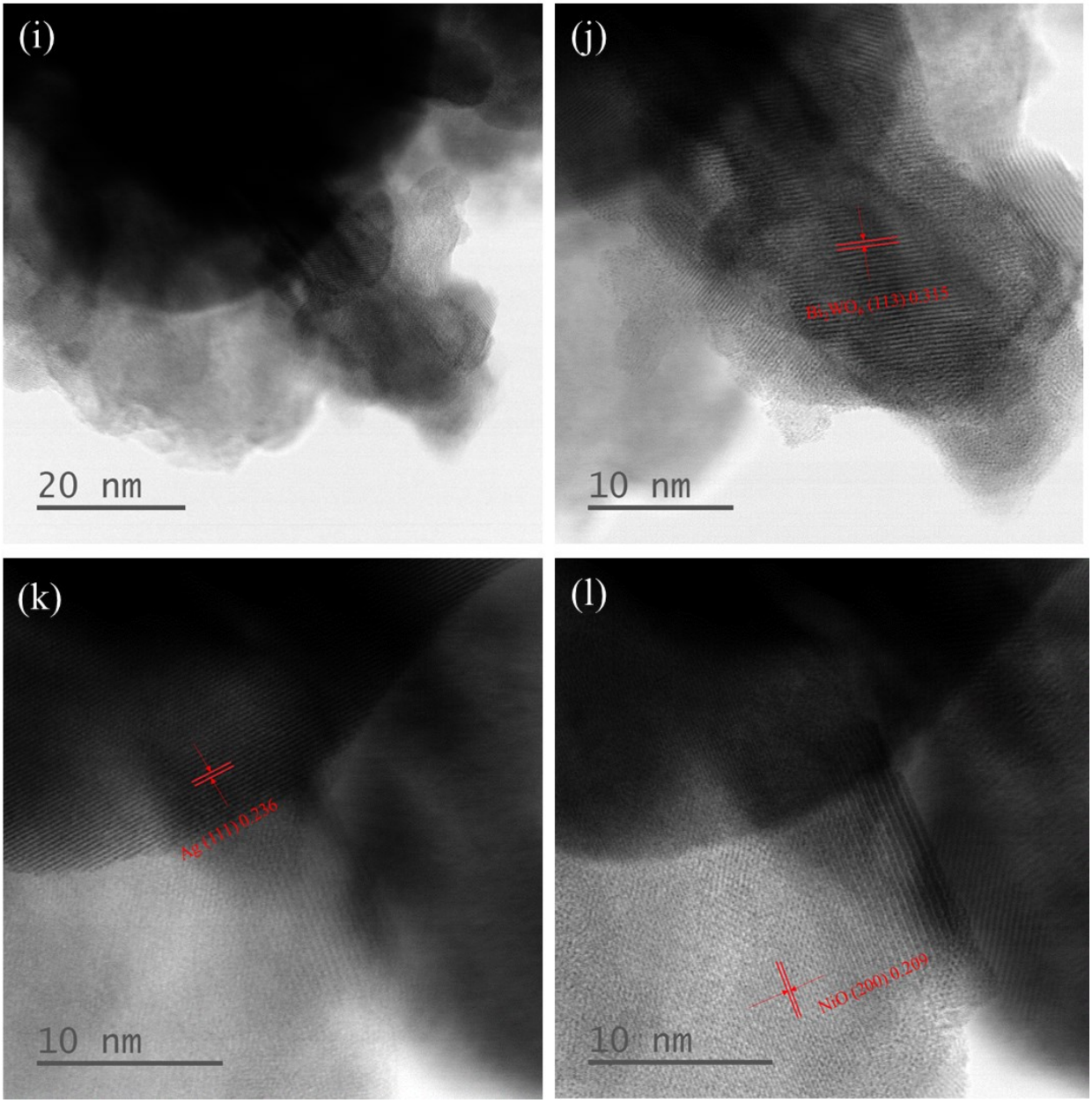

Fig. 3.10 SEM of (a) Bi_2WO_6 and (b) Ag/NiO/Bi_2WO_6; (c) BF-STEM of Ag/NiO/Bi_2WO_6; (d) HAADF-STEM of Ag/NiO/Bi_2WO_6; (e) the enlarged image of the selected area in d; (f) the enlarged image of the selected area in e; (g) the enlarged image of the selected area in f; (h) corresponding element mapping of Ag/NiO/Bi_2WO_6: O, Bi, W, Ag, Ni and overlap of all elements; (i-l) HRTEM of Ag/NiO/Bi_2WO_6 focusing on different areas.

3.3.4 Chemical composition analysis

The surface chemical states of pure Bi_2WO_6 and Bi_2WO_6 /NiO/Ag were explored by XPS. Fig. 3.4a presents the survey scan spectra. Bi, W, O, C elements could be observed in spectrum of Bi_2WO_6, while Ni and Ag were detected in Bi_2WO_6 /NiO/Ag, which implies that the incorporation of NiO and Ag onto Bi_2WO_6 was successful. The corresponding high-resolution XPS spectra of Bi 4f, W 4f, O 1s, Ag 3d and Ni 2p are shown in Fig. 3.4b-f. The binding energies of Bi $4f_{7/2}$ and Bi $4f_{5/2}$ located at 158.9 and 164.3 eV belong to the metallic Bi^{3+} in Bi_2WO_6. For Bi_2WO_6 /NiO/Ag, peaks located at 158.6 and 163.8 eV were ascribed to Bi^{3+} (Meng et al. 2021). As exhibited in Fig. 3.4c, the characteristic peaks of 35.3 and 37.3 eV for Bi_2WO_6 and 34.8 and 36.9 eV for Bi_2WO_6/NiO/Ag were accorded with the binding energies of W $4f_{7/2}$ and W $4f_{5/2}$ of W^{6+} (Meng et al. 2021, Zhou et al. 2019). The O 1s spectrum for Bi_2WO_6 was further deconvoluted into three peaks of 529.9, 530.6 and 532.2eV and in accordance with lattice oxygen (W-O, Bi-O) and O species in adsorbed H_2O (O-H), respectively (Yang et al. 2021). The new peak that appeared in O 1s spectrum of Bi_2WO_6 /NiO/Ag was arisen from Ni-O bonds (Liu et al. 2019). Moreover, slighted shifts in the banding energy of Bi, W, O were recorded in the spectra of Bi_2WO_6 /NiO/Ag, indicating the different electron density induced by interfacial interaction and electron transfer in the heterojunction (Meng et al. 2021, Tang et al. 2018). The characteristic peak of Ag $3d_{5/2}$ was located at 367.5 eV and Ag $3d_{3/2}$ peak was at 373.6 eV, respectively (Fig. 3.4e) (Jiang et al. 2020). The peak located at 872.41 eV and 853.35 eV were assigned to Ni $2p_{1/2}$ and Ni $2p_{3/2}$, demonstrating the presence of Ni^{2+} in NiO. Two satellite peaks at 860.85 eV and 878.85 eV were arisen from shake-up. The peak of Ni $2p_{3/2}$ at 855.15 eV could be designated as Ni^{3+} in Ni_2O_3 (Cao et al. 2019). These findings further confirmed the successful introduction of NiO and Ag, which will increase the photocatalytic performance through the separation of e^- and h^+.

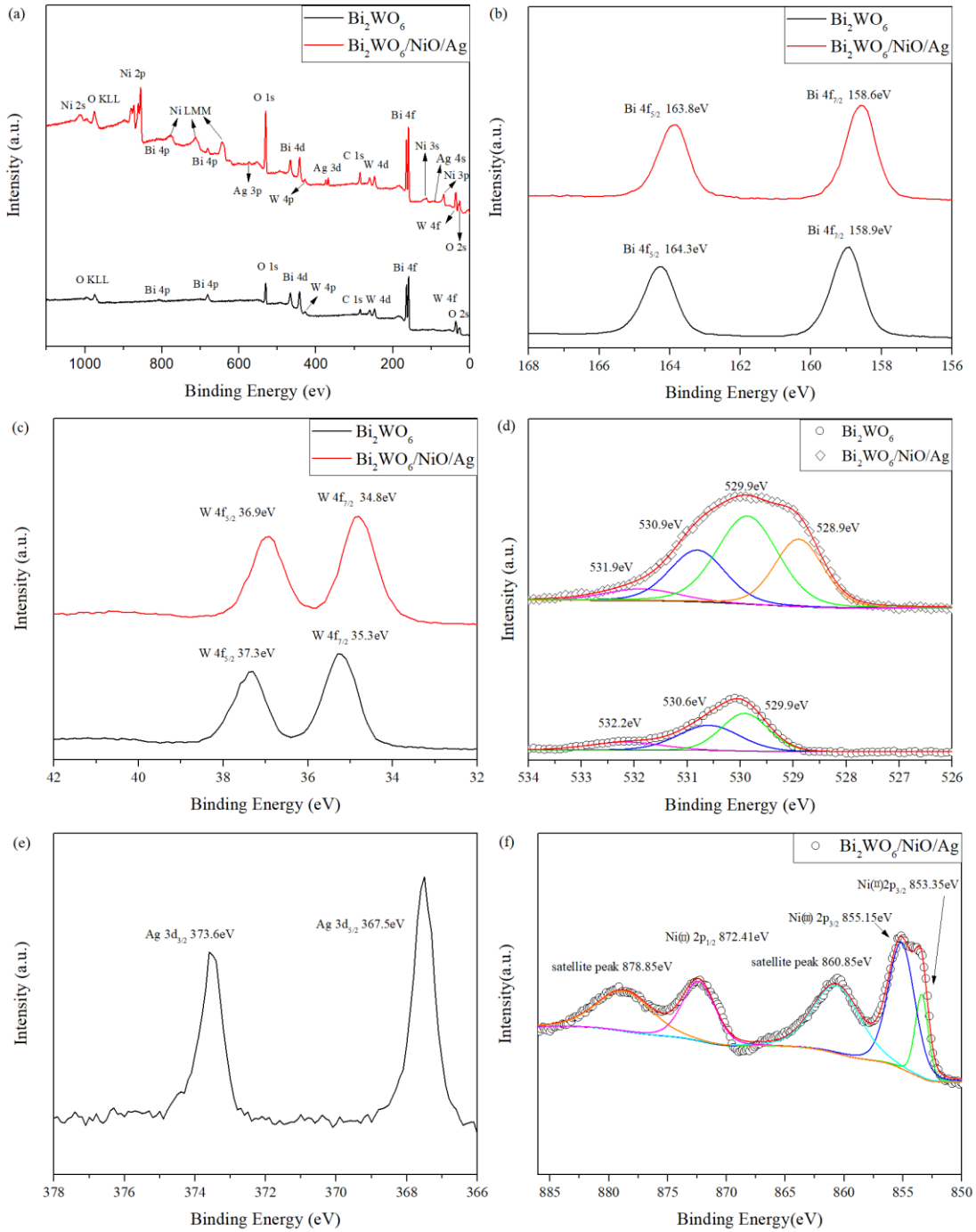

Fig. 3.11 XPS spectra of Bi_2WO_6 and Bi_2WO_6 /NiO/Ag: (a) Survey scan; (b) Bi 4f; (c) W 4f; (d) O 1s; (e) Ag 3d; and (f) Ni 2p.

3.3.5 Optical and photoelectrical property analysis

The trapping, migration and transfer of the photoinduced holes and electrons on the surface of catalysts were studied by photoluminescence (PL) emission spectra and photocurrent responses. Generally, electron was promoted from valence band (VB) to conduction band (CB) under light irradiation. However, the photo-generated charge carriers could simultaneously recombine to release the energy in the form of fluorescence emission, leading to the decreased photocatalytic efficiency. Therefore, the higher intensity of PL signifies the lower separation rate of charge carriers. As shown in the Fig. 3.5(a), the intensity of pure Bi_2WO_6 was relatively high due to the intrinsic low quantum yield. While the loads of Ag and NiO on Bi_2WO_6 could decrease the PL intensity, indicating that the formation of heterojunction facilitated the separation of charge carriers. Fig. 3.5(b) displays both the dark current and photocurrent of Bi_2WO_6, NiO/Bi_2WO_6 and NiO/Ag/Bi_2WO_6. The maximum photocurrent density of NiO/Ag/Bi_2WO_6 compared with other catalysts was recorded, suggesting a more efficient charge transfer and separation efficiency as well as longer lifetime of the charge carriers (Guo et al. 2016). The enhanced current density of NiO/Ag/Bi_2WO_6 perhaps originated from charge transfer between NiO, Ag and Bi_2WO_6 through Z-scheme, which benefits the separation of charge carriers.

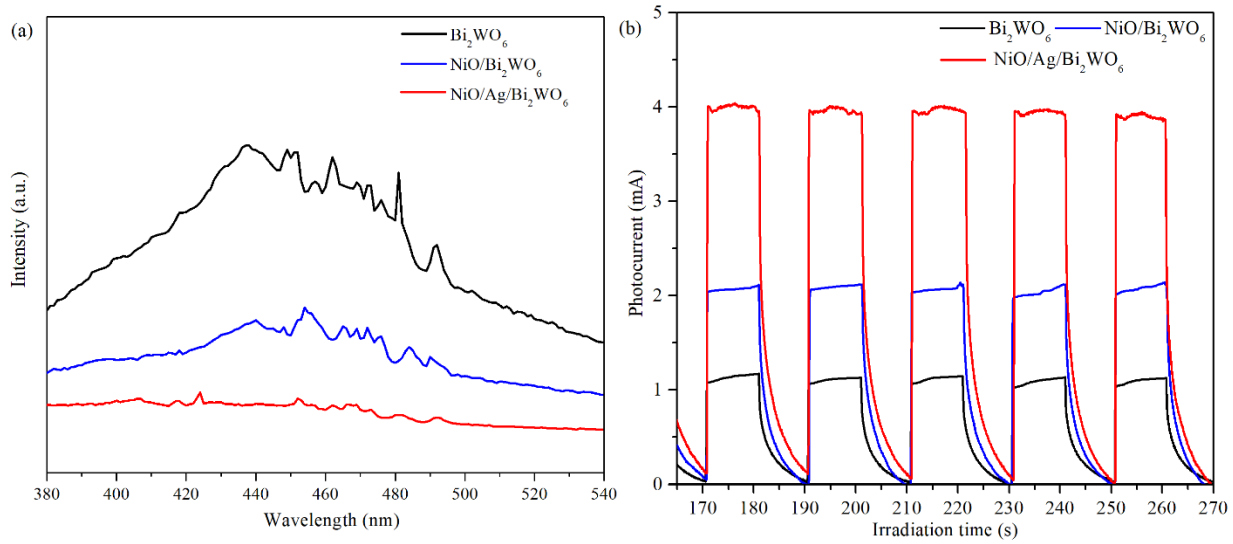

Fig. 3.12 (a) Photoluminescence spectra of samples; (b) Transient photocurrent responses of samples

3.3.6 Active species

Generally, when semiconductor photocatalyst adsorbs photons with energy larger than E_g, the photoinduced e^- and h^+ could react with molecular oxygen and H_2O to produce free radicals. These free radicals were investigated through quenching experiments and detected using EPR. The radical trapping experiments were performed to explore the major oxidative substances during the photocatalytic treatment of ACA. As depicted in Fig. 3.6a, AO, TEMPOL, $K_2Cr_2O_7$ and IPA were used as h^+, $O_2^{\bullet-}$, e^- and $^{\bullet}OH$ scavengers, respectively. The degradation rate of ACA was significantly inhibited (71.2%) after the addition of AO, indicating that h^+ was the main oxidizing species. The inhibitory effects of TEMPOL and IPA were 45.2% and 29.7% for the degradation of ACA, demonstrating that $^{\bullet}OH$ and $O_2^{\bullet-}$ were generated and participated in the photocatalytic degradation. Although O_2 was transformed into $O_2^{\bullet-}$ by photoinduced e^-, the electron scavenger $K_2Cr_2O_7$ had less effect on the degradation efficiency of ACA than TEMPOL. $K_2Cr_2O_7$ could trap electrons to inhibit the recombination of e^- and h^+, leaving more holes to oxidize ACA.

In order to further probe the radical generation and contribution during the photocatalytic process, the EPR spectra with DMPO were used (Fig. 3.6b-c). No peaks were detected for either DMPO-$O_2^{\bullet-}$ or DMPO-$^{\bullet}OH$ in the dark. Under light irradiation, Ag/NiO/Bi_2WO_6 produced both $^{\bullet}OH$ and $O_2^{\bullet-}$, which agreed well with the findings of the quenching tests. Since $^{\bullet}OH$ and $O_2^{\bullet-}$ are derived from isolated photoinduced e^- and h^+, respectively, the higher peak intensities for $^{\bullet}OH$ and $O_2^{\bullet-}$ demonstrated that Ag/NiO/Bi_2WO_6 could improve the separation efficiency of the photogenerated electron-hole pairs in comparison with pure Bi_2WO_6, leading to a boosted photocatalytic performance.

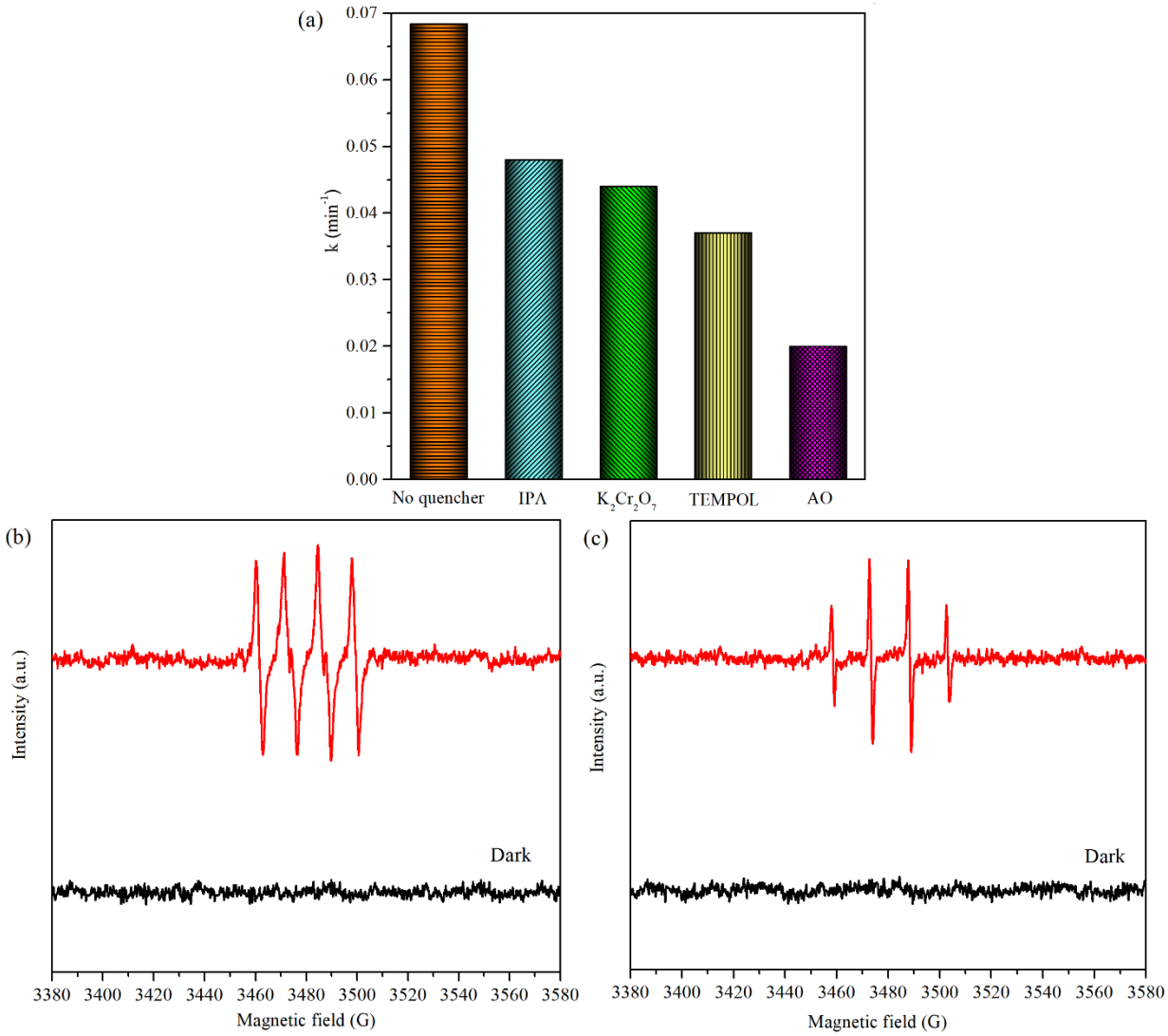

Fig. 3.13 (a) Trapping measurement with 2mM scavengers (IPA→·OH, $K_2Cr_2O_7$→e^-, TEMPOL→·O_2^-, AO→h^+) for photodegradation of ACA using Ag/NiO/Bi_2WO_6; DMPO-EPR spin-trapping spectra of Ag/NiO/Bi_2WO_6 for detection of (b) ·O_2^- and (c) ·OH.

3.3.7 Energy band structure

As illustrated in Fig. 3.7a, the optical properties of pure Bi_2WO_6, NiO, NiO/Bi_2WO_6 and Ag/NiO/Bi_2WO_6 composites were detected using a UV–vis diffuse reflectance spectrometer. The

absorption edge of pure Bi_2WO_6 is 430 nm, while NiO shows considerable adsorption from 200 to 800 nm. Moreover, the optical adsorption of NiO/Bi_2WO_6 and Ag/NiO/Bi_2WO_6 composites were significantly increased in comparison with pure Bi_2WO_6, indicating that the introduction of NiO and Ag onto Bi_2WO_6 obviously widened the absorption range of visible light for the catalysts. The increased visible light absorption range is due to the SPR effect induced by Ag nanoparticles, and the bandgap changes through the addition of NiO and Ag. The band gap (E_g) energies were estimated based on the equation $\alpha h\upsilon = A (h\upsilon - E_g)^n$, where n=0.5 for direct semiconductor and n=2 for indirect semiconductor. Both NiO and Bi_2WO_6 are indirect semiconductors. Therefore, as can be seen from Fig. 3.7b, E_g of as-prepared samples could be estimated from Tauc's plot, which are approximately 2.76, 3.21, 2.62 and 2.35 eV for pure Bi_2WO_6, NiO, NiO/Bi_2WO_6 and Ag/NiO/Bi_2WO_6, respectively. These results revealed that Ag and NiO in the hybrids are markedly reduce the band gap of the catalysts.

The VB potential of Bi_2WO_6 and NiO were obtained by VB-XPS. As illustrated in Fig. 3.8, the VB of Bi_2WO_6 and NiO were estimated as 2.35 and 0.3 eV. The CB values were calculated accordingly as -0.41 and -2.91. To further explore the electron properties of the catalysts, the density of states (DOS) and band structures of Bi_2WO_6 and NiO were calculated by density function theory (DFT) with the CASTEP package in Fig. 3.9. The calculated E_g of Bi_2WO_6 was 2.754 eV, which was consistent with the experimental value of 2.76 eV. The VB edge of Bi_2WO_6 was composed of the hybridization of Bi 6s and O 2p orbitals. However, CB edge was mainly made up of W 5d orbit. The calculated E_g of NiO was 3.419 eV, which was similar with our experimental value of 3.21 eV. The CB edge of NiO was contributed by NiO 3d 4s 3p orbit, whereas the VB edge mainly consisted of Ni 3d 3p, O 2p.

Based on these results, as shown in Fig. 3.10, in a typical Z-scheme structure, the CB of Bi_2WO_6 was negative than the Fermi level of metallic Ag (0.14 eV); therefore, the photoinduced electrons could be easily transferred from CB of Bi_2WO_6 to Ag. After that, the electrons at Ag would migrate to the VB of NiO, eventually recombining with h^+ through a direct electron migration. During this process, the improved electric field intensity around the interface of Ag nanoparticles prompted the interfacial electron transfer and surface electron excitation due to the SPR effect. Meanwhile, the photogenerated holes stayed at the more positive Bi_2WO_6 VB, and electrons were retained in the more negative NiO CB, leading to the production of ·OH and $O_2^{\bullet-}$. Subsequently, the produced ·OH, $O_2^{\bullet-}$ and h^+ could oxidize NAs in OSPW.

In order to confirm the electron transfer mechanism, *in-situ* irradiated XPS were performed. As illustrated in Fig. 3.11 a and b, on one hand, under irradiation, the binding energies of Bi 4f and W 4f in Bi_2WO_6 increased about 0.2 eV in comparison with the values measured in dark. On the other hand, the peak of Ni 2p (Fig. 3.11c) in NiO negatively shifted by about 0.2 eV, compared with the values tested in dark, which implied a decreased electron cloud density of Bi_2WO_6 and increased electron cloud density of NiO. The above *in-situ* irradiated XPS results indicate that the electrons transferred from Bi_2WO_6 to NiO under light illumination.

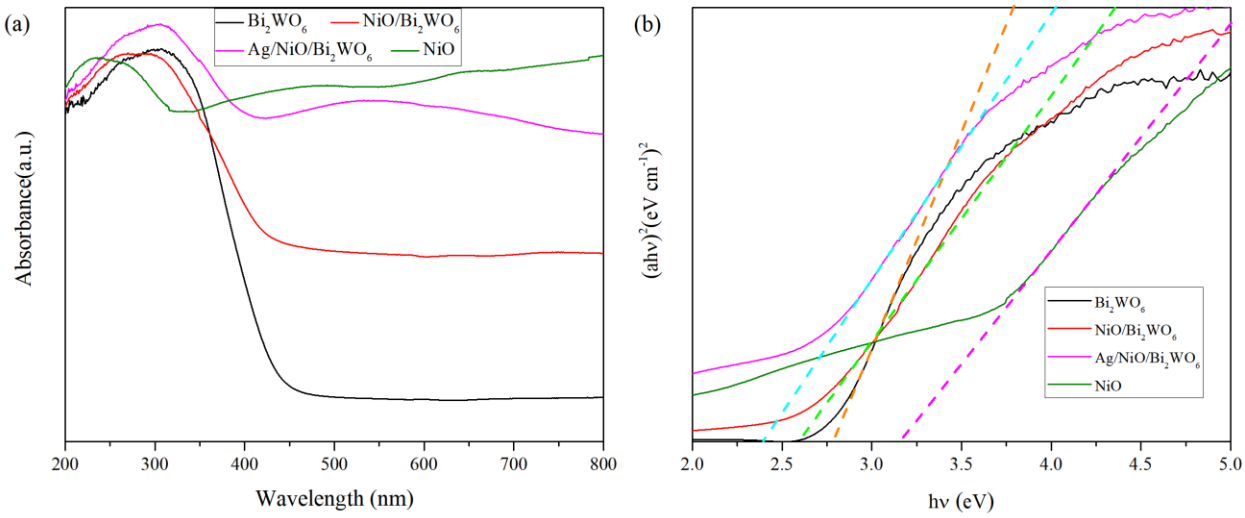

Fig. 3.14 (a) UV–vis diffuses reflectance spectra and (b) Tauc's bandgap plots of Bi_2WO_6, NiO/Bi_2WO_6, $Ag/NiO/Bi_2WO_6$, and NiO.

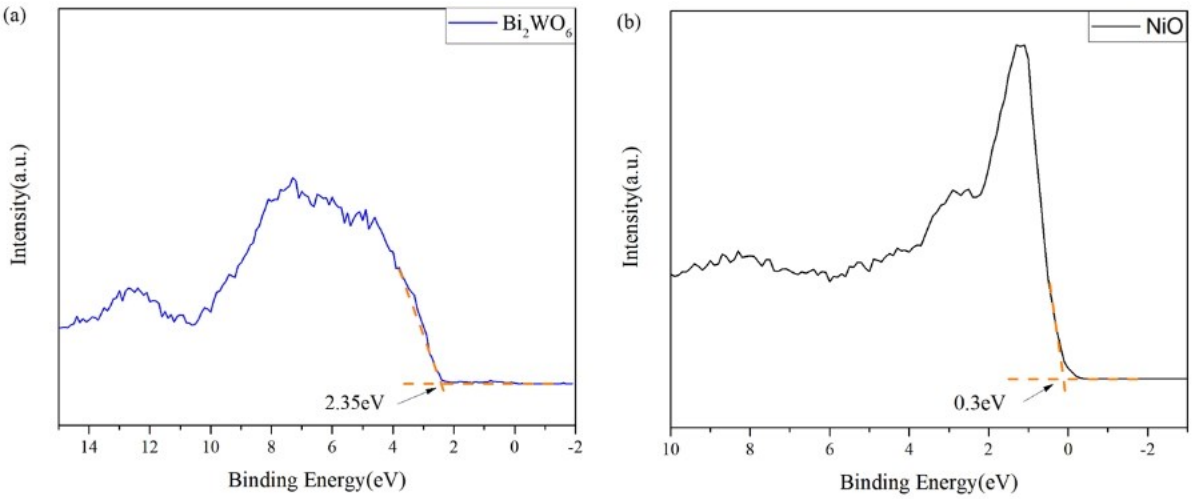

Fig. 3.8 VB-XPS of (a) Bi_2WO_6 and (b) NiO

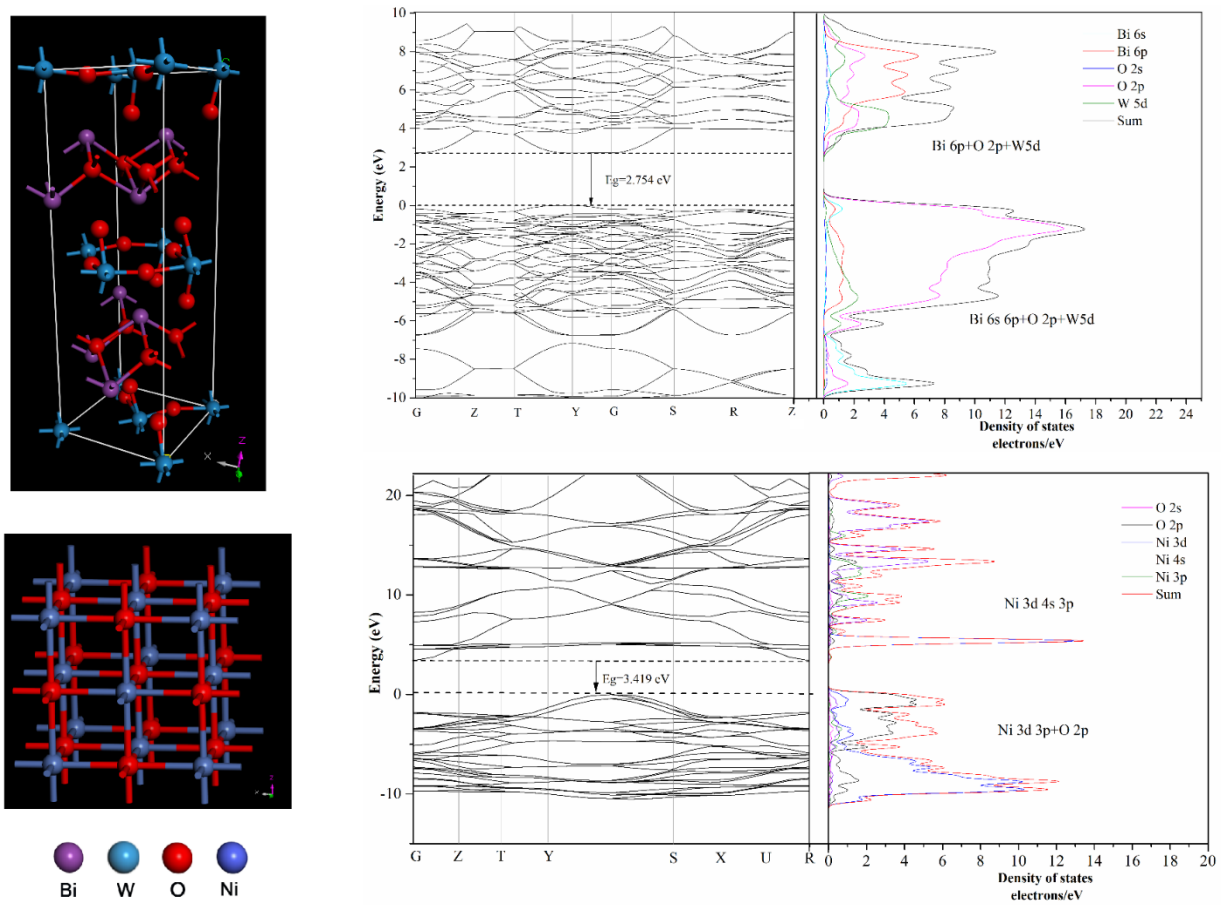

Fig. 3.9 Crystal structures, calculated band structures, density of states (DOS) of Bi_2WO_6 and NiO.

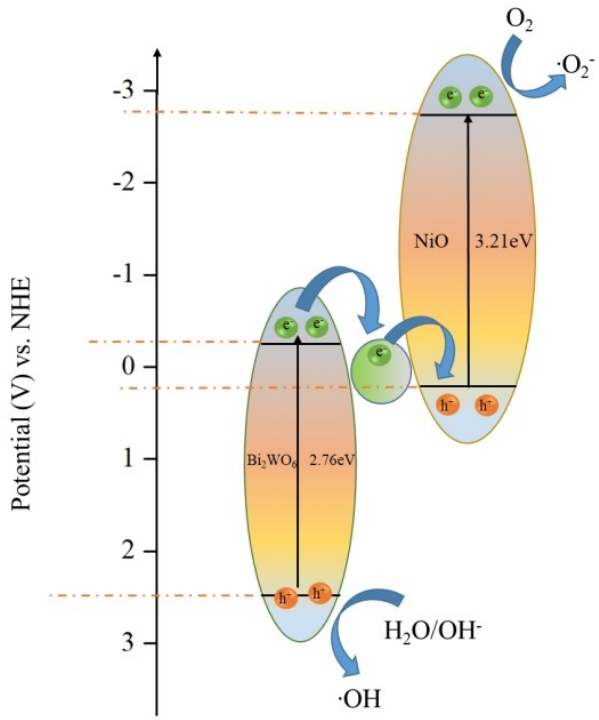

Fig. 3.10 Schematic illustration of proposed photocatalytic mechanisms: the Z-scheme structure.

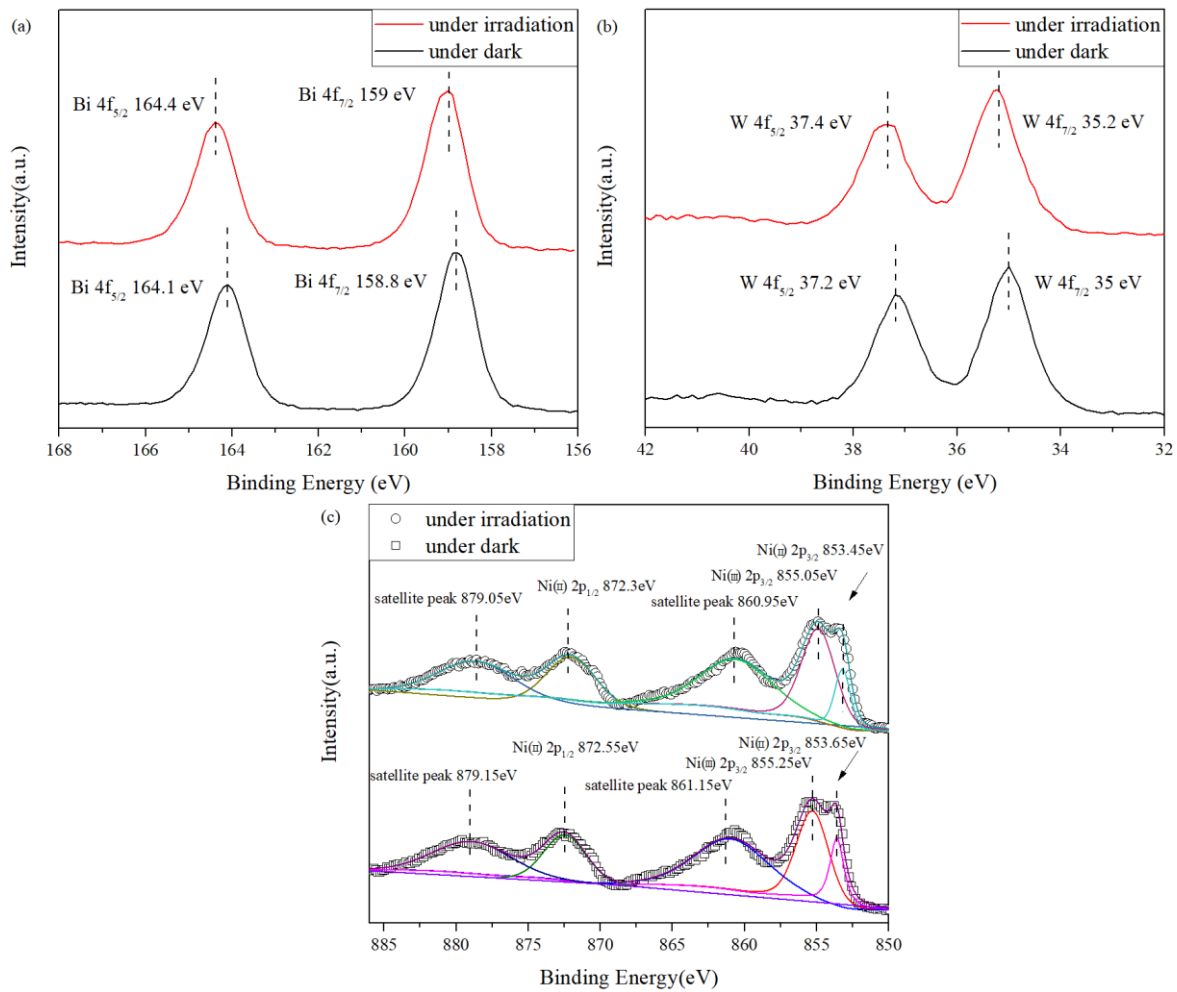

Fig. 3.11 *In-situ* irradiated XPS of Bi, W and Ni

3.3.8 Photocatalytic treatment of OSPW

3.3.8.1 Aromatics degradation

A molecule with a low-energy π/π* transition or n/π* transition is capable of emitting fluoresce when irradiated by UV light (Williams et al. 1983). Therefore, SFS was used to detect fluorophore compounds, which are aromatics containing single-ring or fused rings in OSPW. As depicts in Fig. 3.12, the predominated peak at 267 nm represents the intensity of single-ring aromatics. The other two peaks at 310 nm and 330 nm represent aromatics with two and three fused rings, respectively. The peak areas of all three peaks were generally reduced after photocatalytic treatment by different catalysts. Specifically, after 6 h photocatalytic treatment by Ag/NiO/Bi_2WO_6, all the three peaks were completely removed. The removal rates were 3.4%, 83.5%, 83.3% by Bi_2WO_6; 48.8%, 90.6%, 88.7% by NiO/Bi_2WO_6 for aromatics with one ring, two and three fused rings, respectively. The superior photocatalytic performance for the treatment of OSPW by Bi_2WO_6/NiO/Ag are attributed to the unique Z-scheme electron transfer among NiO, Ag and Bi_2WO_6. The successful separation of e^- and h^+ pairs contribute to the higher production of ·OH, $O_2^{\bullet-}$ and h^+, which are oxidative species reacting with aromatics. It was reported that the generation of $^{\bullet}OH$, $O_2^{\bullet-}$ and h^+ could induce the oxidation of the aromatic functional group through electrophilic addition on the aromatic rings, also, hydrogen abstraction through $^{\bullet}OH$ at the alkyl branches (von Sonntag and von Gunten 2012). Therefore, ring opening and electron withdrawing groups were substituted on aromatic rings, resulting in the loss or weaken of aromaticity of aromatics. The low degradation rate of single-ring aromatics (Fig. 3.12) was due to the transformation of aromatics with multiple rings into single-ring aromatics such as benzoquinone or hydroquinone (Oturan and Aaron 2014). In addition to being oxidized by $^{\bullet}OH$, $O_2^{\bullet-}$ and h^+,

aromatics could also be degraded by direct and sensitized photolysis during the irradiation, with polyaromatics as photosensitizer.

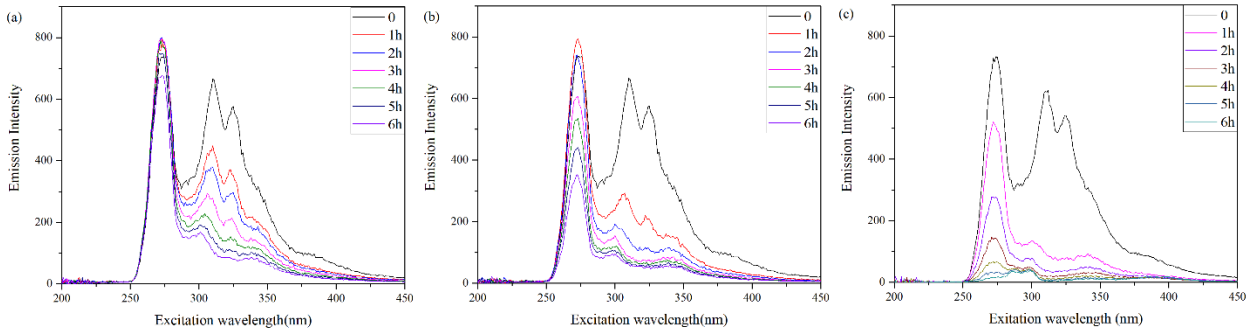

Fig. 3.12 Synchronous fluorescence spectra (SFS) of photocatalytic treatment of OSPW by (a) Bi_2WO_6, (b) Bi_2WO_6/NiO and (c) Bi_2WO_6/NiO/Ag.

3.3.8.2 NAs degradation

According to the retention time in LC and the drift time in drift-gas, NAs with different polarity and molecular volume could be separated. As displayed in Fig. 3.13, there were three clusters of NAs illustrated in the IMS spectra of OSPW, namely, classical NAs (O_2-NAs), oxidized NAs (oxy-NAs), and sulfur containing NAs (S-NAs). The highest intensity of oxy-NAs indicates that they account for the majority of raw OSPW. Compared with raw OSPW, significantly degradation of S-NAs and O_2-NAs and negligible decrease of oxy-NAs could be observed after 6 h of photocatalytic treatment by Bi_2WO_6 and Bi_2WO_6/NiO. Previous study (Meng et al. 2021) reported that the initial oxidation of S-NAs is usually through the addition of O via electrophilic addition on S atom or heterocyclic ring. For O_2-NAs, hydroxyl-substituted or ketone by-products were produced during the reaction with dissolved oxygen at heterocyclic ring (Abdalrhman et al. 2021). Thus, the limited degradation of oxy-NAs maybe because of the slow degradability of the oxy-NAs or owing to the production of new oxy-NAs from the degradation of S-NAs and O_2-NAs.

In contrast, oxy-NAs were partially removed after 6 h of photocatalytic treatment using Bi_2WO_6/NiO/Ag, indicating the improved photocatalytic performance through the construction of Z-scheme heterojunction. The separation of electrons and h^+ and generation of more reactive species could explain this finding.

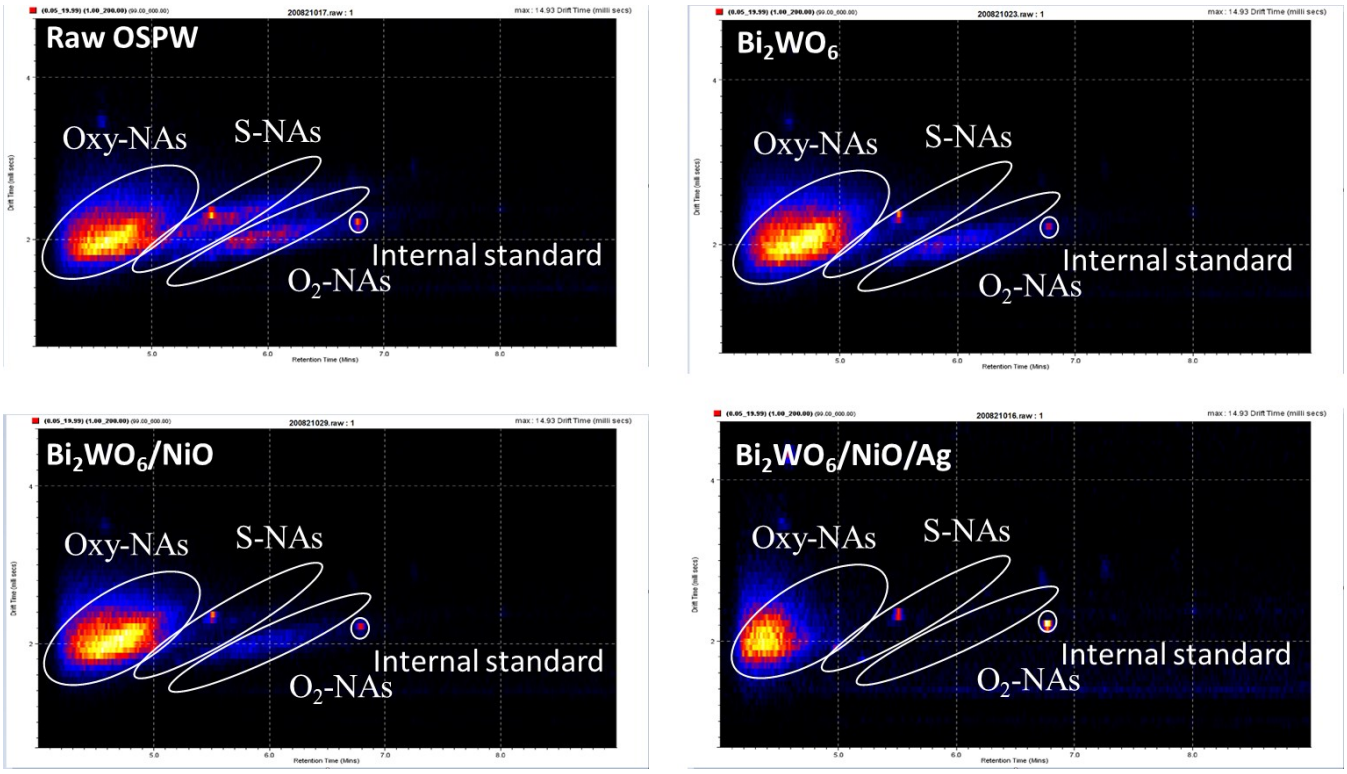

Fig. 3.13 Profiles of ion mobility separation spectra for the untreated and treated OSPW samples. (a) Raw OSPW, photolytic treated OSPW by (b) Bi_2WO_6, (c) Bi_2WO_6/NiO, and (d) Bi_2WO_6/NiO/Ag.

In general, classical NAs were considered to be the main toxic NAs in the OSPW. For example, the acute toxicity data of 15 min Microtox bioassay and 96 h fathead minnow embryo lethality showed that the most toxic fraction is classical NAs (Morandi et al. 2015). The overall distribution of NAs with respect of the DBE (hydrogen deficiency) and carbon numbers before and after treated with the Bi_2WO_6, Bi_2WO_6/NiO and Bi_2WO_6/NiO/Ag are illustrated in Fig. 3.14-

3.18. The concentration of the O_2-NAs and oxy-NAs (the number of O ranging from 3-6) in raw OSPW was 29.5, 18.5, 15.4, 6.3 and 1.4 mg L^{-1}, respectively. The distributions of raw OSPW O_2-NAs based on DBE and carbon number are showed in Fig. 3.14a and Table 3.3. The most abundant species in the O_2-NAs were those with carbon number ranging from 13 to 18 which account for 80.2% of the total O_2-NAs, and O_2-NAs with two and three rings (DBE = 4 and 6) account for 47.5% of the total O_2-NAs (Zhang et al. 2016). The concentration of the O_2-NAs was 29.5 mg L^{-1} in the raw OSPW, and was reduced to 23.7, 15.3 and 3.37 mg L^{-1} after treatment with Bi_2WO_6, Bi_2WO_6/NiO and Bi_2WO_6/NiO/Ag, respectively. When the O_2-NAs removal was corelated as a function of the DBE and carbon number, a clear enhanced removal efficiency of classical NAs by Bi_2WO_6 and Bi_2WO_6/NiO could be recorded with the increasing of DBE and carbon number (Fig. 3.19). Same results were also previously reported for ozone treated OSPW. The reason may be attributed to the increasing available sites of NAs when DBE and carbon number raised (Wang et al. 2016). Whereas the Bi_2WO_6/NiO/Ag showed almost no bias in the removal of NAs regarding to the carbon number and DBE (Fig. 3.19).

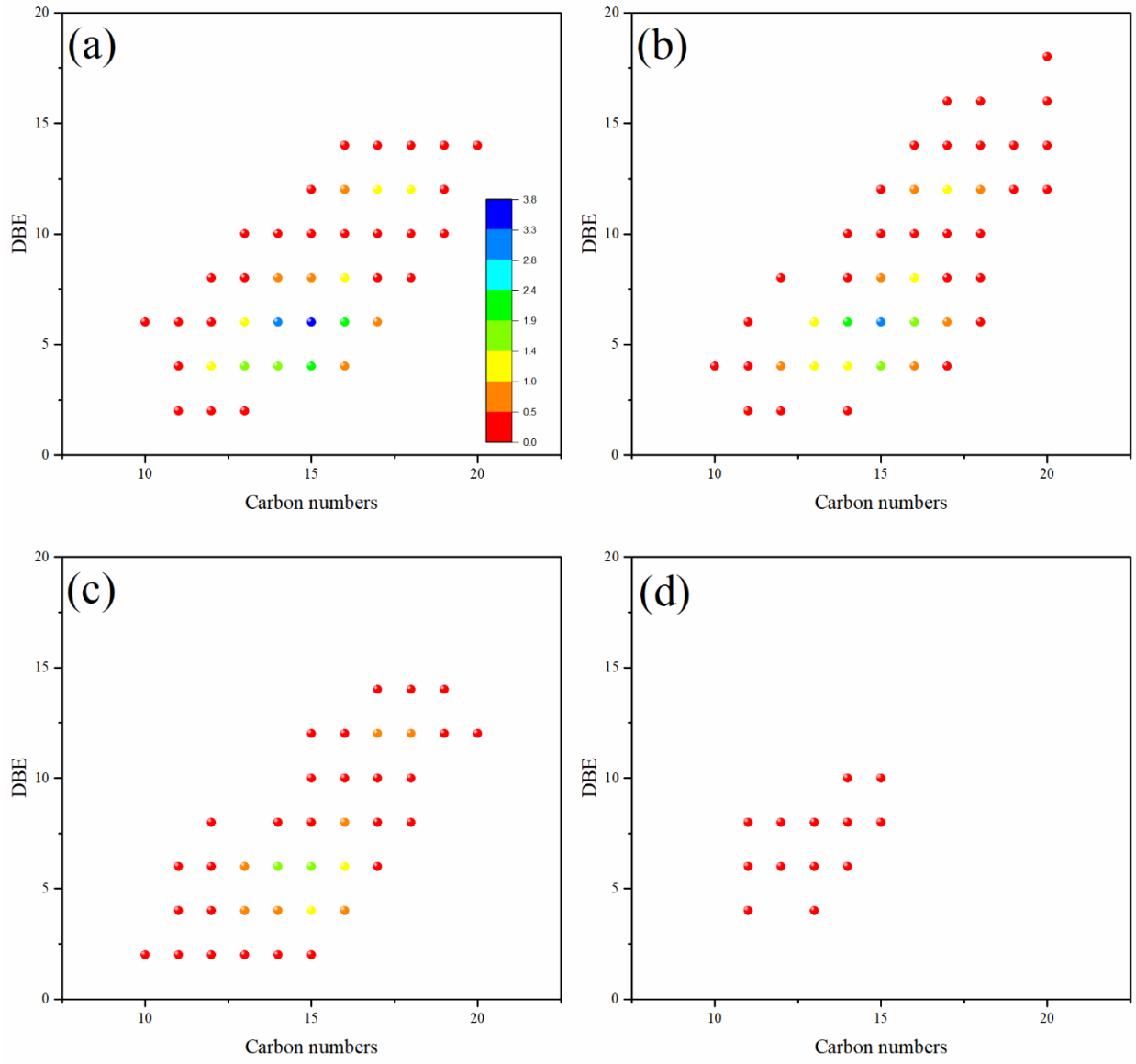

Fig. 3.14 Classical NA distribution in (a) raw OSPW and OSPW treated with (b) Bi_2WO_6, (c) Bi_2WO_6/NiO, and (d) Bi_2WO_6/NiO/Ag after 180 min illumination.

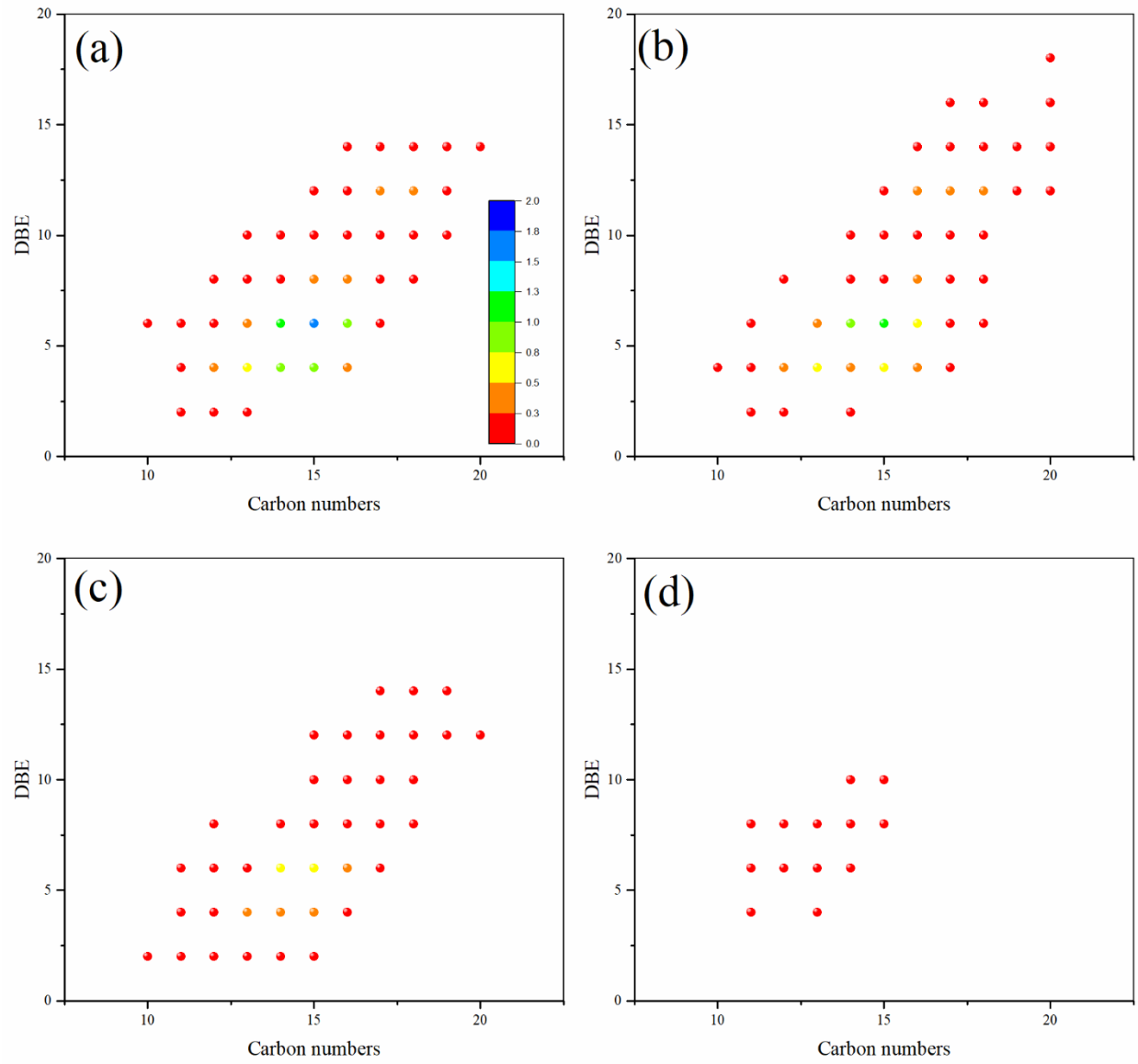

Fig. 3.15 O_3-NA distribution in (a) raw OSPW and OSPW treated with (b) Bi_2WO_6, (c) Bi_2WO_6/NiO, and (d) Bi_2WO_6/NiO/Ag after 180 min illumination.

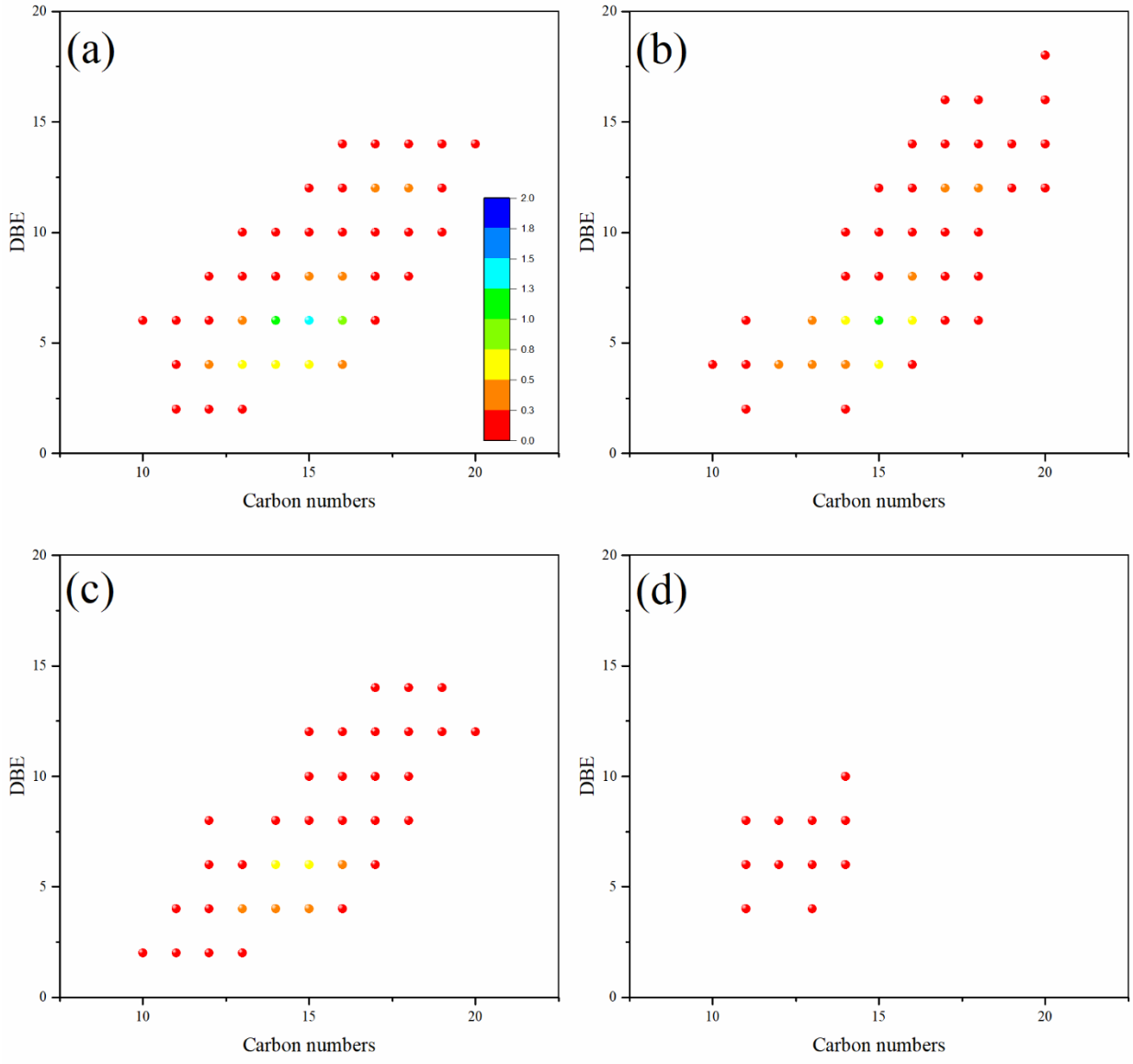

Fig. 3.16 O_4-NA distribution in (a) raw OSPW and OSPW treated with (b) Bi_2WO_6, (c) Bi_2WO_6/NiO, and (d) Bi_2WO_6/NiO/Ag after 180 min illumination.

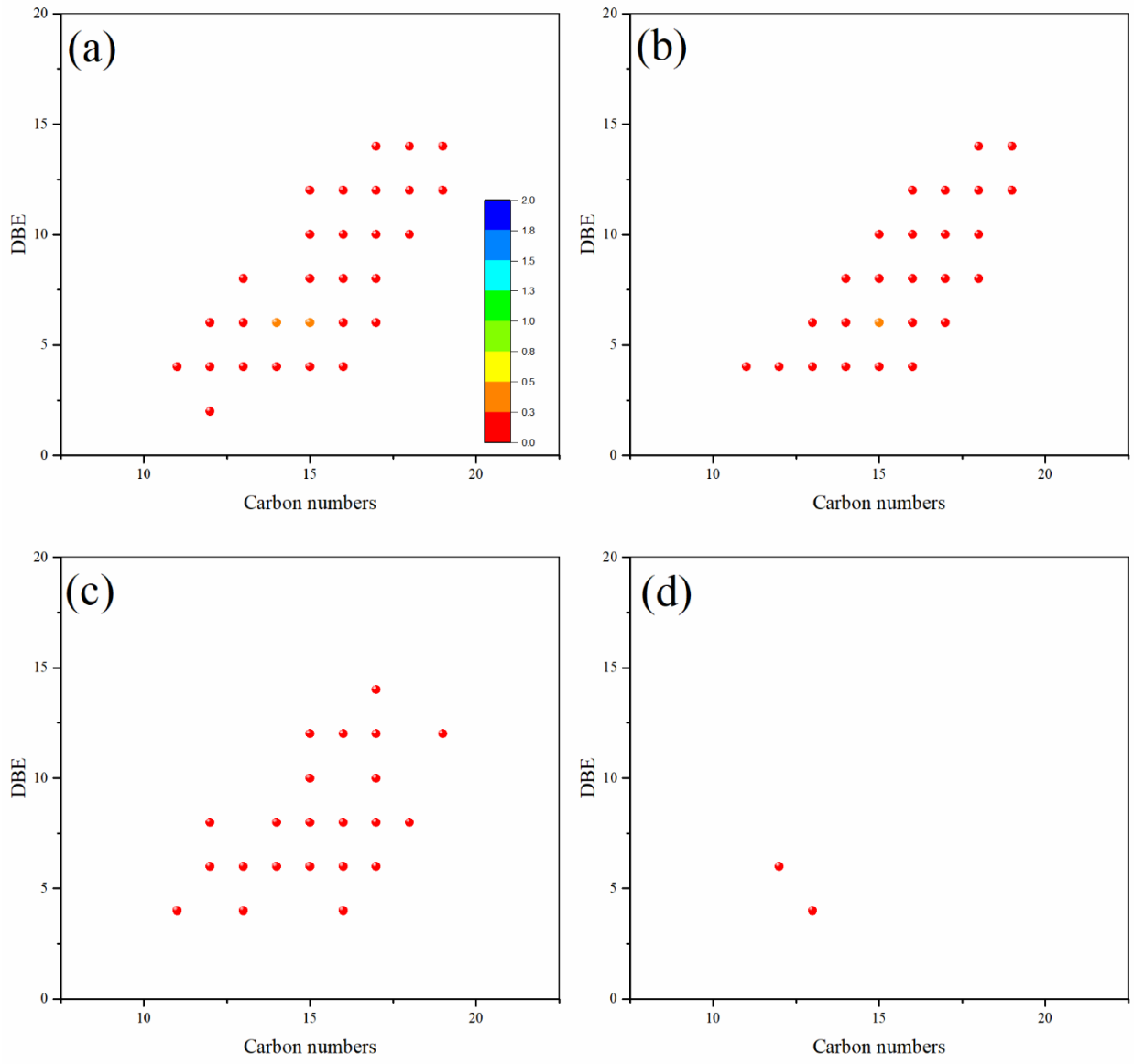

Fig. 3.17 O_5-NA distribution in (a) raw OSPW and OSPW treated with (b) Bi_2WO_6, (c) Bi_2WO_6/NiO, and (d) Bi_2WO_6/NiO/Ag after 180 min illumination.

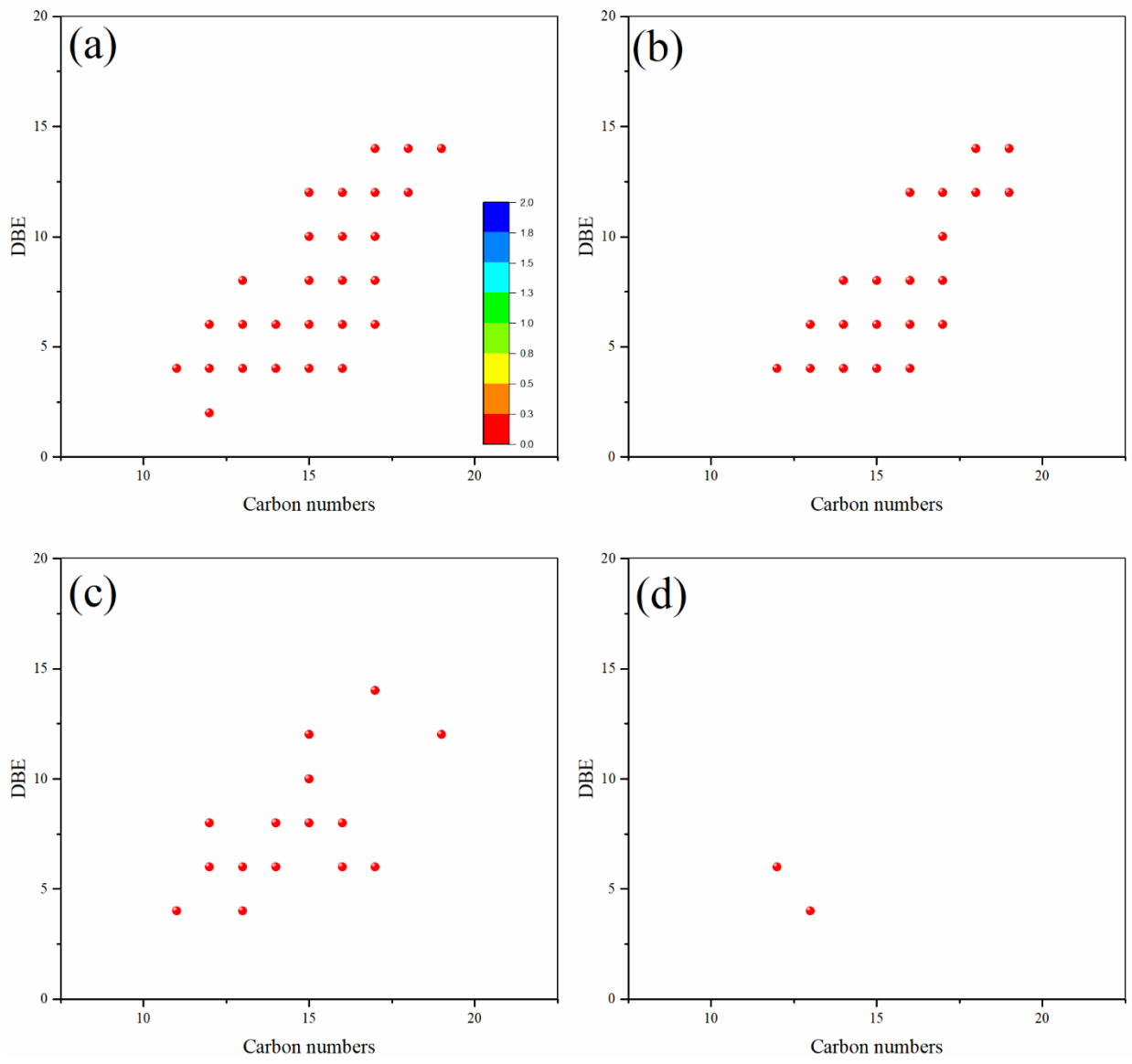

Fig. 3.18 O_6-NA distribution in (a) raw OSPW and OSPW treated with (b) Bi_2WO_6, (c) Bi_2WO_6/NiO, and (d) Bi_2WO_6/NiO/Ag after 180 min illumination

Table 3.6 NA distributions in the OSPW based on carbon and z numbers.

DBE	O_2-NAs (%)	Carbon number	O_2-NAs (%)
0	0	11	1.70%
2	1.43%	12	2.73%
4	19.55%	13	7.45%
6	27.98%	14	12.61%
8	8.58%	15	19.16%
10	5.07%	16	17.06%
12	15.26%	17	12.33%
14	9.40%	18	11.54%
16	8.44%	19	8.93%
18	4.28%	20	4.23%
		21	2.26%

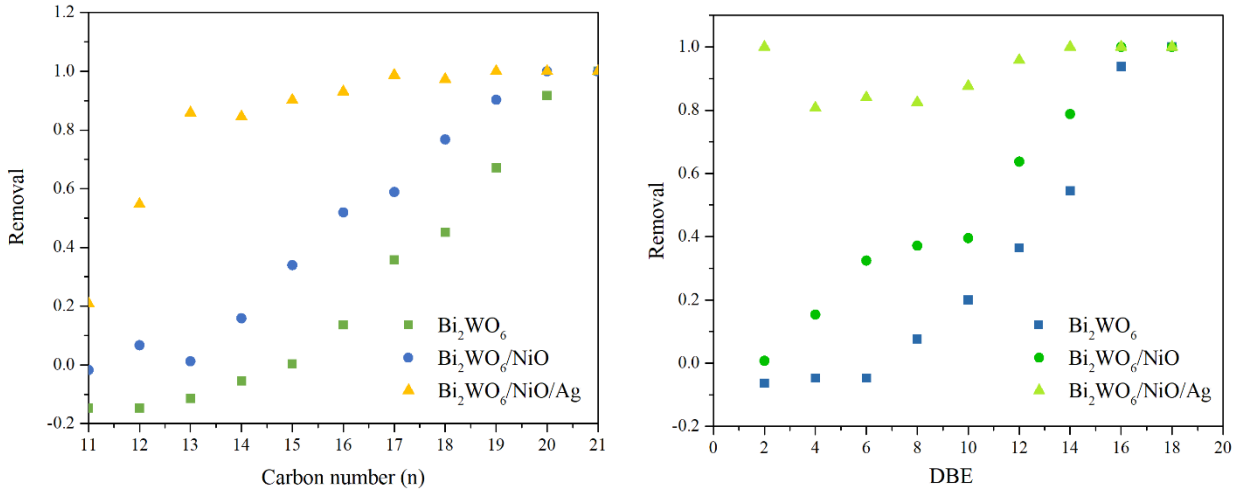

Fig. 3.19 Removal of classical NAs with respect to (a) carbon number and (b) DBE.

3.3.9 Toxicity

As illustrated in Fig. 3.20, the raw OSPW showed 10 % inhibition effect on *Vibrio fischeri*. With prolonged photocatalytic treatment, the inhibition effect was reduced. Specifically, there was no inhibition effects observed after 2 h photocatalytic treatment. Previous study found that classical NAs were the most acute toxic NAs in the OSPW (Morandi et al. 2015). Also, S-containing NAs could induce oxidative stress and inhibit the activity of protein (Alharbi et al. 2016,

Sun et al. 2017). As illustrated in IMS, we predicted the classical NAs and S-containing NAs were completely removed after 2 h, resulting in the reduced toxicity. These results indicated that photocatalytic process is a beneficial method for both removal of contaminates and reduction of toxicity.

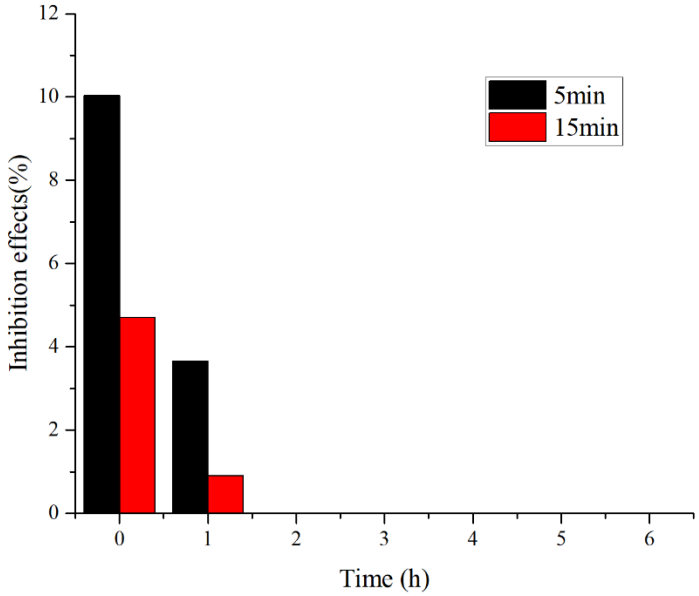

Fig. 3.20 Inhibition effect on *Vibrio fischeri* caused by raw OSPW and OSPW treated with Bi_2WO_6/NiO/Ag after 6h (the inhibition is zero for 2 hours onward).

3.4. Conclusion

A ternary plasmonic Bi_2WO_6/NiO/Ag Z-scheme photocatalyst with excellent photocatalytic activity was first successfully synthesized and applied for the OSPW remediation. After 6 h of photocatalytic treatment by Bi_2WO_6/NiO/Ag, all aromatics were completely removed; S-NAs and O_2-NAs were completely removed, and oxy-NAs were partially degraded. The degradation mechanisms of NAs were discussed in depth. $^{\bullet}OH$, h^+ and $O_2^{\bullet-}$ were detected as the key oxidative species in the photocatalytic system. The improved photocatalytic performance of

Bi_2WO_6/NiO/Ag was owning to the Z-scheme charge transfer pathway and SPR effect, which prevented the recombination of e^- and h^+, broaden the visible light absorption range, while preserving the excellent redox capacity.

3.5 References

Abdalrhman, A.S. and Gamal El-Din, M. (2020) Degradation of organics in real oil sands process water by electro-oxidation using graphite and dimensionally stable anodes. Chemical Engineering Journal 389, 124406.

Abdalrhman, A.S., Wang, C., How, Z.T. and Gamal El-Din, M. (2021) Degradation of cyclohexanecarboxylic acid as a model naphthenic acid by the UV/chlorine process: Kinetics and by-products identification. Journal of Hazardous Materials 402, 123476.

Alharbi, H.A., Saunders, D.M.V., Al-Mousa, A., Alcorn, J., Pereira, A.S., Martin, J.W., Giesy, J.P. and Wiseman, S.B. (2016) Inhibition of ABC transport proteins by oil sands process affected water. Aquatic Toxicology 170, 81-88.

Cao, R., Huang, H., Tian, N., Zhang, Y., Guo, Y. and Zhang, T. (2015) Novel Y doped Bi2WO6 photocatalyst: Hydrothermal fabrication, characterization and enhanced visible-light-driven photocatalytic activity for Rhodamine B degradation and photocurrent generation. Materials Characterization 101, 166-172.

Cao, R., Yang, H., Zhang, S. and Xu, X. (2019) Engineering of Z-scheme 2D/3D architectures with Ni(OH)2 on 3D porous g-C3N4 for efficiently photocatalytic H2 evolution. Applied Catalysis B: Environmental 258, 117997.

Cao, S., Shen, B., Tong, T., Fu, J. and Yu, J. (2018) 2D/2D Heterojunction of Ultrathin MXene/Bi2WO6 Nanosheets for Improved Photocatalytic CO2 Reduction. 28(21),

1800136.

Chen, W., Wu, Y., Fan, J., Djurišić, A.B., Liu, F., Tam, H.W., Ng, A., Surya, C., Chan, W.K., Wang, D. and He, Z.-B. (2018) Understanding the Doping Effect on NiO: Toward High-Performance Inverted Perovskite Solar Cells. Advanced Energy Materials 8(19), 1703519.

Ganiyu, S.O. and Gamal El-Din, M. (2020) Insight into in-situ radical and non-radical oxidative degradation of organic compounds in complex real matrix during electrooxidation with boron doped diamond electrode: A case study of oil sands process water treatment. Applied Catalysis B: Environmental 279, 119366.

Gentes, M.-L., Waldner, C., Papp, Z. and Smits, J.E.G. (2006) Effects of oil sands tailings compounds and harsh weather on mortality rates, growth and detoxification efforts in nestling tree swallows (Tachycineta bicolor). Environmental Pollution 142(1), 24-33.

Guo, Y., Li, J., Gao, Z., Zhu, X., Liu, Y., Wei, Z., Zhao, W. and Sun, C. (2016) A simple and effective method for fabricating novel p–n heterojunction photocatalyst g-C3N4/Bi4Ti3O12 and its photocatalytic performances. Applied Catalysis B: Environmental 192, 57-71.

Hagen, M.O., Katzenback, B.A., Islam, M.D.S., Gamal El-Din, M. and Belosevic, M. (2013) The Analysis of Goldfish (Carassius auratus L.) Innate Immune Responses After Acute and Subchronic Exposures to Oil Sands Process-Affected Water. Toxicological Sciences 138(1), 59-68.

Hersikorn, B.D. and Smits, J.E.G. (2011) Compromised metamorphosis and thyroid hormone changes in wood frogs (Lithobates sylvaticus) raised on reclaimed wetlands on the Athabasca oil sands. Environmental Pollution 159(2), 596-601.

Hotovy, I., Huran, J., Spiess, L., Hascik, S. and Rehacek, V. (1999) Preparation of nickel oxide

thin films for gas sensors applications. Sensors and Actuators B: Chemical 57(1), 147-152.

Huo, W.C., Dong, X.a., Li, J.Y., Liu, M., Liu, X.Y., Zhang, Y.X. and Dong, F. (2019) Synthesis of Bi2WO6 with gradient oxygen vacancies for highly photocatalytic NO oxidation and mechanism study. Chemical Engineering Journal 361, 129-138.

Jiang, H., Xing, Z., Zhao, T., Yang, Z., Wang, K., Li, Z., Yang, S., Xie, L. and Zhou, W. (2020) Plasmon Ag nanoparticle/Bi2S3 ultrathin nanobelt/oxygen-doped flower-like MoS2 nanosphere ternary heterojunctions for promoting charge separation and enhancing solar-driven photothermal and photocatalytic performances. Applied Catalysis B: Environmental 274, 118947.

Jo, W.-K., Kumar, S., Eslava, S. and Tonda, S. (2018) Construction of Bi2WO6/RGO/g-C3N4 2D/2D/2D hybrid Z-scheme heterojunctions with large interfacial contact area for efficient charge separation and high-performance photoreduction of CO2 and H2O into solar fuels. Applied Catalysis B: Environmental 239, 586-598.

Li, C., Fu, L., Stafford, J., Belosevic, M. and Gamal El-Din, M. (2017) The toxicity of oil sands process-affected water (OSPW): A critical review. Science of the Total Environment 601-602, 1785-1802.

Lin, Z., Du, C., Yan, B., Wang, C. and Yang, G. (2018) Two-dimensional amorphous NiO as a plasmonic photocatalyst for solar H2 evolution. Nature Communications 9(1), 4036.

Liu, C.a., Fu, Y., Zhao, J., Wang, H., Huang, H., Liu, Y., Dou, Y., Shao, M. and Kang, Z. (2019) All-solid-state Z-scheme system of NiO/CDs/BiVO4 for visible light-driven efficient overall water splitting. Chemical Engineering Journal 358, 134-142.

Lv, N., Li, Y., Huang, Z., Li, T., Ye, S., Dionysiou, D.D. and Song, X. (2019) Synthesis of GO/TiO2/Bi2WO6 nanocomposites with enhanced visible light photocatalytic degradation

of ethylene. Applied Catalysis B: Environmental 246, 303-311.

Masliyah, J., Zhou, Z.J., Xu, Z., Czarnecki, J. and Hamza, H. (2004) Understanding Water-Based Bitumen Extraction from Athabasca Oil Sands. The Canadian Journal of Chemical Engineering 82(4), 628-654.

Meng, L., How, Z.T., Ganiyu, S.O. and Gamal El-Din, M. (2021) Solar photocatalytic treatment of model and real oil sands process water naphthenic acids by bismuth tungstate: Effect of catalyst morphology and cations on the degradation kinetics and pathways. Journal of Hazardous Materials 413, 125396.

Meng, X., Li, Z., Zeng, H., Chen, J. and Zhang, Z. (2017) MoS2 quantum dots-interspersed Bi2WO6 heterostructures for visible light-induced detoxification and disinfection. Applied Catalysis B: Environmental 210, 160-172.

Morandi, G.D., Wiseman, S.B., Pereira, A., Mankidy, R., Gault, I.G.M., Martin, J.W. and Giesy, J.P. (2015) Effects-Directed Analysis of Dissolved Organic Compounds in Oil Sands Process-Affected Water. Environmental Science & Technology 49(20), 12395-12404.

Oturan, M.A. and Aaron, J.-J. (2014) Advanced Oxidation Processes in Water/Wastewater Treatment: Principles and Applications. A Review. Critical Reviews in Environmental Science and Technology 44(23), 2577-2641.

Qin, R., How, Z.T. and Gamal El-Din, M. (2019) Photodegradation of naphthenic acids induced by natural photosensitizer in oil sands process water. Water Research 164, 114913.

Rabanimehr, F., Farhadian, M., Nazar, A.R.S. and Moghadam, M. (2021) Fabrication of Z-scheme Bi2WO6/CNT/TiO2 heterostructure with enhanced cephalexin photodegradation: Optimization and reaction mechanism. Journal of Molecular Liquids 339, 116728.

Ren, J., Wang, W., Sun, S., Zhang, L. and Chang, J. (2009) Enhanced photocatalytic activity of

Bi2WO6 loaded with Ag nanoparticles under visible light irradiation. Applied Catalysis B: Environmental 92(1), 50-55.

Shang, M., Wang, W., Zhang, L. and Xu, H. (2010) Bi2WO6 with significantly enhanced photocatalytic activities by nitrogen doping. Materials Chemistry and Physics 120(1), 155-159.

Sun, J., Peng, H., Alharbi, H.A., Jones, P.D., Giesy, J.P. and Wiseman, S.B. (2017) Identification of Chemicals that Cause Oxidative Stress in Oil Sands Process-Affected Water. Environmental Science & Technology 51(15), 8773-8781.

Sun, N., Chelme-Ayala, P., Klamerth, N., McPhedran, K.N., Islam, M.S., Perez-Estrada, L., Drzewicz, P., Blunt, B.J., Reichert, M., Hagen, M., Tierney, K.B., Belosevic, M. and Gamal El-Din, M. (2014) Advanced Analytical Mass Spectrometric Techniques and Bioassays to Characterize Untreated and Ozonated Oil Sands Process-Affected Water. Environmental Science & Technology 48(19), 11090-11099.

Tang, J.-y., Guo, R.-t., Zhou, W.-g., Huang, C.-y. and Pan, W.-g. (2018) Ball-flower like NiO/g-C3N4 heterojunction for efficient visible light photocatalytic CO2 reduction. Applied Catalysis B: Environmental 237, 802-810.

Tantardini, C. and Oganov, A.R. (2021) Thermochemical electronegativities of the elements. Nature Communications 12(1), 2087.

von Sonntag, C. and von Gunten, U. (2012) Chemistry of Ozone in Water and Wastewater Treatmentnull, IWA Publishing.

Wang, C., Klamerth, N., Messele, S.A., Singh, A., Belosevic, M. and Gamal El-Din, M. (2016) Comparison of UV/hydrogen peroxide, potassium ferrate(VI), and ozone in oxidizing the organic fraction of oil sands process-affected water (OSPW). Water Research 100, 476-

485.

Wang, H., Zhang, L., Chen, Z., Hu, J., Li, S., Wang, Z., Liu, J. and Wang, X. (2014) Semiconductor heterojunction photocatalysts: design, construction, and photocatalytic performances. Chemical Society Reviews 43(15), 5234-5244.

Wang, N., Chelme-Ayala, P., Perez-Estrada, L., Garcia-Garcia, E., Pun, J., Martin, J.W., Belosevic, M. and Gamal El-Din, M. (2013) Impact of Ozonation on Naphthenic Acids Speciation and Toxicity of Oil Sands Process-Affected Water to Vibrio fischeri and Mammalian Immune System. Environmental Science & Technology 47(12), 6518-6526.

Williams, A.T.R., Winfield, S.A. and Miller, J.N. (1983) Relative fluorescence quantum yields using a computer-controlled luminescence spectrometer. Analyst 108(1290), 1067-1071.

Wu, S., Sun, J., Li, Q., Hood, Z.D., Yang, S., Su, T., Peng, R., Wu, Z., Sun, W., Kent, P.R.C., Jiang, B. and Chisholm, M.F. (2020) Effects of Surface Terminations of 2D Bi2WO6 on Photocatalytic Hydrogen Evolution from Water Splitting. ACS Applied Materials & Interfaces 12(17), 20067-20074.

Yang, P., Chen, C., Wang, D., Ma, H., Du, Y., Cai, D., Zhang, X. and Wu, Z. (2021) Kinetics, reaction pathways, and mechanism investigation for improved environmental remediation by 0D/3D CdTe/Bi2WO6 Z-scheme catalyst. Applied Catalysis B: Environmental 285, 119877.

Yao, D., Ouyang, Y., Jiao, X., Ye, H., Lei, W., Xia, X., Lu, L. and Hao, Q. (2018) Hierarchical NiO@NiCo2O4 Core–shell Nanosheet Arrays on Ni Foam for High-Performance Electrochemical Supercapacitors. Industrial & Engineering Chemistry Research 57(18), 6246-6256.

Zhang, Y., Klamerth, N., Chelme-Ayala, P. and Gamal El-Din, M. (2016) Comparison of

Nitrilotriacetic Acid and [S,S]-Ethylenediamine-N,N′-disuccinic Acid in UV–Fenton for the Treatment of Oil Sands Process-Affected Water at Natural pH. Environmental Science & Technology 50(19), 10535-10544.

Zhang, Y., Zhao, Y., Xiong, Z., Gao, T., Gong, B., Liu, P., Liu, J. and Zhang, J. (2021) Elemental mercury removal by I−-doped Bi2WO6 with remarkable visible-light-driven photocatalytic oxidation. Applied Catalysis B: Environmental 282, 119534.

Zhou, H., Wen, Z., Liu, J., Ke, J., Duan, X. and Wang, S. (2019) Z-scheme plasmonic Ag decorated WO3/Bi2WO6 hybrids for enhanced photocatalytic abatement of chlorinated-VOCs under solar light irradiation. Applied Catalysis B: Environmental 242, 76-84.

Zhu, D. and Zhou, Q. (2020) Novel Bi2WO6 modified by N-doped graphitic carbon nitride photocatalyst for efficient photocatalytic degradation of phenol under visible light. Applied Catalysis B: Environmental 268, 118426.

CHAPTER 4 SOLAR PHOTOCATALYTIC DEGRADATION OF MODEL COMPOUNDS NAS MIXTURES: THE EFFECT OF INORGANIC FRACTION OF OSPW

4.1 Introduction

Oil sands process water (OSPW) is generated during the process of oil sands mining and extraction in northern Alberta, Canada (Meng et al. 2021, Song et al. 2021). In the past decade, the potential environmental problems of OSPW stored on-site have attracted increasing attention. OSPW has been widely demonstrated to trigger detrimental acute and chronic toxicity to different living species (Anderson et al. 2012, Gamal El-Din et al. 2011, Garcia-Garcia et al. 2011, Jones et al. 2011). In terms of chemical compositions, OSPW includes trace metals, suspended particles, inorganic ions, and organic fractions, of which naphthenic acids (NAs) constitute the dominant compounds for the organics. As a class of alkyl-substituted acyclic, cyclic, and polycyclic carboxylic acids, NAs are structurally stable through natural attenuation processes such as photolysis, hydrolysis, and biodegradation. In general, the chemical formula of $C_nH_{2n+Z}O_x$ is used to represented NAs, where n is the carbon number ($7 \leq n \leq 26$), Z is even integer represents the hydrogen deficiency due to the formation of ring or double bond structure ($0 \leq -Z \leq 18$), and x indicates the oxygen number. The heteroatomic NAs are designated as $C_nH_{2n+z}SO_x$ and $C_nH_{2n+z}NO_x$ (Ganiyu and Gamal El-Din 2020, Luo et al. 2022). In particular, NAs could greatly induce oxidative stress, endocrine disruptive, immunotoxicity and inhibit protein synthesis in living organisms (Hagen et al. 2013, He et al. 2012a, He et al. 2011, He et al. 2012b, Wiseman et al. 2013). Therefore, considerable efforts have been devoted to remediating the OSPW, especially the NAs.

Among these treatment techniques, advanced oxidation processes (AOPs) have exhibited outstanding merits in eliminating the organic fractions of OSPW. The studied oxidative systems include UV/H_2O_2 (Afzal et al. 2012, Fang et al. 2019), ozone (Afzal et al. 2015, Wang et al. 2013), UV-Fenton (Zhang et al. 2017, Zhang et al. 2016), ferrate (VI) (Huang et al. 2019, Wang et al. 2016), UV/chlorine (Abdalrhman et al. 2021, Shu et al. 2014), electro-oxidation (Abdalrhman et al. 2019, Abdalrhman et al. 2020), and solar photocatalytic treatment (Meng et al. 2021, Suara et al. 2022). Solar photocatalytic treatment is a green technology and characterized with solar energy and reused nanomaterials. Most of these studies focused on the removal efficiency of model NAs from pure water, whereas the co-existing water components may affect the oxidative performance to different degrees. For example, OSPW inorganic fraction consists of K^+, Na^{2+}, Ca^{2+}, Mg^{2+}, HCO_3^-, Cl^-, SO_4^{2-}, NO_3^- *etc*. It has been reported that bicarbonate could significantly inhibit the nitrate-induced photodegradation of 1-adamantanecarboxylic acid (ACA), which may be due to the consumption of hydroxyl radicals ($^{\bullet}OH$) to produce the less reactive carbonate radicals ($CO_3^{\bullet-}$) (Qin et al. 2019a). Additionally, the presence of ammonia, bicarbonate, and chloride has been shown to decrease the removal of NAs during ozonation (Qin et al. 2020). Moreover, the OSPW toxicity may be attributed to the synergistic or antagonistic chemical effects due to the complexity of OSPW components. For instance, Nero *et al.* (Nero et al. 2006) reported that the addition of salts decreased the gill surface area of yellow perch, leading to less toxicity induced by NAs due to the decreased NAs entry. However, simultaneous effect on the exchange of respiratory gases was also recorded. Therefore, it is necessary to evaluate the real water matrix effect on the remediation performance of NAs. Yet, there is a paucity of literature on the real water matrix effect on the photocatalytic degradation of NAs.

The objectives of this chapter were (1) to evaluate the influence of inorganic fraction (IF) of OSPW on the solar photocatalytic efficiency of the NAs mixtures using Bi_2WO_6 and Bi_2WO_6/NiO/Ag; (2) to investigate the effects of different inorganic ions (e.g., SO_4^{2-}, NO_3^-, HCO_3^-, and Cl^-) on the above treatment processes using the buffer solutions; (3) to study the effects of NO_3^- on the degradation pathways of ACA during photocatalytic processes; 4) to explore the byproducts formation and reaction pathways of a S-NAs model compound. This study could facilitate the understanding of the possible practical application of the solar photocatalytic system in the elimination of NAs and remediation of OSPW.

4.2 Experimental section

4.2.1 Chemicals and materials

Raw OSPW was collected from an active oil sands tailings pond in Fort McMurray, Alberta, Canada, and stored in a cold room at 4 °C. The model NA compounds, 1-adamantanecarboxylic acid (ACA), cyclohexanecarboxylic acid (CHA), tetrahydro-2H-thiopyran-4-carboxylic acid (T-2H-T4CA), tetrahydropyran-4-carboxylic acid (T4CA), isonipecotic acid (IA) and 4,5-dihydronaphtho[1,2-b]thiophene-2-carboxylic acid (DTCA) were purchased from Sigma Aldrich. Details and the structures of these six surrogate organic acids are listed in Table 4.1. Inorganic salts Na_2SO_4, K_2SO_4, $NaNO_3$, $NaHCO_3$, and NaCl were purchased from Fisher Scientific. Ultrapure water ($R \geq 18.2$ MΩ) produced in-house by a Millipore Milli-Q system was used to prepare the reaction solutions.

Table 4.8 Model compounds for NAs mixture.

Structure	Abbreviation	Name	Formula	MW
	ACA	1-adamantanecarboxylic acid	$C_{11}H_{16}O_2$	180.24
	CHA	cyclohexanecarboxylic acid	$C_7H_{12}O_2$	128.1691
	T4CA	Tetrahydropyran-4-carboxylic acid	$C_6H_{10}O_3$	130.1419
	T-2H-T4CA	Tetrahydro-2H-thiopyran-4-carboxylic acid	$C_6H_{10}O_2S$	146.21
	IA	Isonipecotic acid	$C_6H_{11}O_2N$	129.16
	DTCA	4,5-dihydronaphtho[1,2-b]thiophene-2-carboxylic acid	$C_{13}H_{10}O_2S$	230.23

4.2.2 Preparation of OSPW containing inorganic fraction only

OSPW inorganic fraction (OSPW-IF) was prepared using the method described by Qin *et al.* (Qin et al. 2019b). Briefly, granular activated carbon (GAC) was used as adsorbent. Firstly, the GAC was washed using 0.1 mM NaOH and HCl alternately for several times to remove impurities. After that, the GAC was rinsed by ultrapure water to remove the acid/base solution and dried overnight at 100 °C. Then, 30 g of clean dry GAC was packed in a glass column with a depth of 15 cm and a diameter of 2.5 cm. In order to hold the GAC inside the vertical column, place a polyethylene terephthalate disk at the bottom of the column. Using 2 L ultrapure water to wash the GAC packed column and collect the last 50 mL of the effluent as blank. Negligible inorganic ions were detected in the blank. Finally, 2 L OSPW was passed through the GAC column at a flow rate

of 1 mL/min. The effluent was filtered with a 0.2 µm nylon membrane filter and denoted as the OSPW-IF. The properties, major ions and trace metals of blank and OSPW-IF are listed in Table 4.2.

Table 4.9 Properties, major ions and trace metals of blank and raw OSPW-IF

Parameter	Blank	OSPW-IF
pH	8.5±0.1	8.7±0.2
Ions (ppm)		
Ag	<LOD	<LOD
Al	0.001±0.000	0.142±0.021
As	0.001±0.000	0.047±0.000
B	0.001±0.000	5.989±0.063
Ba	<LOD	0.297±0.006
Be	<LOD	<LOD
Ca	0.131±0.000	4.295±0.074
Cd	<LOD	<LOD
Co	<LOD	<LOD
Cr	<LOD	<LOD
Cu	0.003±0.000	0.003±0.000
Fe	<LOD	0.005±0.000
K	0.077±0.000	41.56±0.702
Li	0.001±0.000	0.343±0.003
Mg	0.054±0.000	4.984±0.025
Mn	0.001±0.000	0.002±0.000
Mo	0.003±0.000	0.096±0.000
Na	0.124±0.001	1,182±8.306
Ni	0.007±0.000	0.004±0.000
P	0.001±0.000	0.776±0.014
Pb	<LOD	0.003±0.000
S	0.003±0.000	51.69±0.661
Sb	0.001±0.000	0.013±0.000
Se	0.002±0.000	0.036±0.000
Si	0.317±0.012	3.003±0.037
Sr	0.007±0.000	0.394±0.005
Ti	<LOD	0.016±0.000
Tl	<LOD	0.003±0.000
V	<LOD	0.063±0.004
Zn	0.010±0.000	<LOD
Fluoride (F^-)	0.0157±0.000	2.3931±0.123
Chloride (Cl^-)	0.5453±0.014	615.3760±5.312
Nitrite (NO_2^-)	n.a.	10.6883±0.578
Sulfate (SO_4^{2-})	0.0566±0.000	93.4347±5.0320
Bromide (Br^-)	0.0156±0.000	n.a.

Nitrate (NO_3^-)	0.0609±0.002	19.5539±0.910
Bicarbonate (HCO_3^-)	0.0812±0.004	801.2376±7.432
Phosphate (PO_4^{3-})	n.a.	n.a.

4.2.3 Preparation of model compound mixtures in buffer with individual ions and OSPW-IF

Six model compounds: ACA, CHA, T-2H-T4CA, T4CA, IA, and DTCA were selected to represent classical (O_2-NAs), oxidized (Oxy-NAs), sulfur (S-NAs) and nitrogen (N-NAs) containing NAs in OSPW (Table 4.1). 5 mM $NaHCO_3$ buffer with pH adjusted to 8.7 was used to simulate the pH of real OSPW. Each model compound was spiked into either a buffer solution to obtain a 60 mg/L NAs mixture solution in buffer (NAs-Buffer) or into OSPW-IF to prepare a 60 mg/L NAs mixture solution in OSPW-IF (NAs-OSPW-IF). Appropriate volumes of Na_2SO_4, K_2SO_4, $NaNO_3$, $NaHCO_3$, and NaCl from individual stock solutions were added to obtain the NAs-Buffer with individual ions (Table 4.3), whose concentration was similar to that in real OSPW (Table 4.2).

Table 4.10 Concentration of inorganic salts in the experiments conducted to investigate the influence of individual ions.

Salts	Concentration a (mM)	concentration b (mM)	Concentration c (mM)
Na_2SO_4	4	13	25
K_2SO_4	0.05	0.5	2
$NaNO_3$	0.05	0.5	2
$NaHCO_3$	4	8	12
NaCl	5	10	20

4.2.4 Preparation of catalysts

The preparation methods of Bi_2WO_6 and Bi_2WO_6/NiO/Ag were described in the experimental section of Chapter 2 and 3.

4.2.5 Photocatalytic experiments

A solar simulator equipped with a 300 W Xenon lamp was used during the degradation processes. The simulated solar light irradiance was measured by a black-comet-sr spectroradiometer with a CR2 UV-VIS-NIR cosine receptor and the software program SpectraWiz® (StellarNet Inc.). In a typical experiment, 0.5 g L^{-1} catalyst was dispersed in a 50 mL of solution in an open reactor containing the targeted pollutant, which was placed on a magnetic stirrer under the direct irradiation of the simulated solar rays. The irradiance of effective wavelengths (200–800 nm) was set at 19.9 mW cm^{-2} (Table 4.4). Samples (3 mL) were taken at regular intervals and the suspended solids were filtered from the solution using a 0.2 µm Nylon filter (Thermo Scientific).

Table 4.11 The irradiance of different wavelength range

Wavelength (nm)	400-500	500-600	600-700	700-800	Total
Irradiance (Watts/m^2)	48.69	49.68	49.63	33.81	198.524
Wavelength (nm)	UVa (320-420)		UVb (275-320)	UVc (200-275)	
Irradiance (Watts/m^2)	14.26		0.256	2.198	

4.2.6 Analytical method

The concentrations of model NA compounds were measured by ultra-performance liquid chromatography (UPLC) coupled with a single quadrupole mass spectrometry (SQ Detector 2, Waters). Chromatographic separation was performed at a flow rate of 400 µL·min^{-1} by a BEH C18 column (2.1 mm × 100 mm × 1.7 µm, Waters) maintained at 40 °C. The mobile phase was 2 mM ammonia acetate in water (A) and acetonitrile (B). The MS was operating in a negative ion mode

using an ESI source in a single ion monitoring mode. The intermediate by-products formed during the photocatalytic degradation of heteroatomic NAs were identified by ultraperformance liquid chromatography coupled with time-of-flight mass spectrometry (UPLC-TOF-MS) (Synapt G2, Waters). The chromatographic separation was achieved by a Waters BEH Phenyl column with 2 mM ammonia acetate buffer in both water (A) and 50/50 methanol/acetonitrile (B). TOF-MS was operated at ESI negative mode using MS scan over the mass range of 50–1200 Da in high-resolution mode (mass resolution = 40,000 FWHM at *m/z* 1431). Leucine enkephalin (*m/z* = 554.2611) was used as lock mass for the mass correction and was continuously infused via the lock spray ESI. The data were acquired by MassLynx (Waters) and processed by TargetLynx (Waters).

The anion concentrations were quantified by ion chromatography (ICS-2000 and 2500, Dionex, Sunnyvale, CA, USA). The analysis of trace elements was performed by inductively coupled plasma mass spectrometry (ICP-MS, Elan 6000 ICP mass spectrometer, PerkinElmer, Waltham, MA, USA).

4.2.7 Calculation of frontier electron densities (FEDs) of DTCA

The molecular structure of DTCA was optimized using hybrid density functional theory (DFT) method (B3LYP) and Gaussian 09 software package. The basis sets employed were 6–311G** for C, H, O, and S. Molecular orbital calculations were carried out based on the optimized conformation.

4.3 Results and discussions

4.3.1 The photocatalytic degradation of NAs mixtures in buffer and OSPW-IF

The solar photocatalytic degradation of the mixtures of six model NA compounds (i.e., ACA, CHA, T-2H-T4CA, T4CA, IA, and DTCA) was investigated in buffer (5 mM HCO_3^-) and OSPW-

IF solutions, respectively. CHA, T-2H-T4CA, T4CA and IA were used to investigate the structure-relative degradation of NAs. Two different photocatalysts (i.e., Bi_2WO_6 and Bi_2WO_6/NiO/Ag) were added for comparison of the degradation efficiency of these model NAs. The obtained results are illustrated in Fig. 4.1a-f. It can be seen from Fig. 4.1 that the photocatalytic elimination of all six model compounds followed the pseudo-first-order reaction. The fitted rate constants suggested that Bi_2WO_6/NiO/Ag generally had higher photocatalytic activity than that of Bi_2WO_6 in both OSPW-IF and buffer solutions. For example, in the buffer solutions, the photocatalytic rate constants of ACA, CHA, T4CA, T-2H-T4CA, IA and DTCA were individually 0.011 min^{-1}, 0.009 min^{-1}, 0.002 min^{-1}, 0.122 min^{-1}, 0.003 min^{-1}, and 0.053 min^{-1} for Bi_2WO_6, which were enhanced to 0.048 min^{-1}, 0.036 min^{-1}, 0.019 min^{-1}, 0.283 min^{-1}, 0.026 min^{-1}, and 0.075 min^{-1} for Bi_2WO_6/NiO/Ag. These results demonstrated the synergistic effect of different composites in the heterojunction photocatalyst in promoting the catalytic performance of model NA compounds. The degradation rate of the four structure-relative model NAs decreased in the following order: T-2H-T4CA > CHA > IA > T4CA. The preferential degradation of T-2H-T4CA was because of the highly reactive S atoms (Meng et al. 2021). CHA, a typical classical NAs, was found to generally oxidized at the secondary and tertiary carbon (Abdalrhman et al. 2021), which are much lower in reactivity as compared to the electron-rich S atom in T-2H-T4CA. The lower apparent activity of T4CA was due to the fact that the O_2-NAs and S-NAs were oxidized into Oxy-NAs as demonstrated from the previous studies (Abdalrhman et al. 2021, Fang et al. 2020, Qin et al. 2019a). Notably, the rate constants in both reaction systems indicated that the removal of mixtures of ACA, CHA, T-2H-T4CA, T4CA, and DTCA in IF solutions was apparently lower than that in buffer solutions. On the contrary, the photocatalytic elimination of IA exhibited a higher reactivity in IF solution (i.e., 0.0101 min^{-1} for Bi_2WO_6 and 0.0328 min^{-1} for Bi_2WO_6/NiO/Ag) as compared to that

in buffer solutions (i.e., 0.0026 min^{-1} for Bi_2WO_6 and 0.026 min^{-1} for Bi_2WO_6/NiO/Ag). The distinct phenomena were studied and discussed in detail in Section 4.3.2.

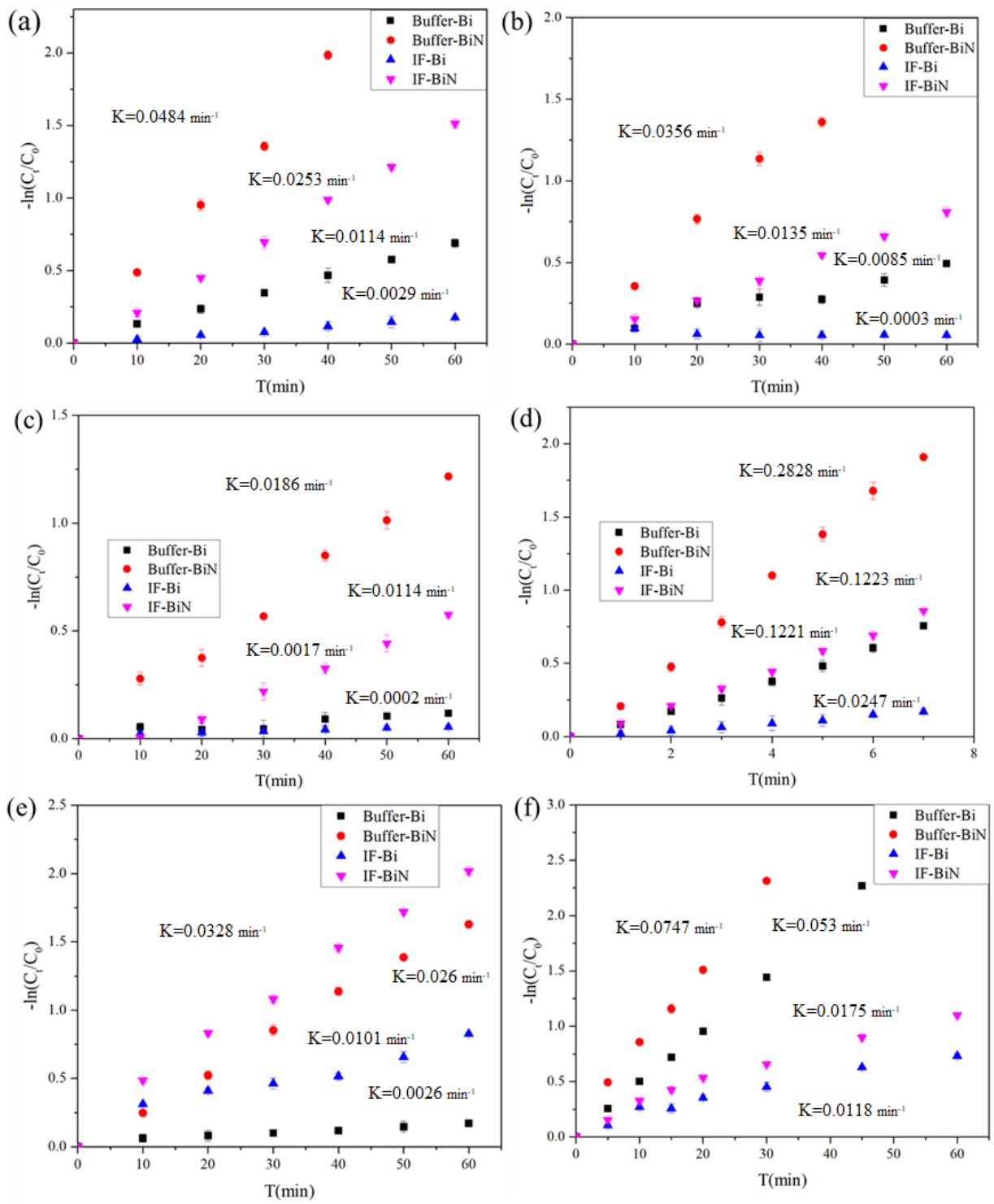

Fig. 4.11 The photocatalytic degradation of a) ACA, b) CHA, c) T4CA, d) T-2H-T4CA, e) IA, f) DCTA in buffer and OSPW-IF using Bi_2WO_6 (Bi) and Bi_2WO_6/NiO/Ag (BiN) [Buffer: [$NaHCO_3$]= 5mM, [Catalyst] = 0.5g/L, concentration of mixtures = 60 mg/L.]

4.3.2 The effects of inorganic salts on the degradation of mixtures

In order to understand the phenomena observed in section 4.3.1, related experiments were performed to explore the underlying water components or mechanisms contributing to different removal efficiencies of the NAs mixtures in buffer and IF solutions. According to the measured levels of trace metals and inorganic ions in IF, the higher concentrations go to K, Na, S, Cl^-, SO_4^{2-}, NO_3^- and HCO_3^- (Table 4.2). Therefore, three different concentrations (Table 4.3) were tested using K_2SO_4, Na_2SO_4, $NaNO_3$, NaCl, and $NaHCO_3$, respectively. The obtained results were summarized and are individually presented in Figs. 4.2-4.7 for ACA, CHA, T4CA, T-2H-T4CA, IA, and DTCA. It can be observed that the presence of K_2SO_4 and Na_2SO_4 exhibited a negligible effect on the photocatalytic treatments of six model NAs using Bi_2WO_6 and Bi_2WO_6/NiO/Ag. In contrary, the dose-dependent inhibitions of NaCl and $NaHCO_3$ were observed for the photocatalytic removal of all model NA compounds except IA in the buffered solution. The decreased removal performance of model NAs in the presence of chloride ions may be due to its role as the hole scavenger, which could inhibit the photocatalytic processes (Iguchi et al. 2015). Regarding the addition of HCO_3^-, this anion could react with the highly reactive $^{\bullet}OH$ to form the less reactive $CO_3^{\bullet-}$, which mainly initiated the oxidation by selectively attacking the electron-rich moiety of the organic compounds. Considering the lack of electron-withdrawing groups for these model NA compounds, the diminished photocatalytic removal efficiencies were therefore observed in the presence of $NaHCO_3$. Therefore, the phenomenon that decreased the removal efficiency of ACA, CHA, T-2H-T4CA, T4CA, and DTCA in IF solutions compared to that in buffer solutions could be explained by the presence of Cl^- and HCO_3^-.

By comparison, the increased introduction of $NaNO_3$ caused a significant enhancement in the photocatalytic removal of mixtures, especially for IA. The reason may be due to the generation of $NO_2^{\bullet}$, $^{\bullet}OH$ and $NO^{\bullet}$ from photosensitization of NO_3^-, which presented a higher reactivity with NAs (Qin et al. 2019a). The different degradation behavior of IA compared to other five NAs was owing to the specific transformation pathway of IA. Meng *et.al* (Meng et al. 2021) reported that the degradation of IA continues even after the lamp was turned off, indicating the spontaneous degradation of the IA in the absence of the oxidative species ($^{\bullet}OH$, h^+ and $O_2^{\bullet-}$). In alkaline environment, IA was activated to aminyl radicals under solar irradiation, which act as dominant reactive species for its degradation. The aminyl radicals initiate the spontaneous, chain and continuous degradation of the IA. Therefore, the effect of the reduced concentration of other oxidative species on the degradation of IA is negligible. Whereas NO_3^- was predicted to accelerate the production of aminyl radicals, resulting in the enhanced degradation of IA in OSPW-IF.

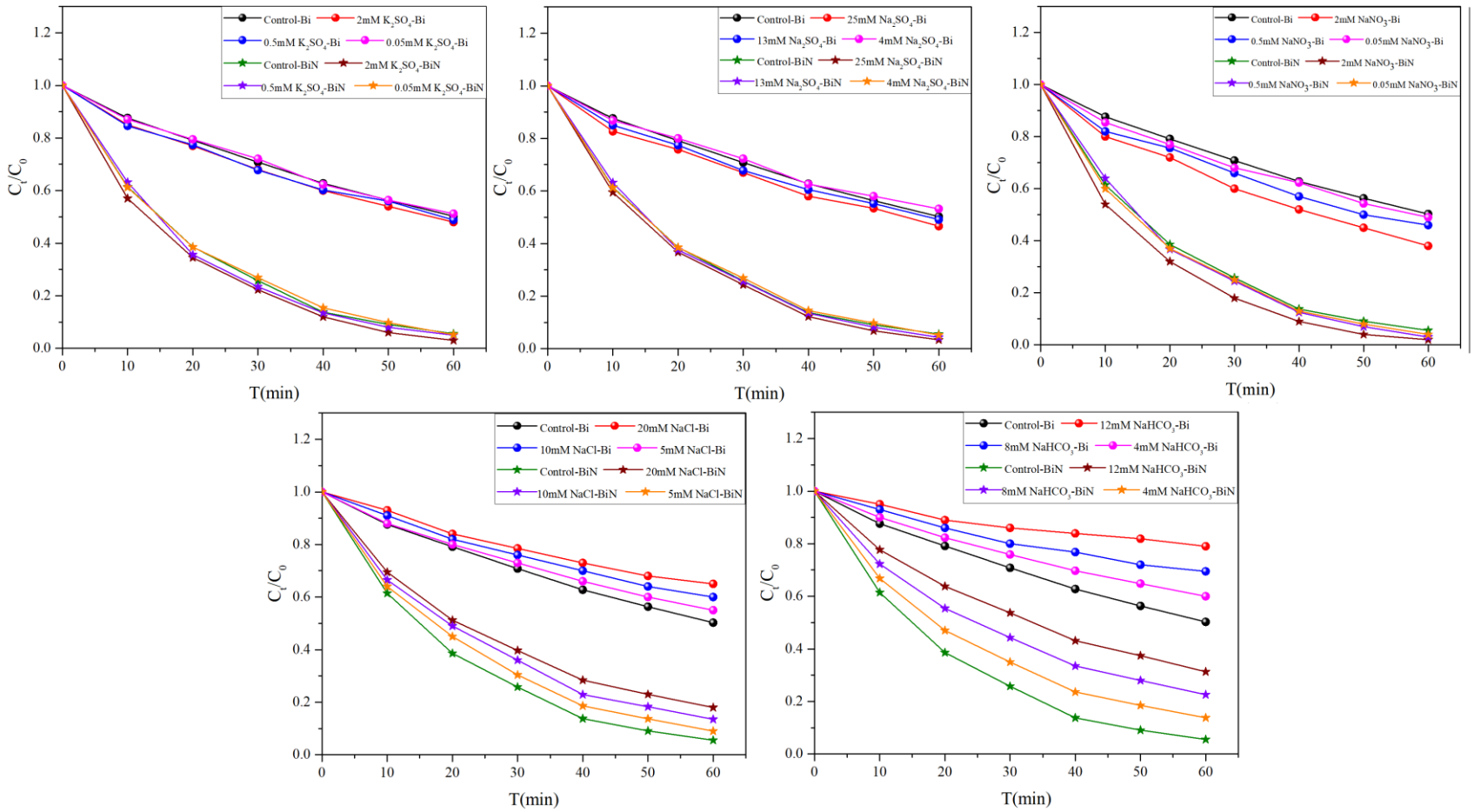

Fig. 4.12 The effects of different salts on the photocatalytic degradation of ACA using Bi_2WO_6 and Bi_2WO_6 /NiO/Ag. [Buffer: [$NaHCO_3$]=5mM, [Catalyst] = 0.5g/L, concentration of mixtures = 60 mg/L].

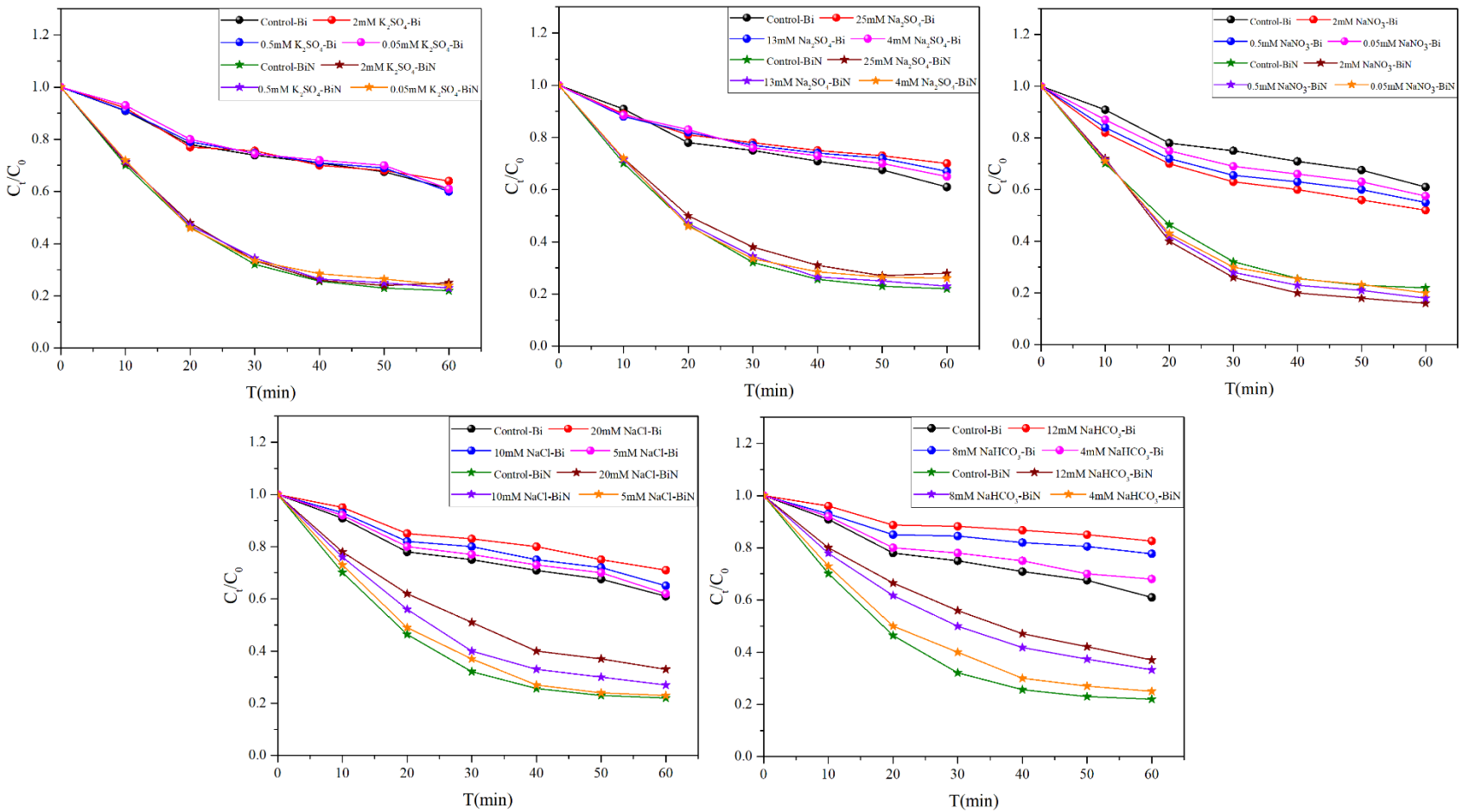

Fig. 4.13 The effects of different salts on the photocatalytic degradation of CHA using Bi_2WO_6 and Bi_2WO_6 /NiO/Ag. [Buffer: [$NaHCO_3$]=5mM, [Catalyst] = 0.5g/L, concentration of mixtures = 60 mg/L].

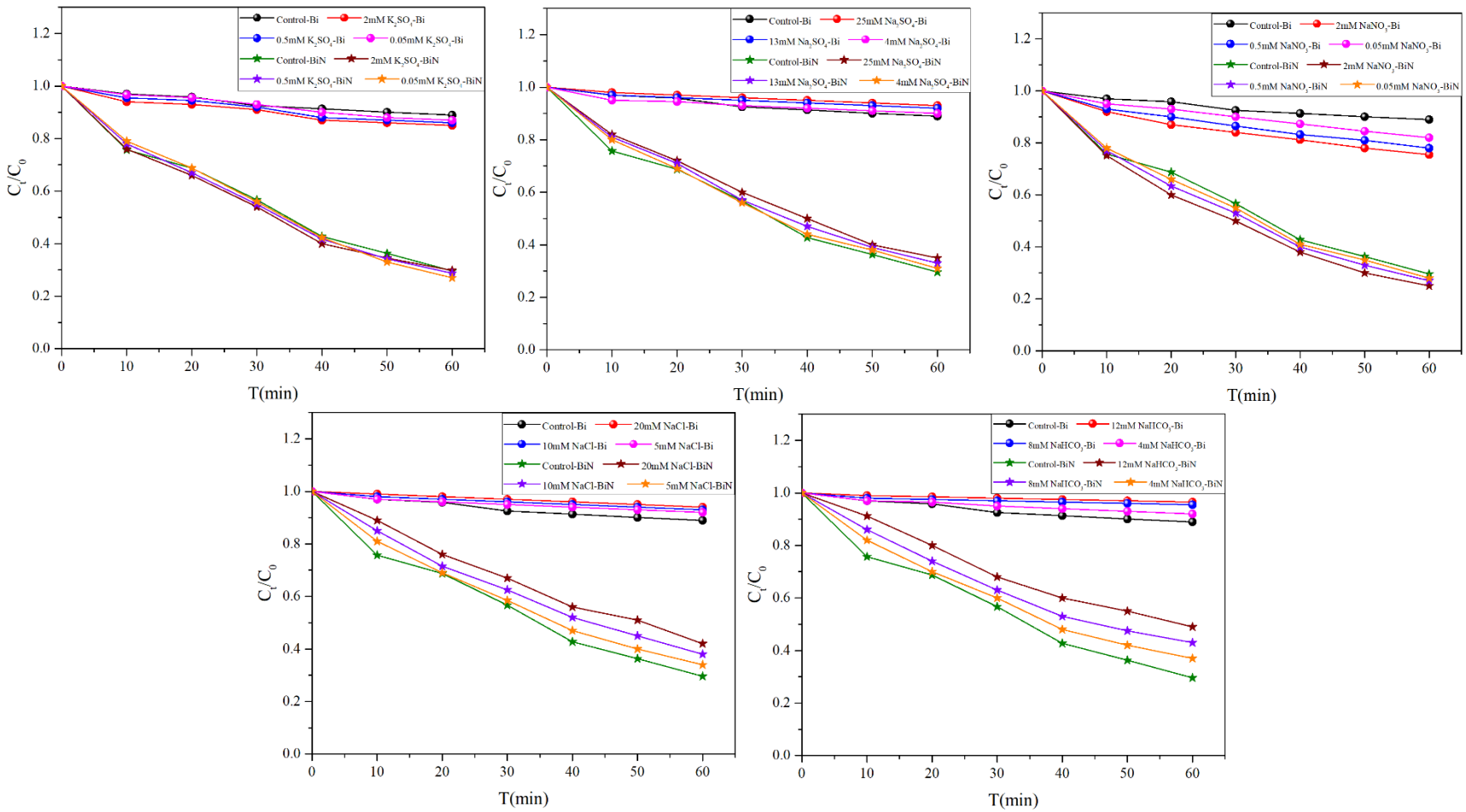

Fig. 4.14 The effects of different salts on the photocatalytic degradation of T4CA using Bi_2WO_6 and Bi_2WO_6 /NiO/Ag. [Buffer: [$NaHCO_3$]=5mM, [Catalyst] = 0.5g/L, concentration of mixtures = 60 mg/L].

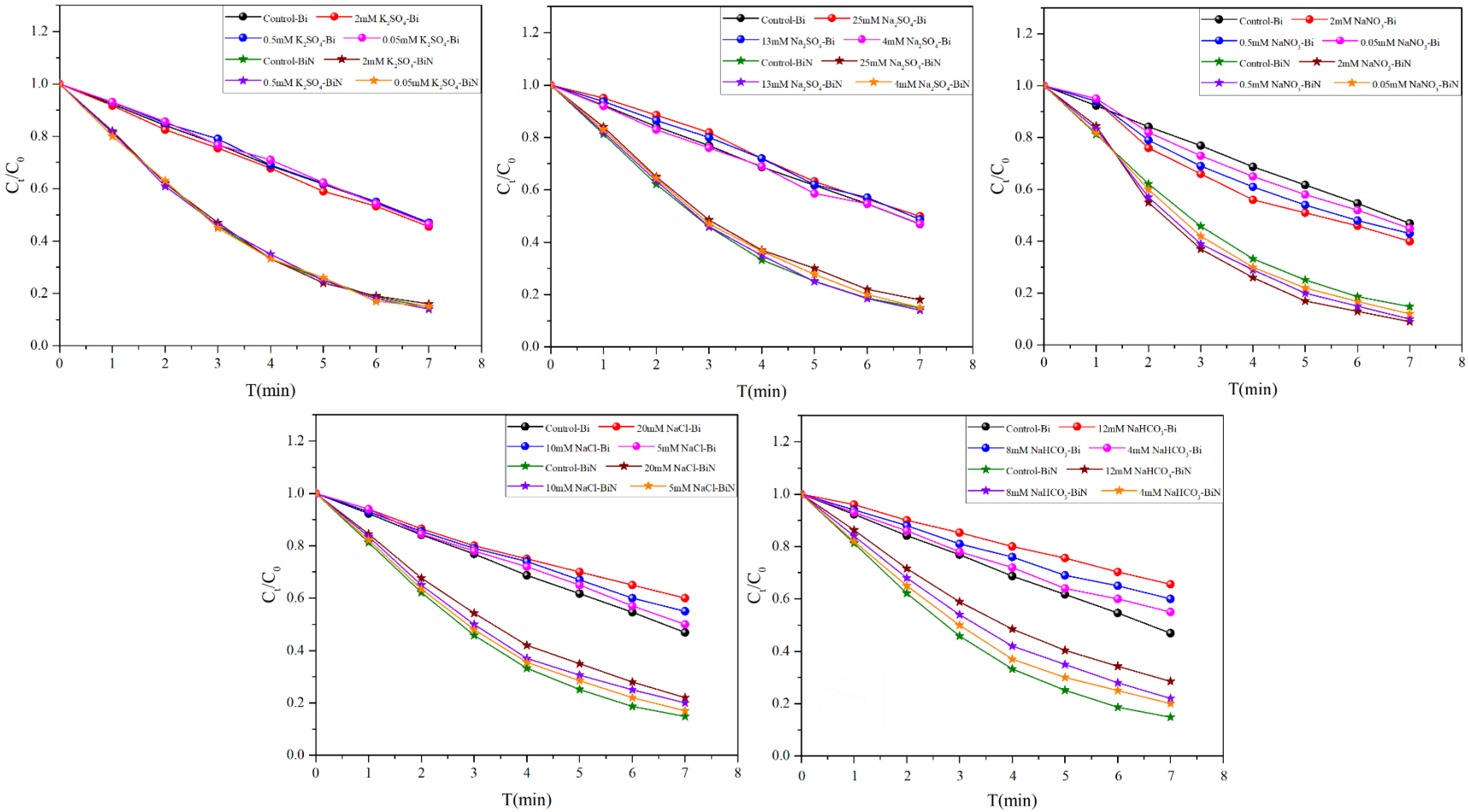

Fig. 4.15 The effects of different salts on the photocatalytic degradation of T2HT4CA using Bi_2WO_6 and Bi_2WO_6 /NiO/Ag. [Buffer: [$NaHCO_3$]=5mM, [Catalyst] = 0.5g/L, concentration of mixtures = 60 mg/L].

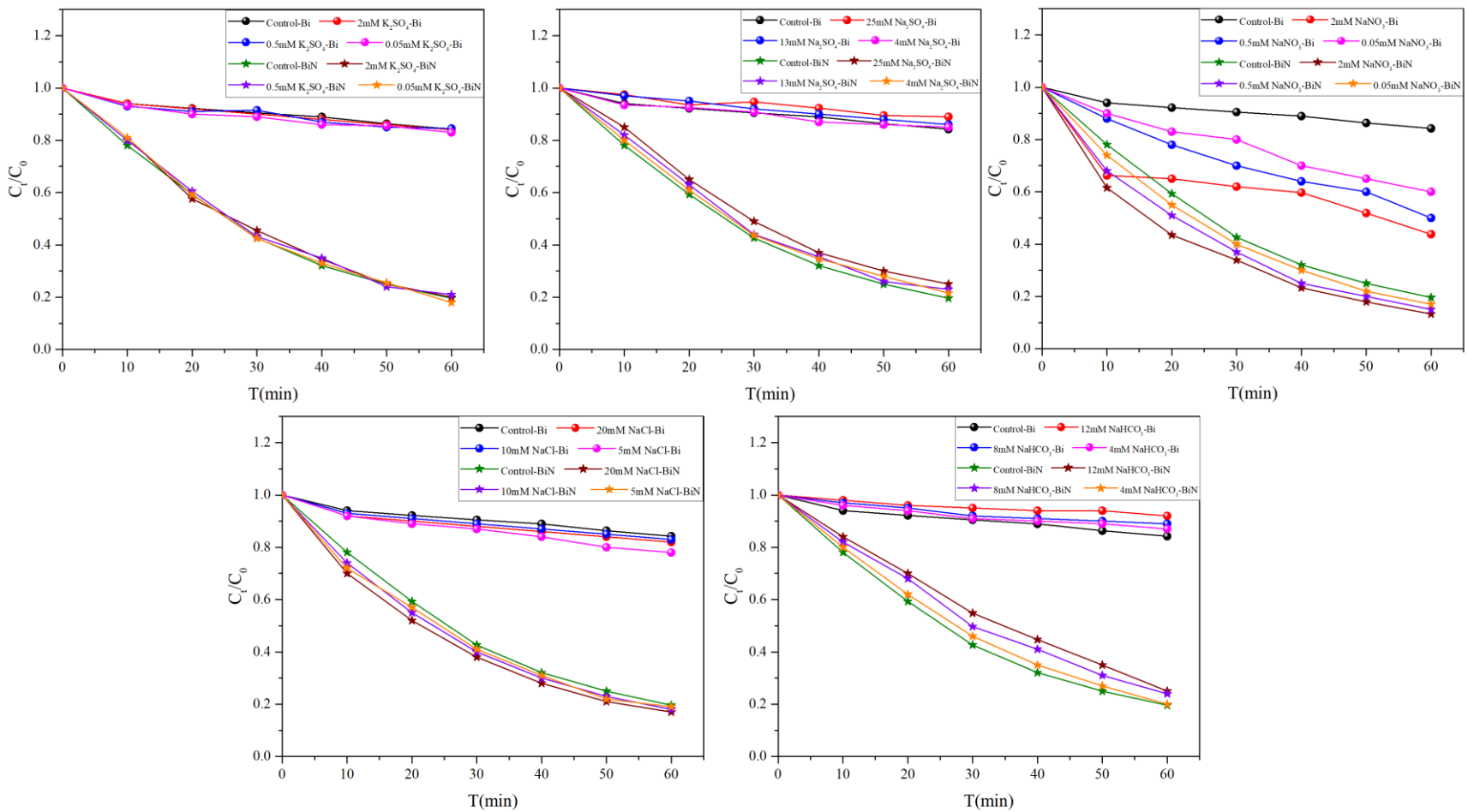

Fig. 4.16 The effects of different salts on the photocatalytic degradation of IA using Bi_2WO_6 and Bi_2WO_6 /NiO/Ag. [Buffer: [$NaHCO_3$]=5mM, [Catalyst] = 0.5g/L, concentration of mixtures = 60 mg/L].

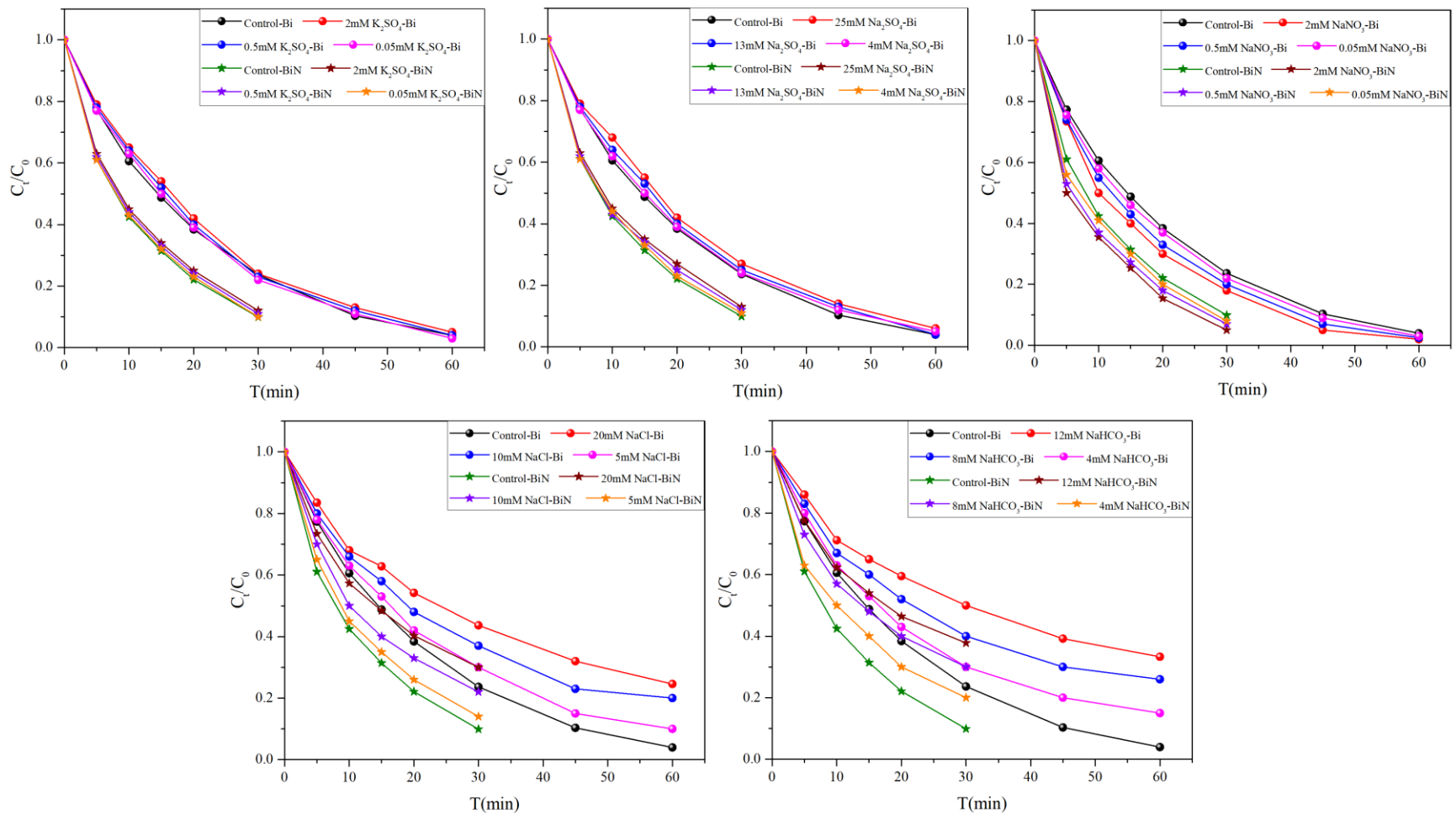

Fig. 4.17 The effects of different salts on the photocatalytic degradation of DCTA using Bi_2WO_6 and Bi_2WO_6 /NiO/Ag. [Buffer: [$NaHCO_3$]=5mM, [Catalyst] = 0.5g/L, concentration of mixtures = 60 mg/L].

4.3.3 The effect of NO_3^- on the degradation pathway of ACA

In order to understand the impact of photocatalyst on the degradation pathways of NAs in the presence of nitrate, the degradation of ACA as a model NA in the presence of nitrate and catalyst, only nitrate and only catalyst were studied (Table B2 in appendix B and Fig. 4.8). The degradation pathways of ACA (Fig. 4.8) in the presence of nitrate with direct photolysis only was similar to our previous study on the phtotodegradation of ACA (Qin et al. 2019a). Only single hydroxylated and carbonyl substituted by-products (P1, P2 and P3, Fig. 4.8) were detected when using catalyst without nitrate. When treated with catalyst in the presence of nitrate, in addition to P1, P2, and P3, by-products with multiple hydroxyls, nitroso or nitro substitution were produced (P7 and P8). The difference in the by-products form between photocatalytic degradation and direct photodegradation might be due to the difference in their degradation mechanism. In direct photodegradation, $^{\bullet}OH$ was the main reactive species resulting in by-products with hydroxylated and carbonyl substitution (Qin et al. 2019a). While in the photocatalytic degradation, the main reactive species were h^+ and $O_2^{\bullet-}$, and $^{\bullet}OH$ generated as a secondary reactive species (Meng et al. 2021), thus the only single hydroxyl and carbonyl substituted by-products were generated in the absences of nitrate. In the presence of nitrate, h^+ and $O_2^{\bullet-}$ could react with nitrate to generate $NO^{\bullet}$, which can in turn generate $^{\bullet}OH$. This resulted in the formation of multiple hydroxyls, nitroso or nitro substituted by-products. The observation of only P7 and P8 and without the detection of P4 to P6 after irradiation was that the rate of reaction in the photocatalytic was much faster than direct photodegradation only.

The acute and chronic toxicity towards aquatic organism of the by-products was predicted using Ecological Structure Activity Relationships (ECOSAR, US EPA) (Table 4.5 and 4.6). Table 4.6 illustrated that only the parent compound, ACA, demonstrated both acute and chronic toxicity.

By-products P5 and P6, which are produced by photodegradation in the presence of nitrate demonstrated chronic toxicity towards Daphnid. As nitrate is definitely present in OSPW, these by-products can also be expected to be formed in OSPW after photodegradation. The by-products formed (P7 and P8) from the photocatalytic degradation do not demonstrate acute and chronic toxicity towards aquatic organism. This showed that the photocatalytic process not only speed up the degradation of NAs but also help to migrate the possible toxic by-products.

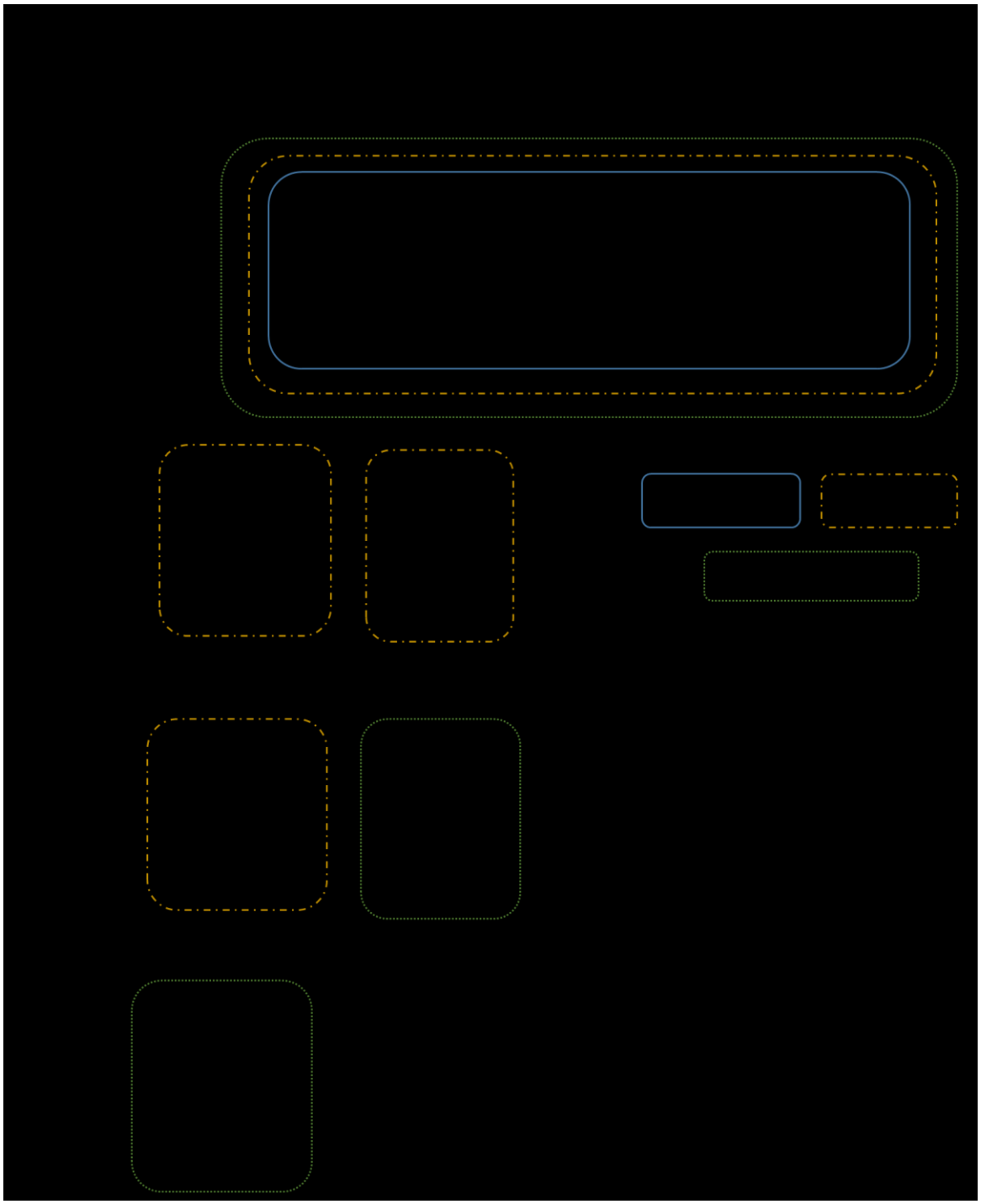

Fig. 4.18 The degradation pathways of ACA by treatments of catalyst only, nitrate only and catalyst + nitrate.

Table 4.12 Toxicity classification according to the Globally Harmonized System of Classification and Labelling of Chemicals.

Toxicity range (mg/L)	Class
LC_{50}/EC_{50} [a] ≤ 1	Very toxic
$1 < LC_{50}/EC_{50} \leq 10$	Toxic
$10 < LC_{50}/EC_{50} \leq 100$	Harmful
$LC_{50}/EC_{50} > 100$	Not harmful

[a] LC_{50}, half lethal concentration; EC_{50}, half effective concentration.

Table 4.13 Predicted toxicity of ACA and its degradation products based on ECOSAR program.

Compounds	Acute toxicity (mg/L)			Chronic toxicity (mg/L)		
	Fish 96 h-LC_{50}	Daphnid 48 h-LC_{50}	Green algae 96 h-EC_{50}	Fish	Daphnid	Green algae
ACA	136.249	85.798	83.769	15.101	11.289	33.060
P1	3315.686	1823.016	1188.710	312.018	162.546	289.759
P2	3571.209	1957.009	1258.711	334.752	172.891	304.566
P3	2371.360	1322.861	915.898	227.005	122.809	230.588
P4	34588.21	17186.82	7375.039	2888.64	1156.29	1435.02
P5	2659.524	1344.777	620.234	226.730	94.976	125.465
P6	5782.273	567.733	687.571	608.086	38.621	198.467
P7	29461.23	13418.63	4017.39	2220.32	708.52	643.919
P8	35427.80	3053.477	4785.482	5542.25	182.999	1257.48

4.3.4 The transformation pathway of DTCA

Previously, classical NAs were regarded as the most toxic NAs in the OSPW (Morandi et al. 2015). However, in latest studies, SO_3^+ and O_3^+ species, rather than classical NAs, were predicted to be potential chemicals causing Nrf2 response of Japanese medaka (*Oryzias latipes*) (Sun et al. 2017). Furthermore, oxygen-, sulfur, and nitrogen-containing chemical species but not classical NAs inhibited the activity of multidrug-resistance protein (Alharbi et al. 2016). Therefore, there is an increasing need to explore the degradation details of heteroatomic NAs. The transformation products and reaction pathways of DTCA were firstly studied and proposed in Fig. 4.9. DCTA

first underwent a decarboxylation to produce TP1 as the β carbon was the most reactive carbon in the structure as confirmed by the DFT calculation (Table 4.7). In addition, the β carbon is also the most electron rich atom (Fig 4.10) and thus it is easier to donate an electron to h^+. As the thiol's sulphur can be easily oxidized, TP1 was degraded to TP2 through the removal of a sulphate. TP2 was then oxidized into a carboxylic acid to TP3 by either the oxidation from $^{\bullet}OH$ or a combination of $O_2^{\bullet-}$ and $^{\bullet}OH$. The benzene of TP3 would then be oxidized by $^{\bullet}OH$ to generate a phenolic TP4 or with to $O_2^{\bullet-}$ form a ketone (TP5). TP5 could also be formed from the further oxidation of the phenolic group in TP4.

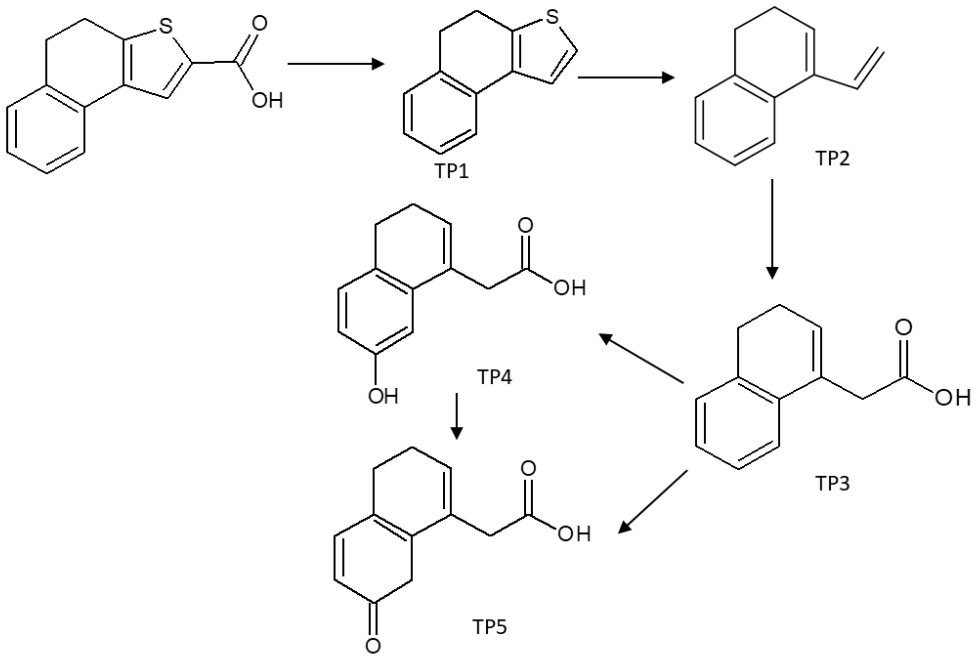

Fig. 4.19 Possible transformation pathway of photocatalytic degradation of DTCA.

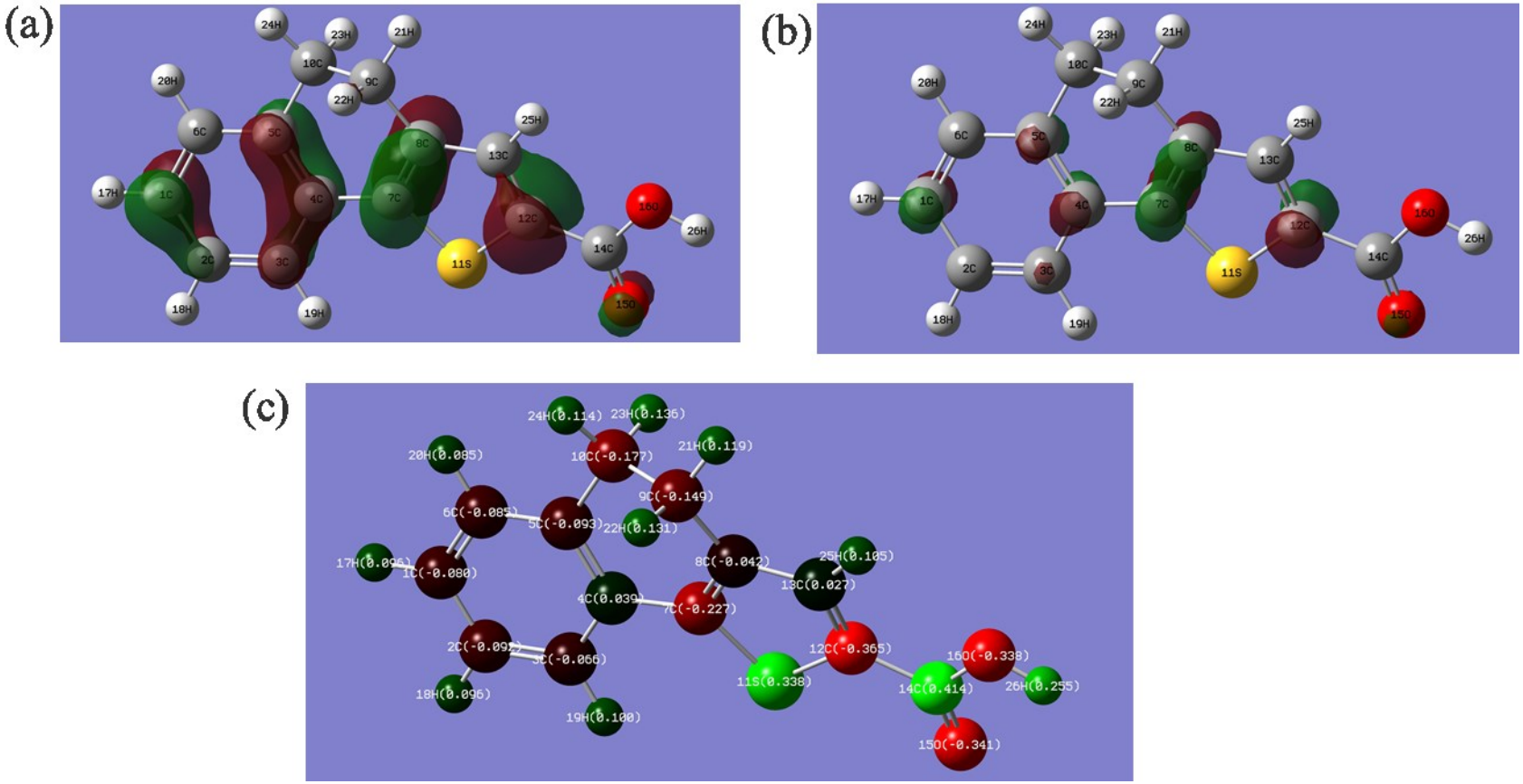

Fig. 4.20 Isodensity surfaces of HOMO with an isovalue of (a) 0.08 and (b) 0.05; (c) Mulliken atomic charge.

Table 4.14 Frontier electron densities on atoms of DCTA calculated by Gaussian 09 program at B3LYP/6-311 + G** level.

Number (atom)	$2FED^2_{HOMO}$
1C	0.115620813
2C	0.029023546
3C	0.049656879
4C	0.107972985
5C	0.087225671
6C	0.003511692
7C	0.17603944
8C	0.138187508
9C	0.014179639
10C	0.010222333
11S	0.005693117
12C	0.206999476
13C	0.014081077
14C	0.004249125
15O	0.045845305
16O	0.010147165
17H	0.000152209
18H	0.000115706
19H	0.000105204
20H	0.000141519
21H	0.002436297

22H	0.022693641
23H	0.01479271
24H	0.000233576
25H	3.75836E-05
26H	5.33504E-05

4.4 Conclusions

In this study, we have investigated the comparative photocatalytic performance of six model NA compounds mixtures by Bi_2WO_6 and Bi_2WO_6/NiO/Ag in buffered and IF matrices. The higher removal efficiencies of these organic pollutants were found using the heterojunction catalysts. The distinct water matrices significantly affected the removal of model NA compounds. Further experimental analysis suggested that chloride and bicarbonate could commonly produce the inhibited effects for photocatalytic pollutant elimination, while NO_3^- could accelerate the degradation. The effects of NO_3^- on the photocatalytic degradation of ACA were also studied. Additionally, the transformation products of DTCA were characterized based on the UPLC-TOF-MS analysis, from which the reaction pathways were proposed for the photocatalytic system. The use of frontier molecular orbital calculations further confirmed the initial reaction sites for these organic compounds. Overall, these findings facilitate the understanding of the water matrix-induced transformation process of model NA compounds during photocatalytic treatment.

4.5 References

Abdalrhman, A.S., Ganiyu, S.O. and Gamal El-Din, M. (2019) Degradation kinetics and structure-reactivity relation of naphthenic acids during anodic oxidation on graphite electrodes. Chemical Engineering Journal 370, 997-1007.

Abdalrhman, A.S., Wang, C., How, Z.T. and Gamal El-Din, M. (2021) Degradation of cyclohexanecarboxylic acid as a model naphthenic acid by the UV/chlorine process: Kinetics and by-products identification. Journal of Hazardous Materials 402, 123476.

Abdalrhman, A.S., Zhang, Y., Arslan, M. and Gamal El-Din, M. (2020) Low-current electro-oxidation enhanced the biodegradation of the recalcitrant naphthenic acids in oil sands process water. Journal of Hazardous Materials 398, 122807.

Afzal, A., Chelme-Ayala, P., Drzewicz, P., Martin, J.W. and Gamal El-Din, M. (2015) Effects of Ozone and Ozone/Hydrogen Peroxide on the Degradation of Model and Real Oil-Sands-Process-Affected-Water Naphthenic Acids. Ozone: Science & Engineering 37(1), 45-54.

Afzal, A., Drzewicz, P., Pérez-Estrada, L.A., Chen, Y., Martin, J.W. and Gamal El-Din, M. (2012) Effect of Molecular Structure on the Relative Reactivity of Naphthenic Acids in the UV/H2O2 Advanced Oxidation Process. Environmental Science & Technology 46(19), 10727-10734.

Alharbi, H.A., Saunders, D.M.V., Al-Mousa, A., Alcorn, J., Pereira, A.S., Martin, J.W., Giesy, J.P. and Wiseman, S.B. (2016) Inhibition of ABC transport proteins by oil sands process affected water. Aquatic Toxicology 170, 81-88.

Anderson, J., Wiseman, S.B., Moustafa, A., Gamal El-Din, M., Liber, K. and Giesy, J.P. (2012) Effects of exposure to oil sands process-affected water from experimental reclamation ponds on Chironomus dilutus. Water Research 46(6), 1662-1672.

Fang, Z., Huang, R., Chelme-Ayala, P., Shi, Q., Xu, C. and Gamal El-Din, M. (2019) Comparison of UV/Persulfate and UV/H2O2 for the removal of naphthenic acids and acute toxicity towards Vibrio fischeri from petroleum production process water. Science of the Total Environment 694, 133686.

Fang, Z., Huang, R., How, Z.T., Jiang, B., Chelme-Ayala, P., Shi, Q., Xu, C. and Gamal El-Din, M. (2020) Molecular transformation of dissolved organic matter in process water from oil and gas operation during UV/H2O2, UV/chlorine, and UV/persulfate processes. Science of the Total Environment 730, 139072.

Gamal El-Din, M., Fu, H., Wang, N., Chelme-Ayala, P., Pérez-Estrada, L., Drzewicz, P., Martin, J.W., Zubot, W. and Smith, D.W. (2011) Naphthenic acids speciation and removal during petroleum-coke adsorption and ozonation of oil sands process-affected water. Science of the Total Environment 409(23), 5119-5125.

Ganiyu, S.O. and Gamal El-Din, M. (2020) Insight into in-situ radical and non-radical oxidative degradation of organic compounds in complex real matrix during electrooxidation with boron doped diamond electrode: A case study of oil sands process water treatment. Applied Catalysis B: Environmental 279, 119366.

Garcia-Garcia, E., Ge, J.Q., Oladiran, A., Montgomery, B., El-Din, M.G., Perez-Estrada, L.C., Stafford, J.L., Martin, J.W. and Belosevic, M. (2011) Ozone treatment ameliorates oil sands process water toxicity to the mammalian immune system. Water Research 45(18), 5849-5857.

Hagen, M.O., Katzenback, B.A., Islam, M.D.S., Gamal El-Din, M. and Belosevic, M. (2013) The Analysis of Goldfish (Carassius auratus L.) Innate Immune Responses After Acute and

Subchronic Exposures to Oil Sands Process-Affected Water. Toxicological Sciences 138(1), 59-68.

He, Y., Patterson, S., Wang, N., Hecker, M., Martin, J.W., El-Din, M.G., Giesy, J.P. and Wiseman, S.B. (2012a) Toxicity of untreated and ozone-treated oil sands process-affected water (OSPW) to early life stages of the fathead minnow (Pimephales promelas). Water Research 46(19), 6359-6368.

He, Y., Wiseman, S.B., Hecker, M., Zhang, X., Wang, N., Perez, L.A., Jones, P.D., Gamal El-Din, M., Martin, J.W. and Giesy, J.P. (2011) Effect of Ozonation on the Estrogenicity and Androgenicity of Oil Sands Process-Affected Water. Environmental Science & Technology 45(15), 6268-6274.

He, Y., Wiseman, S.B., Wang, N., Perez-Estrada, L.A., El-Din, M.G., Martin, J.W. and Giesy, J.P. (2012b) Transcriptional Responses of the Brain–Gonad–Liver Axis of Fathead Minnows Exposed to Untreated and Ozone-Treated Oil Sands Process-Affected Water. Environmental Science & Technology 46(17), 9701-9708.

Huang, R., Wang, C., Chelme-Ayala, P., Fang, Z., Shi, Q., Xu, C. and Gamal El-Din, M. (2019) Ferrate oxidation of distinct naphthenic acids species isolated from process water of unconventional petroleum production. Science of the Total Environment 672, 906-915.

Iguchi, S., Teramura, K., Hosokawa, S. and Tanaka, T. (2015) Effect of the chloride ion as a hole scavenger on the photocatalytic conversion of CO2 in an aqueous solution over Ni–Al layered double hydroxides. Physical Chemistry Chemical Physics 17(27), 17995-18003.

Jones, D., Scarlett, A.G., West, C.E. and Rowland, S.J. (2011) Toxicity of Individual Naphthenic Acids to Vibrio fischeri. Environmental Science & Technology 45(22), 9776-9782.

Luo, Z., Meng, L., How, Z.T., Chelme-Ayala, P., Yang, L., Benally, C. and Gamal El-Din, M. (2022) Treatment of oil sands process water by the ferric citrate under visible light irradiation. Chemical Engineering Journal 429, 132419.

Meng, L., How, Z.T., Ganiyu, S.O. and Gamal El-Din, M. (2021) Solar photocatalytic treatment of model and real oil sands process water naphthenic acids by bismuth tungstate: Effect of catalyst morphology and cations on the degradation kinetics and pathways. Journal of Hazardous Materials 413, 125396.

Morandi, G.D., Wiseman, S.B., Pereira, A., Mankidy, R., Gault, I.G.M., Martin, J.W. and Giesy, J.P. (2015) Effects-Directed Analysis of Dissolved Organic Compounds in Oil Sands Process-Affected Water. Environmental Science & Technology 49(20), 12395-12404.

Nero, V., Farwell, A., Lee, L.E.J., Van Meer, T., MacKinnon, M.D. and Dixon, D.G. (2006) The effects of salinity on naphthenic acid toxicity to yellow perch: Gill and liver histopathology. Ecotoxicology and Environmental Safety 65(2), 252-264.

Qin, R., Chelme-Ayala, P. and El-Din, M.G. (2020) The impact of oil sands process water matrix on the ozonation of naphthenic acids: from a model compound to a natural mixture. 47(10), 1166-1174.

Qin, R., How, Z.T. and Gamal El-Din, M. (2019a) Photodegradation of naphthenic acids induced by natural photosensitizer in oil sands process water. Water Research 164, 114913.

Qin, R., Lillico, D., How, Z.T., Huang, R., Belosevic, M., Stafford, J. and Gamal El-Din, M. (2019b) Separation of oil sands process water organics and inorganics and examination of their acute toxicity using standard in-vitro bioassays. Science of the Total Environment 695, 133532.

Shu, Z., Li, C., Belosevic, M., Bolton, J.R. and El-Din, M.G. (2014) Application of a Solar UV/Chlorine Advanced Oxidation Process to Oil Sands Process-Affected Water Remediation. Environmental Science & Technology 48(16), 9692-9701.

Song, J., Messele, S.A., Meng, L., Huang, Z. and Gamal El-Din, M. (2021) Adsorption of metals from oil sands process water (OSPW) under natural pH by sludge-based Biochar/Chitosan composite. Water Research 194, 116930.

Suara, M.A., Ganiyu, S.O., Paul, S., Stafford, J.L. and Gamal El-Din, M. (2022) Solar-activated zinc oxide photocatalytic treatment of real oil sands process water: Effect of treatment parameters on naphthenic acids, polyaromatic hydrocarbons and acute toxicity removal. Science of the Total Environment 819, 153029.

Sun, J., Peng, H., Alharbi, H.A., Jones, P.D., Giesy, J.P. and Wiseman, S.B. (2017) Identification of Chemicals that Cause Oxidative Stress in Oil Sands Process-Affected Water. Environmental Science & Technology 51(15), 8773-8781.

Wang, C., Klamerth, N., Huang, R., Elnakar, H. and Gamal El-Din, M. (2016) Oxidation of Oil Sands Process-Affected Water by Potassium Ferrate(VI). Environmental Science & Technology 50(8), 4238-4247.

Wang, N., Chelme-Ayala, P., Perez-Estrada, L., Garcia-Garcia, E., Pun, J., Martin, J.W., Belosevic, M. and Gamal El-Din, M. (2013) Impact of Ozonation on Naphthenic Acids Speciation and Toxicity of Oil Sands Process-Affected Water to Vibrio fischeri and Mammalian Immune System. Environmental Science & Technology 47(12), 6518-6526.

Wiseman, S.B., Anderson, J.C., Liber, K. and Giesy, J.P. (2013) Endocrine disruption and oxidative stress in larvae of Chironomus dilutus following short-term exposure to fresh or aged oil sands process-affected water. Aquatic Toxicology 142-143, 414-421.

Zhang, Y., Chelme-Ayala, P., Klamerth, N. and Gamal El-Din, M. (2017) Application of UV-irradiated Fe(III)-nitrilotriacetic acid (UV-Fe(III)NTA) and UV-NTA-Fenton systems to degrade model and natural occurring naphthenic acids. Chemosphere 179, 359-366.

Zhang, Y., Klamerth, N., Chelme-Ayala, P. and Gamal El-Din, M. (2016) Comparison of Nitrilotriacetic Acid and [S,S]-Ethylenediamine-N,N′-disuccinic Acid in UV–Fenton for the Treatment of Oil Sands Process-Affected Water at Natural pH. Environmental Science & Technology 50(19), 10535-10544.

CHAPTER 5 COMPARISION OF DIFFERENT OXIDANT ASSISTED PHOTOCATALYTIC TREATMENT OF OSPW: H_2O_2, PMS and $KMnO_4$

5.1 Introduction

The ever-growing contaminants in water produced by industrial activities have resulted in extensive concerns due to their compositional complexity, non-biodegradability, and high toxicity. Conventional wastewater treatment technologies such as biodegradation and adsorption suffer from problems like long periodicity, low stability, and secondary pollution. Therefore, novel treatment technologies are highly desired. So far, various advanced oxidation processes (AOPs) have shown the potential for the degradation of recalcitrant organics in wastewater, categorized into ozone based AOPs (Wang et al. 2011, Zhao et al. 2017), permanganate ($KMnO_4$) based AOPs (Jiang et al. 2009, Tian et al. 2019), Fenton, photo-Fenton (Michael et al. 2012, Trovó et al. 2011), UV based AOPs (Meng et al. 2017, Tang et al. 2020), photocatalysis (Meng et al. 2021, Xu et al. 2021), electrochemical oxidation (García-Espinoza et al. 2018, Loos et al. 2018), radiation (Liu et al. 2016b, Wang and Wang 2018) and sonolysis (Güyer and Ince 2011, Serna-Galvis et al. 2016). Among these technologies, photocatalysis has attracted considerable interest due to the potential capability for the utilization of solar energy and reusable nanomaterials. The synergistic effects of photocatalyst and oxidant especially peroxymonosulfate (PMS) could further improve the efficiency of oxidants, meanwhile accelerating the separation of electron and hole in catalysts and promoting the photocatalytic activity. However, the studies of comparison of different oxidant-assisted photocatalysis are rare and the removal mechanisms are unclear. Therefore, hydrogen peroxide (H_2O_2), PMS and $KMnO_4$ assisted photocatalysis were selected to compare the different performance for the treatment of real oil sands process water (OSPW).

H_2O_2 is the typical oxidant used in hydroxyl radical-based AOPs (HR-AOPs). It was reported that H_2O_2 enhances the photocatalytic degradation of target pollutants. For example, the treatment efficiency of real textile effluents decreased as: UV/TiO_2/H_2O_2 > UV/Fe^{2+}/H_2O_2 > UV/TiO_2 > UV/H_2O_2 (Garcia et al. 2007). MoSx/hemin supported fibrous catalysts achieved significant degradation rate of dye and stable catalytic performance in the presence of H_2O_2 under visible light irradiation (Ji et al. 2019). However, Bessa *et al.* (Bessa et al. 2001) reported that the addition of H_2O_2 for the photocatalytic treatment of contaminants in oil field produced waters is undesirable due to the corrosion of H_2O_2 for photocatalyst TiO_2.

Extensive research has been reported related to the sulfate radical-based advanced oxidation processes (SR-AOPs), which are regarded as interesting alternatives to HR-AOPs. Compared to non-selective $^{\bullet}OH$, $SO_4^{\bullet-}$ is an electron transfer oxidant, and has a comparable oxidizing ability with $^{\bullet}OH$ (E_0 = 2.5–3.1 V). It can exist in a wider pH range and has longer half-time ($t_{1/2}$ = 30-40μs) than $^{\bullet}OH$ ($t_{1/2}$ = 10ns) in aquatic systems (Oh et al. 2016). Various single and heterojunction catalysts were successfully applied for PMS assisted photocatalytic system such as α-Sulfur (Andrew Lin and Zhang 2016), metal and metal oxides based catalyst (Gao et al. 2018, Liu et al. 2016a, Liu et al. 2017), bismuth-based catalyst (Chen et al. 2020, Feng et al. 2019, Sun et al. 2021, Zhong et al. 2020), and carbon based catalysts (Duan et al. 2016, Wang et al. 2017b). For instance, after 5 min irradiation, 86.2% removal of ciprofloxacin was achieved by Co_3O_4/Bi_2WO_6 photocatalysis in the presence of PMS due to the formation of p-n heterojunction and PMS worked as electron accepter (Sun et al. 2021). It was reported that TiO_2/PMS is more efficient than TiO_2/persulfate, TiO_2/H_2O_2 and single TiO_2 for the degradation of Acid Orange 7 under visible light (Chen et al. 2012).

Initially, $KMnO_4$ is mainly used to remove dissolved iron and manganese in water, taste and odor and inhibit the growth of microorganisms. The potential of removing organic pollutants from water by $KMnO_4$ based AOP is gradually became a research hotspot because of the diversity of active species during oxidation processes and the complexity of reaction mechanisms. It was reported that $KMnO_4$ could be activated by visible light in the presence of biochar. The removal of sulfamethoxazole significantly increased to 97% in 30 min by the addition of biochar powder, and simultaneous removal of the total organic carbon was more than 58%. The increased removal was attributed to the generation of intermediate reactive manganese species and the adsorption of biochar (Tian et al. 2019).

Oil sands process water (OSPW) is generated during the process of oil sands mining and extraction and is a complex mixture of inorganic and organic matters such as naphthenic acids (NAs). OSPW has shown acute and chronic toxicity to different living species and the organic fraction was suspected to be the major contributor to the toxicity. Thus, OSPW needs to be treated before releasing into the environment (Arslan et al. 2022, Fuchylo et al. 2022, Ganiyu et al. 2022, Luo et al. 2022).

Therefore, in this study, we firstly applied H_2O_2, PMS, $KMnO_4$ for photocatalytic remediation of real OSPW using z-scheme photocatalyst Bi_2WO_6/NiO/Ag. The removal efficiencies were compared through the degradation of aromatic organics. The toxicity was evaluated through Microtox assays. The mechanisms were studied using quenching experiments and electron paramagnetic resonance (EPR). The degradation of organic compounds in OSPW were monitored through synchronous fluorescence spectra (SFS) and ultra-performance liquid chromatography coupled with time-of-flight mass spectrometry (UPLC-TOF-MS). This study will provide new

insights into the oxidant assisted photocatalytic mechanisms and will benefit the design of environmentally friendly catalytic processes for passive OSPW treatment.

5.2 Materials and methods

5.2.1 Chemicals and materials

Raw OSPW was collected from an active oil sands tailings pond in Fort McMurray, Alberta, Canada, and stored in a cold room at 4 °C. Table 5.1 lists the properties of the raw OSPW. Methanol (MeOH), 1-adamantanecarboxylic acid (ACA), ammonium oxalate (AO), H_2O_2, tert-butyl alcohol (TBA), PMS, 4-hydroxy 2, 2, 6, 6-tetramethylpiperidinyloxy (TEMPOL) and $KMnO_4$ were purchased from Sigma Aldrich. The spin-trapping agents 5,5-dimethyl-1-pyrroline-N-oxide (DMPO) was obtained from Dojindo Molecular Technologies Inc. All chemicals were of analytical grade and used as received without further purification. Ultrapure water (R ≥ 18.2 MΩ) produced in-house by Millipore Milli-Q system was used to prepare solutions.

Table 5.3 Properties, major ions and organic composition of raw OSPW.

Parameter	Value
pH	8.5 ± 0.2
Alkalinity (mg L^{-1} as $CaCO_3$)	470 ± 10
Conductivity (mS cm^{-1})	3.3 ± 0.4
Total suspended solids (mg L^{-1})	76 ± 7
Ions (mg L^{-1})	
K	56.32 ± 0.622
Na	1,273 ± 8.734
S	40.37 ± 0.554
Cl^-	523.6755 ± 4.786
SO_4^{2-}	87.5553 ± 6.012
CO_3^{2-}	1078.4523 ± 27.3
NO_3^-	21.002 ± 0.876
Organic parameters (mg L^{-1})	
Dissolved organic carbon (mg L^{-1} as C)	66.2 ± 4.5
Classical NAs (O_2-NAs)	31.46 ± 1.7
O_3-NAs	19.85 ± 0.6
O_4-NAs	17.4 ± 0.8
O_5-NAs	7.3 ± 0.3
O_6-NAs	2.5 ±0.3

5.2.2 Photocatalytic degradation

The photocatalytic degradation of NAs in the presence or absence of oxidants were performed under 300W Xenon lamp solar simulator (Newport, USA) irradiation. 0.5 g/L Bi_2WO_6/NiO/Ag was dispersed to 100 mL glass beaker containing 50 mL pre-filtered raw OSPW samples. Before irradiation, 0.1, 1 or 5 mM of H_2O_2, PMS or $KMnO_4$ was added into the suspensions, respectively. At regular interval, 3 mL OSPW was taken and filtrated by 0.22 μm nylon membranes. The saturated sodium thiosulfate solution (Fang et al. 2020, Wang and Wang 2022) and hydroxylamine hydrochloride (Tian et al. 2019) were used to quench the oxidative radicals and stop the further oxidation of NAs by residual H_2O_2, PMS and $KMnO_4$, respectively.

5.2.3 Analytical methods

Active species of photocatalysis in aqueous solution were determined by EPR with an ELEXSYS – II EPR spectrometer (Bruker E–500, Billerica). The running parameters were as follows: The center field of the spectrometer was 3897 G and resonance frequency (empty) of 9.81 GHz. The EPR spectra were detected with a 100 kHz magnetic field modulation with amplitude of 1.0 G at microwave power of 20 mW and 60 s sweep time. DMPO was used as superoxide radical ($O_2^{\bullet-}$), $^{\bullet}OH$ and $SO_4^{\bullet-}$ spin-trapping agent.

SFS before and after treatment were recorded with Varian Cary Eclipse fluorescence spectrometer. Excitation wavelengths ranged from 200 to 600 nm, and emission wavelengths were recorded from 218 to 618 nm. Scanning speed was 600 nm/min and the photomultiplier (PMT) voltage was 800 mV. SFS of OSPW provide specific information on fluorescing compounds: peak I at 267 nm is assigned to one ring aromatics, while peak II at 310 nm and peak III at 330 nm are assigned to aromatics with two and three fused rings, respectively.

The concentration of model NA compound ACA, was measured by an UPLC coupled with a single quadrupole mass spectrometry (SQ Detector 2, Waters). Chromatographic separation was performed at a flow rate of 400 μL·min^{-1} by a BEH C18 column (2.1 mm × 100 mm × 1.7 μm, Waters) maintained at 40 °C. The mobile phase was 0.1% formic acid in water (A) and MeOH (B). The MS was operating in a negative ion mode using an ESI source in single ion monitoring mode. For raw and treated OSPW samples, 1 mL of each water sample was centrifuged at 10000 RPM for 10 min. The injection solution was prepared with 500 μL of the supernatant, 100 μL of 4.0 mg L^{-1} internal standard (ISTD) compound (Myristic acid-1-^{13}C) in MeOH, and 400 μL methanol to reach a final sample volume of 1 mL. The samples were analyzed using UPLC-TOF-MS in high-resolution mode (mass resolution = 40000 FWHM at 1431 m/z) at mass range of 100-600 (m/z). The electrospray ionization source was operated in the negative mode to measure NAs in the samples. Data acquisition was controlled using MassLynx (Waters) and data analysis was performed using TargetLynx (Waters). One raw OSPW sample was used as the quality control sample to ensure the method stability. This method was developed previously for the semi-quantification of NAs based on the signal of a compound versus the signal of spiked ISTD. The chromatographic separation was achieved by a method developed in our previous reports for the separation of NAs (Wang et al. 2013).

5.2.4 Microtox assays

After treated by H_2O_2, PMS and $KMnO_4$ assisted photocatalysis, a Model 500 Microtox toxicity analyzer was employed to test the acute toxicity of OSPW using *Vibrio fischeri* (*V. fischeri*). Due to the potential toxicity of oxidants, OSPW organics were extracted by H_2SO_4. After that, the extract was dissolved in 0.05 N NaOH. Then, the pH of the resulting solution was adjusted

to 8 (Sohrabi et al. 2013). The toxicity bioassay was performed based on the luminescence intensity of *V. fischeri* and the reduction of luminescence induced by the toxicity of organics in OSPW.

5.3 Results and discussion

5.3.1 Aromatics degradation

SFS was a commonly used qualitative and semi-quantitative analysis for fluorophore compounds, which could be used to determine aromatics in OSPW. Fig. 5.1-5.3 illustrated the SFS of OSPW treated by H_2O_2, PMS and $KMnO_4$ assisted photocatalysis at different oxidant doses. The characteristic peaks located at 267 nm, 310 nm and 330 nm were ascribed to aromatics with single, two and three fused rings in OSPW, respectively. The highest intensity of peak 267 nm indicates that single-ring aromatics are the most abundant in OSPW. Bi_2WO_6/NiO/Ag only showed efficient photocatalytic performance for oxidative degradation of aromatics NAs after 6 h illumination with the completely removal of polycyclic aromatics and 78.1% removal of one-ring aromatics due to the production of h^+, $^{\bullet}OH$ and $O_2^{\bullet-}$. It was reported that polycyclic aromatics were degraded to one-ring aromatics such as hydroquinone or benzoquinone, leading to the slow degradation rate of single-ring aromatics (Oturan and Aaron 2014). There are no effects on the photocatalytic degradation of aromatics when 0.1 and 1mM H_2O_2 were added into the solution. However, all the peak areas were significantly reduced in the presence of 5mM H_2O_2 due to the higher production of unselective $^{\bullet}OH$. As for $KMnO_4$ photocatalytic oxidation, with the increase of $KMnO_4$ concentration, the inhibition of aromatics degradation becomes more obvious until the degradation stops. The reason may be the photo shielding effect of $KMnO_4$, in which the purple color hindered the adsorption of photons by catalyst. Another reasonable explanation is that alkaline pH of OSPW resulted in adverse impact on the activation of $KMnO_4$ to produce reactive species. After adding 0.1 mM PMS, the enhanced removal rate of all the three peaks were not

obvious. However, when the concentration increased to 1 mM, after 1h treatment, the removal rate increased from 6.4%, 45.3%, 54.7% at 0.1 mM to 30.5%, 72.6%, 85.9% at 1 mM for aromatics with single-ring, two fused rings and three fused rings, respectively. All the three peaks were completely removed after 1h at the presence of 5 mM PMS, demonstrating the synergistic effects of PMS and photocatalyst for degradation of aromatic NAs.

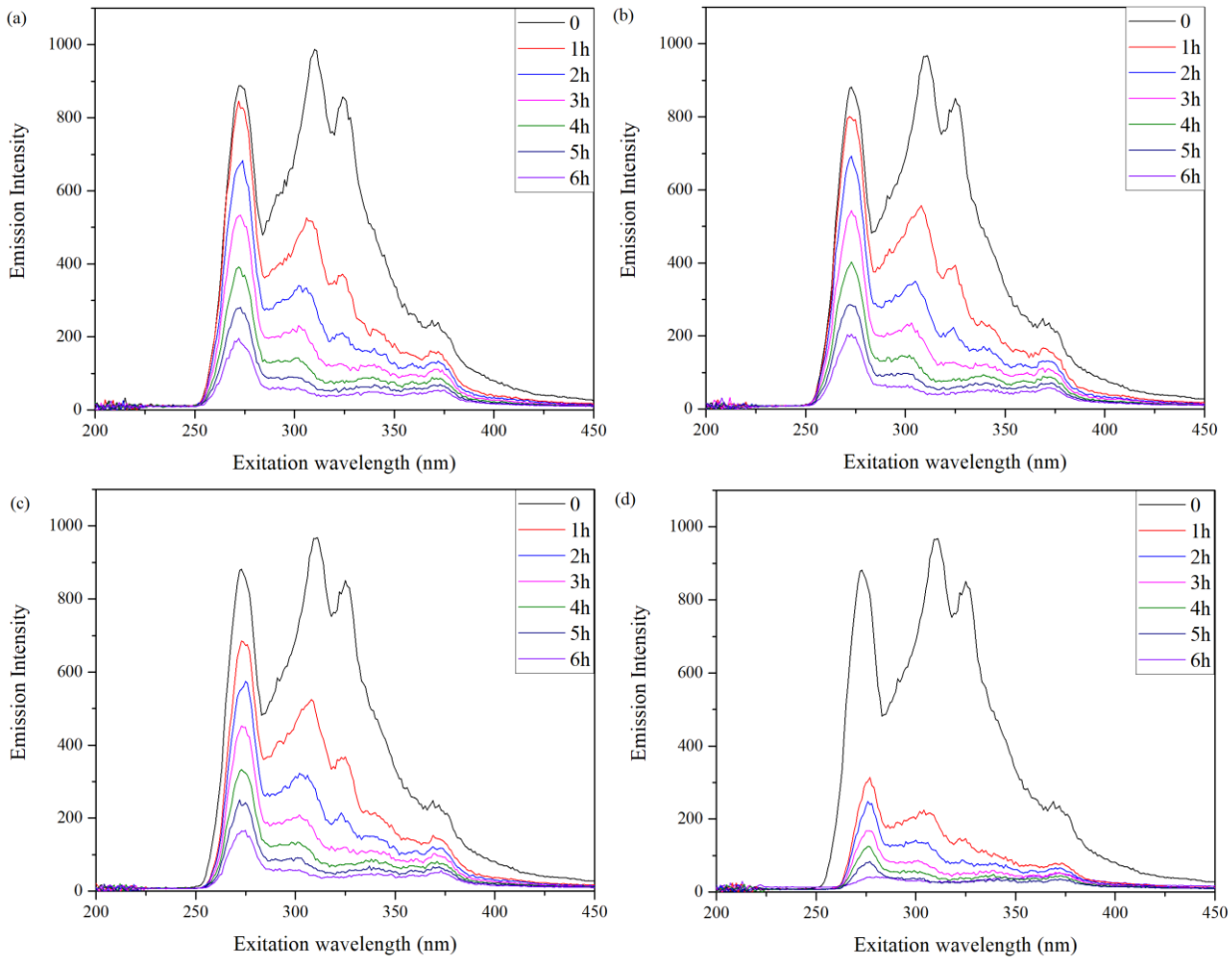

Fig. 5.14 Synchronous fluorescence spectra (SFS) of photocatalytic treatment of OSPW by 0.5g/L Bi_2WO_6/NiO/Ag (a) control; (b) 0.1mM H_2O_2; (c) 1mM H_2O_2 and (d) 5mM H_2O_2.

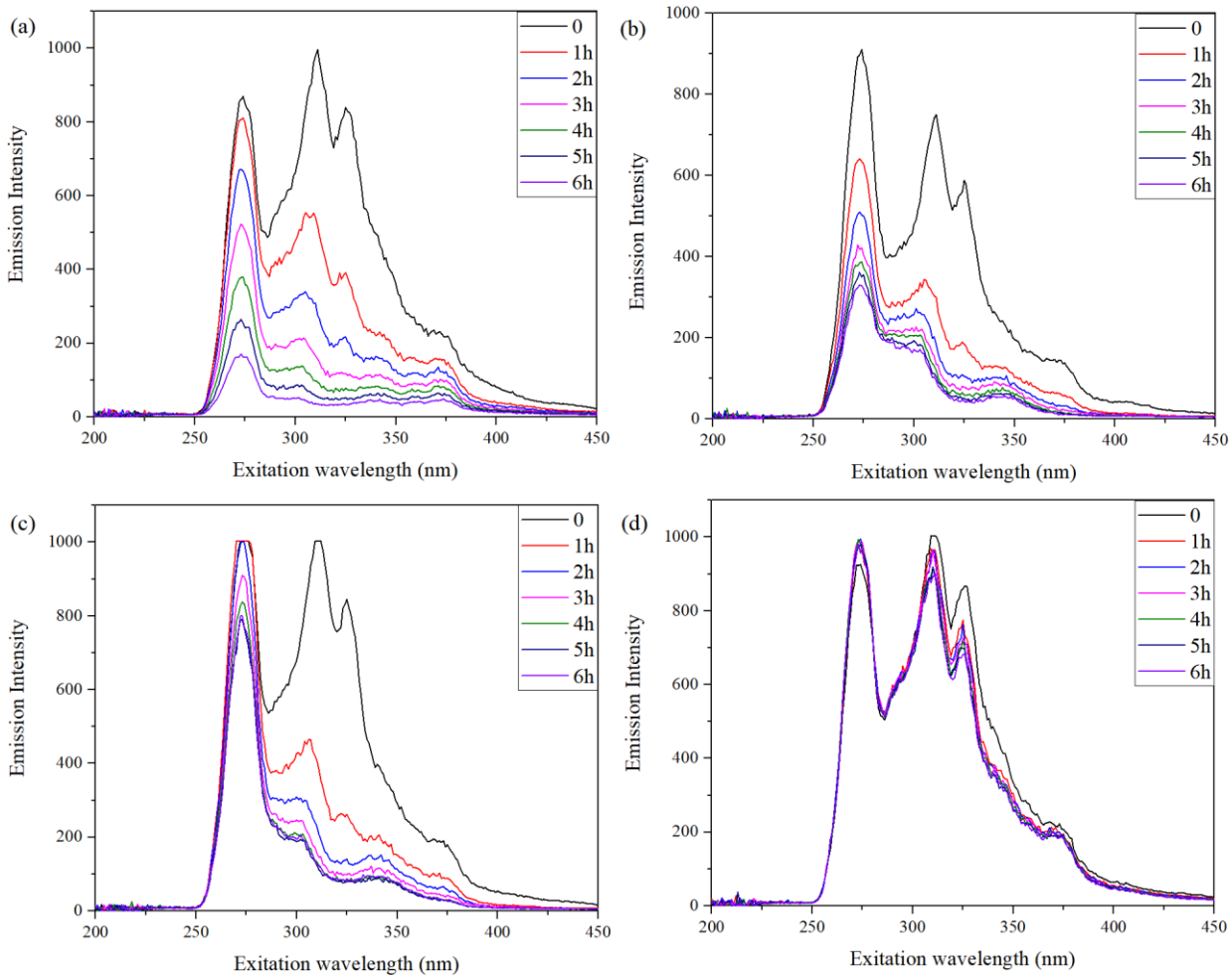

Fig. 5.15 Synchronous fluorescence spectra (SFS) of photocatalytic treatment of OSPW by 0.5g/L Bi_2WO_6/NiO/Ag (a) control; (b) 0.1mM $KMnO_4$; (c) 1mM $KMnO_4$ and (d) 5mM $KMnO_4$.

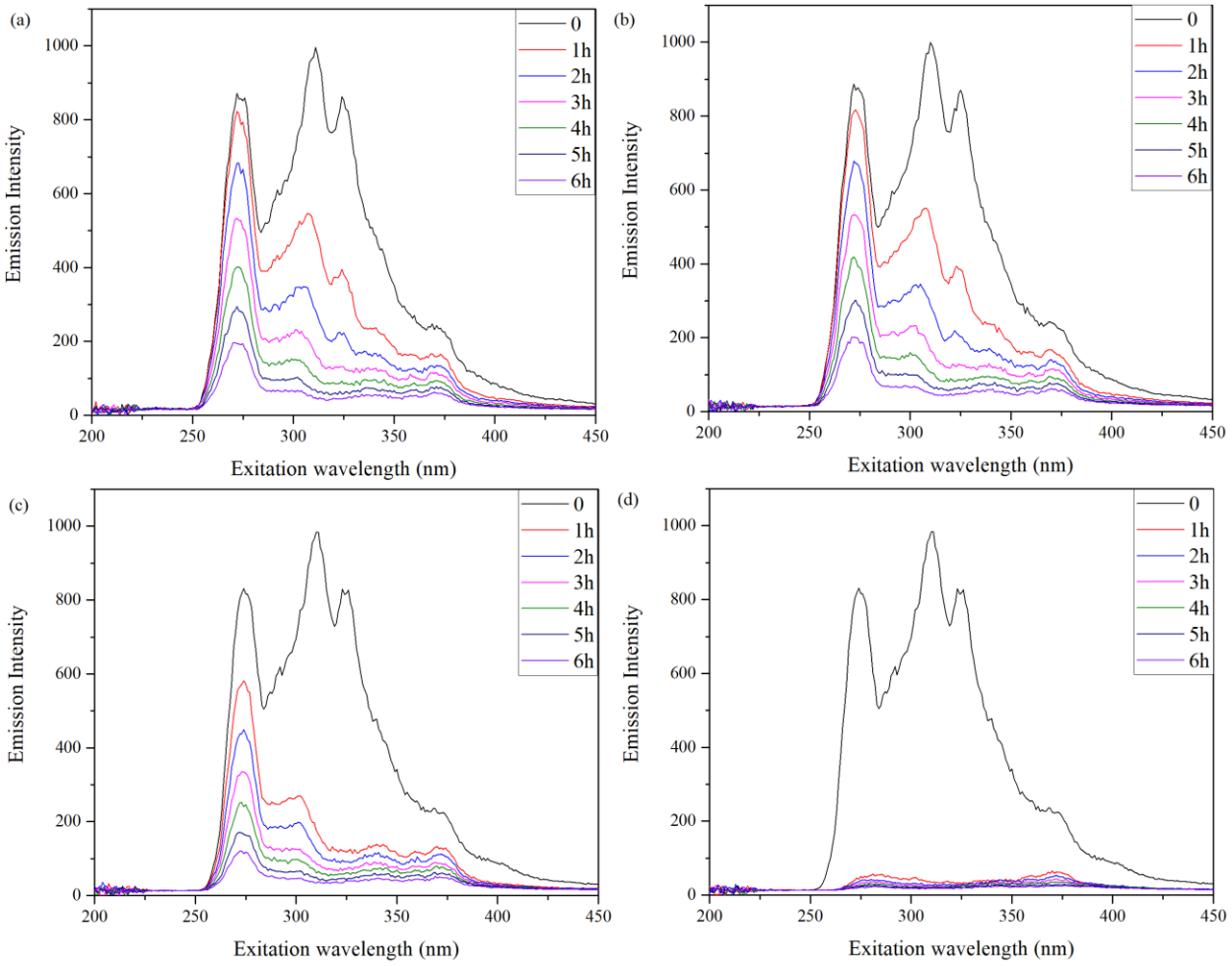

Fig. 5.16 Synchronous fluorescence spectra (SFS) of photocatalytic treatment of OSPW by 0.5g/L Bi_2WO_6/NiO/Ag (a) control; (b) 0.1mM PMS; (c) 1mM PMS and (d) 5mM PMS

5.3.2 Toxicity

Since NAs and their transformation byproducts in OSPW may induce acute toxicity, the Microtox assay was conducted to evaluate the toxicity of OSPW treated by H_2O_2, PMS and $KMnO_4$ assisted photocatalysis after 1h illumination at different dosage of oxidants. As displayed in Fig. 5.4, the inhibition effects of luminescence of *V. fischeri* were 10.7% and 2.9% for OSPW samples treated by 1 mM H_2O_2, PMS assisted photocatalysis, respectively. No inhibition effects

observed of OSPW treated by 5 mM H_2O_2 and PMS assisted photocatalysis, implying H_2O_2 and PMS showed a well detoxification effect on OSPW at high concentration, and the detoxification effect of PMS is better than that of H_2O_2 at low concentration. However, $KMnO_4$ could not efficiently eliminates the toxicity. The increasing inhibition effects were due to the antagonism of $KMnO_4$ and photocatalyst. Based on the results of SFS and toxicity, H_2O_2 and PMS assisted photocatalysis are confirmed to be effective approaches for OSPW treatment and detoxification.

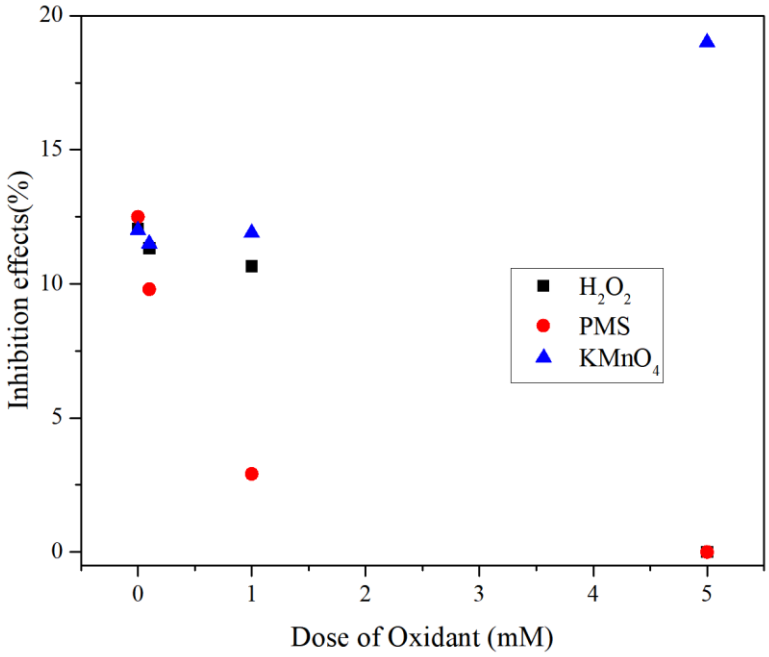

Fig. 5.17 Inhibition effect on Vibrio fischeri caused by OSPW treated with 0.5g/L Bi_2WO_6/NiO/Ag at the presence of different concentrations of H_2O_2, PMS and $KMnO_4$ after 1h illumination

5.3.3 NAs degradation

As the PMS-assisted photocatalysis showed the highest degradation efficiency and the highest reduction of toxicity, only the degradation of NAs by PMS-assisted photocatalysis was

investigated. The overall distribution of NAs based on the carbon numbers and DBE (hydrogen deficiency) in the raw OSPW and in the OSPW treated with the PMS assisted Bi_2WO_6/NiO/Ag photocatalysis after 1h illumination was illustrated in Fig. 5.5-5.9. The concentration of the O_2-NAs, O_3-NAs, O_4-NAs, O_5-NAs and O_6-NAs in raw OSPW was 31.5 mg L^{-1}, 19.9 mg L^{-1}, 17.4 mg L^{-1}, 7.3 mg L^{-1} and 2.5 mg L^{-1}, respectively. The variations of O_2-NAs are commonly employed to evaluate the efficiency of different treatment methods (Shu et al. 2014, Zhang et al. 2016, Zhang et al. 2015). The distributions of O_2-NAs in the raw OSPW with respect of carbon number and DBE are provided in Fig. 5.5 and Table 5.2. The most abundant species in the O_2-NAs were NAs with two (DBE = 4) and three rings (DBE = 6) (46.7% of the total O_2-NAs), and O_2-NAs with carbon number ranging from 13 to 18 (87.6% of the total O_2-NAs) (Zhang et al. 2016). The concentration of the O_2-NAs in the raw OSPW was 31.5 mg L^{-1}, and it decreased to 17.4 mg L^{-1}, 16.1 mg L^{-1}, and 8.76 mg L^{-1} and 1.25 mg L^{-1} after treatment with 0.5 g/L Bi_2WO_6/NiO/Ag with concentrations of 0, 0.1 mM, 1 mM, 5 mM of OSPW, respectively, implying the synergistic effects of PMS and photocatalyst for the elimination of NAs in OSPW.

Table 5.4 NA distributions in the OSPW based on carbon and z numbers.

DBE	O_2-NAs (%)	Carbon number	O_2-NAs (%)
0	0	11	0.91%
2	2.74%	12	1.45%
4	25.47%	13	8.32%
6	21.22%	14	15.01%
8	6.94%	15	21.03%
10	6.32%	16	17.76%
12	16.47%	17	13.66%
14	7.86%	18	11.81%
16	7.44%	19	4.67%
18	5.54%	20	2.83%
		21	2.55%

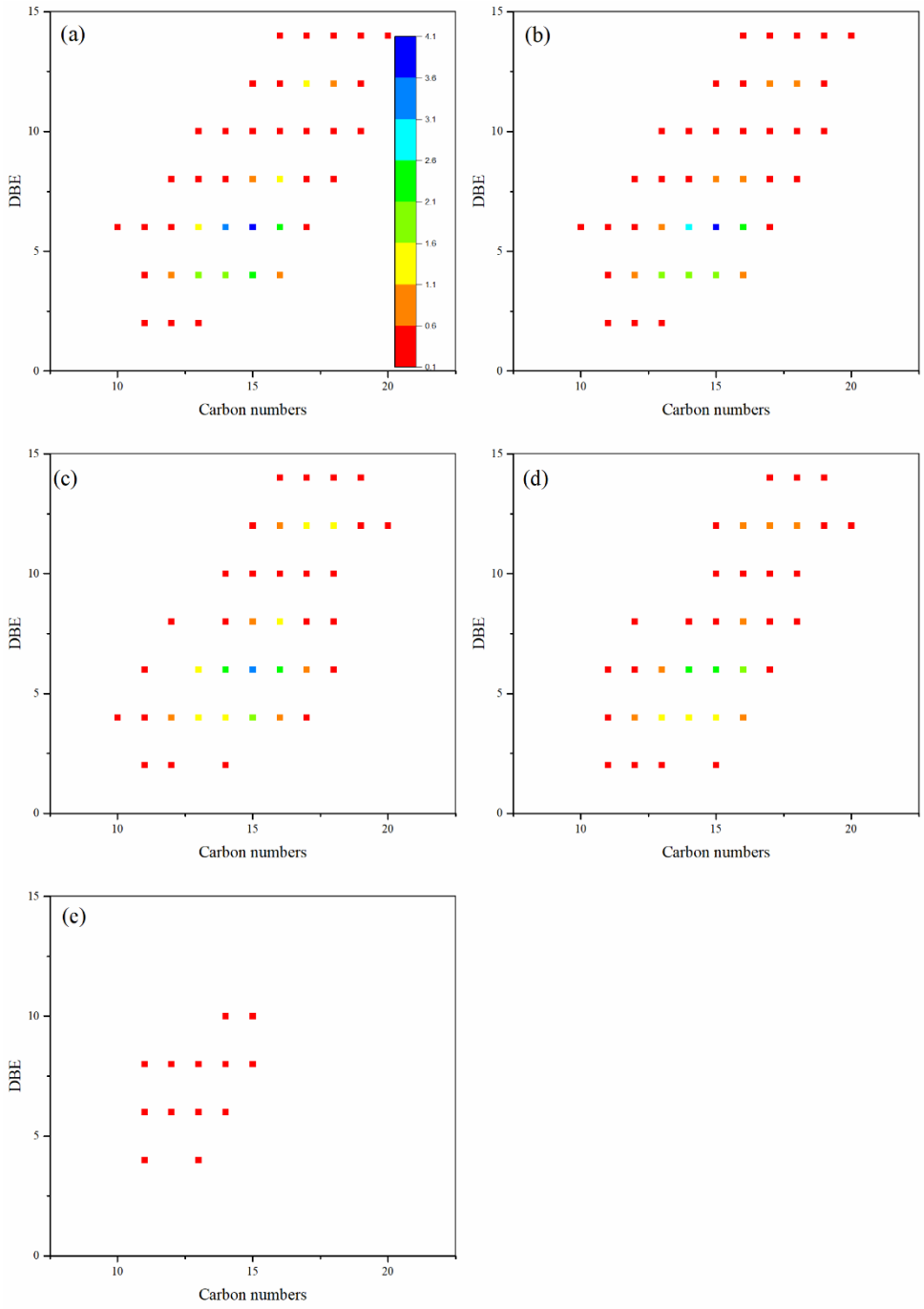

Fig. 5.18 Classical NA distribution in (a) raw OSPW and OSPW photocatalytic treated by 0.5 g/L Bi_2WO_6/NiO/Ag with (b) control (c) 0.1 mM PMS (d) 1 mM PMS, and (e) 5 mM PMS after 1h illumination.

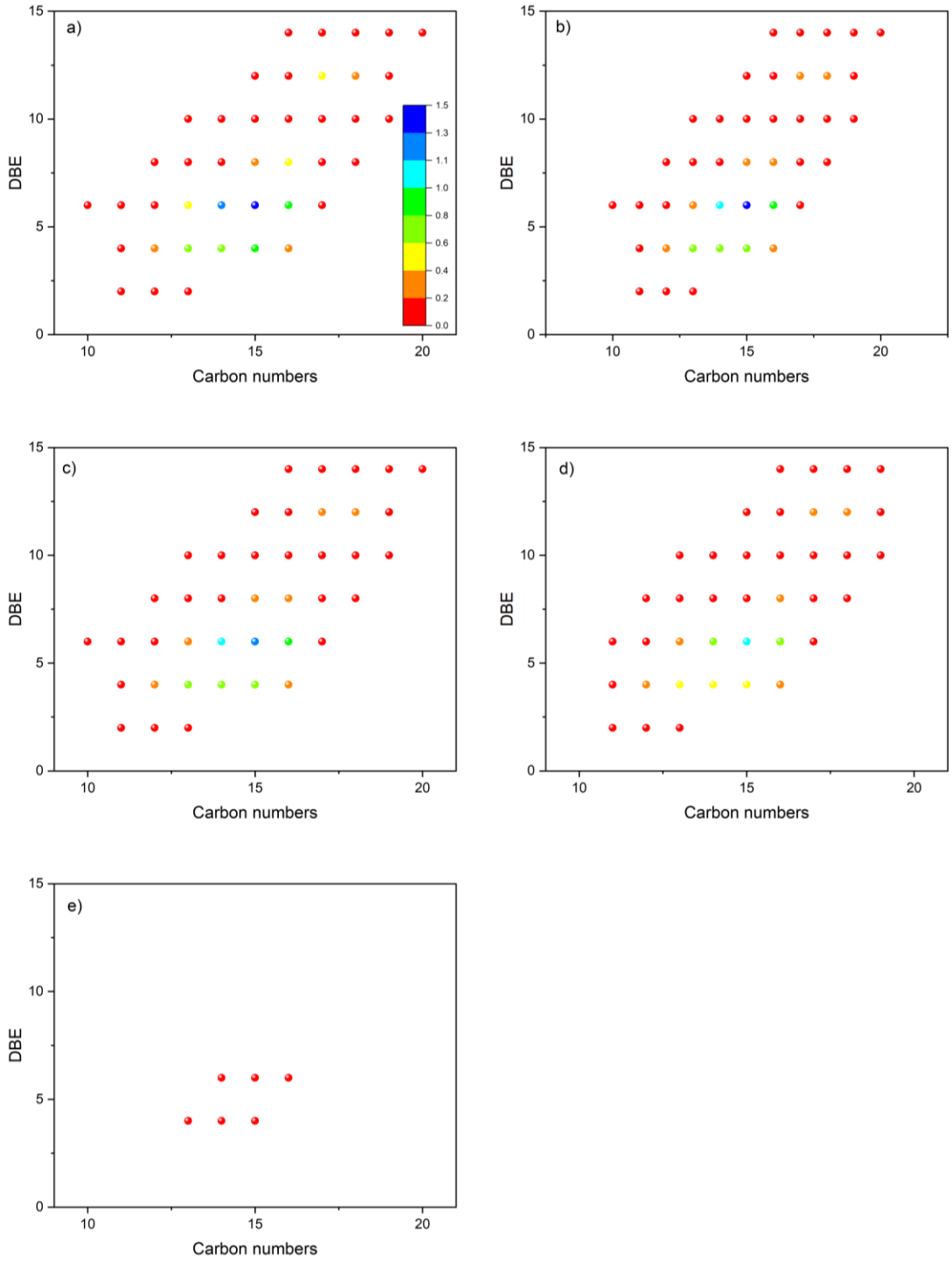

Fig. 5.19 O_3-NA distribution in (a) raw OSPW and OSPW photocatalytic treated by 0.5 g/L Bi_2WO_6/NiO/Ag with (b) control (c) 0.1 mM PMS (d) 1 mM PMS, and (e) 5 mM PMS after 1h illumination.

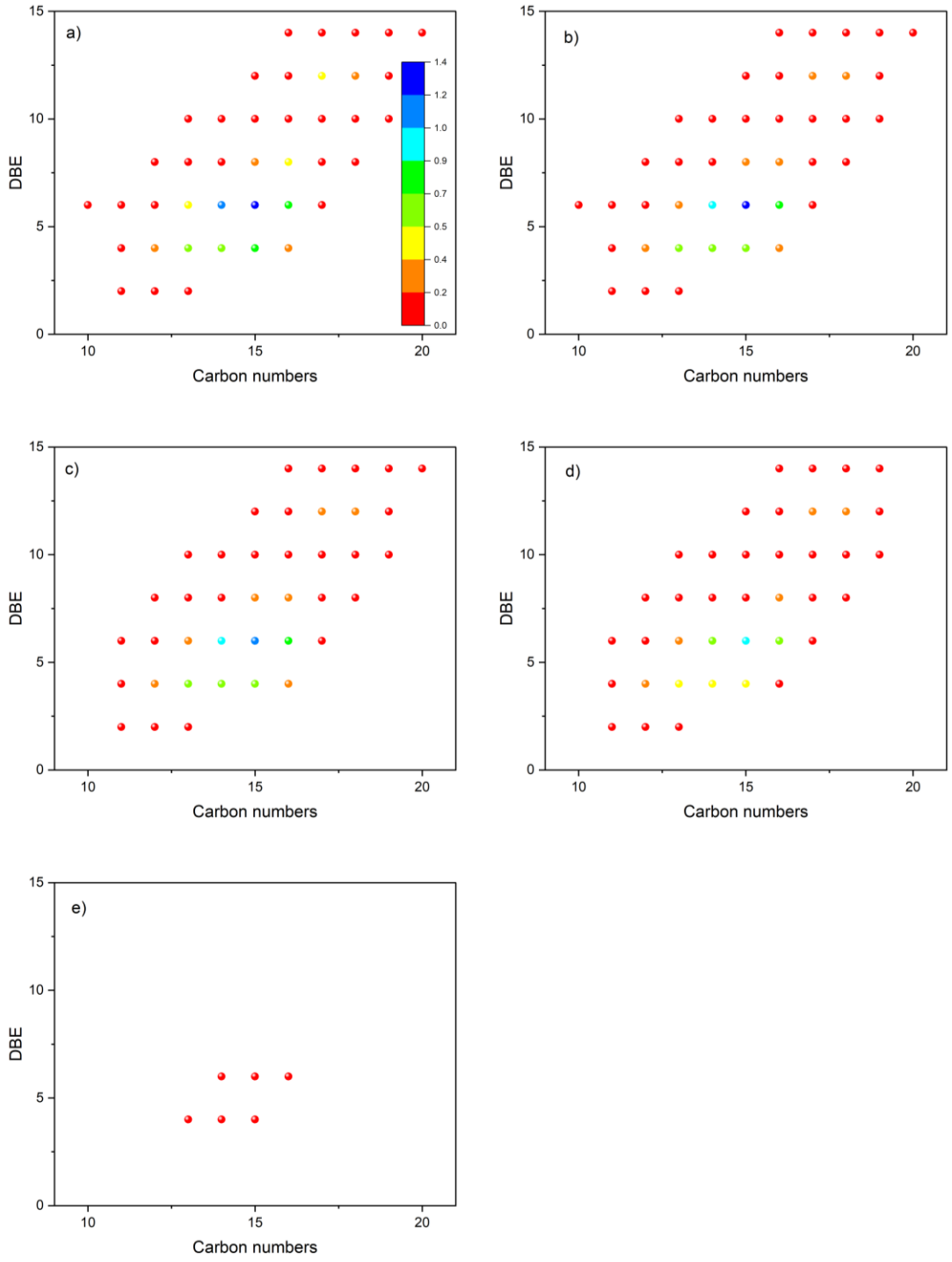

Fig. 5.20 O_4-NA distribution in (a) raw OSPW and OSPW photocatalytic treated by 0.5 g/L Bi_2WO_6/NiO/Ag with (b) control (c) 0.1mM PMS (d) 1 mM PMS, and (e) 5 mM PMS after 1h illumination.

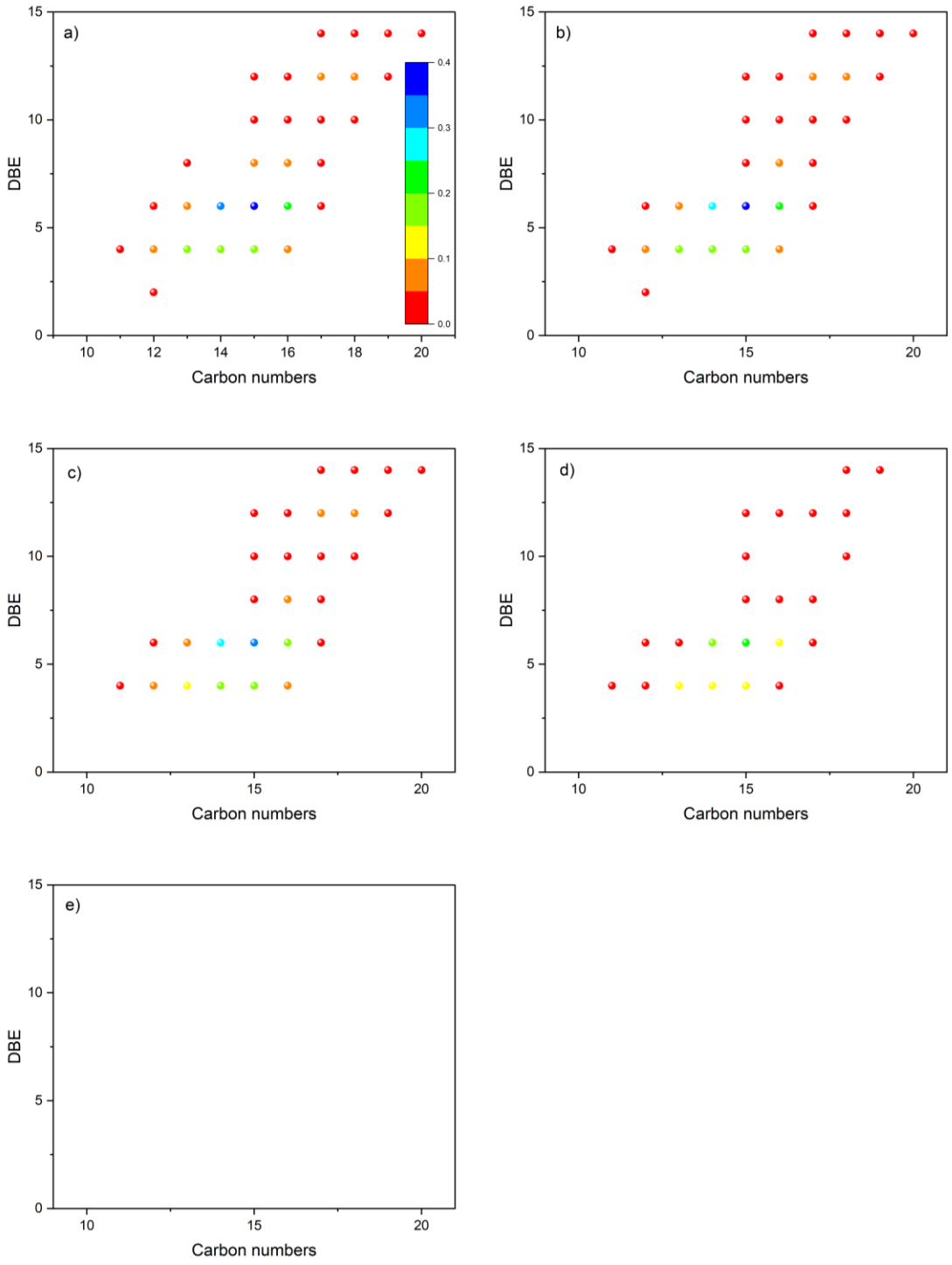

Fig. 5.21 O_5-NA distribution in (a) raw OSPW and OSPW photocatalytic treated by 0.5 g/L Bi_2WO_6/NiO/Ag with (b) control (c) 0.1 mM PMS (d) 1 mM PMS, and (e) 5 mM PMS after 1h illumination.

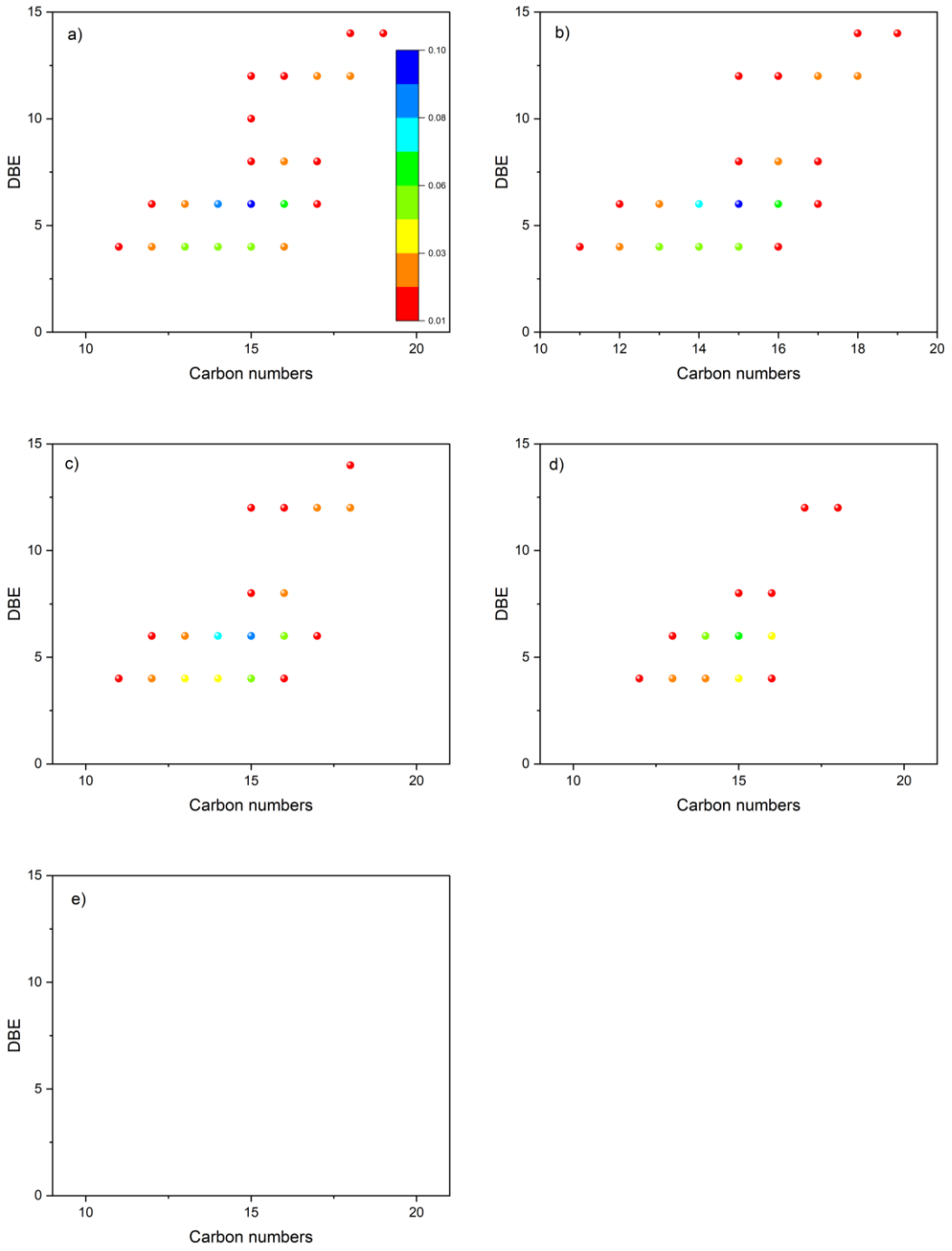

Fig. 5.22 O_6-NA distribution in (a) raw OSPW and OSPW photocatalytic treated by 0.5 g/L Bi_2WO_6/NiO/Ag with (b) control (c) 0.1 mM PMS, (d) 1mM PMS, and (e) 5 mM PMS after 1h illumination

5.3.4 H_2O_2 photocatalytic mechanism

In order to reveal the underlying mechanism, the quenching experiments of free radicals, electrons (e^-) and h^+ and EPR were employed to identify the main reactive species in H_2O_2-assisted photocatalytic degradation process of ACA. AO, TEMPOL, $K_2Cr_2O_7$ and IPA were selected as h^+, $O_2^{\bullet-}$, e^- and $^{\bullet}OH$ scavengers, respectively. Fig. 5.10 illustrated the photocatalytic degradation of ACA using Bi_2WO_6/NiO/Ag in the presence of 5 mM H_2O_2. The removal efficiency of ACA was obviously suppressed (82.9%) by $^{\bullet}OH$ scavengers IPA, demonstrating that $^{\bullet}OH$ was the main radicals. AO also showed significant inhibitory effect (77.2%) on the degradation of ACA, inferring h^+ were essential oxidizing species. Meanwhile, the photocatalytic degradation rate of ACA was also suppressed by TEMPOL and $K_2Cr_2O_7$ to some extent, implying the generation of $O_2^{\bullet-}$ and e^-. In brief, h^+, $O_2^{\bullet-}$, e^- and $^{\bullet}OH$ were all participated in the H_2O_2-assisted photocatalytic degradation process. The DMPO-EPR spin trapping was further conducted to analyze free radicals. As shown in Fig. 5b-c, the high peak intensity of the DMPO-$^{\bullet}OH$ and DMPO-$O_2^{\bullet-}$ involving H_2O_2-assisted photocatalysis, indicating the presence of radicals $O_2^{\bullet-}$ and $^{\bullet}OH$. As discussed in Chapter 3 and results obtained above, the mechanism was listed below and illustrated in Fig. 5.11. The accumulated e^- at conducting band (CB) of NiO and h^+ at valance band (VB) of Bi_2WO_6 could react with H_2O_2 to produce $^{\bullet}OH$ and O_2 (eq 5.8 and 5.10), which then oxidize NAs in OSPW and accelerate the e^- and h^+ seperation.

$$Bi_2WO_6 + hv \rightarrow h^+(Bi_2WO_6) + e^-(Bi_2WO_6) \quad (5.1)$$

$$NiO + hv \rightarrow h^+(NiO) + e^-(NiO) \quad (5.2)$$

$$Ag + hv \rightarrow h^+(Ag) + e^-(Ag) \quad (5.3)$$

$$e^-(Bi_2WO_6) \rightarrow e^-(Ag) \quad (5.4)$$

$e^{-}(Ag) + h^{+}(NiO) \rightarrow$ recombination (5.5)

$h^{+}(Bi_2WO_6) + OH^{-} \rightarrow \cdot OH$ (5.6)

$h^{+}(Bi_2WO_6) + H_2O \rightarrow \cdot OH + H^{+}$ (5.7)

$2h^{+}(Bi_2WO_6) + H_2O_2 \rightarrow O_2 + 2H^{+}$ (5.8)

$e^{-}(NiO) + O_2 \rightarrow O_2^{\bullet -}$ (5.9)

$2e^{-}(NiO) + H_2O_2 \rightarrow \cdot OH + OH^{-}$ (5.10)

$O_2^{\bullet -}$, $\cdot OH$, and h^{+} + pollutant $\rightarrow$ pollutant$^{+\bullet} \rightarrow$ Intermediates (5.11)

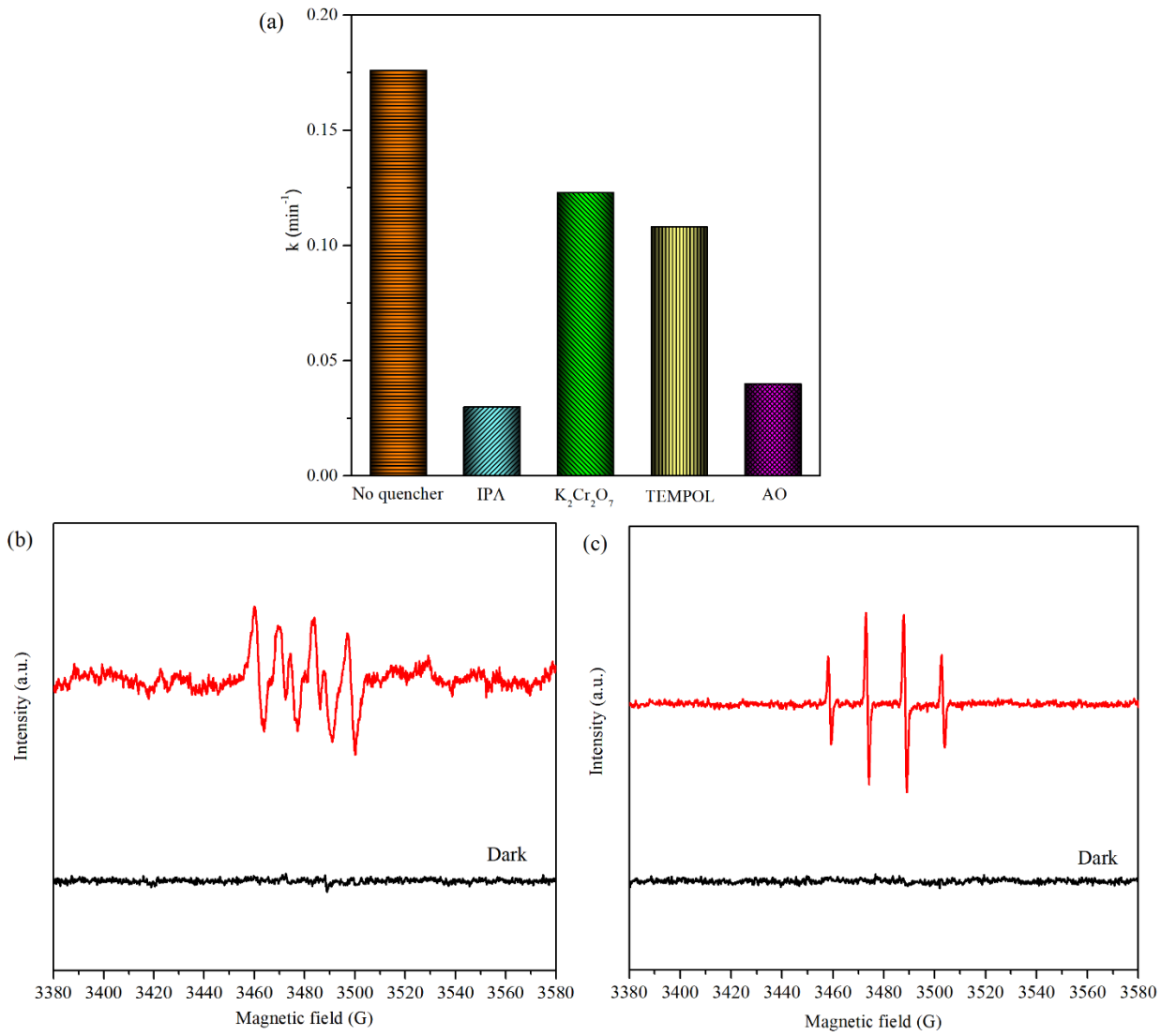

Fig. 5.23 (a) Trapping measurement with 2mM scavengers (IPA→·OH, $K_2Cr_2O_7$→e^-, TEMPOL→·O_2^-, AO→h^+) for the photodegradation of ACA using 0.5 g/L Bi_2WO_6/NiO/Ag in the presence of 5 mM H_2O_2; DMPO-EPR spin-trapping spectra for detection of (b) ·O_2^- and (c) ·OH.

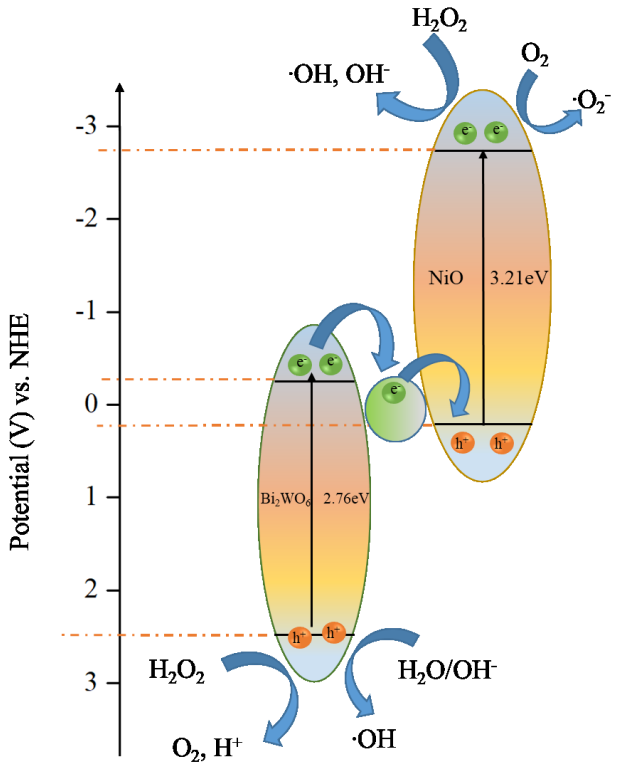

Fig. 5.24 Schematic illustration of proposed H_2O_2 assisted photocatalytic mechanism.

5.3.5 PMS photocatalytic mechanism

Fig. 5.12a illustrated the effects of different scavengers on the degradation of ACA over the Bi_2WO_6/NiO/Ag heterojunction system in the presence of 1mM PMS. The second-order rate constant of MeOH with $^{\bullet}OH$ and $SO_4^{\bullet-}$ is $9.7 \times 10^8\ M^{-1}s^{-1}$ and $2.5 \times 10^7\ M^{-1}\ s^{-1}$, respectively (Wang et al. 2017a, Zeng et al. 2015), whereas that of TBA with $^{\bullet}OH$ and $SO_4^{\bullet-}$ is 3.8–$7.6 \times 10^8\ M^{-1}s^{-1}$ and 4.0–$9.1 \times 10^5\ M^{-1}\ s^{-1}$ (Gong et al. 2018). Therefore, MeOH was used as scavenger of both $^{\bullet}OH$ and $SO_4^{\bullet-}$, while TBA used for $^{\bullet}OH$ only. The second-order rate constant of TEMPOL with $O_2^{\bullet-}$ is $6.5 \times 10^4\ M^1\ s^1$ (Samuni et al. 1990). Moreover, AO are commonly used in quenching experiments for h^+ (Xu et al. 2021). As depicted in Fig. 5.12a, the degradation rate of ACA was significantly hindered (92.5% and 72.4%) after the addition of AO and TEMPOL,

inferring that h^+ and $O_2^{\bullet-}$ were the main oxidizing species. The inhibitory effects of MeOH and TBA were 77.6% and 47.8% for the degradation of ACA, implying that $^{\bullet}OH$ and $SO_4^{\bullet-}$ were generated and contributed to the improved photocatalytic activity. In order to further verify and gain insight about the radical generation in PMS assisted photocatalytic system, the EPR spectra were presented in Fig. 5.12b-c. The signal of $SO_4^{\bullet-}$, $^{\bullet}OH$ and $O_2^{\bullet-}$ were observed under the illumination, which agree with scavenging results. The mechanism was listed below and illustrated in Fig. 5.13. In the presence of PMS, the NiO CB e^- could be trapped by HSO_5^- to generate $SO_4^{\bullet-}$, h^+ at the VB of Bi_2WO_6 could oxidize HSO_5^- to $SO_4^{\bullet-}$ and $SO_5^{\bullet-}$, which further promoted the separation of electrons and holes. Subsequently, the produced $SO_4^{\bullet-}$, ·OH, $O_2^{\bullet-}$ and h^+ could oxidize NAs in OSPW. During this process, the dual role of PMS as electron accepter and radical precursor were confirmed.

$$Bi_2WO_6 + hv \rightarrow h^+(Bi_2WO_6) + e^-(Bi_2WO_6) \quad (5.12)$$

$$NiO + hv \rightarrow h^+(NiO) + e^-(NiO) \quad (5.13)$$

$$Ag + hv \rightarrow h^+(Ag) + e^-(Ag) \quad (5.14)$$

$$e^-(Bi_2WO_6) \rightarrow e^-(Ag) \quad (5.15)$$

$$e^-(Ag) + h^+(NiO) \rightarrow \text{recombination} \quad (5.16)$$

$$h^+(Bi_2WO_6) + OH^- \rightarrow \cdot OH \quad (5.17)$$

$$h^+(Bi_2WO_6) + H_2O \rightarrow \cdot OH + H^+ \quad (5.18)$$

$$e^-(NiO) + O_2 \rightarrow O_2^{\bullet-} \quad (5.19)$$

$$HSO_5^- + e^-(NiO) \rightarrow \cdot OH + SO_4^{2-} \quad (5.20)$$

$$HSO_5^- + e^-(NiO) \rightarrow OH^- + SO_4^{\cdot-} \quad (5.21)$$

$$HSO_5^- + h^+(Bi_2WO_6) \rightarrow H^+ + SO_5^{\cdot -} \quad (5.22)$$

$$SO_5^{\cdot -} + SO_5^{\cdot -} \rightarrow 2SO_4^{\cdot -} + O_2 \quad (5.23)$$

$$O_2^{\bullet -}, \cdot OH, SO_4^{\bullet -} \text{ and } h^+ + \text{pollutant} \rightarrow \text{pollutant}^{+\bullet} \rightarrow \text{Intermediates} \quad (5.24)$$

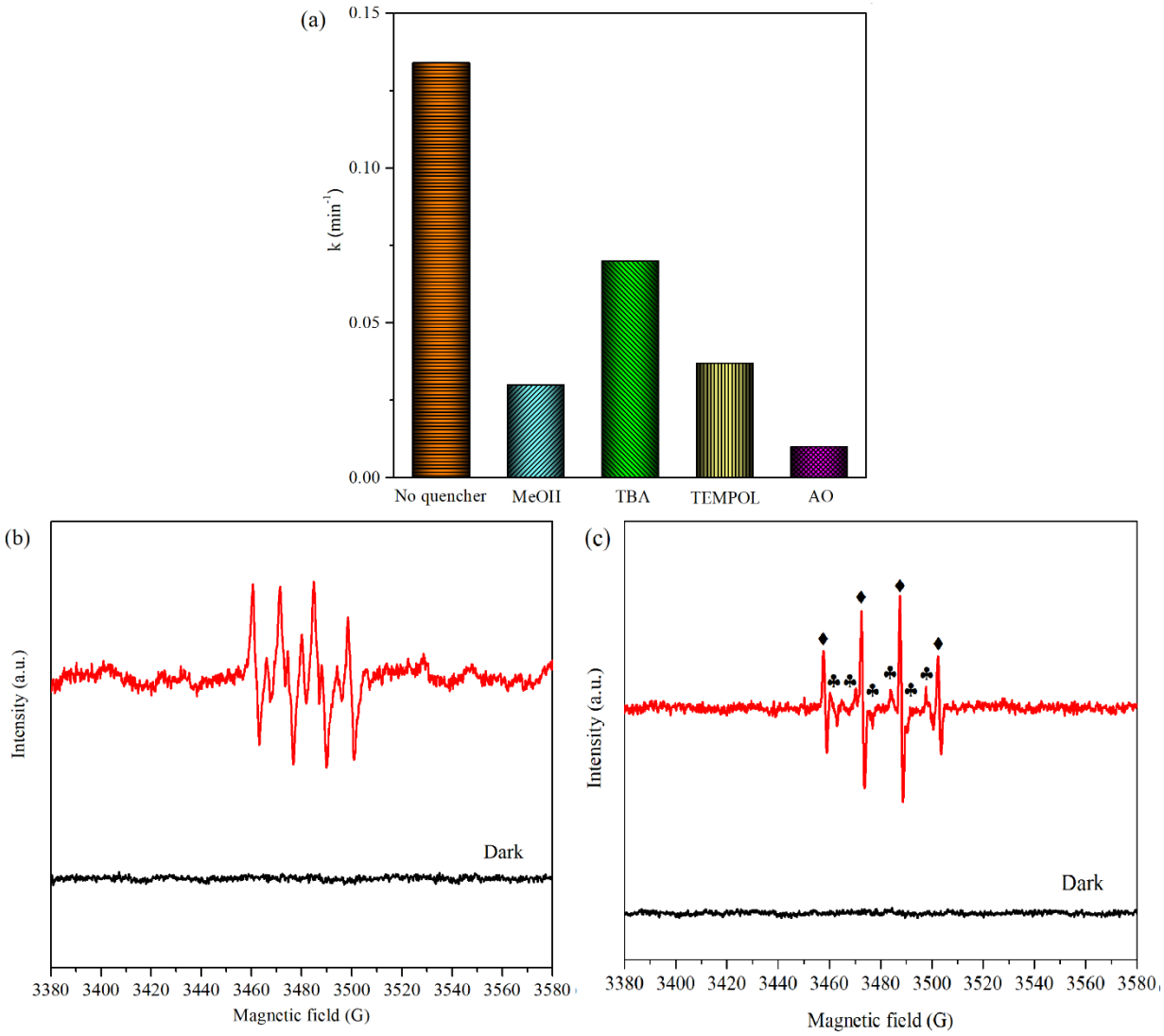

Fig. 5.25 (a) Trapping measurement with 2mM scavengers (MeOH→·OH and $SO_4^{\cdot-}$, TBA→·OH, TEMPOL→$\cdot O_2^-$, AO→h^+) for the photodegradation of ACA using 0.5g/L Bi_2WO_6/NiO/Ag in the presence of 1mM PMS; DMPO-EPR spin-trapping spectra for detection of (b) $\cdot O_2^-$ and (c)♦— ·OH and ♣—$SO_4^{\cdot-}$

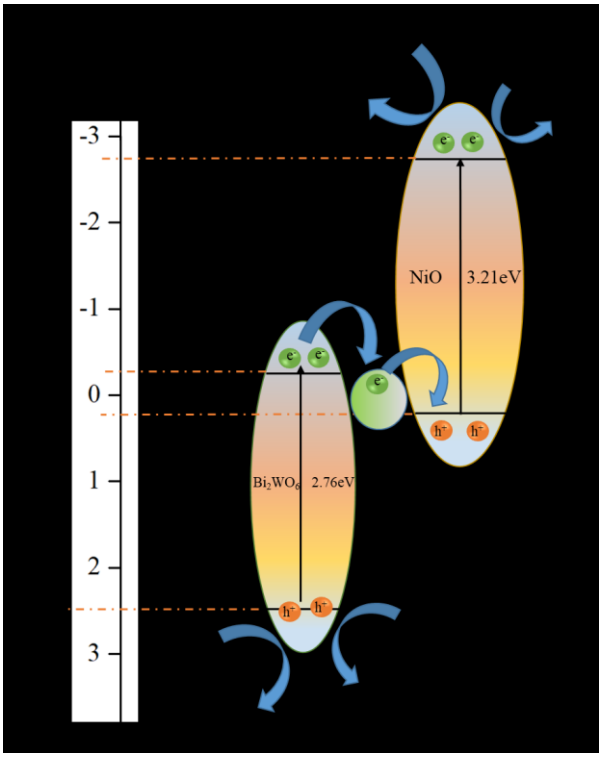

Fig. 5.26 Schematic illustration of proposed PMS assisted photocatalytic mechanism

5.4 Conclusion

In this study, single-ring, two-rings and three-rings aromatics in OSPW were significantly eliminated in H_2O_2 assisted photocatalysis system in the presence of 5 mM H_2O_2. All the three types of aromatics were completely removed by PMS assisted photocatalysis in the presence of 5 mM PMS after only 1h illumination. However, no degradation of aromatics was recorded when 5 mM $KMnO_4$ was added, implying the inhibition effect of $KMnO_4$ on the removal of aromatics. The inhibition effects (%) of bacteria *Vibrio fischeri* were decreased with the increasing concentration of H_2O_2 and PMS, demonstrating organics in OSPW transfer to nontoxic products in H_2O_2 and PMS assisted photocatalytic system. Whereas $KMnO_4$ showed no detoxification for OSPW. h^+, $O_2^{\bullet-}$, e^- and $^{\bullet}OH$ were main reactive species in H_2O_2 assisted photocatalysis. Moreover,

$SO_4^{\bullet-}$, h^+, $O_2^{\bullet-}$ and $^{\bullet}OH$ were responsible for the degradation of organics in PMS assisted photocatalysis. In addition, PMS assisted photocatalysis was able to fully degrade all classes of NAs at with 0.5 g/L of catalyst and 5 mM PMS. This study confirmed H_2O_2, and PMS assisted photocatalysis are efficient passive treatment methods for OSPW.

5.5 References

Andrew Lin, K.-Y. and Zhang, Z.-Y. (2016) α-Sulfur as a metal-free catalyst to activate peroxymonosulfate under visible light irradiation for decolorization. RSC Advances 6(18), 15027-15034.

Arslan, M., Müller, J.A. and Gamal El-Din, M. (2022) Aerobic naphthenic acid-degrading bacteria in petroleum-coke improve oil sands process water remediation in biofilters: DNA-stable isotope probing reveals methylotrophy in Schmutzdecke. Science of the Total Environment 815, 151961.

Bessa, E., Sant'Anna, G.L. and Dezotti, M. (2001) Photocatalytic/H2O2 treatment of oil field produced waters. Applied Catalysis B: Environmental 29(2), 125-134.

Chen, F., Huang, G.-X., Yao, F.-B., Yang, Q., Zheng, Y.-M., Zhao, Q.-B. and Yu, H.-Q. (2020) Catalytic degradation of ciprofloxacin by a visible-light-assisted peroxymonosulfate activation system: Performance and mechanism. Water Research 173, 115559.

Chen, X., Wang, W., Xiao, H., Hong, C., Zhu, F., Yao, Y. and Xue, Z. (2012) Accelerated TiO2 photocatalytic degradation of Acid Orange 7 under visible light mediated by peroxymonosulfate. Chemical Engineering Journal 193-194, 290-295.

Duan, X., Ao, Z., Zhou, L., Sun, H., Wang, G. and Wang, S. (2016) Occurrence of radical and nonradical pathways from carbocatalysts for aqueous and nonaqueous catalytic oxidation. Applied Catalysis B: Environmental 188, 98-105

Fang, Z., Huang, R., How, Z.T., Jiang, B., Chelme-Ayala, P., Shi, Q., Xu, C. and Gamal El-Din, M. (2020) Molecular transformation of dissolved organic matter in process water from oil and gas operation during UV/H_2O_2, UV/chlorine, and UV/persulfate processes. Science of the Total Environment 730, 139072.

Feng, Q., Zhou, J. and Zhang, Y. (2019) Coupling Bi_2MoO_6 with persulfate for photocatalytic oxidation of tetracycline hydrochloride under visible light. Journal of Materials Science: Materials in Electronics 30(21), 19108-19118.

Fuchylo, U., Alharbi, H.A., Alcaraz, A.J., Jones, P.D., Giesy, J.P., Hecker, M. and Brinkmann, M. (2022) Inflammation of Gill Epithelia in Fish Causes Increased Permeation of Petrogenic Polar Organic Chemicals via Disruption of Tight Junctions. Environmental Science & Technology 56(3), 1820-1829.

Ganiyu, S.O., Arslan, M. and Gamal El-Din, M. (2022) Combined solar activated sulfate radical-based advanced oxidation processes (SR-AOPs) and biofiltration for the remediation of dissolved organics in oil sands produced water. Chemical Engineering Journal 433, 134579.

Gao, H., Yang, H., Xu, J., Zhang, S. and Li, J. (2018) Strongly Coupled g-C3N4 Nanosheets-Co3O4 Quantum Dots as 2D/0D Heterostructure Composite for Peroxymonosulfate Activation. Small 14(31), 1801353.

García-Espinoza, J.D., Mijaylova-Nacheva, P. and Avilés-Flores, M. (2018) Electrochemical carbamazepine degradation: Effect of the generated active chlorine, transformation pathways and toxicity. Chemosphere 192, 142-151.

Garcia, J.C., Oliveira, J.L., Silva, A.E.C., Oliveira, C.C., Nozaki, J. and de Souza, N.E. (2007) Comparative study of the degradation of real textile effluents by photocatalytic reactions involving UV/TiO2/H2O2 and UV/Fe2+/H2O2 systems. Journal of Hazardous Materials 147(1), 105-110.

Gong, Y., Zhao, X., Zhang, H., Yang, B., Xiao, K., Guo, T., Zhang, J., Shao, H., Wang, Y. and Yu, G. (2018) MOF-derived nitrogen doped carbon modified g-C3N4 heterostructure composite with enhanced photocatalytic activity for bisphenol A degradation with peroxymonosulfate under visible light irradiation. Applied Catalysis B: Environmental 233, 35-45.

Güyer, G.T. and Ince, N.H. (2011) Degradation of diclofenac in water by homogeneous and heterogeneous sonolysis. Ultrasonics Sonochemistry 18(1), 114-119.

Ji, X., Han, Z., Li, J., Deng, Y., Han, X., Zhao, J., Zhao, X. and Chen, C. (2019) MoSx co-catalytic activation of H2O2 by heterogeneous hemin catalyst under visible light irradiation. Journal of Colloid and Interface Science 557, 301-310.

Jiang, J., Pang, S.-Y. and Ma, J. (2009) Oxidation of Triclosan by Permanganate (Mn(VII)): Importance of Ligands and In Situ Formed Manganese Oxides. Environmental Science & Technology 43(21), 8326-8331.

Liu, M., Hou, L.-a., Li, Q., Hu, X. and Yu, S. (2016a) Heterogeneous degradation of tetracycline by magnetic Ag/AgCl/modified zeolite X–persulfate system under visible light. RSC Advances 6(42), 35216-35227.

Liu, M., Zhang, L., Xi, B.-d., Yu, S., Hu, X. and Hou, L.-a. (2017) Degradation of ciprofloxacin by TiO2/Fe2O3/zeolite catalyst-activated persulfate under visible LED light irradiation. RSC Advances 7(81), 51512-51520.

Liu, N., Lei, Z.-D., Wang, T., Wang, J.-J., Zhang, X.-D., Xu, G. and Tang, L. (2016b) Radiolysis of carbamazepine aqueous solution using electron beam irradiation combining with hydrogen peroxide: Efficiency and mechanism. Chemical Engineering Journal 295, 484-493.

Loos, G., Scheers, T., Van Eyck, K., Van Schepdael, A., Adams, E., Van der Bruggen, B., Cabooter, D. and Dewil, R. (2018) Electrochemical oxidation of key pharmaceuticals using a boron doped diamond electrode. Separation and Purification Technology 195, 184-191.

Luo, Z., Meng, L., How, Z.T., Chelme-Ayala, P., Yang, L., Benally, C. and Gamal El-Din, M. (2022) Treatment of oil sands process water by the ferric citrate under visible light irradiation. Chemical Engineering Journal 429, 132419.

Meng, L., How, Z.T., Ganiyu, S.O. and Gamal El-Din, M. (2021) Solar photocatalytic treatment of model and real oil sands process water naphthenic acids by bismuth tungstate: Effect of catalyst morphology and cations on the degradation kinetics and pathways. Journal of Hazardous Materials 413, 125396.

Meng, L., Yang, S., Sun, C., He, H., Xian, Q., Li, S., Wang, G., Zhang, L. and Jiang, D. (2017) A novel method for photo-oxidative degradation of diatrizoate in water via electromagnetic induction electrodeless lamp. Journal of Hazardous Materials 337, 34-46.

Michael, I., Hapeshi, E., Michael, C., Varela, A.R., Kyriakou, S., Manaia, C.M. and Fatta-Kassinos, D. (2012) Solar photo-Fenton process on the abatement of antibiotics at a pilot scale: Degradation kinetics, ecotoxicity and phytotoxicity assessment and removal of antibiotic resistant enterococci. Water Research 46(17), 5621-5634.

Oh, W.-D., Dong, Z. and Lim, T.-T. (2016) Generation of sulfate radical through heterogeneous catalysis for organic contaminants removal: Current development, challenges and prospects. Applied Catalysis B: Environmental 194, 169-201.

Oturan, M.A. and Aaron, J.-J. (2014) Advanced Oxidation Processes in Water/Wastewater Treatment: Principles and Applications. A Review. Critical Reviews in Environmental Science and Technology 44(23), 2577-2641.

Samuni, A., Krishna, C.M., Mitchell, J.B., Collins, C.R. and Russo, A. (1990) Superoxide Reaction with Nitroxides. Free Radical Research Communications 9(3-6), 241-249.

Serna-Galvis, E.A., Silva-Agredo, J., Giraldo-Aguirre, A.L., Flórez-Acosta, O.A. and Torres-Palma, R.A. (2016) High frequency ultrasound as a selective advanced oxidation process to remove penicillinic antibiotics and eliminate its antimicrobial activity from water. Ultrasonics Sonochemistry 31, 276-283.

Shu, Z., Li, C., Belosevic, M., Bolton, J.R. and El-Din, M.G. (2014) Application of a Solar UV/Chlorine Advanced Oxidation Process to Oil Sands Process-Affected Water Remediation. Environmental Science & Technology 48(16), 9692-9701.

Sohrabi, V., Ross, M.S., Martin, J.W. and Barker, J.F. (2013) Potential for in situ chemical oxidation of acid extractable organics in oil sands process affected groundwater. Chemosphere 93(11), 2698-2703.

Sun, J., Shen, C.-H., Guo, J., Guo, H., Yin, Y.-F., Xu, X.-J., Fei, Z.-H., Liu, Z.-T. and Wen, X.-J. (2021) Highly efficient activation of peroxymonosulfate by Co3O4/Bi2WO6 p-n heterojunction composites for the degradation of ciprofloxacin under visible light irradiation. Journal of Colloid and Interface Science 588, 19-30.

Tang, S., Tang, J., Yuan, D., Wang, Z., Zhang, Y. and Rao, Y. (2020) Elimination of humic acid in water: comparison of UV/PDS and UV/PMS. RSC Advances 10(30), 17627-17634.

Tian, S.-Q., Wang, L., Liu, Y.-L., Yang, T., Huang, Z.-S., Wang, X.-S., He, H.-Y., Jiang, J. and Ma, J. (2019) Enhanced Permanganate Oxidation of Sulfamethoxazole and Removal of Dissolved Organics with Biochar: Formation of Highly Oxidative Manganese Intermediate Species and in Situ Activation of Biochar. Environmental Science & Technology 53(9), 5282-5291.

Trovó, A.G., Pupo Nogueira, R.F., Agüera, A., Fernandez-Alba, A.R. and Malato, S. (2011) Degradation of the antibiotic amoxicillin by photo-Fenton process – Chemical and toxicological assessment. Water Research 45(3), 1394-1402.

Wang, N., Chelme-Ayala, P., Perez-Estrada, L., Garcia-Garcia, E., Pun, J., Martin, J.W., Belosevic, M. and Gamal El-Din, M. (2013) Impact of Ozonation on Naphthenic Acids Speciation and Toxicity of Oil Sands Process-Affected Water to Vibrio fischeri and Mammalian Immune System. Environmental Science & Technology 47(12), 6518-6526.

Wang, S. and Wang, J. (2018) Degradation of carbamazepine by radiation-induced activation of peroxymonosulfate. Chemical Engineering Journal 336, 595-601.

Wang, S. and Wang, J. (2022) Magnetic 2D/2D oxygen doped g-C3N4/biochar composite to activate peroxymonosulfate for degradation of emerging organic pollutants. Journal of Hazardous Materials 423, 127207.

Wang, Y., Cao, D. and Zhao, X. (2017a) Heterogeneous degradation of refractory pollutants by peroxymonosulfate activated by CoOx-doped ordered mesoporous carbon. Chemical Engineering Journal 328, 1112-1121.

Wang, Y., Zhang, H., Zhang, J., Lu, C., Huang, Q., Wu, J. and Liu, F. (2011) Degradation of tetracycline in aqueous media by ozonation in an internal loop-lift reactor. Journal of Hazardous Materials 192(1), 35-43.

Wang, Y., Zhao, X., Cao, D., Wang, Y. and Zhu, Y. (2017b) Peroxymonosulfate enhanced visible light photocatalytic degradation bisphenol A by single-atom dispersed Ag mesoporous g-C3N4 hybrid. Applied Catalysis B: Environmental 211, 79-88.

Xu, X., Meng, L., Luo, J., Zhang, M., Wang, Y., Dai, Y., Sun, C., Wang, Z., Yang, S., He, H. and Wang, S. (2021) Self-assembled ultrathin CoO/Bi quantum dots/defective Bi2MoO6 hollow Z-scheme heterojunction for visible light-driven degradation of diazinon in water matrix: Intermediate toxicity and photocatalytic mechanism. Applied Catalysis B: Environmental 293, 120231.

Zeng, T., Zhang, X., Wang, S., Niu, H. and Cai, Y. (2015) Spatial Confinement of a Co3O4 Catalyst in Hollow Metal–Organic Frameworks as a Nanoreactor for Improved Degradation of Organic Pollutants. Environmental Science & Technology 49(4), 2350-2357.

Zhang, Y., Klamerth, N., Chelme-Ayala, P. and Gamal El-Din, M. (2016) Comparison of Nitrilotriacetic Acid and [S,S]-Ethylenediamine-N,N′-disuccinic Acid in UV–Fenton for the Treatment of Oil Sands Process-Affected Water at Natural pH. Environmental Science & Technology 50(19), 10535-10544.

Zhang, Y., McPhedran, K.N. and Gamal El-Din, M. (2015) Pseudomonads biodegradation of aromatic compounds in oil sands process-affected water. Science of the Total Environment 521-522, 59-67.

Zhao, Y., Kuang, J., Zhang, S., Li, X., Wang, B., Huang, J., Deng, S., Wang, Y. and Yu, G. (2017) Ozonation of indomethacin: Kinetics, mechanisms and toxicity. Journal of Hazardous Materials 323, 460-470.

Zhong, X., Zhang, K.-X., Wu, D., Ye, X.-Y., Huang, W. and Zhou, B.-X. (2020) Enhanced photocatalytic degradation of levofloxacin by Fe-doped BiOCl nanosheets under LED light irradiation. Chemical Engineering Journal 383, 123148.

CHAPTER 6. GENERAL CONCLUSIONS AND RECOMMENDATIONS

6.1 Thesis overview

Alberta's oil sands possess the third-largest oil reserves in the world, which is the important pillar in Alberta and main source of Canada's Gross Domestic Product. The extraction, upgrading and refining of oil sands into petroleum products produce oil sands process water (OSPW). Currently, environmental problems related to OSPW pose severe threats to the sustainable development of humankind. Therefore, it is crucial to manage increasing volume of OSPW and oil sands tailings with more stringent environmental regulations. Naphthenic acids (NAs), being the dominant toxic organics in OSPW, are structurally stable through natural attenuation processes such as hydrolysis, photolysis, and biodegradation. During the past few years, various physical, chemical, biological and combined remediation technologies have been investigated for the removal of NAs from OSPW at the bench scale level. Generally, biodegradation and adsorption suffer from problems such as long periodicity, low stability, and secondary pollution. To address these significant problems, advanced oxidation processes (AOPs) with higher NAs removal efficiencies were applied for the treatment of OSPW due to the production of reactive species such as $SO_4^{\bullet-}$, $O_2^{\bullet-}$and $^{\bullet}OH$. Among them, semiconductor photocatalysis offers a novel green and energy saving solution to eliminate NAs from OSPW. To date, it has been proven that the semiconductor TiO_2 can be used for the oxidative decomposition of NAs. Unfortunately, because of its wide bandgap of 3.2 eV, TiO_2 could only be excited by UV light, which covers about 4% of the solar light spectrum. Herein, visible light driven catalyst Bi_2WO_6 was prepared in this research for OSPW remediation to make effective use of solar energy.

More importantly, pure Bi_2WO_6 suffers from disadvantage of recombination of electrons and holes, which affects the photocatalytic performance. Recently, researchers have invented different kinds of Bi_2WO_6 based photocatalysts with enhanced photocatalytic performance through anionic and cationic dopants, noble metal deposition, and heterojunction photocatalysts. Nickel oxide (NiO) is a p-type semiconductor with a band gap around 3.6 eV, which could form p-n heterojunction with Bi_2WO_6. Nevertheless, the photocatalytic activities of p-n heterojunction may be restricted due to the reduced redox ability of original electrons and holes. Therefore, Z-scheme systems were employed to avoid the decrease of redox potential, meanwhile keeping the capability to separate photo-generated electron-hole pairs effectively. However, the directional migration of traditional charge carriers usually competes with that in two phase Z-scheme heterojunction. In this case, an electron mediator Ag is introduced to enhance Z-scheme charge transfer based on the difference of electrical resistances between different phases. Therefore, Bi_2WO_6/NiO/Ag Z-scheme heterojunction was firstly synthesized in this thesis and applied for the oxidative degradation of NAs.

Another effective photocatalyst-enhancing technology is to establish a catalytic oxidation system by combining different oxidants. H_2O_2, peroxymonosulfate (PMS) and $KMnO_4$ were firstly employed for the photocatalytic treatment of OSPW. Compared with H_2O_2 and $KMnO_4$, PMS and catalyst showed synergistic effect in promoting NAs removal in OSPW and PMS worked as an electron acceptor and a radical precursor.

On the other hand, NAs could be divided into four groups: classical NAs (O_2-NAs), oxidized NAs (oxy-NAs), nitrogen-containing NAs (N-NAs) and sulphur-containing NAs (S-NAs). Although classical and oxidized NAs have been widely studied, there is limited information on the environmental fates of heteroatomic NAs, especially their degradation and reaction mechanisms.

Hence, the transformation pathways of selected S-NAs and N-NAs model compounds were firstly studied in this thesis. The effects of OSPW inorganic fraction on the photocatalytic degradation of NAs were also explored.

6.2 Conclusions

The results generated from this research showed that novel Bi_2WO_6 based semiconductor photocatalysts were successfully developed for OSPW remediation. With the combination of oxidants, the improvement of NAs removal by photocatalysis was investigated. The main conclusions of each chapter are as follows:

Chapter 2: Solar photocatalytic treatment of model and real oil sands process water naphthenic acids by Bi_2WO_6

- This study confirmed the capability of Bi_2WO_6 to degrade model NAs and real OSPW.
- Nanoplate (NP), swirl-like (SL) and flower-like (FL) structures of Bi_2WO_6 semiconductor catalysts were successfully prepared by hydrothermal method, among which FL showed the highest specific surface area and total pore volume.
- The highest photocatalytic degradation rate of cyclohexanoic acid (CHA) at fluence-based rate constant 0.0929 cm^2/J was observed by using FL Bi_2WO_6.
- Trapping measurements confirmed that the main reactive species were holes (h^+) and superoxide radicals ($O_2^{\bullet-}$) in Bi_2WO_6 photocatalysis system.
- Mn^{2+} and Fe^{3+} inhibited the photocatalytic degradation of tetrahydro-2H-thiopyran-4-carboxylic acid (T-2H-T4CA) and 5-Hexyl-2-thiophenecarboxylic acid (5H-2THCA), whereas, they had no effects on the degradation of isonipecotic acid (IA).

- S and N atoms played a crucial role in the degradation mechanisms of T-2H-T4CA, 5H-2THCA, and IA.
- For the treatment of real OSPW using 1 g/L FL Bi_2WO_6, S-NAs were completely degraded, and classical NAs were partially oxidized during the photocatalytic treatment. Oxy-NAs, on the other hand, were difficult to remove.
- This investigation showed the potential of solar light-driven photocatalysis as a passive treatment approach for the remediation of OSPW and fill the research gap for the information related to the environmental fates of heteroatom NAs.

Chapter 3: Solar photocatalytic treatment of model and real oil sands process water naphthenic acids by Bi_2WO_6/NiO/Ag

- Solar photocatalytic degradation using Z-scheme photocatalyst Bi_2WO_6/NiO/Ag was a promising method for the treatment of OSPW.
- The loading amounts of NiO and Ag were optimized using the degradation of 1-adamantanecarboxylic acid (ACA) and were found to be 5% of NiO and 2% of Ag.
- The bandgap of Bi_2WO_6/NiO/Ag was 0.4 eV lower than that of Bi_2WO_6 (2.76 eV).
- In addition, cycling experiments indicated that Bi_2WO_6/NiO/Ag still retained its photocatalytic properties after multiple runs.
- The results of quenching experiments and electron paramagnetic resonance showed that h^+, $O_2^{\bullet-}$, e^- and $^{\bullet}OH$ were the major reactive species.
- Bi_2WO_6/NiO/Ag was capable of completely degrading the aromatic, classical NAs and heteroatomic NAs in real OSPW. In contrast, Bi_2WO_6 partially degraded the aromatics and classical NAs after 6 h irradiation.

- The removal efficiency of classical NAs by Bi_2WO_6 was increased with an increase of double bond equivalents (DBE) and carbon number. Whereas the Bi_2WO_6/NiO/Ag showed almost no bias in the removal of NAs regarding to the carbon number and DBE.
- The improved photocatalytic performance of Bi_2WO_6/NiO/Ag was attributed to: (1) the introduction of NiO and Ag broadened the visible light absorption range; (2) the improved electric field intensity around the interface of Ag nanoparticles prompted the interfacial electron transfer and surface electron excitation due to the surface plasmon resonance effect; and (3) z-scheme heterojunction separated the electrons and holes efficiently.
- The organic compounds in OSPW would eventually be converted into harmless products based on the toxicity assessment toward *Vibrio fischeri*.
- A novel z-scheme heterojunction catalyst Bi_2WO_6/NiO/Ag was developed for the removal of NAs in OSPW and provides valuable information for the design of engineered passive solar-based treatment approaches.

Chapter 4: Solar photocatalytic degradation of model compounds NAs mixtures: The effect of inorganic fraction of OSPW

- Solar photocatalysis was able to effectively degrade the mixtures of commercial NA compounds dissolved in OSPW inorganic fraction (OSPW-IF)
- The removal of mixtures of ACA, CHA, T-2H-T4CA, tetrahydropyran-4-carboxylic acid (T4CA), and 4,5-dihydronaphtho[1,2-b]thiophene-2-carboxylic acid (DTCA) in IF solutions was apparently lower than that in buffer solutions due to the dose-dependent inhibitions of Cl^- and HCO_3^-.

- Photocatalytic elimination of IA exhibited a higher reactivity in IF solution as compared to that in buffer solutions, which could be explained by the production of aminyl radicals in the presence of NO_3^-.
- The addition of catalysts in the presence of NO_3^- accelerated the degradation rate of ACA and reduced the toxicity of by-products.
- The transformation pathways of DCTA were proposed and verified by the isodensity surfaces of HOMO and Mulliken atomic charges.
- This study revealed the effects of complex inorganic matrix on the degradation of NAs, which will be beneficial for the understanding of the possible practical application of the solar photocatalytic system in the elimination of NAs and treatment of OSPW.

Chapter 5: Enhanced treatment of OSPW by catalyst through the addition of oxidants

- $KMnO_4$ inhibited the photocatalytic degradation of aromatic NAs, while H_2O_2 accelerated the photocatalytic degradation of aromatic NAs at higher concentration.
- Peroxymonosulfate could highly promote the photocatalytic treatment of aromatic NAs, and the degradation rate was increased with the increase of peroxymonosulfate concentration.
- $SO_4^{\bullet-}$, h^+, $O_2^{\bullet-}$ and $^{\bullet}OH$ were determined as major reactive species by quenching experiments and electron paramagnetic resonance in PMS assisted photocatalytic system.
- H_2O_2, PMS assisted photocatalytic technology was confirmed effective in this study for OSPW remediation. Different performance of oxidants is conducive to achieve complete removal of organic matters in alkaline wastewater.

6.3 Recommendations

Given these results obtained from the research, Bi_2WO_6 based semiconductor photocatalyst appeared to be an efficient passive treatment option for OSPW remediation. Recommendations for future works are proposed here:

- All photocatalytic experiments in this research were carried out in batch reactors using catalyst powders. Herein, floating catalysts are suggested in the future work for scaling-up and practical applications. One of the key points of floating catalyst is the selection of supporting materials. Basalt fiber mesh has advantages as it is alkali resistant, corrosion resistant, and chemical resistant. It can be fixed on the water surface for easy recycling. Hollow glass beads are characterized with small size, lightweight, heat insulation and high temperature resistance, which can greatly reduce the density of catalyst. Organic polymer-based photocatalyst are hydrophobic, leading to easier adsorption of organic contaminants on the surface. They have good thermoplasticity and can be made into various shapes and fully combined with catalysts. Hence, floating catalysts with proper supporting materials could be used for *in-situ* OSPW treatment as they can float on the surface of tailings or constructed wetlands.

- For PMS assisted photocatalysis, a continuous-flow reactor could be used. The reactor can be continuously filled with OSPW and PMS by a peristaltic pump at constant flow rate. Notably, the concentrations of secondary products SO_4^{2-} in effluent after treatment by PMS assisted photocatalysis would be high. Therefore, post-treatment would be necessary. For example: Anaerobic biological treatment, membrane treatment or electrochemical oxidation coupled with boron-doped diamond anode materials.

- Among the different available photocatalysts, Bi_2WO_6 based semiconductor catalysts are not the only choice. The evaluation of photocatalytic treatment of OSPW by using other catalysts is highly recommended. Currently, ZnO with cheap price and high efficiency was used in our laboratory. Other catalysts such as BiOI, $BiVO_4$; metal organic frame photocatalysts could be used in OSPW treatment. BiOI (~1.9 eV) and $BiVO_4$ (~2.4 eV) with narrow bandgap have many advantages such as low costs, high stability, relatively efficient electron-hole pairs separation under visible light, and broad-spectrum light absorption. MOFs can provide a significant reaction platform that contains both active sites and light harvesters. Furthermore, the ultrahigh surface area, tailorable versatility and structural flexibility of MOFs are contributed for better photocatalytic performance. On the other hand, except for z-scheme heterojunction structures, many other attempts may be used to further improve the photocatalytic performance such as surface defect, facets exposure as well as morphology control.
- Although $KMnO_4$ oxidation is not suitable for OSPW treatment due to the higher pH, the enhancement methods have been proposed. Ligands such as phosphate, pyrophosphate, EDTA, and humic acid could improve the performance of $KMnO_4$ due to the production of ligand-stabilized reactive manganese intermediates. UV/$KMnO_4$ is also an efficiency method for elimination of organics. The results observed in this research indicated that Bi_2WO_6 based catalysts were incapable to activate $KMnO_4$. Alternative catalysts could be MnO_2, biochar or ruthenium catalysts.

BIBLIOGRAPHY

Abdalrhman, A.S. and Gamal El-Din, M. (2020) Degradation of organics in real oil sands process water by electro-oxidation using graphite and dimensionally stable anodes. Chemical Engineering Journal 389, 124406.

Abdalrhman, A.S., Ganiyu, S.O. and Gamal El-Din, M. (2019) Degradation kinetics and structure-reactivity relation of naphthenic acids during anodic oxidation on graphite electrodes. Chemical Engineering Journal 370, 997-1007.

Abdalrhman, A.S., Wang, C., How, Z.T. and Gamal El-Din, M. (2021) Degradation of cyclohexanecarboxylic acid as a model naphthenic acid by the UV/chlorine process: Kinetics and by-products identification. Journal of Hazardous Materials 402, 123476.

Abdalrhman, A.S., Zhang, Y., Arslan, M. and Gamal El-Din, M. (2020) Low-current electro-oxidation enhanced the biodegradation of the recalcitrant naphthenic acids in oil sands process water. Journal of Hazardous Materials 398, 122807.

Afzal, A., Chelme-Ayala, P., Drzewicz, P., Martin, J.W. and Gamal El-Din, M. (2015) Effects of Ozone and Ozone/Hydrogen Peroxide on the Degradation of Model and Real Oil-Sands-Process-Affected-Water Naphthenic Acids. Ozone: Science & Engineering 37(1), 45-54.

Afzal, A., Drzewicz, P., Martin, J.W. and Gamal El-Din, M. (2012) Decomposition of cyclohexanoic acid by the UV/H2O2 process under various conditions. Science of the Total Environment 426, 387-392.

Afzal, A., Drzewicz, P., Pérez-Estrada, L.A., Chen, Y., Martin, J.W. and Gamal El-Din, M. (2012) Effect of Molecular Structure on the Relative Reactivity of Naphthenic Acids in the UV/H2O2 Advanced Oxidation Process. Environmental Science & Technology 46(19), 10727-10734.

Alharbi, H.A., Saunders, D.M.V., Al-Mousa, A., Alcorn, J., Pereira, A.S., Martin, J.W., Giesy, J.P. and Wiseman, S.B. (2016) Inhibition of ABC transport proteins by oil sands process affected water. Aquatic Toxicology 170, 81-88.

Allen, E.W.A.W. (2008) Process water treatment in Canada's oil sands industry: I. Target pollutants and treatment objectives. 7(2), 123-138.

Anderson, J., Wiseman, S.B., Moustafa, A., Gamal El-Din, M., Liber, K. and Giesy, J.P. (2012) Effects of exposure to oil sands process-affected water from experimental reclamation ponds on Chironomus dilutus. Water Research 46(6), 1662-1672.

Andrew Lin, K.-Y. and Zhang, Z.-Y. (2016) α-Sulfur as a metal-free catalyst to activate peroxymonosulfate under visible light irradiation for decolorization. RSC Advances 6(18), 15027-15034.

Anipsitakis, G.P. and Dionysiou, D.D. (2004) Transition metal/UV-based advanced oxidation technologies for water decontamination. Applied Catalysis B: Environmental 54(3), 155-163.

Arslan, M., Müller, J.A. and Gamal El-Din, M. (2022) Aerobic naphthenic acid-degrading bacteria in petroleum-coke improve oil sands process water remediation in biofilters: DNA-stable isotope probing reveals methylotrophy in Schmutzdecke. Science of the Total Environment 815, 151961.

Babaei, A.A. and Ghanbari, F. (2016) COD removal from petrochemical wastewater by UV/hydrogen peroxide, UV/persulfate and UV/percarbonate: biodegradability improvement and cost evaluation. Journal of Water Reuse and Desalination 6(4), 484-494.

Barzegar, G., Jorfi, S., Zarezade, V., Khatebasreh, M., Mehdipour, F. and Ghanbari, F. (2018) 4-Chlorophenol degradation using ultrasound/peroxymonosulfate/nanoscale zero valent iron:

Reusability, identification of degradation intermediates and potential application for real wastewater. Chemosphere 201, 370-379.

Benally, C., Messele, S.A. and Gamal El-Din, M. (2019) Adsorption of organic matter in oil sands process water (OSPW) by carbon xerogel. Water Research 154, 402-411.

Bessa, E., Sant'Anna, G.L. and Dezotti, M. (2001) Photocatalytic/H2O2 treatment of oil field produced waters. Applied Catalysis B: Environmental 29(2), 125-134.

Biryukova, O.V., Fedorak, P.M. and Quideau, S.A. (2007) Biodegradation of naphthenic acids by rhizosphere microorganisms. Chemosphere 67(10), 2058-2064.

Bolton, J.R. and Linden, K.G. (2003) Standardization of Methods for Fluence (UV Dose) Determination in Bench-Scale UV Experiments. Journal of Environmental Engineering 129(3), 209-215.

Bouchard, J., Maine, C., Argyropoulos, D. and Berry, R. (1998) Kraft pulp bleaching using in-situ dimethyldioxirane: mechanism and reactivity of the oxidants.

Buxton, G.V., Greenstock, C.L., Helman, W.P. and Ross, A.B. (1988) Critical Review of rate constants for reactions of hydrated electrons, hydrogen atoms and hydroxyl radicals (·OH/·O− in Aqueous Solution. 17(2), 513-886.

Cao, R., Huang, H., Tian, N., Zhang, Y., Guo, Y. and Zhang, T. (2015) Novel Y doped Bi2WO6 photocatalyst: Hydrothermal fabrication, characterization and enhanced visible-light-driven photocatalytic activity for Rhodamine B degradation and photocurrent generation. Materials Characterization 101, 166-172.

Cao, R., Yang, H., Zhang, S. and Xu, X. (2019) Engineering of Z-scheme 2D/3D architectures with Ni(OH)2 on 3D porous g-C3N4 for efficiently photocatalytic H2 evolution. Applied Catalysis B: Environmental 258, 117997.

Cao, S., Shen, B., Tong, T., Fu, J. and Yu, J. (2018) 2D/2D Heterojunction of Ultrathin MXene/Bi2WO6 Nanosheets for Improved Photocatalytic CO2 Reduction. 28(21), 1800136.

Chen, F., Huang, G.-X., Yao, F.-B., Yang, Q., Zheng, Y.-M., Zhao, Q.-B. and Yu, H.-Q. (2020) Catalytic degradation of ciprofloxacin by a visible-light-assisted peroxymonosulfate activation system: Performance and mechanism. Water Research 173, 115559.

Chen, J., Ling, J., Sun, B., Wang, J., Zhou, B., Guan, X. and Sun, Y. (2021) Trace organic contaminants abatement by permanganate/bisulfite pretreatment coupled with conventional water treatment processes: Lab- and pilot-scale tests. Journal of Hazardous Materials 401, 123380.

Chen, J., Rao, D., Dong, H., Sun, B., Shao, B., Cao, G. and Guan, X. (2020) The role of active manganese species and free radicals in permanganate/bisulfite process. Journal of Hazardous Materials 388, 121735.

Chen, W., Wu, Y., Fan, J., Djurišić, A.B., Liu, F., Tam, H.W., Ng, A., Surya, C., Chan, W.K., Wang, D. and He, Z.-B. (2018) Understanding the Doping Effect on NiO: Toward High-Performance Inverted Perovskite Solar Cells. Advanced Energy Materials 8(19), 1703519.

Chen, X., Wang, W., Xiao, H., Hong, C., Zhu, F., Yao, Y. and Xue, Z. (2012) Accelerated TiO2 photocatalytic degradation of Acid Orange 7 under visible light mediated by peroxymonosulfate. Chemical Engineering Journal 193-194, 290-295.

Clemente, J.S., MacKinnon, M.D. and Fedorak, P.M. (2004) Aerobic Biodegradation of Two Commercial Naphthenic Acids Preparations. Environmental Science & Technology 38(4), 1009-1016.

Connick, R.E. and Zhang, Y.-X. (1996) Kinetics and Mechanism of the Oxidation of HSO3- by O2. 2. The Manganese(II)-Catalyzed Reaction. Inorganic Chemistry 35(16), 4613-4621.

Criquet, J. and Karpel Vel Leitner, N. (2011) Electron beam irradiation of aqueous solution of persulfate ions. Chemical Engineering Journal 169(1), 258-262.

Dai, Z., Qin, F., Zhao, H., Tian, F., Liu, Y. and Chen, R. (2015) Time-dependent evolution of the Bi3.64Mo0.36O6.55/Bi2MoO6 heterostructure for enhanced photocatalytic activity via the interfacial hole migration. Nanoscale 7(28), 11991-11999.

de Oliveira Livera, D., Leshuk, T., Peru, K.M., Headley, J.V. and Gu, F. (2018) Structure-reactivity relationship of naphthenic acids in the photocatalytic degradation process. Chemosphere 200, 180-190.

Debenest, T., Turcotte, P., Gagné, F., Gagnon, C. and Blaise, C. (2012) Ecotoxicological impacts of effluents generated by oil sands bitumen extraction and oil sands lixiviation on Pseudokirchneriella subcapitata. Aquatic Toxicology 112-113, 83-91.

Dong, S., Ding, X., Guo, T., Yue, X., Han, X. and Sun, J. (2017) Self-assembled hollow sphere shaped Bi2WO6/RGO composites for efficient sunlight-driven photocatalytic degradation of organic pollutants. Chemical Engineering Journal 316, 778-789.

Drzewicz, P., Perez-Estrada, L., Alpatova, A., Martin, J.W. and Gamal El-Din, M. (2012) Impact of Peroxydisulfate in the Presence of Zero Valent Iron on the Oxidation of Cyclohexanoic Acid and Naphthenic Acids from Oil Sands Process-Affected Water. Environmental Science & Technology 46(16), 8984-8991.

Duan, X., Ao, Z., Zhou, L., Sun, H., Wang, G. and Wang, S. (2016) Occurrence of radical and nonradical pathways from carbocatalysts for aqueous and nonaqueous catalytic oxidation. Applied Catalysis B: Environmental 188, 98-105.

Ernst, T., Cyfert, M. and Wilgocki, M. (1992) Kinetics and mechanism of sulfite oxidation by permanganate in basic medium. 24(10), 903-908.

Eslami, A., Hashemi, M. and Ghanbari, F. (2018) Degradation of 4-chlorophenol using catalyzed peroxymonosulfate with nano-MnO2/UV irradiation: Toxicity assessment and evaluation for industrial wastewater treatment. Journal of Cleaner Production 195, 1389-1397.

Fang, Z., Huang, R., Chelme-Ayala, P., Shi, Q., Xu, C. and Gamal El-Din, M. (2019) Comparison of UV/Persulfate and UV/H2O2 for the removal of naphthenic acids and acute toxicity towards Vibrio fischeri from petroleum production process water. Science of The Total Environment 694, 133686.

Fang, Z., Huang, R., How, Z.T., Jiang, B., Chelme-Ayala, P., Shi, Q., Xu, C. and Gamal El-Din, M. (2020) Molecular transformation of dissolved organic matter in process water from oil and gas operation during UV/H2O2, UV/chlorine, and UV/persulfate processes. Science of The Total Environment 730, 139072.

Feng, Q., Zhou, J. and Zhang, Y. (2019) Coupling Bi2MoO6 with persulfate for photocatalytic oxidation of tetracycline hydrochloride under visible light. Journal of Materials Science: Materials in Electronics 30(21), 19108-19118.

Fennell, J. and Arciszewski, T.J. (2019) Current knowledge of seepage from oil sands tailings ponds and its environmental influence in northeastern Alberta. Science of the Total Environment 686, 968-985.

Fu, H., Zhang, L., Yao, W. and Zhu, Y. (2006) Photocatalytic properties of nanosized Bi2WO6 catalysts synthesized via a hydrothermal process. Applied Catalysis B: Environmental 66(1), 100-110.

Fuchylo, U., Alharbi, H.A., Alcaraz, A.J., Jones, P.D., Giesy, J.P., Hecker, M. and Brinkmann, M. (2022) Inflammation of Gill Epithelia in Fish Causes Increased Permeation of Petrogenic Polar Organic Chemicals via Disruption of Tight Junctions. Environmental Science & Technology 56(3), 1820-1829.

Furman, O.S., Teel, A.L. and Watts, R.J. (2010) Mechanism of Base Activation of Persulfate. Environmental Science & Technology 44(16), 6423-6428.

Gagné, F., Bruneau, A., Turcotte, P., Gagnon, C. and Lacaze, E. (2017) An investigation of the immunotoxicity of oil sands processed water and leachates in trout leukocytes. Ecotoxicology and Environmental Safety 141, 43-51.

Gamal El-Din, M., Fu, H., Wang, N., Chelme-Ayala, P., Pérez-Estrada, L., Drzewicz, P., Martin, J.W., Zubot, W. and Smith, D.W. (2011) Naphthenic acids speciation and removal during petroleum-coke adsorption and ozonation of oil sands process-affected water. Science of The Total Environment 409(23), 5119-5125.

Ganiyu, S.O. and Gamal El-Din, M. (2020) Insight into in-situ radical and non-radical oxidative degradation of organic compounds in complex real matrix during electrooxidation with boron doped diamond electrode: A case study of oil sands process water treatment. Applied Catalysis B: Environmental 279, 119366.

Ganiyu, S.O., Arslan, M. and Gamal El-Din, M. (2022) Combined solar activated sulfate radical-based advanced oxidation processes (SR-AOPs) and biofiltration for the remediation of dissolved organics in oil sands produced water. Chemical Engineering Journal 433, 134579.

Gao, H., Yang, H., Xu, J., Zhang, S. and Li, J. (2018) Strongly Coupled g-C3N4 Nanosheets-Co3O4 Quantum Dots as 2D/0D Heterostructure Composite for Peroxymonosulfate Activation. Small 14(31), 1801353.

Gao, Y., Jiang, J., Zhou, Y., Pang, S.-Y., Jiang, C., Guo, Q. and Duan, J.-B. (2018) Does Soluble Mn(III) Oxidant Formed in Situ Account for Enhanced Transformation of Triclosan by Mn(VII) in the Presence of Ligands? Environmental Science & Technology 52(8), 4785-4793.

Gao, Y., Jiang, J., Zhou, Y., Pang, S.-Y., Ma, J., Jiang, C., Wang, Z., Wang, P.-X., Wang, L.-H. and Li, J. (2017) Unrecognized role of bisulfite as Mn(III) stabilizing agent in activating permanganate (Mn(VII)) for enhanced degradation of organic contaminants. Chemical Engineering Journal 327, 418-422.

Garcia, J.C., Oliveira, J.L., Silva, A.E.C., Oliveira, C.C., Nozaki, J. and de Souza, N.E. (2007) Comparative study of the degradation of real textile effluents by photocatalytic reactions involving UV/TiO2/H2O2 and UV/Fe2+/H2O2 systems. Journal of Hazardous Materials 147(1), 105-110.

García-Espinoza, J.D., Mijaylova-Nacheva, P. and Avilés-Flores, M. (2018) Electrochemical carbamazepine degradation: Effect of the generated active chlorine, transformation pathways and toxicity. Chemosphere 192, 142-151.

Garcia-Garcia, E., Ge, J.Q., Oladiran, A., Montgomery, B., El-Din, M.G., Perez-Estrada, L.C., Stafford, J.L., Martin, J.W. and Belosevic, M. (2011) Ozone treatment ameliorates oil sands process water toxicity to the mammalian immune system. Water Research 45(18), 5849-5857.

Ge, M., Li, Y., Liu, L., Zhou, Z. and Chen, W. (2011) Bi2O3−Bi2WO6 Composite Microspheres: Hydrothermal Synthesis and Photocatalytic Performances. The Journal of Physical Chemistry C 115(13), 5220-5225.

Gentes, M.-L., Waldner, C., Papp, Z. and Smits, J.E.G. (2006) Effects of oil sands tailings compounds and harsh weather on mortality rates, growth and detoxification efforts in nestling tree swallows (Tachycineta bicolor). Environmental Pollution 142(1), 24-33.

Ghauch, A., Baalbaki, A., Amasha, M., El Asmar, R. and Tantawi, O. (2017) Contribution of persulfate in UV-254nm activated systems for complete degradation of chloramphenicol antibiotic in water. Chemical Engineering Journal 317, 1012-1025.

Ghauch, A., Tuqan, A.M. and Kibbi, N. (2012) Ibuprofen removal by heated persulfate in aqueous solution: A kinetics study. Chemical Engineering Journal 197, 483-492.

Gong, Y., Zhao, X., Zhang, H., Yang, B., Xiao, K., Guo, T., Zhang, J., Shao, H., Wang, Y. and Yu, G. (2018) MOF-derived nitrogen doped carbon modified g-C3N4 heterostructure composite with enhanced photocatalytic activity for bisphenol A degradation with peroxymonosulfate under visible light irradiation. Applied Catalysis B: Environmental 233, 35-45.

Govindan, K., Raja, M., Noel, M. and James, E.J. (2014) Degradation of pentachlorophenol by hydroxyl radicals and sulfate radicals using electrochemical activation of peroxomonosulfate, peroxodisulfate and hydrogen peroxide. Journal of Hazardous Materials 272, 42-51.

Guan, Y.-H., Ma, J., Li, X.-C., Fang, J.-Y. and Chen, L.-W. (2011) Influence of pH on the Formation of Sulfate and Hydroxyl Radicals in the UV/Peroxymonosulfate System. Environmental Science & Technology 45(21), 9308-9314.

Gunawan, Y., Nemati, M. and Dalai, A. (2014) Biodegradation of a surrogate naphthenic acid under denitrifying conditions. Water Research 51, 11-24.

Guo, K., Zhang, J., Li, A., Xie, R., Liang, Z., Wang, A., Ling, L., Li, X., Li, C. and Fang, J. (2018) Ultraviolet Irradiation of Permanganate Enhanced the Oxidation of Micropollutants by Producing HO• and Reactive Manganese Species. Environmental Science & Technology Letters 5(12), 750-756.

Guo, Y., Li, J., Gao, Z., Zhu, X., Liu, Y., Wei, Z., Zhao, W. and Sun, C. (2016) A simple and effective method for fabricating novel p–n heterojunction photocatalyst g-C3N4/Bi4Ti3O12 and its photocatalytic performances. Applied Catalysis B: Environmental 192, 57-71.

Güyer, G.T. and Ince, N.H. (2011) Degradation of diclofenac in water by homogeneous and heterogeneous sonolysis. Ultrasonics Sonochemistry 18(1), 114-119.

Hagen, M.O., Katzenback, B.A., Islam, M.D.S., Gamal El-Din, M. and Belosevic, M. (2013) The Analysis of Goldfish (Carassius auratus L.) Innate Immune Responses After Acute and Subchronic Exposures to Oil Sands Process-Affected Water. Toxicological Sciences 138(1), 59-68.

He, Q., Si, S., Song, L., Yan, H., Yao, Y., Zhao, D. and Cai, Q. (2019) Refractory petrochemical wastewater treatment by K2S2O8 assisted photocatalysis. Saudi Journal of Biological Sciences 26(4), 849-853.

He, Y., Patterson, S., Wang, N., Hecker, M., Martin, J.W., El-Din, M.G., Giesy, J.P. and Wiseman, S.B. (2012a) Toxicity of untreated and ozone-treated oil sands process-affected water (OSPW) to early life stages of the fathead minnow (Pimephales promelas). Water Research 46(19), 6359-6368.

He, Y., Wiseman, S.B., Hecker, M., Zhang, X., Wang, N., Perez, L.A., Jones, P.D., Gamal El-Din, M., Martin, J.W. and Giesy, J.P. (2011) Effect of Ozonation on the Estrogenicity and

Androgenicity of Oil Sands Process-Affected Water. Environmental Science & Technology 45(15), 6268-6274.

He, Y., Wiseman, S.B., Wang, N., Perez-Estrada, L.A., El-Din, M.G., Martin, J.W. and Giesy, J.P. (2012b) Transcriptional Responses of the Brain–Gonad–Liver Axis of Fathead Minnows Exposed to Untreated and Ozone-Treated Oil Sands Process-Affected Water. Environmental Science & Technology 46(17), 9701-9708.

Hersikorn, B.D. and Smits, J.E.G. (2011) Compromised metamorphosis and thyroid hormone changes in wood frogs (Lithobates sylvaticus) raised on reclaimed wetlands on the Athabasca oil sands. Environmental Pollution 159(2), 596-601.

Hersikorn, B.D., Ciborowski, J.J.C. and Smits, J.E.G. (2010) The effects of oil sands wetlands on wood frogs (Rana sylvatica). Toxicological & Environmental Chemistry 92(8), 1513-1527.

Hotovy, I., Huran, J., Spiess, L., Hascik, S. and Rehacek, V. (1999) Preparation of nickel oxide thin films for gas sensors applications. Sensors and Actuators B: Chemical 57(1), 147-152.

Hu, L., Martin, H.M. and Strathmann, T.J. (2010) Oxidation Kinetics of Antibiotics during Water Treatment with Potassium Permanganate. Environmental Science & Technology 44(16), 6416-6422.

Hu, L., Martin, H.M., Arce-Bulted, O., Sugihara, M.N., Keating, K.A. and Strathmann, T.J. (2009) Oxidation of Carbamazepine by Mn(VII) and Fe(VI): Reaction Kinetics and Mechanism. Environmental Science & Technology 43(2), 509-515.

Hu, L., Stemig, A.M., Wammer, K.H. and Strathmann, T.J. (2011) Oxidation of Antibiotics during Water Treatment with Potassium Permanganate: Reaction Pathways and Deactivation. Environmental Science & Technology 45(8), 3635-3642.

Hu, T., Li, H., Zhang, R., Du, N. and Hou, W. (2016) Thickness-determined photocatalytic

performance of bismuth tungstate nanosheets. RSC Advances 6(38), 31744-31750.

Huang, C., Shi, Y., Gamal El-Din, M. and Liu, Y. (2015) Treatment of oil sands process-affected water (OSPW) using ozonation combined with integrated fixed-film activated sludge (IFAS). Water Research 85, 167-176.

Huang, R., Chen, Y., Meshref, M.N.A., Chelme-Ayala, P., Dong, S., Ibrahim, M.D., Wang, C., Klamerth, N., Hughes, S.A., Headley, J.V., Peru, K.M., Brown, C., Mahaffey, A. and Gamal El-Din, M. (2018) Characterization and determination of naphthenic acids species in oil sands process-affected water and groundwater from oil sands development area of Alberta, Canada. Water Research 128, 129-137.

Huang, R., Sun, N., Chelme-Ayala, P., McPhedran, K.N., Changalov, M. and Gamal El-Din, M. (2015) Fractionation of oil sands-process affected water using pH-dependent extractions: A study of dissociation constants for naphthenic acids species. Chemosphere 127, 291-296.

Huang, R., Wang, C., Chelme-Ayala, P., Fang, Z., Shi, Q., Xu, C. and Gamal El-Din, M. (2019) Ferrate oxidation of distinct naphthenic acids species isolated from process water of unconventional petroleum production. Science of the Total Environment 672, 906-915.

Huo, W.C., Dong, X.a., Li, J.Y., Liu, M., Liu, X.Y., Zhang, Y.X. and Dong, F. (2019) Synthesis of Bi2WO6 with gradient oxygen vacancies for highly photocatalytic NO oxidation and mechanism study. Chemical Engineering Journal 361, 129-138.

Iguchi, S., Teramura, K., Hosokawa, S. and Tanaka, T. (2015) Effect of the chloride ion as a hole scavenger on the photocatalytic conversion of CO2 in an aqueous solution over Ni–Al layered double hydroxides. Physical Chemistry Chemical Physics 17(27), 17995-18003.

Islam, M.S., Zhang, Y., McPhedran, K.N., Liu, Y. and Gamal El-Din, M. (2015) Granular activated carbon for simultaneous adsorption and biodegradation of toxic oil sands process-affected water organic compounds. Journal of Environmental Management 152, 49-57.

Ji, X., Han, Z., Li, J., Deng, Y., Han, X., Zhao, J., Zhao, X. and Chen, C. (2019) MoSx co-catalytic activation of H2O2 by heterogeneous hemin catalyst under visible light irradiation. Journal of Colloid and Interface Science 557, 301-310.

Jiang, H., Xing, Z., Zhao, T., Yang, Z., Wang, K., Li, Z., Yang, S., Xie, L. and Zhou, W. (2020) Plasmon Ag nanoparticle/Bi2S3 ultrathin nanobelt/oxygen-doped flower-like MoS2 nanosphere ternary heterojunctions for promoting charge separation and enhancing solar-driven photothermal and photocatalytic performances. Applied Catalysis B: Environmental 274, 118947.

Jiang, J., Gao, Y., Pang, S.-Y., Lu, X.-T., Zhou, Y., Ma, J. and Wang, Q. (2015) Understanding the Role of Manganese Dioxide in the Oxidation of Phenolic Compounds by Aqueous Permanganate. Environmental Science & Technology 49(1), 520-528.

Jiang, J., Gao, Y., Pang, S.-Y., Wang, Q., Huangfu, X., Liu, Y. and Ma, J. (2014) Oxidation of Bromophenols and Formation of Brominated Polymeric Products of Concern during Water Treatment with Potassium Permanganate. Environmental Science & Technology 48(18), 10850-10858.

Jiang, J., Pang, S.-Y. and Ma, J. (2009) Oxidation of Triclosan by Permanganate (Mn(VII)): Importance of Ligands and In Situ Formed Manganese Oxides. Environmental Science & Technology 43(21), 8326-8331.

Jo, W.-K., Kumar, S., Eslava, S. and Tonda, S. (2018) Construction of Bi2WO6/RGO/g-C3N4 2D/2D/2D hybrid Z-scheme heterojunctions with large interfacial contact area for efficient

charge separation and high-performance photoreduction of CO2 and H2O into solar fuels. Applied Catalysis B: Environmental 239, 586-598.

Jones, D., Scarlett, A.G., West, C.E. and Rowland, S.J. (2011) Toxicity of Individual Naphthenic Acids to Vibrio fischeri. Environmental Science & Technology 45(22), 9776-9782.

Kalebaila, K.K. and Fairbridge, C. (2014) UV Photocatalytic Degradation of Commercial Naphthenic Acid Using TiO₂-Zeolite Composites %J Journal of Water Resource and Protection. Vol.06No.12, 9.

Kirschenbaum, L.J. and Sutter, J.R. (1966) Kinetic Studies of Permanganate Oxidation Reactions. I. Reaction with Iodide Ion. The Journal of Physical Chemistry 70(12), 3863-3866.

Kormali, P., Triantis, T., Dimotikali, D., Hiskia, A. and Papaconstantinou, E. (2006) On the photooxidative behavior of TiO2 and PW12O403−: OH radicals versus holes. Applied Catalysis B: Environmental 68(3), 139-146.

Lawani, S.A. and Sutter, J.R. (1973) Kinetic studies of permanganate oxidation reactions. IV. Reaction with bromide ion. The Journal of Physical Chemistry 77(12), 1547-1551.

Leclair, L.A., Pohler, L., Wiseman, S.B., He, Y., Arens, C.J., Giesy, J.P., Scully, S., Wagner, B.D., van den Heuvel, M.R. and Hogan, N.S. (2015) In Vitro Assessment of Endocrine Disrupting Potential of Naphthenic Acid Fractions Derived from Oil Sands-Influenced Water. Environmental Science & Technology 49(9), 5743-5752.

Legrini, O., Oliveros, E. and Braun, A.M. (1993) Photochemical processes for water treatment. Chemical Reviews 93(2), 671-698.

Leshuk, T., de Oliveira Livera, D., Peru, K.M., Headley, J.V., Vijayaraghavan, S., Wong, T. and Gu, F. (2016a) Photocatalytic degradation kinetics of naphthenic acids in oil sands process-

affected water: Multifactorial determination of significant factors. Chemosphere 165, 10-17.

Leshuk, T., Peru, K.M., de Oliveira Livera, D., Tripp, A., Bardo, P., Headley, J.V. and Gu, F. (2018) Petroleomic analysis of the treatment of naphthenic organics in oil sands process-affected water with buoyant photocatalysts. Water Research 141, 297-306.

Leshuk, T., Wong, T., Linley, S., Peru, K.M., Headley, J.V. and Gu, F. (2016b) Solar photocatalytic degradation of naphthenic acids in oil sands process-affected water. Chemosphere 144, 1854-1861.

Li, B., Lai, C., Zeng, G., Qin, L., Yi, H., Huang, D., Zhou, C., Liu, X., Cheng, M., Xu, P., Zhang, C., Huang, F. and Liu, S. (2018) Facile Hydrothermal Synthesis of Z-Scheme Bi2Fe4O9/Bi2WO6 Heterojunction Photocatalyst with Enhanced Visible Light Photocatalytic Activity. ACS Applied Materials & Interfaces 10(22), 18824-18836.

Li, B., Yang, Q., Peng, Y., Chen, J., Deng, L., Wang, D., Hong, X. and Li, J. (2019) Enhanced low-temperature activity of LaMnO3 for toluene oxidation: The effect of treatment with an acidic KMnO4. Chemical Engineering Journal 366, 92-99.

Li, C., Chen, G., Sun, J., Rao, J., Han, Z., Hu, Y., Xing, W. and Zhang, C. (2016) Doping effect of phosphate in Bi2WO6 and universal improved photocatalytic activity for removing various pollutants in water. Applied Catalysis B: Environmental 188, 39-47.

Li, C., Fu, L., Lillico, D.M.E., Belosevic, M., Stafford, J.L. and Gamal El-Din, M. (2019) Exposure to Organic Fraction Extracted from Oil Sands Process-Affected Water Has Negligible Impact on Pregnancy and Lactation of Mice. Environmental Science & Technology 53(12), 7083-7094.

Li, C., Fu, L., Stafford, J., Belosevic, M. and Gamal El-Din, M. (2017) The toxicity of oil sands

process-affected water (OSPW): A critical review. Science of the Total Environment 601-602, 1785-1802.

Liang, X., Zhu, X. and Butler, E.C. (2011) Comparison of four advanced oxidation processes for the removal of naphthenic acids from model oil sands process water. Journal of Hazardous Materials 190(1), 168-176.

Lin, Z., Du, C., Yan, B., Wang, C. and Yang, G. (2018) Two-dimensional amorphous NiO as a plasmonic photocatalyst for solar H2 evolution. Nature Communications 9(1), 4036.

Liu, C.a., Fu, Y., Zhao, J., Wang, H., Huang, H., Liu, Y., Dou, Y., Shao, M. and Kang, Z. (2019) All-solid-state Z-scheme system of NiO/CDs/BiVO4 for visible light-driven efficient overall water splitting. Chemical Engineering Journal 358, 134-142.

Liu, J., Wang, L., Tang, J. and Ma, J. (2016a) Photocatalytic degradation of commercially sourced naphthenic acids by TiO2-graphene composite nanomaterial. Chemosphere 149, 328-335.

Liu, J., Zhao, Z., Shao, P. and Cui, F. (2015) Activation of peroxymonosulfate with magnetic Fe3O4–MnO2 core–shell nanocomposites for 4-chlorophenol degradation. Chemical Engineering Journal 262, 854-861.

Liu, M., Hou, L.-a., Li, Q., Hu, X. and Yu, S. (2016a) Heterogeneous degradation of tetracycline by magnetic Ag/AgCl/modified zeolite X–persulfate system under visible light. RSC Advances 6(42), 35216-35227.

Liu, M., Zhang, L., Xi, B.-d., Yu, S., Hu, X. and Hou, L.-a. (2017) Degradation of ciprofloxacin by TiO2/Fe2O3/zeolite catalyst-activated persulfate under visible LED light irradiation. RSC Advances 7(81), 51512-51520.

Liu, N., Lei, Z.-D., Wang, T., Wang, J.-J., Zhang, X.-D., Xu, G. and Tang, L. (2016b) Radiolysis of carbamazepine aqueous solution using electron beam irradiation combining with

hydrogen peroxide: Efficiency and mechanism. Chemical Engineering Journal 295, 484-493.

Lo, C.C., Brownlee, B.G. and Bunce, N.J. (2006) Mass spectrometric and toxicological assays of Athabasca oil sands naphthenic acids. Water Research 40(4), 655-664.

Loos, G., Scheers, T., Van Eyck, K., Van Schepdael, A., Adams, E., Van der Bruggen, B., Cabooter, D. and Dewil, R. (2018) Electrochemical oxidation of key pharmaceuticals using a boron doped diamond electrode. Separation and Purification Technology 195, 184-191.

Luo, C., Ma, J., Jiang, J., Liu, Y., Song, Y., Yang, Y., Guan, Y. and Wu, D. (2015) Simulation and comparative study on the oxidation kinetics of atrazine by UV/H2O2, UV/HSO5− and UV/S2O82−. Water Research 80, 99-108.

Luo, Z., Meng, L., How, Z.T., Chelme-Ayala, P., Yang, L., Benally, C. and Gamal El-Din, M. (2022) Treatment of oil sands process water by the ferric citrate under visible light irradiation. Chemical Engineering Journal 429, 132419.

Lutze, H. (2013) Sulfate radical based oxidation in water treatment, Universität Duisburg-Essen.

Lutze, H.V., Bakkour, R., Kerlin, N., von Sonntag, C. and Schmidt, T.C. (2014) Formation of bromate in sulfate radical based oxidation: Mechanistic aspects and suppression by dissolved organic matter. Water Research 53, 370-377.

Lutze, H.V., Bircher, S., Rapp, I., Kerlin, N., Bakkour, R., Geisler, M., von Sonntag, C. and Schmidt, T.C. (2015) Degradation of Chlorotriazine Pesticides by Sulfate Radicals and the Influence of Organic Matter. Environmental Science & Technology 49(3), 1673-1680.

Lv, N., Li, Y., Huang, Z., Li, T., Ye, S., Dionysiou, D.D. and Song, X. (2019) Synthesis of GO/TiO2/Bi2WO6 nanocomposites with enhanced visible light photocatalytic degradation of ethylene. Applied Catalysis B: Environmental 246, 303-311.

Lv, Y.-R., He, R.-K., Chen, Z.-Y., Li, X. and Xu, Y.-H. (2020) Fabrication of hierarchical copper sulfide/bismuth tungstate p-n heterojunction with two-dimensional (2D) interfacial coupling for enhanced visible-light photocatalytic degradation of glyphosate. Journal of Colloid and Interface Science 560, 293-302.

Mao, D., Ding, S., Meng, L., Dai, Y., Sun, C., Yang, S. and He, H. (2017) One-pot microemulsion-mediated synthesis of Bi-rich Bi4O5Br2 with controllable morphologies and excellent visible-light photocatalytic removal of pollutants. Applied Catalysis B: Environmental 207, 153-165.

Masliyah, J., Zhou, Z.J., Xu, Z., Czarnecki, J. and Hamza, H. (2004) Understanding Water-Based Bitumen Extraction from Athabasca Oil Sands. The Canadian Journal of Chemical Engineering 82(4), 628-654.

Mavinakere Ramesh, A., Shivanna, S. (2018) Visible light assisted photocatalytic degradation of chromium (VI) by using nanoporous Fe_2O_3. Journal of Materials, 2018.

McQueen, A.D., Kinley, C.M., Kiekhaefer, R.L., Calomeni, A.J., Rodgers, J.H. and Castle, J.W. (2016) Photocatalysis of a Commercial Naphthenic Acid in Water Using Fixed-Film TiO2. Water, Air, & Soil Pollution 227(5), 132.

Meng, L., How, Z.T., Ganiyu, S.O. and Gamal El-Din, M. (2021) Solar photocatalytic treatment of model and real oil sands process water naphthenic acids by bismuth tungstate: Effect of catalyst morphology and cations on the degradation kinetics and pathways. Journal of Hazardous Materials 413, 125396.

Meng, L., Yang, S., Sun, C., He, H., Xian, Q., Li, S., Wang, G., Zhang, L. and Jiang, D. (2017a) A novel method for photo-oxidative degradation of diatrizoate in water via electromagnetic induction electrodeless lamp. Journal of Hazardous Materials 337, 34-46.

Meng, X., Li, Z., Zeng, H., Chen, J. and Zhang, Z. (2017) MoS2 quantum dots-interspersed Bi2WO6 heterostructures for visible light-induced detoxification and disinfection. Applied Catalysis B: Environmental 210, 160-172.

Michael, I., Hapeshi, E., Michael, C., Varela, A.R., Kyriakou, S., Manaia, C.M. and Fatta-Kassinos, D. (2012) Solar photo-Fenton process on the abatement of antibiotics at a pilot scale: Degradation kinetics, ecotoxicity and phytotoxicity assessment and removal of antibiotic resistant enterococci. Water Research 46(17), 5621-5634.

Miklos, D.B., Remy, C., Jekel, M., Linden, K.G., Drewes, J.E. and Hübner, U. (2018) Evaluation of advanced oxidation processes for water and wastewater treatment – A critical review. Water Research 139, 118-131.

Morandi, G.D., Wiseman, S.B., Pereira, A., Mankidy, R., Gault, I.G.M., Martin, J.W. and Giesy, J.P. (2015) Effects-Directed Analysis of Dissolved Organic Compounds in Oil Sands Process-Affected Water. Environmental Science & Technology 49(20), 12395-12404.

Nawaz, T. and Sengupta, S. (2021) Handbook of Water Purity and Quality (Second Edition). Ahuja, S. (ed), pp. 293-337, Academic Press, Amsterdam.

Nero, V., Farwell, A., Lee, L.E.J., Van Meer, T., MacKinnon, M.D. and Dixon, D.G. (2006) The effects of salinity on naphthenic acid toxicity to yellow perch: Gill and liver histopathology. Ecotoxicology and Environmental Safety 65(2), 252-264.

NRC (2022a) Oil Resources, Natural Resource Canada, Canada.

NRC (2022b) Water Management in oil sands, Natural Resource Canada, Canada.

Nyakas, A., Han, J., Peru, K.M., Headley, J.V. and Borchers, C.H. (2013) Comprehensive Analysis of Oil Sands Processed Water by Direct-Infusion Fourier-Transform Ion Cyclotron

Resonance Mass Spectrometry with and without Offline UHPLC Sample Prefractionation. Environmental Science & Technology 47(9), 4471-4479.

Oh, W.-D., Dong, Z. and Lim, T.-T. (2016) Generation of sulfate radical through heterogeneous catalysis for organic contaminants removal: Current development, challenges and prospects. Applied Catalysis B: Environmental 194, 169-201.

Oturan, M.A. and Aaron, J.-J. (2014) Advanced Oxidation Processes in Water/Wastewater Treatment: Principles and Applications. A Review. Critical Reviews in Environmental Science and Technology 44(23), 2577-2641.

Parajulee, A. and Wania, F. (2014) Evaluating officially reported polycyclic aromatic hydrocarbon emissions in the Athabasca oil sands region with a multimedia fate model. 111(9), 3344-3349.

Peng, J., Zhou, P., Zhou, H., Liu, W., Zhang, H., Zhou, C., Lai, L., Ao, Z., Su, S. and Lai, B. (2021) Insights into the Electron-Transfer Mechanism of Permanganate Activation by Graphite for Enhanced Oxidation of Sulfamethoxazole. Environmental Science & Technology 55(13), 9189-9198.

Peng, W., Liu, S., Sun, H., Yao, Y., Zhi, L. and Wang, S. (2013) Synthesis of porous reduced graphene oxide as metal-free carbon for adsorption and catalytic oxidation of organics in water. Journal of Materials Chemistry A 1(19), 5854-5859.

Pérez-Estrada, L.A., Han, X., Drzewicz, P., Gamal El-Din, M., Fedorak, P.M. and Martin, J.W. (2011) Structure–Reactivity of Naphthenic Acids in the Ozonation Process. Environmental Science & Technology 45(17), 7431-7437.

Pollet, I. and Bendell-Young, L.I. (2000) Amphibians as indicators of wetland quality in wetlands formed from oil sands effluent. 19(10), 2589-2597.

Poveda, C. and Lipsett, M. (2013) The Canadian oil sands: environmental, economic, social, health, and other impacts. WIT Transactions on Ecology and the Environment 173, 575-587.

Pramanik, S. (2016) Review of biological processes in oil sands: a feasible solution for tailings water treatment. 24(3), 274-284.

Qi, C., Liu, X., Ma, J., Lin, C., Li, X. and Zhang, H. (2016) Activation of peroxymonosulfate by base: Implications for the degradation of organic pollutants. Chemosphere 151, 280-288.

Qin, R., Chelme-Ayala, P. and El-Din, M.G. (2020) The impact of oil sands process water matrix on the ozonation of naphthenic acids: from a model compound to a natural mixture. 47(10), 1166-1174.

Qin, R., How, Z.T. and Gamal El-Din, M. (2019a) Photodegradation of naphthenic acids induced by natural photosensitizer in oil sands process water. Water Research 164, 114913.

Qin, R., Lillico, D., How, Z.T., Huang, R., Belosevic, M., Stafford, J. and Gamal El-Din, M. (2019b) Separation of oil sands process water organics and inorganics and examination of their acute toxicity using standard in-vitro bioassays. Science of the Total Environment 695, 133532.

Rabanimehr, F., Farhadian, M., Nazar, A.R.S. and Moghadam, M. (2021) Fabrication of Z-scheme Bi2WO6/CNT/TiO2 heterostructure with enhanced cephalexin photodegradation: Optimization and reaction mechanism. Journal of Molecular Liquids 339, 116728.

Rastogi, A., Al-Abed, S.R. and Dionysiou, D.D. (2009) Sulfate radical-based ferrous–peroxymonosulfate oxidative system for PCBs degradation in aqueous and sediment systems. Applied Catalysis B: Environmental 85(3), 171-179.

Redpath, J.L. and Willson, R.L. (1975) Chain Reactions and Radiosensitization: Model Enzyme Studies. International Journal of Radiation Biology and Related Studies in Physics, Chemistry and Medicine 27(4), 389-398.

Reinardy, H.C., Scarlett, A.G., Henry, T.B., West, C.E., Hewitt, L.M., Frank, R.A. and Rowland, S.J. (2013) Aromatic Naphthenic Acids in Oil Sands Process-Affected Water, Resolved by GCxGC-MS, Only Weakly Induce the Gene for Vitellogenin Production in Zebrafish (Danio rerio) Larvae. Environmental Science & Technology 47(12), 6614-6620.

Ren, J., Wang, W., Sun, S., Zhang, L. and Chang, J. (2009) Enhanced photocatalytic activity of Bi2WO6 loaded with Ag nanoparticles under visible light irradiation. Applied Catalysis B: Environmental 92(1), 50-55.

Rogers, V., MacKinnon, M. and Brownlee, B. (2007) Analytical approaches to characterising fish tainting potential of oil sands process waters. Water Science and Technology 55(5), 311-318.

Rowland, S.J., West, C.E., Jones, D., Scarlett, A.G., Frank, R.A. and Hewitt, L.M. (2011) Steroidal Aromatic 'Naphthenic Acids' in Oil Sands Process-Affected Water: Structural Comparisons with Environmental Estrogens. Environmental Science & Technology 45(22), 9806-9815.

Samuni, A., Krishna, C.M., Mitchell, J.B., Collins, C.R. and Russo, A. (1990) Superoxide Reaction with Nitroxides. Free Radical Research Communications 9(3-6), 241-249.

Sánchez-Polo, M., Abdel daiem, M.M., Ocampo-Pérez, R., Rivera-Utrilla, J. and Mota, A.J. (2013) Comparative study of the photodegradation of bisphenol A by HO, SO4− and CO3−/HCO3 radicals in aqueous phase. Science of the Total Environment 463-464, 423-431.

Scarlett, A.G., Reinardy, H.C., Henry, T.B., West, C.E., Frank, R.A., Hewitt, L.M. and Rowland, S.J. (2013) Acute toxicity of aromatic and non-aromatic fractions of naphthenic acids extracted from oil sands process-affected water to larval zebrafish. Chemosphere 93(2), 415-420.

Scarlett, A.G., West, C.E., Jones, D., Galloway, T.S. and Rowland, S.J. (2012) Predicted toxicity of naphthenic acids present in oil sands process-affected waters to a range of environmental and human endpoints. Science of the Total Environment 425, 119-127.

Serna-Galvis, E.A., Silva-Agredo, J., Giraldo-Aguirre, A.L., Flórez-Acosta, O.A. and Torres-Palma, R.A. (2016) High frequency ultrasound as a selective advanced oxidation process to remove penicillinic antibiotics and eliminate its antimicrobial activity from water. Ultrasonics Sonochemistry 31, 276-283.

Shang, M., Wang, W., Zhang, L. and Xu, H. (2010) Bi2WO6 with significantly enhanced photocatalytic activities by nitrogen doping. Materials Chemistry and Physics 120(1), 155-159.

Shu, Z., Li, C., Belosevic, M., Bolton, J.R. and El-Din, M.G. (2014) Application of a Solar UV/Chlorine Advanced Oxidation Process to Oil Sands Process-Affected Water Remediation. Environmental Science & Technology 48(16), 9692-9701.

Sohrabi, V., Ross, M.S., Martin, J.W. and Barker, J.F. (2013) Potential for in situ chemical oxidation of acid extractable organics in oil sands process affected groundwater. Chemosphere 93(11), 2698-2703.

Song, J., Messele, S.A., Meng, L., Huang, Z. and Gamal El-Din, M. (2021) Adsorption of metals from oil sands process water (OSPW) under natural pH by sludge-based Biochar/Chitosan composite. Water Research 194, 116930.

Suara, M.A., Ganiyu, S.O., Paul, S., Stafford, J.L. and Gamal El-Din, M. (2022) Solar-activated zinc oxide photocatalytic treatment of real oil sands process water: Effect of treatment parameters on naphthenic acids, polyaromatic hydrocarbons and acute toxicity removal. Science of the Total Environment 819, 153029.

Sun, B., Bao, Q. and Guan, X. (2018a) Critical role of oxygen for rapid degradation of organic contaminants in permanganate/bisulfite process. Journal of Hazardous Materials 352, 157-164.

Sun, B., Dong, H., He, D., Rao, D. and Guan, X. (2016) Modeling the Kinetics of Contaminants Oxidation and the Generation of Manganese(III) in the Permanganate/Bisulfite Process. Environmental Science & Technology 50(3), 1473-1482.

Sun, B., Guan, X., Fang, J. and Tratnyek, P.G. (2015) Activation of Manganese Oxidants with Bisulfite for Enhanced Oxidation of Organic Contaminants: The Involvement of Mn(III). Environmental Science & Technology 49(20), 12414-12421.

Sun, B., Li, D., Linghu, W. and Guan, X. (2018b) Degradation of ciprofloxacin by manganese(III) intermediate: Insight into the potential application of permanganate/bisulfite process. Chemical Engineering Journal 339, 144-152.

Sun, B., Zhang, J., Du, J., Qiao, J. and Guan, X. (2013) Reinvestigation of the Role of Humic Acid in the Oxidation of Phenols by Permanganate. Environmental Science & Technology 47(24), 14332-14340.

Sun, C., Shotyk, W., Cuss, C.W., Donner, M.W., Fennell, J., Javed, M., Noernberg, T., Poesch, M., Pelletier, R., Sinnatamby, N., Siddique, T. and Martin, J.W. (2017) Characterization of Naphthenic Acids and Other Dissolved Organics in Natural Water from the Athabasca Oil Sands Region, Canada. Environmental Science & Technology 51(17), 9524-9532.

Sun, H., Kwan, C., Suvorova, A., Ang, H.M., Tadé, M.O. and Wang, S. (2014) Catalytic oxidation of organic pollutants on pristine and surface nitrogen-modified carbon nanotubes with sulfate radicals. Applied Catalysis B: Environmental 154-155, 134-141.

Sun, J., Peng, H., Alharbi, H.A., Jones, P.D., Giesy, J.P. and Wiseman, S.B. (2017) Identification of Chemicals that Cause Oxidative Stress in Oil Sands Process-Affected Water. Environmental Science & Technology 51(15), 8773-8781.

Sun, J., Shen, C.-H., Guo, J., Guo, H., Yin, Y.-F., Xu, X.-J., Fei, Z.-H., Liu, Z.-T. and Wen, X.-J. (2021) Highly efficient activation of peroxymonosulfate by Co3O4/Bi2WO6 p-n heterojunction composites for the degradation of ciprofloxacin under visible light irradiation. Journal of Colloid and Interface Science 588, 19-30.

Sun, N., Chelme-Ayala, P., Klamerth, N., McPhedran, K.N., Islam, M.S., Perez-Estrada, L., Drzewicz, P., Blunt, B.J., Reichert, M., Hagen, M., Tierney, K.B., Belosevic, M. and Gamal El-Din, M. (2014) Advanced Analytical Mass Spectrometric Techniques and Bioassays to Characterize Untreated and Ozonated Oil Sands Process-Affected Water. Environmental Science & Technology 48(19), 11090-11099.

Svejstrup, T.D., Ruffoni, A., Juliá, F., Aubert, V.M. and Leonori, D. (2017) Synthesis of Arylamines via Aminium Radicals. Angewandte Chemie International Edition 56(47), 14948-14952.

Takdastan, A., Ravanbakhsh, M., Hazrati, M. and Safapour, S. (2019) Removal of dinitrotoluene from petrochemical wastewater by Fenton oxidation, kinetics and the optimum experiment conditions. SN Applied Sciences 1(7), 794.

Tan, X., Bai, J., Zheng, J., Zhang, Y., Li, J., Zhou, T., Xia, L., Xu, Q. and Zhou, B. (2019) Photocatalytic fuel cell based on sulfate radicals converted from sulfates in situ for wastewater treatment and chemical energy utilization. Catalysis Today 335, 485-491.

Tang, J.-y., Guo, R.-t., Zhou, W.-g., Huang, C.-y. and Pan, W.-g. (2018) Ball-flower like NiO/g-C3N4 heterojunction for efficient visible light photocatalytic CO2 reduction. Applied Catalysis B: Environmental 237, 802-810.

Tang, S., Tang, J., Yuan, D., Wang, Z., Zhang, Y. and Rao, Y. (2020) Elimination of humic acid in water: comparison of UV/PDS and UV/PMS. RSC Advances 10(30), 17627-17634.

Tantardini, C. and Oganov, A.R. (2021) Thermochemical electronegativities of the elements. Nature Communications 12(1), 2087.

Tian, S.-Q., Wang, L., Liu, Y.-L., Yang, T., Huang, Z.-S., Wang, X.-S., He, H.-Y., Jiang, J. and Ma, J. (2019) Enhanced Permanganate Oxidation of Sulfamethoxazole and Removal of Dissolved Organics with Biochar: Formation of Highly Oxidative Manganese Intermediate Species and in Situ Activation of Biochar. Environmental Science & Technology 53(9), 5282-5291.

Trovó, A.G., Pupo Nogueira, R.F., Agüera, A., Fernandez-Alba, A.R. and Malato, S. (2011) Degradation of the antibiotic amoxicillin by photo-Fenton process – Chemical and toxicological assessment. Water Research 45(3), 1394-1402.

von Gunten, U. (2003) Ozonation of drinking water: Part II. Disinfection and by-product formation in presence of bromide, iodide or chlorine. Water Research 37(7), 1469-1487.

von Gunten, U. and Oliveras, Y. (1998) Advanced Oxidation of Bromide-Containing Waters: Bromate Formation Mechanisms. Environmental Science & Technology 32(1), 63-70.

von Sonntag, C. and von Gunten, U. (2012) Chemistry of Ozone in Water and Wastewater

Treatmentnull, IWA Publishing.

Wang, C., Klamerth, N., Huang, R., Elnakar, H. and Gamal El-Din, M. (2016a) Oxidation of Oil Sands Process-Affected Water by Potassium Ferrate(VI). Environmental Science & Technology 50(8), 4238-4247.

Wang, C., Klamerth, N., Messele, S.A., Singh, A., Belosevic, M. and Gamal El-Din, M. (2016b) Comparison of UV/hydrogen peroxide, potassium ferrate(VI), and ozone in oxidizing the organic fraction of oil sands process-affected water (OSPW). Water Research 100, 476-485.

Wang, H., Zhang, L., Chen, Z., Hu, J., Li, S., Wang, Z., Liu, J. and Wang, X. (2014) Semiconductor heterojunction photocatalysts: design, construction, and photocatalytic performances. Chemical Society reviews 43(15), 5234-5244.

Wang, J., Cao, X., Huang, Y. and Tang, X. (2015) Developmental toxicity and endocrine disruption of naphthenic acids on the early life stage of zebrafish (Danio rerio). 35(12), 1493-1501.

Wang, N., Chelme-Ayala, P., Perez-Estrada, L., Garcia-Garcia, E., Pun, J., Martin, J.W., Belosevic, M. and Gamal El-Din, M. (2013) Impact of Ozonation on Naphthenic Acids Speciation and Toxicity of Oil Sands Process-Affected Water to Vibrio fischeri and Mammalian Immune System. Environmental Science & Technology 47(12), 6518-6526.

Wang, P., Huang, B., Lou, Z., Zhang, X., Qin, X., Dai, Y., Zheng, Z. and Wang, X. (2010a) Synthesis of Highly Efficient Ag@AgCl Plasmonic Photocatalysts with Various Structures. 16(2), 538-544.

Wang, P., Huang, B., Zhang, Q., Zhang, X., Qin, X., Dai, Y., Zhan, J., Yu, J., Liu, H. and Lou, Z. (2010b) Highly Efficient Visible Light Plasmonic Photocatalyst Ag@Ag(Br,I). 16(33), 10042-10047.

Wang, S. and Wang, J. (2018) Degradation of carbamazepine by radiation-induced activation of peroxymonosulfate. Chemical Engineering Journal 336, 595-601.

Wang, S. and Wang, J. (2022) Magnetic 2D/2D oxygen doped g-C3N4/biochar composite to activate peroxymonosulfate for degradation of emerging organic pollutants. Journal of Hazardous Materials 423, 127207.

Wang, Y., Cao, D. and Zhao, X. (2017a) Heterogeneous degradation of refractory pollutants by peroxymonosulfate activated by CoOx-doped ordered mesoporous carbon. Chemical Engineering Journal 328, 1112-1121.

Wang, Y., Zhang, H., Zhang, J., Lu, C., Huang, Q., Wu, J. and Liu, F. (2011) Degradation of tetracycline in aqueous media by ozonation in an internal loop-lift reactor. Journal of Hazardous Materials 192(1), 35-43.

Wang, Y., Zhao, X., Cao, D., Wang, Y. and Zhu, Y. (2017b) Peroxymonosulfate enhanced visible light photocatalytic degradation bisphenol A by single-atom dispersed Ag mesoporous g-C3N4 hybrid. Applied Catalysis B: Environmental 211, 79-88.

Wei, T. T., Wu, T., Lin, Y. W. (2019) Controlled synthesis of Ag_3PO_4 microparticles with different morphologies and their photocatalytic degradation of rhodamine B under white light-emitting diode irradiation. Micro & Nano Letters, 14(4), 363-366.

Wei, W., Guo, K., Kang, X., Zhang, J., Li, C. and Fang, J. (2021) Complete Removal of Organoarsenic by the UV/Permanganate Process via HO• Oxidation and in Situ-Formed Manganese Dioxide Adsorption. ACS ES&T Engineering 1(4), 794-803.

Whyte, J.J., Jung, R.E., Schmitt, C.J. and Tillitt, D.E. (2000) Ethoxyresorufin-O-deethylase (EROD) Activity in Fish as a Biomarker of Chemical Exposure. Critical Reviews in Toxicology 30(4), 347-570.

Williams, A.T.R., Winfield, S.A. and Miller, J.N. (1983) Relative fluorescence quantum yields using a computer-controlled luminescence spectrometer. Analyst 108(1290), 1067-1071.

Wiseman, S.B., Anderson, J.C., Liber, K. and Giesy, J.P. (2013) Endocrine disruption and oxidative stress in larvae of Chironomus dilutus following short-term exposure to fresh or aged oil sands process-affected water. Aquatic Toxicology 142-143, 414-421.

Wu, S., Sun, J., Li, Q., Hood, Z.D., Yang, S., Su, T., Peng, R., Wu, Z., Sun, W., Kent, P.R.C., Jiang, B. and Chisholm, M.F. (2020) Effects of Surface Terminations of 2D Bi2WO6 on Photocatalytic Hydrogen Evolution from Water Splitting. ACS Applied Materials & Interfaces 12(17), 20067-20074.

Xiao, Y., Zhang, L., Zhang, W., Lim, K.-Y., Webster, R.D. and Lim, T.-T. (2016) Comparative evaluation of iodoacids removal by UV/persulfate and UV/H2O2 processes. Water Research 102, 629-639.

Xu, X., Meng, L., Dai, Y., Zhang, M., Sun, C., Yang, S., He, H., Wang, S. and Li, H. (2020) Bi spheres SPR-coupled Cu2O/Bi2MoO6 with hollow spheres forming Z-scheme Cu2O/Bi/Bi2MoO6 heterostructure for simultaneous photocatalytic decontamination of sulfadiazine and Ni(II). Journal of Hazardous Materials 381, 120953.

Xu, X., Meng, L., Luo, J., Zhang, M., Wang, Y., Dai, Y., Sun, C., Wang, Z., Yang, S., He, H. and Wang, S. (2021) Self-assembled ultrathin CoO/Bi quantum dots/defective Bi2MoO6 hollow Z-scheme heterojunction for visible light-driven degradation of diazinon in water

matrix: Intermediate toxicity and photocatalytic mechanism. Applied Catalysis B: Environmental 293, 120231.

Xue, J., Zhang, Y., Liu, Y. and Gamal El-Din, M. (2016) Treatment of oil sands process-affected water (OSPW) using a membrane bioreactor with a submerged flat-sheet ceramic microfiltration membrane. Water Research 88, 1-11.

Yang, A.-M., Han, Y., Li, S.-S., Xing, H.-W., Pan, Y.-H. and Liu, W.-X. (2017) Synthesis and comparison of photocatalytic properties for Bi2WO6 nanofibers and hierarchical microspheres. Journal of Alloys and Compounds 695, 915-921.

Yang, P., Chen, C., Wang, D., Ma, H., Du, Y., Cai, D., Zhang, X. and Wu, Z. (2021) Kinetics, reaction pathways, and mechanism investigation for improved environmental remediation by 0D/3D CdTe/Bi2WO6 Z-scheme catalyst. Applied Catalysis B: Environmental 285, 119877.

Yao, D., Ouyang, Y., Jiao, X., Ye, H., Lei, W., Xia, X., Lu, L. and Hao, Q. (2018) Hierarchical NiO@NiCo2O4 Core–shell Nanosheet Arrays on Ni Foam for High-Performance Electrochemical Supercapacitors. Industrial & Engineering Chemistry Research 57(18), 6246-6256.

Ye, T., Xu, B., Lin, Y.-L., Hu, C.-Y., Lin, L., Zhang, T.-Y. and Gao, N.-Y. (2013) Formation of iodinated disinfection by-products during oxidation of iodide-containing waters with chlorine dioxide. Water Research 47(9), 3006-3014.

Ye, T., Xu, B., Lin, Y.-L., Hu, C.-Y., Xia, S.-J., Lin, L., Mwakagenda, S.A. and Gao, N.-Y. (2012) Formation of iodinated disinfection by-products during oxidation of iodide-containing water with potassium permanganate. Journal of Hazardous Materials 241-242, 348-354.

Yousefi, N., Pourfadakari, S., Esmaeili, S. and Babaei, A.A. (2019) Mineralization of high saline petrochemical wastewater using Sonoelectro-activated persulfate: Degradation mechanisms and reaction kinetics. Microchemical Journal 147, 1075-1082.

Yuan, S., Liao, P. and Alshawabkeh, A.N. (2014) Electrolytic Manipulation of Persulfate Reactivity by Iron Electrodes for Trichloroethylene Degradation in Groundwater. Environmental Science & Technology 48(1), 656-663.

Zeng, T., Zhang, X., Wang, S., Niu, H. and Cai, Y. (2015) Spatial Confinement of a Co3O4 Catalyst in Hollow Metal–Organic Frameworks as a Nanoreactor for Improved Degradation of Organic Pollutants. Environmental Science & Technology 49(4), 2350-2357.

Zhang, C. and Zhu, Y. (2005) Synthesis of Square Bi2WO6 Nanoplates as High-Activity Visible-Light-Driven Photocatalysts. Chemistry of Materials 17(13), 3537-3545.

Zhang, J., Sun, B., Guan, X., Wang, H., Bao, H., Huang, Y., Qiao, J. and Zhou, G. (2013) Ruthenium Nanoparticles Supported on CeO2 for Catalytic Permanganate Oxidation of Butylparaben. Environmental Science & Technology 47(22), 13011-13019.

Zhang, J., Sun, B., Huang, Y. and Guan, X. (2015a) Catalyzing the oxidation of sulfamethoxazole by permanganate using molecular sieves supported ruthenium nanoparticles. Chemosphere 141, 154-161.

Zhang, J., Sun, B., Xiong, X., Gao, N., Song, W., Du, E., Guan, X. and Zhou, G. (2014) Removal of emerging pollutants by Ru/TiO2-catalyzed permanganate oxidation. Water Research 63, 262-270.

Zhang, L., Wang, W., Chen, Z., Zhou, L., Xu, H. and Zhu, W. (2007a) Fabrication of flower-like Bi2WO6 superstructures as high performance visible-light driven photocatalysts. Journal

of Materials Chemistry 17(24), 2526-2532.

Zhang, L., Wang, W., Zhou, L. and Xu, H. (2007b) Bi2WO6 Nano- and Microstructures: Shape Control and Associated Visible-Light-Driven Photocatalytic Activities. Small 3(9), 1618-1625.

Zhang, L., Zhang, Y. and Gamal El-Din, M. (2018) Degradation of recalcitrant naphthenic acids from raw and ozonated oil sands process-affected waters by a semi-passive biofiltration process. Water Research 133, 310-318.

Zhang, T.-Y., Xu, B., Hu, C.-Y., Lin, Y.-L., Lin, L., Ye, T. and Tian, F.-X. (2015b) A comparison of iodinated trihalomethane formation from chlorine, chlorine dioxide and potassium permanganate oxidation processes. Water Research 68, 394-403.

Zhang, Y., Chelme-Ayala, P., Klamerth, N. and Gamal El-Din, M. (2017) Application of UV-irradiated Fe(III)-nitrilotriacetic acid (UV-Fe(III)NTA) and UV-NTA-Fenton systems to degrade model and natural occurring naphthenic acids. Chemosphere 179, 359-366.

Zhang, Y., Klamerth, N. and Gamal El-Din, M. (2016b) Degradation of a model naphthenic acid by nitrilotriacetic acid – modified Fenton process. Chemical Engineering Journal 292, 340-347.

Zhang, Y., Klamerth, N., Chelme-Ayala, P. and Gamal El-Din, M. (2016) Comparison of Nitrilotriacetic Acid and [S,S]-Ethylenediamine-N,N′-disuccinic Acid in UV–Fenton for the Treatment of Oil Sands Process-Affected Water at Natural pH. Environmental Science & Technology 50(19), 10535-10544.

Zhang, Y., McPhedran, K.N. and Gamal El-Din, M. (2015) Pseudomonads biodegradation of aromatic compounds in oil sands process-affected water. Science of the Total Environment 521-522, 59-67.

Zhang, Y., Zhao, Y., Xiong, Z., Gao, T., Gong, B., Liu, P., Liu, J. and Zhang, J. (2021) Elemental mercury removal by I−-doped Bi2WO6 with remarkable visible-light-driven photocatalytic oxidation. Applied Catalysis B: Environmental 282, 119534.

Zhao, L., Hou, H., Fujii, A., Hosomi, M. and Li, F. (2014) Degradation of 1,4-dioxane in water with heat- and Fe2+-activated persulfate oxidation. Environmental Science and Pollution Research 21(12), 7457-7465.

Zhao, X., Ma, J. and von Gunten, U. (2017a) Reactions of hypoiodous acid with model compounds and the formation of iodoform in absence/presence of permanganate. Water Research 119, 126-135.

Zhao, X., Ma, J., Jiang, J., Bao, Y. and Liu, H. (2016a) Phenols and anilines degradation by permanganate in the absence/presence of carbon nanotubes: Oxidation and dehalogenation. Separation and Purification Technology 170, 344-352.

Zhao, X., Salhi, E., Liu, H., Ma, J. and von Gunten, U. (2016b) Kinetic and Mechanistic Aspects of the Reactions of Iodide and Hypoiodous Acid with Permanganate: Oxidation and Disproportionation. Environmental Science & Technology 50(8), 4358-4365.

Zhao, Y., Kuang, J., Zhang, S., Li, X., Wang, B., Huang, J., Deng, S., Wang, Y. and Yu, G. (2017b) Ozonation of indomethacin: Kinetics, mechanisms and toxicity. Journal of Hazardous Materials 323, 460-470.

Zhong, X., Zhang, K.-X., Wu, D., Ye, X.-Y., Huang, W. and Zhou, B.-X. (2020) Enhanced photocatalytic degradation of levofloxacin by Fe-doped BiOCl nanosheets under LED light irradiation. Chemical Engineering Journal 383, 123148.

Zhou, H., Wen, Z., Liu, J., Ke, J., Duan, X. and Wang, S. (2019) Z-scheme plasmonic Ag decorated WO3/Bi2WO6 hybrids for enhanced photocatalytic abatement of chlorinated-VOCs under

solar light irradiation. Applied Catalysis B: Environmental 242, 76-84.

Zhu, D. and Zhou, Q. (2020) Novel Bi2WO6 modified by N-doped graphitic carbon nitride photocatalyst for efficient photocatalytic degradation of phenol under visible light. Applied Catalysis B: Environmental 268, 118426.

Zhu, Y., Wang, X., Zhang, J., Ding, L., Li, J., Zheng, H. and Zhao, C. (2019a) Generation of Active Mn(III)aq by a Novel Heterogeneous Electro-permanganate Process with Manganese(II) as Promoter and Stabilizer. Environmental Science & Technology 53(15), 9063-9072.

Zhu, Y., Yang, X., Qiao, J., Zhang, X. and Guan, X. (2019b) Effects of KMnO4/NaHSO3 pre-oxidation on the formation potential of disinfection by-products during subsequent chlorination. Chemical Engineering Journal 372, 825-835.

Zhu, Y., Zhao, C., Liang, J., Shang, R., Zhu, X., Ding, L., Deng, H., Zheng, H. and Strathmann, T.J. (2019c) Rapid removal of diclofenac in aqueous solution by soluble Mn(III) (aq) generated in a novel Electro-activated carbon fiber-permanganate (E-ACF-PM) process. Water Research 165, 114975.

Zubot, W., MacKinnon, M.D., Chelme-Ayala, P., Smith, D.W. and Gamal El-Din, M. (2012) Petroleum coke adsorption as a water management option for oil sands process-affected water. Science of the Total Environment 427-428, 364-372.

APPENDIX A

A-1. Calculation of frontier electron densities (FEDs) of 5H-2THCA and DTCA

The frontier electron densities (FEDs) theory is commonly used to evaluate the degradation of organics. Molecular orbital calculations were conducted using the Gaussian 03 program. The hybrid density functional B3LYP method with the 6-31G(d,p) basis set were used. The FEDs of the highest occupied molecular orbital (HOMO) and the lowest unoccupied molecular orbital (LUMO) were obtained from the Gaussian output files. The values of $2FED^2_{HOMO}$ were calculated to predict the initial reaction sites for electrophilic reaction.

The input coordinate of 5H-2THCA is illustrated below:

C	3.04348200	2.25994201	1.52213376
C	3.02492436	1.71946063	0.27454953
C	1.59811191	1.28212732	-0.15197879
C	0.67496066	1.53394296	0.81410112
S	1.39458391	2.47145113	2.13334157
C	4.32087678	2.63129556	2.29799400
O	4.22304312	3.19311119	3.60936419
O	5.45078443	2.44034671	1.77797688
C	-0.79107460	1.06449760	0.76981020
C	-0.88432098	-0.25366656	-0.02097950
C	-2.35035623	-0.72311192	-0.06527042
C	-2.44360261	-2.04127608	-0.85606013
C	-3.90963787	-2.51072144	-0.90035105

C	-4.00288425	-3.82888560	-1.69114076
H	3.89447484	1.59862782	-0.33715415
H	1.36963583	0.82475255	-1.09192932
H	4.97074496	3.77479282	3.76489051
H	-1.39022378	1.81071036	0.29118010
H	-1.14574626	0.90797907	1.76711154
H	-0.28517180	-0.99987932	0.45765060
H	-0.52964931	-0.09714803	-1.01828084
H	-2.94950541	0.02310084	-0.54390053
H	-2.70502790	-0.87963045	0.93203091
H	-1.84445344	-2.78748884	-0.37743002
H	-2.08893095	-1.88475755	-1.85336147
H	-4.50878705	-1.76450868	-1.37898116
H	-4.26430953	-2.66723997	0.09695029
H	-5.02149316	-4.15505868	-1.72191432
H	-3.40373507	-4.57509836	-1.21251065
H	-3.64821258	-3.67236707	-2.68844209

The input coordinate of DTCA is illustrated below:

C	-4.30253069	-0.62189235	0.05872840
C	-3.88567413	0.84197805	-0.18934269
C	-2.57257214	1.16901694	-0.27310130

C	-1.50280625	0.07371875	-0.12233878
C	-1.86533026	-1.20943170	0.14114826
C	-3.35702923	-1.58194139	0.21683074
C	-0.01001316	0.39738075	-0.25950485
C	0.91112119	-0.57214616	-0.34745121
C	0.47681382	-2.03491623	-0.48267355
C	-0.77345979	-2.28127262	0.39827461
S	0.74133053	1.99722377	-0.34379516
C	2.38141734	1.33050941	-0.19067796
C	2.36109181	-0.02783977	-0.30998844
C	3.64994074	2.17014662	0.04902552
O	3.56659198	3.42188814	0.14785216
O	4.92256981	1.52737619	0.15930431
H	-5.33959648	-0.88058452	0.10845682
H	-4.63330184	1.59984746	-0.29698453
H	-2.28165474	2.18395222	-0.44680634
H	-3.64770957	-2.59575817	0.39733137
H	1.25795676	-2.69440861	-0.16678510
H	0.24650718	-2.22170487	-1.51076346
H	-0.49645455	-2.22006408	1.42998271
H	-1.15494430	-3.25765979	0.18371073
H	3.23625285	-0.64144046	-0.35986194
H	5.60868314	2.11962241	-0.15707034

A-2. Calculation of UV fluence of solar simulator

			Reflection Factor	Decadic absorption coefficient	vertical path length	Water Factor	Divergence Factor		Petri Factor	
wavelength/ nm	irradiance/ mW cm^{-2} nm^{-1}	relative spectral irradiance	1-R	a	l	WF	DF	Corrected WF X DF	PF	Correct Factor
201	0.003410804	0.000523595	0.975	2.6567	3.6	0.045408724	0.5625	1.33739E-05	0.9	1.17356E-05
202	0.0089778	0.00137819	0.975	2.6337	3.6	0.045805276	0.5625	3.55097E-05	0.9	3.11598E-05
203	0.010854	0.001666207	0.975	2.6438	3.6	0.045630288	0.5625	4.27666E-05	0.9	3.75277E-05
204	0.00798715	0.001226114	0.975	2.6488	3.6	0.045544154	0.5625	3.14113E-05	0.9	2.75634E-05
205	0.00506475	0.000777494	0.975	2.6279		0.045906372	0.5625	2.00767E-05	0.9	1.76173E-05
206	0.0049381	0.000758052	0.975	2.5952	3.6	0.046484801	0.5625	1.98213E-05	0.9	1.73932E-05
207	0.00680705	0.001044956	0.975	2.5644	3.6	0.047043112	0.5625	2.76514E-05	0.9	2.42641E-05
208	0.00648315	0.000995234	0.975	2.5123	3.6	0.04801869	0.5625	2.68818E-05	0.9	2.35888E-05
209	0.00517805	0.000794887	0.975	2.4435	3.6	0.049370721	0.5625	2.20748E-05	0.9	1.93707E-05
210	0.0040425	0.000620568	0.975	2.3832	3.6	0.050619904	0.5625	1.76699E-05	0.9	1.55053E-05
211	0.00335415	0.000514898	0.975	2.3081	3.6	0.052266954	0.5625	1.51381E-05	0.9	1.32837E-05
212	0.00246005	0.000377644	0.975	2.2183	3.6	0.054382795	0.5625	1.15523E-05	0.9	1.01371E-05
213	0.00189555	0.000290987	0.975	2.1298	3.6	0.056642574	0.5625	9.27128E-06	0.9	8.13555E-06
214	0.002234	0.000342943	0.975	2.0135	3.6	0.059914253	0.5625	1.15578E-05	0.9	1.0142E-05
215	0.0031976	0.000490866	0.975	1.8992	3.6	0.063520081	0.5625	1.75387E-05	0.9	1.53902E-05
216	0.00338815	0.000520118	0.975	1.7827	3.6	0.067671122	0.5625	1.97983E-05	0.9	1.7373E-05

217	0.00338855	0.000520179	0.975	1.6426	3.6	0.07344284	0.5625	2.14894E-05	0.9	1.8857E-05
218	0.00360615	0.000553583	0.975	1.5117	3.6	0.079802157	0.5625	2.48496E-05	0.9	2.18056E-05
219	0.00339165	0.000520655	0.975	1.3853	3.6	0.087083024	0.5625	2.55039E-05	0.9	2.23796E-05
220	0.00255055	0.000391537	0.975	1.2638	3.6	0.095453358	0.5625	2.10226E-05	0.9	1.84473E-05
221	0.00203255	0.000312018	0.975	1.1394	3.6	0.105869593	0.5625	1.85812E-05	0.9	1.6305E-05
222	0.00234355	0.00035976	0.975	1.024	3.6	0.117785664	0.5625	2.38357E-05	0.9	2.09158E-05
223	0.00251105	0.000385473	0.975	0.9217	3.6	0.130822789	0.5625	2.83661E-05	0.9	2.48913E-05
224	0.00219585	0.000337087	0.975	0.8156	3.6	0.147741069	0.5625	2.80134E-05	0.9	2.45817E-05
225	0.0015315	0.000235102	0.975	0.723	3.6	0.166440216	0.5625	2.20109E-05	0.9	1.93145E-05
226	0.0012956	0.000198889	0.975	0.6377	3.6	0.188218205	0.5625	2.10569E-05	0.9	1.84774E-05
227	0.00138705	0.000212927	0.975	0.5536	3.6	0.215699544	0.5625	2.58347E-05	0.9	2.26699E-05
228	0.0014488	0.000222407	0.975	0.4841	3.6	0.244693295	0.5625	3.0612E-05	0.9	2.68621E-05
229	0.00150335	0.000230781	0.975	0.4185	3.6	0.279283165	0.5625	3.62549E-05	0.9	3.18137E-05
230	0.0013238	0.000203218	0.975	0.3704	3.6	0.310581105	0.5625	3.55025E-05	0.9	3.11534E-05
231	0.00094221	0.000144639	0.975	0.3332	3.6	0.339187383	0.5625	2.75962E-05	0.9	2.42156E-05
232	0.000827785	0.000127074	0.975	0.2929	3.6	0.375537389	0.5625	2.68431E-05	0.9	2.35548E-05
233	0.00094838	0.000145587	0.975	0.2558	3.6	0.415023123	0.5625	3.39873E-05	0.9	2.98238E-05
234	0.0011076	0.000170029	0.975	0.2266	3.6	0.451010664	0.5625	4.31352E-05	0.9	3.78511E-05
235	0.00096548	0.000148212	0.975	0.1988	3.6	0.490043186	0.5625	4.08544E-05	0.9	3.58498E-05

236	0.00105345	0.000161716	0.975	0.1778	3.6	0.523093503	0.5625	4.75833E-05	0.9	4.17544E-05
237	0.00111155	0.000170635	0.975	0.1596	3.6	0.55455223	0.5625	5.32271E-05	0.9	4.67068E-05
238	0.000992035	0.000152288	0.975	0.1457	3.6	0.580526166	0.5625	4.97291E-05	0.9	4.36373E-05
239	0.000693275	0.000106425	0.975	0.1322	3.6	0.607515301	0.5625	3.63684E-05	0.9	3.19133E-05
240	0.00049486	7.59664E-05	0.975	0.1221	3.6	0.62892859	0.5625	2.68748E-05	0.9	2.35826E-05
241	0.00055834	8.57112E-05	0.975	0.1139	3.6	0.647131703	0.5625	3.11999E-05	0.9	2.73779E-05
242	0.00060071	9.22155E-05	0.975	0.1066	3.6	0.663985492	0.5625	3.44417E-05	0.9	3.02226E-05
243	0.00068775	0.000105577	0.975	0.1012	3.6	0.676862278	0.5625	4.01969E-05	0.9	3.52728E-05
244	0.000713465	0.000109525	0.975	0.0978	3.6	0.685154349	0.5625	4.22107E-05	0.9	3.70399E-05
245	0.000747495	0.000114749	0.975	0.0948	3.6	0.69259205	0.5625	4.47041E-05	0.9	3.92278E-05
246	0.00066581	0.000102209	0.975	0.092	3.6	0.69963828	0.5625	4.0224E-05	0.9	3.52966E-05
247	0.000636045	9.76398E-05	0.975	0.0893	3.6	0.706529927	0.5625	3.88043E-05	0.9	3.40508E-05
248	0.00061027	9.36831E-05	0.975	0.0873	3.6	0.711697216	0.5625	3.75041E-05	0.9	3.29099E-05
249	0.00054826	8.41639E-05	0.975	0.0862	3.6	0.714562113	0.5625	3.38289E-05	0.9	2.96849E-05
250	0.00054672	8.39274E-05	0.975	0.0853	3.6	0.716918297	0.5625	3.38451E-05	0.9	2.96991E-05
251	0.00061132	9.38442E-05	0.975	0.0842	3.6	0.719813053	0.5625	3.79971E-05	0.9	3.33424E-05
252	0.00064559	9.91051E-05	0.975	0.0831	3.6	0.722724386	0.5625	4.02894E-05	0.9	3.5354E-05
253	0.000646115	9.91857E-05	0.975	0.0823	3.6	0.724852193	0.5625	4.04409E-05	0.9	3.54869E-05
254	0.00067413	0.000103486	0.975	0.0819	3.6	0.725919419	0.5625	4.22565E-05	0.9	3.70801E-05

255	0.00062525	9.59827E-05	0.975	0.0811	3.6	0.728060544	0.5625	3.93082E-05	0.9	3.44929E-05
256	0.000510075	7.8302E-05	0.975	0.0807	3.6	0.729134453	0.5625	3.21147E-05	0.9	2.81806E-05
257	0.00042008	6.44868E-05	0.975	0.0801	3.6	0.730749515	0.5625	2.65071E-05	0.9	2.326E-05
258	0.000422585	6.48714E-05	0.975	0.0795	3.6	0.732369631	0.5625	2.67243E-05	0.9	2.34506E-05
259	0.000385705	5.92099E-05	0.975	0.0791	3.6	0.733452526	0.5625	2.44281E-05	0.9	2.14356E-05
260	0.00039073	5.99813E-05	0.975	0.0786	3.6	0.734809323	0.5625	2.47921E-05	0.9	2.17551E-05
261	0.00041402	6.35566E-05	0.975	0.0782	3.6	0.735897311	0.5625	2.63087E-05	0.9	2.30859E-05
262	0.0004322	6.63474E-05	0.975	0.0779	3.6	0.736714792	0.5625	2.74945E-05	0.9	2.41264E-05
263	0.000384905	5.90871E-05	0.975	0.0775	3.6	0.737806759	0.5625	2.45221E-05	0.9	2.15181E-05
264	0.000344415	5.28714E-05	0.975	0.077	3.6	0.739174927	0.5625	2.19832E-05	0.9	1.92903E-05
265	0.000269185	4.13228E-05	0.975	0.0765	3.6	0.740546671	0.5625	1.72133E-05	0.9	1.51047E-05
266	0.000198085	3.04082E-05	0.975	0.076	3.6	0.741922002	0.5625	1.26903E-05	0.9	1.11357E-05
267	0.000255185	3.91737E-05	0.975	0.0754	3.6	0.743577149	0.5625	1.63849E-05	0.9	1.43777E-05
268	0.000361215	5.54504E-05	0.975	0.0751	3.6	0.744406671	0.5625	2.32187E-05	0.9	2.03744E-05
269	0.00038996	5.98631E-05	0.975	0.0746	3.6	0.745792102	0.5625	2.5113E-05	0.9	2.20367E-05
270	0.000323475	4.96569E-05	0.975	0.074	3.6	0.747459409	0.5625	2.0878E-05	0.9	1.83205E-05
271	0.000318475	4.88894E-05	0.975	0.0733	3.6	0.749411229	0.5625	2.0609E-05	0.9	1.80844E-05
272	0.00036486	5.601E-05	0.975	0.0729	3.6	0.75052977	0.5625	2.36459E-05	0.9	2.07493E-05
273	0.000376285	5.77638E-05	0.975	0.072	3.6	0.753055073	0.5625	2.44684E-05	0.9	2.1471E-05

274	0.000367265	5.63792E-05	0.975	0.0715	3.6	0.754463174	0.5625	2.39265E-05	0.9	2.09955E-05
275	0.000329505	5.05826E-05	0.975	0.0709	3.6	0.756157776	0.5625	2.15147E-05	0.9	1.88792E-05
276	0.00032457	4.9825E-05	0.975	0.0702	3.6	0.758141564	0.5625	2.12481E-05	0.9	1.86452E-05
277	0.000352645	5.41348E-05	0.975	0.0697	3.6	0.759563024	0.5625	2.31293E-05	0.9	2.0296E-05
278	0.000361195	5.54473E-05	0.975	0.0692	3.6	0.76098822	0.5625	2.37346E-05	0.9	2.08271E-05
279	0.000390695	5.99759E-05	0.975	0.0688	3.6	0.762131075	0.5625	2.57116E-05	0.9	2.25619E-05
280	0.000375645	5.76656E-05	0.975	0.0681	3.6	0.764136861	0.5625	2.47862E-05	0.9	2.17499E-05
281	0.00037886	5.81591E-05	0.975	0.0675	3.6	0.76586199	0.5625	2.50548E-05	0.9	2.19856E-05
282	0.000401865	6.16906E-05	0.975	0.0669	3.6	0.767592571	0.5625	2.66362E-05	0.9	2.33733E-05
283	0.00042271	6.48906E-05	0.975	0.0667	3.6	0.768170647	0.5625	2.8039E-05	0.9	2.46042E-05
284	0.00044302	6.80084E-05	0.975	0.0661	3.6	0.769908529	0.5625	2.94526E-05	0.9	2.58447E-05
285	0.000454835	6.98221E-05	0.975	0.0653	3.6	0.772234263	0.5625	3.03294E-05	0.9	2.66141E-05
286	0.00049307	7.56916E-05	0.975	0.0649	3.6	0.77340081	0.5625	3.29287E-05	0.9	2.88949E-05
287	0.000485975	7.46024E-05	0.975	0.0643	3.6	0.775155249	0.5625	3.25285E-05	0.9	2.85438E-05
288	0.00044879	6.88941E-05	0.975	0.0638	3.6	0.776621527	0.5625	3.00964E-05	0.9	2.64096E-05
289	0.00039644	6.08578E-05	0.975	0.0632	3.6	0.778386172	0.5625	2.66461E-05	0.9	2.3382E-05
290	0.00034351	5.27325E-05	0.975	0.0627	3.6	0.779860984	0.5625	2.31323E-05	0.9	2.02986E-05
291	0.00034074	5.23073E-05	0.975	0.0621	3.6	0.781635904	0.5625	2.2998E-05	0.9	2.01807E-05
292	0.000392425	6.02415E-05	0.975	0.0617	3.6	0.782822313	0.5625	2.65266E-05	0.9	2.32771E-05

293	0.00047293	7.25999E-05	0.975	0.0612	3.6	0.784308854	0.5625	3.20292E-05	0.9	2.81056E-05
294	0.000502935	7.7206E-05	0.975	0.0604	3.6	0.786695506	0.5625	3.41649E-05	0.9	2.99797E-05
295	0.00047825	7.34166E-05	0.975	0.0602	3.6	0.787293748	0.5625	3.25127E-05	0.9	2.85299E-05
296	0.000418335	6.4219E-05	0.975	0.0596	3.6	0.789092276	0.5625	2.85045E-05	0.9	2.50127E-05
297	0.000379755	5.82965E-05	0.975	0.0589	3.6	0.791197789	0.5625	2.59448E-05	0.9	2.27666E-05
298	0.000325375	4.99486E-05	0.975	0.0585	3.6	0.792404447	0.5625	2.22635E-05	0.9	1.95362E-05
299	0.00030467	4.67701E-05	0.975	0.0579	3.6	0.794219234	0.5625	2.08945E-05	0.9	1.83349E-05
300	0.00032969	5.0611E-05	0.975	0.0575	3.6	0.795432301	0.5625	2.26449E-05	0.9	1.98709E-05
301	0.000400525	6.14849E-05	0.975	0.0569	3.6	0.797256731	0.5625	2.75733E-05	0.9	2.41956E-05
302	0.000403735	6.19777E-05	0.975	0.0563	3.6	0.799086974	0.5625	2.78581E-05	0.9	2.44455E-05
303	0.00035408	5.43551E-05	0.975	0.0559	3.6	0.800310376	0.5625	2.44693E-05	0.9	2.14718E-05
304	0.00035452	5.44227E-05	0.975	0.0554	3.6	0.801843286	0.5625	2.45466E-05	0.9	2.15397E-05
305	0.000439215	6.74243E-05	0.975	0.0547	3.6	0.803996206	0.5625	3.04925E-05	0.9	2.67572E-05
306	0.000514485	7.8979E-05	0.975	0.0544	3.6	0.804921339	0.5625	3.57592E-05	0.9	3.13787E-05
307	0.000535235	8.21644E-05	0.975	0.0538	3.6	0.806776035	0.5625	3.72871E-05	0.9	3.27195E-05
308	0.0005624	8.63345E-05	0.975	0.0533	3.6	0.808326139	0.5625	3.92549E-05	0.9	3.44461E-05
309	0.000622805	9.56073E-05	0.975	0.0528	3.6	0.809880369	0.5625	4.35547E-05	0.9	3.82192E-05
310	0.000664635	0.000102029	0.975	0.0525	3.6	0.810814894	0.5625	4.65336E-05	0.9	4.08332E-05
311	0.00068305	0.000104856	0.975	0.0519	3.6	0.812688423	0.5625	4.79334E-05	0.9	4.20615E-05

312	0.00071414	0.000109628	0.975	0.0515	3.6	0.813940771	0.5625	5.01924E-05	0.9	4.40438E-05
313	0.00078429	0.000120397	0.975	0.051	3.6	0.815509961	0.5625	5.5229E-05	0.9	4.84635E-05
314	0.000864595	0.000132725	0.975	0.0504	3.6	0.817398513	0.5625	6.1025E-05	0.9	5.35495E-05
315	0.000930455	0.000142835	0.975	0.0501	3.6	0.818345056	0.5625	6.57496E-05	0.9	5.76953E-05
316	0.001022585	0.000156978	0.975	0.0496	3.6	0.819925995	0.5625	7.23995E-05	0.9	6.35306E-05
317	0.00114485	0.000175747	0.975	0.0495	3.6	0.820242688	0.5625	8.10872E-05	0.9	7.11541E-05
318	0.0012917	0.00019829	0.975	0.0491	3.6	0.821511154	0.5625	9.16298E-05	0.9	8.04051E-05
319	0.00145665	0.000223612	0.975	0.0488	3.6	0.82246428	0.5625	0.000103451	0.9	9.07781E-05
320	0.00163985	0.000251735	0.975	0.0483	3.6	0.824056218	0.5625	0.000116687	0.9	0.000102393
321	0.00181625	0.000278814	0.975	0.0478	3.6	0.825652411	0.5625	0.000129489	0.9	0.000113627
322	0.00199475	0.000306216	0.975	0.0477	3.6	0.825972161	0.5625	0.000142271	0.9	0.000124843
323	0.0021262	0.000326395	0.975	0.0471	3.6	0.827894251	0.5625	0.000151999	0.9	0.000133379
324	0.00223965	0.000343811	0.975	0.0468	3.6	0.828857608	0.5625	0.000160296	0.9	0.000140659
325	0.00231645	0.0003556	0.975	0.0463	3.6	0.83046664	0.5625	0.000166114	0.9	0.000145765
326	0.0023877	0.000366538	0.975	0.046	3.6	0.831434125	0.5625	0.000171423	0.9	0.000150424
327	0.00246155	0.000377875	0.975	0.0457	3.6	0.832403163	0.5625	0.000176931	0.9	0.000155257
328	0.0025604	0.000393049	0.975	0.0454	3.6	0.833373756	0.5625	0.000184251	0.9	0.00016168
329	0.0026326	0.000404133	0.975	0.045	3.6	0.834670306	0.5625	0.000189741	0.9	0.000166498
330	0.00263815	0.000404985	0.975	0.0448	3.6	0.835319623	0.5625	0.000190289	0.9	0.000166979

331	0.00263115	0.00040391	0.975	0.0444	3.6	0.836620342	0.5625	0.00019008	0.9	0.000166795
332	0.0026267	0.000403227	0.975	0.0443	3.6	0.836945957	0.5625	0.000189832	0.9	0.000166578
333	0.0026124	0.000401032	0.975	0.044	3.6	0.837923849	0.5625	0.000189019	0.9	0.000165864
334	0.00258725	0.000397171	0.975	0.0439	3.6	0.838250162	0.5625	0.000187272	0.9	0.000164331
335	0.0025694	0.000394431	0.975	0.0436	3.6	0.839230151	0.5625	0.000186198	0.9	0.000163389
336	0.00252545	0.000387684	0.975	0.0434	3.6	0.839884352	0.5625	0.000183155	0.9	0.000160719
337	0.0024401	0.000374582	0.975	0.0433	3.6	0.840211716	0.5625	0.000177035	0.9	0.000155348
338	0.00238755	0.000366515	0.975	0.0432	3.6	0.840539255	0.5625	0.000173289	0.9	0.000152061
339	0.0024786	0.000380492	0.975	0.0429	3.6	0.841522925	0.5625	0.000180108	0.9	0.000158045
340	0.00266995	0.000409866	0.975	0.0427	3.6	0.842179584	0.5625	0.000194164	0.9	0.000170379
341	0.0027583	0.000423429	0.975	0.0424	3.6	0.843165894	0.5625	0.000200824	0.9	0.000176223
342	0.0027446	0.000421326	0.975	0.0426	3.6	0.842508178	0.5625	0.000199671	0.9	0.000175211
343	0.00275175	0.000422423	0.975	0.0424	3.6	0.843165894	0.5625	0.000200347	0.9	0.000175805
344	0.0028123	0.000431719	0.975	0.0422	3.6	0.843824315	0.5625	0.000204916	0.9	0.000179814
345	0.00289425	0.000444299	0.975	0.0421	3.6	0.844153791	0.5625	0.000210969	0.9	0.000185126
346	0.0030862	0.000473765	0.975	0.0419	3.6	0.844813272	0.5625	0.000225137	0.9	0.000197557
347	0.0033748	0.000518068	0.975	0.0418	3.6	0.845143278	0.5625	0.000246286	0.9	0.000216116
348	0.00366165	0.000562103	0.975	0.0416	3.6	0.845803822	0.5625	0.000267429	0.9	0.000234669
349	0.00387625	0.000595046	0.975	0.0414	3.6	0.846465074	0.5625	0.000283323	0.9	0.000248616

350	0.00407475	0.000625518	0.975	0.0413	3.6	0.846795966	0.5625	0.000297949	0.9	0.00026145
351	0.0043408	0.00066636	0.975	0.0413	3.6	0.846795966	0.5625	0.000317402	0.9	0.000278521
352	0.00473245	0.000726482	0.975	0.0412	3.6	0.847127036	0.5625	0.000346175	0.9	0.000303769
353	0.00523925	0.000804282	0.975	0.0412	3.6	0.847127036	0.5625	0.000383247	0.9	0.0003363
354	0.00580625	0.000891322	0.975	0.0411	3.6	0.847458283	0.5625	0.000424889	0.9	0.00037284
355	0.00650085	0.000997951	0.975	0.0409	3.6	0.848121312	0.5625	0.000476091	0.9	0.00041777
356	0.0072504	0.001113015	0.975	0.041	3.6	0.847789709	0.5625	0.000530776	0.9	0.000465756
357	0.0080098	0.001229591	0.975	0.0407	3.6	0.848785053	0.5625	0.000587058	0.9	0.000515143
358	0.00876325	0.001345254	0.975	0.0407	3.6	0.848785053	0.5625	0.00064228	0.9	0.000563601
359	0.00978435	0.001502004	0.975	0.0406	3.6	0.84911719	0.5625	0.0007174	0.9	0.000629518
360	0.0108755	0.001669507	0.975	0.0403	3.6	0.850114673	0.5625	0.000798341	0.9	0.000700544
361	0.012201	0.001872986	0.975	0.0404	3.6	0.849782	0.5625	0.000895292	0.9	0.000785618
362	0.013892	0.002132573	0.975	0.0401	3.6	0.850780555	0.5625	0.001020573	0.9	0.000895552
363	0.0159525	0.002448882	0.975	0.0404	3.6	0.849782	0.5625	0.001170571	0.9	0.001027176
364	0.0180865	0.002776474	0.975	0.0402	3.6	0.850447525	0.5625	0.0013282	0.9	0.001165496
365	0.020071	0.003081116	0.975	0.0401	3.6	0.850780555	0.5625	0.001474511	0.9	0.001293884
366	0.02214	0.00339873	0.975	0.0398	3.6	0.85178072	0.5625	0.001628422	0.9	0.00142894
367	0.024285	0.003728011	0.975	0.0397	3.6	0.852114466	0.5625	0.001786889	0.9	0.001567995
368	0.0266125	0.004085307	0.975	0.0399	3.6	0.851447153	0.5625	0.001956613	0.9	0.001716928

369	0.0289635	0.004446211	0.975	0.0395	3.6	0.852782497	0.5625	0.002132804	0.9	0.001871535
370	0.031195	0.004788771	0.975	0.0396	3.6	0.852448392	0.5625	0.002296226	0.9	0.002014938
371	0.033073	0.005077064	0.975	0.0396	3.6	0.852448392	0.5625	0.002434463	0.9	0.002136242
372	0.0343525	0.005273481	0.975	0.0395	3.6	0.852782497	0.5625	0.002529637	0.9	0.002219756
373	0.0349815	0.005370039	0.975	0.0395	3.6	0.852782497	0.5625	0.002575955	0.9	0.002260401
374	0.035392	0.005433056	0.975	0.0394	3.6	0.853116782	0.5625	0.002607205	0.9	0.002287822
375	0.036333	0.005577509	0.975	0.0391	3.6	0.854120715	0.5625	0.002679675	0.9	0.002351415
376	0.036786	0.00564705	0.975	0.039	3.6	0.854455719	0.5625	0.002714149	0.9	0.002381666
377	0.036316	0.0055749	0.975	0.0392	3.6	0.853785891	0.5625	0.002677371	0.9	0.002349393
378	0.0355955	0.005464295	0.975	0.0393	3.6	0.853451247	0.5625	0.002623224	0.9	0.002301879
379	0.0354775	0.005446181	0.975	0.039	3.6	0.854455719	0.5625	0.002617605	0.9	0.002296949
380	0.0353055	0.005419777	0.975	0.039	3.6	0.854455719	0.5625	0.002604915	0.9	0.002285813
381	0.0350785	0.00538493	0.975	0.0389	3.6	0.854790903	0.5625	0.002589181	0.9	0.002272007
382	0.035	0.005372879	0.975	0.0388	3.6	0.855126267	0.5625	0.002584401	0.9	0.002267812
383	0.034875	0.005353691	0.975	0.0389	3.6	0.854790903	0.5625	0.002574161	0.9	0.002258826
384	0.034597	0.005311014	0.975	0.0387	3.6	0.855461812	0.5625	0.002555646	0.9	0.002242579
385	0.034279	0.005262198	0.975	0.0386	3.6	0.855797537	0.5625	0.002533149	0.9	0.002222838
386	0.0343215	0.005268722	0.975	0.0386	3.6	0.855797537	0.5625	0.00253629	0.9	0.002225594
387	0.034933	0.005362594	0.975	0.0386	3.6	0.855797537	0.5625	0.002581478	0.9	0.002265247

388	0.0357095	0.005481795	0.975	0.0386	3.6	0.855797537	0.5625	0.00263886	0.9	0.0023156
389	0.036326	0.005576435	0.975	0.0385	3.6	0.856133443	0.5625	0.002685472	0.9	0.002356502
390	0.0365785	0.005615196	0.975	0.0382	3.6	0.857142243	0.5625	0.002707325	0.9	0.002375678
391	0.0368835	0.005662017	0.975	0.0384	3.6	0.856469529	0.5625	0.002727757	0.9	0.002393606
392	0.0371485	0.005702697	0.975	0.0385	3.6	0.856133443	0.5625	0.002746277	0.9	0.002409858
393	0.0376005	0.005772084	0.975	0.0382	3.6	0.857142243	0.5625	0.002782967	0.9	0.002442054
394	0.038357	0.005888215	0.975	0.0382	3.6	0.857142243	0.5625	0.002838959	0.9	0.002491186
395	0.039265	0.006027603	0.975	0.0384	3.6	0.856469529	0.5625	0.002903883	0.9	0.002548157
396	0.0403475	0.006193779	0.975	0.0383	3.6	0.856805796	0.5625	0.002985112	0.9	0.002619436
397	0.0409905	0.006292486	0.975	0.0383	3.6	0.856805796	0.5625	0.003032684	0.9	0.00266118
398	0.0414765	0.006367092	0.975	0.0381	3.6	0.857478872	0.5625	0.003071052	0.9	0.002694848
399	0.0416215	0.006389351	0.975	0.0381	3.6	0.857478872	0.5625	0.003081788	0.9	0.002704269
400	0.041368	0.006350436	0.975	0.0381	3.6	0.857478872	0.5625	0.003063018	0.9	0.002687798
401	0.041174	0.006320655	0.975	0.0381	3.6	0.857478872	0.5625	0.003048653	0.9	0.002675193
402	0.0411625	0.00631889	0.975	0.0381	3.6	0.857478872	0.5625	0.003047802	0.9	0.002674446
403	0.041053	0.00630208	0.975	0.0381	3.6	0.857478872	0.5625	0.003039694	0.9	0.002667332
404	0.0410185	0.006296784	0.975	0.0381	3.6	0.857478872	0.5625	0.00303714	0.9	0.00266509
405	0.0411125	0.006311214	0.975	0.0381	3.6	0.857478872	0.5625	0.0030441	0.9	0.002671198
406	0.0411895	0.006323035	0.975	0.0381	3.6	0.857478872	0.5625	0.003049801	0.9	0.0026762

407	0.0412345	0.006329943	0.975	0.0381	3.6	0.857478872	0.5625	0.003053133	0.9	0.002679124
408	0.041415	0.006357651	0.975	0.0381	3.6	0.857478872	0.5625	0.003066498	0.9	0.002690852
409	0.041864	0.006426578	0.975	0.0381	3.6	0.857478872	0.5625	0.003099743	0.9	0.002720025
410	0.042182	0.006475394	0.975	0.0381	3.6	0.857478872	0.5625	0.003123289	0.9	0.002740686
411	0.042315	0.006495811	0.975	0.0381	3.6	0.857478872	0.5625	0.003133137	0.9	0.002749327
412	0.0421295	0.006467335	0.975	0.0381	3.6	0.857478872	0.5625	0.003119402	0.9	0.002737275
413	0.0418805	0.006429111	0.975	0.0381	3.6	0.857478872	0.5625	0.003100965	0.9	0.002721097
414	0.041628	0.006390349	0.975	0.0381	3.6	0.857478872	0.5625	0.003082269	0.9	0.002704691
415	0.0419215	0.006435405	0.975	0.0381	3.6	0.857478872	0.5625	0.003104001	0.9	0.002723761
416	0.042054	0.006455745	0.975	0.0381	3.6	0.857478872	0.5625	0.003113811	0.9	0.00273237
417	0.041991	0.006446074	0.975	0.0381	3.6	0.857478872	0.5625	0.003109147	0.9	0.002728276
418	0.042215	0.00648046	0.975	0.0381	3.6	0.857478872	0.5625	0.003125732	0.9	0.00274283
419	0.0428465	0.006577402	0.975	0.0381	3.6	0.857478872	0.5625	0.003172491	0.9	0.002783861
420	0.0430845	0.006613938	0.975	0.0381	3.6	0.857478872	0.5625	0.003190113	0.9	0.002799324
421	0.042578	0.006536184	0.975	0.0381	3.6	0.857478872	0.5625	0.00315261	0.9	0.002766415
422	0.042028	0.006451754	0.975	0.0381	3.6	0.857478872	0.5625	0.003111886	0.9	0.00273068
423	0.041859	0.00642581	0.975	0.0381	3.6	0.857478872	0.5625	0.003099373	0.9	0.0027197
424	0.041885	0.006429801	0.975	0.0381	3.6	0.857478872	0.5625	0.003101298	0.9	0.002721389
425	0.041875	0.006428266	0.975	0.0381	3.6	0.857478872	0.5625	0.003100558	0.9	0.002720739

426	0.041795	0.006415986	0.975	0.0381	3.6	0.857478872	0.5625	0.003094634	0.9	0.002715542
427	0.041812	0.006418595	0.975	0.0381	3.6	0.857478872	0.5625	0.003095893	0.9	0.002716646
428	0.041966	0.006442236	0.975	0.0381	3.6	0.857478872	0.5625	0.003107296	0.9	0.002726652
429	0.0418975	0.00643172	0.975	0.0381	3.6	0.857478872	0.5625	0.003102224	0.9	0.002722201
430	0.0418615	0.006426194	0.975	0.0381	3.6	0.857478872	0.5625	0.003099558	0.9	0.002719862
431	0.041818	0.006419516	0.975	0.0381	3.6	0.857478872	0.5625	0.003096337	0.9	0.002717036
432	0.041883	0.006429494	0.975	0.0381	3.6	0.857478872	0.5625	0.00310115	0.9	0.002721259
433	0.041917	0.006434714	0.975	0.0381	3.6	0.857478872	0.5625	0.003103668	0.9	0.002723468
434	0.042215	0.00648046	0.975	0.0381	3.6	0.857478872	0.5625	0.003125732	0.9	0.00274283
435	0.0428175	0.00657295	0.975	0.0381	3.6	0.857478872	0.5625	0.003170343	0.9	0.002781976
436	0.0434045	0.006663061	0.975	0.0381	3.6	0.857478872	0.5625	0.003213807	0.9	0.002820115
437	0.0441125	0.006771747	0.975	0.0381	3.6	0.857478872	0.5625	0.003266229	0.9	0.002866116
438	0.044882	0.006889873	0.975	0.0381	3.6	0.857478872	0.5625	0.003323206	0.9	0.002916113
439	0.045337	0.006959721	0.975	0.0381	3.6	0.857478872	0.5625	0.003356895	0.9	0.002945676
440	0.04512	0.006926409	0.975	0.0381	3.6	0.857478872	0.5625	0.003340828	0.9	0.002931576
441	0.0449125	0.006894556	0.975	0.0381	3.6	0.857478872	0.5625	0.003325464	0.9	0.002918095
442	0.0450545	0.006916354	0.975	0.0381	3.6	0.857478872	0.5625	0.003335978	0.9	0.002927321
443	0.045244	0.006945444	0.975	0.0381	3.6	0.857478872	0.5625	0.003350009	0.9	0.002939633
444	0.045312	0.006955883	0.975	0.0381	3.6	0.857478872	0.5625	0.003355044	0.9	0.002944051

445	0.045453	0.006977528	0.975	0.0381	3.6	0.857478872	0.5625	0.003365484	0.9	0.002953212
446	0.045823	0.007034327	0.975	0.0381	3.6	0.857478872	0.5625	0.00339288	0.9	0.002977252
447	0.046262	0.007101718	0.975	0.0381	3.6	0.857478872	0.5625	0.003425385	0.9	0.003005775
448	0.0472655	0.007255767	0.975	0.0381	3.6	0.857478872	0.5625	0.003499687	0.9	0.003070976
449	0.049837	0.00765052	0.975	0.0381	3.6	0.857478872	0.5625	0.003690089	0.9	0.003238053
450	0.0525285	0.008063694	0.975	0.0381	3.6	0.857478872	0.5625	0.003889377	0.9	0.003412928
451	0.0532105	0.008168388	0.975	0.0381	3.6	0.857478872	0.5625	0.003939874	0.9	0.003457239
452	0.0523935	0.00804297	0.975	0.0381	3.6	0.857478872	0.5625	0.003879381	0.9	0.003404157
453	0.0514575	0.007899284	0.975	0.0381	3.6	0.857478872	0.5625	0.003810076	0.9	0.003343342
454	0.050293	0.007720521	0.975	0.0381	3.6	0.857478872	0.5625	0.003723853	0.9	0.003267681
455	0.0495885	0.007612372	0.975	0.0381	3.6	0.857478872	0.5625	0.00367169	0.9	0.003221908
456	0.0500815	0.007688053	0.975	0.0381	3.6	0.857478872	0.5625	0.003708193	0.9	0.003253939
457	0.051474	0.007901817	0.975	0.0381	3.6	0.857478872	0.5625	0.003811298	0.9	0.003344414
458	0.052385	0.008041665	0.975	0.0381	3.6	0.857478872	0.5625	0.003878751	0.9	0.003403604
459	0.052515	0.008061622	0.975	0.0381	3.6	0.857478872	0.5625	0.003888377	0.9	0.003412051
460	0.0527685	0.008100537	0.975	0.0381	3.6	0.857478872	0.5625	0.003907147	0.9	0.003428521
461	0.0545005	0.008366417	0.975	0.0381	3.6	0.857478872	0.5625	0.00403539	0.9	0.003541055
462	0.0575385	0.008832783	0.975	0.0381	3.6	0.857478872	0.5625	0.004260333	0.9	0.003738442
463	0.05963	0.009153851	0.975	0.0381	3.6	0.857478872	0.5625	0.004415194	0.9	0.003874333

464	0.0593865	0.009116471	0.975	0.0381	3.6	0.857478872	0.5625	0.004397165	0.9	0.003858512
465	0.05865	0.009003411	0.975	0.0381	3.6	0.857478872	0.5625	0.004342632	0.9	0.003810659
466	0.0614665	0.009435774	0.975	0.0381	3.6	0.857478872	0.5625	0.004551174	0.9	0.003993656
467	0.0675495	0.01036958	0.975	0.0381	3.6	0.857478872	0.5625	0.005001579	0.9	0.004388886
468	0.0712125	0.010931891	0.975	0.0381	3.6	0.857478872	0.5625	0.005272799	0.9	0.004626881
469	0.069046	0.010599309	0.975	0.0381	3.6	0.857478872	0.5625	0.005112385	0.9	0.004486118
470	0.064268	0.009865835	0.975	0.0381	3.6	0.857478872	0.5625	0.004758606	0.9	0.004175677
471	0.0604365	0.009277658	0.975	0.0381	3.6	0.857478872	0.5625	0.00447491	0.9	0.003926734
472	0.059605	0.009150014	0.975	0.0381	3.6	0.857478872	0.5625	0.004413343	0.9	0.003872709
473	0.060345	0.009263612	0.975	0.0381	3.6	0.857478872	0.5625	0.004468135	0.9	0.003920789
474	0.058975	0.009053302	0.975	0.0381	3.6	0.857478872	0.5625	0.004366696	0.9	0.003831776
475	0.0549935	0.008442098	0.975	0.0381	3.6	0.857478872	0.5625	0.004071893	0.9	0.003573086
476	0.0516965	0.007935973	0.975	0.0381	3.6	0.857478872	0.5625	0.003827773	0.9	0.003358871
477	0.0500515	0.007683448	0.975	0.0381	3.6	0.857478872	0.5625	0.003705972	0.9	0.00325199
478	0.049766	0.00763962	0.975	0.0381	3.6	0.857478872	0.5625	0.003684832	0.9	0.00323344
479	0.050997	0.007828592	0.975	0.0381	3.6	0.857478872	0.5625	0.00377598	0.9	0.003313422
480	0.05369	0.008241997	0.975	0.0381	3.6	0.857478872	0.5625	0.003975378	0.9	0.003488394
481	0.0561185	0.008614798	0.975	0.0381	3.6	0.857478872	0.5625	0.004155192	0.9	0.003646181
482	0.056901	0.00873492	0.975	0.0381	3.6	0.857478872	0.5625	0.00421313	0.9	0.003697022

483	0.056197	0.008626849	0.975	0.0381	3.6	0.857478872	0.5625	0.004161004	0.9	0.003651281
484	0.0546605	0.008390979	0.975	0.0381	3.6	0.857478872	0.5625	0.004047237	0.9	0.00355145
485	0.0527465	0.008097159	0.975	0.0381	3.6	0.857478872	0.5625	0.003905518	0.9	0.003427092
486	0.0509925	0.007827901	0.975	0.0381	3.6	0.857478872	0.5625	0.003775646	0.9	0.00331313
487	0.049938	0.007666024	0.975	0.0381	3.6	0.857478872	0.5625	0.003697568	0.9	0.003244616
488	0.0494675	0.007593797	0.975	0.0381	3.6	0.857478872	0.5625	0.00366273	0.9	0.003214046
489	0.04936	0.007577295	0.975	0.0381	3.6	0.857478872	0.5625	0.003654771	0.9	0.003207061
490	0.0503485	0.00772904	0.975	0.0381	3.6	0.857478872	0.5625	0.003727963	0.9	0.003271287
491	0.0530375	0.008141831	0.975	0.0381	3.6	0.857478872	0.5625	0.003927065	0.9	0.003445999
492	0.055453	0.008512637	0.975	0.0381	3.6	0.857478872	0.5625	0.004105916	0.9	0.003602941
493	0.0553315	0.008493985	0.975	0.0381	3.6	0.857478872	0.5625	0.00409692	0.9	0.003595047
494	0.053162	0.008160943	0.975	0.0381	3.6	0.857478872	0.5625	0.003936283	0.9	0.003454088
495	0.051007	0.007830127	0.975	0.0381	3.6	0.857478872	0.5625	0.00377672	0.9	0.003314072
496	0.049744	0.007636243	0.975	0.0381	3.6	0.857478872	0.5625	0.003683203	0.9	0.003232011
497	0.049098	0.007537075	0.975	0.0381	3.6	0.857478872	0.5625	0.003635372	0.9	0.003190039
498	0.048847	0.007498544	0.975	0.0381	3.6	0.857478872	0.5625	0.003616787	0.9	0.00317373
499	0.0486825	0.007473291	0.975	0.0381	3.6	0.857478872	0.5625	0.003604607	0.9	0.003163042
500	0.048621	0.00746385	0.975	0.0381	3.6	0.857478872	0.5625	0.003600053	0.9	0.003159046
501	0.0532105	0.002689288	0.975	0.0302	3.6	0.884653979	0.5625	0.001338238	0.9	0.001174304

502	0.0532105	0.002689288	0.975	0.0302	3.6	0.884653979	0.5625	0.001338238	0.9	0.001174304
503	0.0523935	0.002647997	0.975	0.0302	3.6	0.884653979	0.5625	0.00131769	0.9	0.001156273
504	0.0523935	0.002647997	0.975	0.0302	3.6	0.884653979	0.5625	0.00131769	0.9	0.001156273
505	0.0514575	0.002600691	0.975	0.0235	3.6	0.908628696	0.5625	0.001329223	0.9	0.001166393
506	0.0514575	0.002600691	0.975	0.0235	3.6	0.908628696	0.5625	0.001329223	0.9	0.001166393
507	0.050293	0.002541836	0.975	0.0235	3.6	0.908628696	0.5625	0.001299142	0.9	0.001139997
508	0.050293	0.002541836	0.975	0.0235	3.6	0.908628696	0.5625	0.001299142	0.9	0.001139997
509	0.0495885	0.00250623	0.975	0.0235	3.6	0.908628696	0.5625	0.001280944	0.9	0.001124028
510	0.0495885	0.00250623	0.975	0.0235	3.6	0.908628696	0.5625	0.001280944	0.9	0.001124028
511	0.0500815	0.002531147	0.975	0.0235	3.6	0.908628696	0.5625	0.001293678	0.9	0.001135203
512	0.0500815	0.002531147	0.975	0.0235	3.6	0.908628696	0.5625	0.001293678	0.9	0.001135203
513	0.051474	0.002601525	0.975	0.0235	3.6	0.908628696	0.5625	0.001329649	0.9	0.001166767
514	0.051474	0.002601525	0.975	0.0235	3.6	0.908628696	0.5625	0.001329649	0.9	0.001166767
515	0.052385	0.002647567	0.975	0.0235	3.6	0.908628696	0.5625	0.001353181	0.9	0.001187416
516	0.052385	0.002647567	0.975	0.0235	3.6	0.908628696	0.5625	0.001353181	0.9	0.001187416
517	0.052515	0.002654137	0.975	0.0235	3.6	0.908628696	0.5625	0.001356539	0.9	0.001190363
518	0.052515	0.002654137	0.975	0.0235	3.6	0.908628696	0.5625	0.001356539	0.9	0.001190363
519	0.0527685	0.002666949	0.975	0.0235	3.6	0.908628696	0.5625	0.001363088	0.9	0.001196109
520	0.0527685	0.002666949	0.975	0.0235	3.6	0.908628696	0.5625	0.001363088	0.9	0.001196109

521	0.0545005	0.002754486	0.975	0.0235	3.6	0.908628696	0.5625	0.001407828	0.9	0.001235369
522	0.0545005	0.002754486	0.975	0.0235	3.6	0.908628696	0.5625	0.001407828	0.9	0.001235369
523	0.0575385	0.002908028	0.975	0.0235	3.6	0.908628696	0.5625	0.001486304	0.9	0.001304231
524	0.0575385	0.002908028	0.975	0.0235	3.6	0.908628696	0.5625	0.001486304	0.9	0.001304231
525	0.05963	0.003013733	0.975	0.0235	3.6	0.908628696	0.5625	0.00154033	0.9	0.00135164
526	0.05963	0.003013733	0.975	0.0235	3.6	0.908628696	0.5625	0.00154033	0.9	0.00135164
527	0.0593865	0.003001427	0.975	0.0235	3.6	0.908628696	0.5625	0.00153404	0.9	0.00134612
528	0.0593865	0.003001427	0.975	0.0235	3.6	0.908628696	0.5625	0.00153404	0.9	0.00134612
529	0.05865	0.002964204	0.975	0.0235	3.6	0.908628696	0.5625	0.001515015	0.9	0.001329426
530	0.05865	0.002964204	0.975	0.0235	3.6	0.908628696	0.5625	0.001515015	0.9	0.001329426
531	0.0614665	0.003106551	0.975	0.0235	3.6	0.908628696	0.5625	0.00158777	0.9	0.001393268
532	0.0614665	0.003106551	0.975	0.0235	3.6	0.908628696	0.5625	0.00158777	0.9	0.001393268
533	0.0675495	0.003413989	0.975	0.0235	3.6	0.908628696	0.5625	0.001744902	0.9	0.001531152
534	0.0675495	0.003413989	0.975	0.0235	3.6	0.908628696	0.5625	0.001744902	0.9	0.001531152
535	0.0712125	0.003599119	0.975	0.0235	3.6	0.908628696	0.5625	0.001839523	0.9	0.001614181
536	0.0712125	0.003599119	0.975	0.0235	3.6	0.908628696	0.5625	0.001839523	0.9	0.001614181
537	0.069046	0.003489623	0.975	0.0235	3.6	0.908628696	0.5625	0.001783559	0.9	0.001565073
538	0.069046	0.003489623	0.975	0.0235	3.6	0.908628696	0.5625	0.001783559	0.9	0.001565073
539	0.064268	0.003248141	0.975	0.0235	3.6	0.908628696	0.5625	0.001660136	0.9	0.00145677

540	0.064268	0.003248141	0.975	0.0235	3.6	0.908628696	0.5625	0.001660136	0.9	0.00145677
541	0.0604365	0.003054494	0.975	0.0235	3.6	0.908628696	0.5625	0.001561163	0.9	0.001369921
542	0.0604365	0.003054494	0.975	0.0235	3.6	0.908628696	0.5625	0.001561163	0.9	0.001369921
543	0.059605	0.00301247	0.975	0.0235	3.6	0.908628696	0.5625	0.001539684	0.9	0.001351073
544	0.059605	0.00301247	0.975	0.0235	3.6	0.908628696	0.5625	0.001539684	0.9	0.001351073
545	0.060345	0.00304987	0.975	0.0235	3.6	0.908628696	0.5625	0.0015588	0.9	0.001367847
546	0.060345	0.00304987	0.975	0.0235	3.6	0.908628696	0.5625	0.0015588	0.9	0.001367847
547	0.058975	0.002980629	0.975	0.0235	3.6	0.908628696	0.5625	0.001523411	0.9	0.001336793
548	0.058975	0.002980629	0.975	0.0235	3.6	0.908628696	0.5625	0.001523411	0.9	0.001336793
549	0.0549935	0.002779402	0.975	0.0235	3.6	0.908628696	0.5625	0.001420563	0.9	0.001246544
550	0.0549935	0.002779402	0.975	0.0235	3.6	0.908628696	0.5625	0.001420563	0.9	0.001246544
551	0.0516965	0.00261277	0.975	0.0235	3.6	0.908628696	0.5625	0.001335396	0.9	0.00117181
552	0.0516965	0.00261277	0.975	0.0235	3.6	0.908628696	0.5625	0.001335396	0.9	0.00117181
553	0.0500515	0.002529631	0.975	0.0235	3.6	0.908628696	0.5625	0.001292903	0.9	0.001134523
554	0.0500515	0.002529631	0.975	0.0235	3.6	0.908628696	0.5625	0.001292903	0.9	0.001134523
555	0.049766	0.002515201	0.975	0.0235	3.6	0.908628696	0.5625	0.001285529	0.9	0.001128051
556	0.049766	0.002515201	0.975	0.0235	3.6	0.908628696	0.5625	0.001285529	0.9	0.001128051
557	0.050997	0.002577417	0.975	0.0235	3.6	0.908628696	0.5625	0.001317327	0.9	0.001155955
558	0.050997	0.002577417	0.975	0.0235	3.6	0.908628696	0.5625	0.001317327	0.9	0.001155955

559	0.05369	0.002713523	0.975	0.0235	3.6	0.908628696	0.5625	0.001386891	0.9	0.001216997
560	0.05369	0.002713523	0.975	0.0235	3.6	0.908628696	0.5625	0.001386891	0.9	0.001216997
561	0.0561185	0.00283626	0.975	0.0235	3.6	0.908628696	0.5625	0.001449623	0.9	0.001272044
562	0.0561185	0.00283626	0.975	0.0235	3.6	0.908628696	0.5625	0.001449623	0.9	0.001272044
563	0.056901	0.002875808	0.975	0.0235	3.6	0.908628696	0.5625	0.001469836	0.9	0.001289781
564	0.056901	0.002875808	0.975	0.0235	3.6	0.908628696	0.5625	0.001469836	0.9	0.001289781
565	0.056197	0.002840228	0.975	0.0235	3.6	0.908628696	0.5625	0.001451651	0.9	0.001273824
566	0.056197	0.002840228	0.975	0.0235	3.6	0.908628696	0.5625	0.001451651	0.9	0.001273824
567	0.0546605	0.002762572	0.975	0.0235	3.6	0.908628696	0.5625	0.001411961	0.9	0.001238996
568	0.0546605	0.002762572	0.975	0.0235	3.6	0.908628696	0.5625	0.001411961	0.9	0.001238996
569	0.0527465	0.002665838	0.975	0.0235	3.6	0.908628696	0.5625	0.001362519	0.9	0.001195611
570	0.0527465	0.002665838	0.975	0.0235	3.6	0.908628696	0.5625	0.001362519	0.9	0.001195611
571	0.0509925	0.002577189	0.975	0.0235	3.6	0.908628696	0.5625	0.001317211	0.9	0.001155853
572	0.0509925	0.002577189	0.975	0.0235	3.6	0.908628696	0.5625	0.001317211	0.9	0.001155853
573	0.049938	0.002523894	0.975	0.0235	3.6	0.908628696	0.5625	0.001289972	0.9	0.00113195
574	0.049938	0.002523894	0.975	0.0235	3.6	0.908628696	0.5625	0.001289972	0.9	0.00113195
575	0.0494675	0.002500115	0.975	0.0235	3.6	0.908628696	0.5625	0.001277818	0.9	0.001121285
576	0.0494675	0.002500115	0.975	0.0235	3.6	0.908628696	0.5625	0.001277818	0.9	0.001121285
577	0.04936	0.002494682	0.975	0.0235	3.6	0.908628696	0.5625	0.001275041	0.9	0.001118848

578	0.04936	0.002494682	0.975	0.0235	3.6	0.908628696	0.5625	0.001275041	0.9	0.001118848
579	0.0503485	0.002544641	0.975	0.0235	3.6	0.908628696	0.5625	0.001300575	0.9	0.001141255
580	0.0503485	0.002544641	0.975	0.0235	3.6	0.908628696	0.5625	0.001300575	0.9	0.001141255
581	0.0530375	0.002680545	0.975	0.0235	3.6	0.908628696	0.5625	0.001370036	0.9	0.001202207
582	0.0530375	0.002680545	0.975	0.0235	3.6	0.908628696	0.5625	0.001370036	0.9	0.001202207
583	0.055453	0.002802626	0.975	0.0235	3.6	0.908628696	0.5625	0.001432432	0.9	0.001256959
584	0.055453	0.002802626	0.975	0.0235	3.6	0.908628696	0.5625	0.001432432	0.9	0.001256959
585	0.0553315	0.002796485	0.975	0.0235	3.6	0.908628696	0.5625	0.001429294	0.9	0.001254205
586	0.0553315	0.002796485	0.975	0.0235	3.6	0.908628696	0.5625	0.001429294	0.9	0.001254205
587	0.053162	0.002686837	0.975	0.0235	3.6	0.908628696	0.5625	0.001373252	0.9	0.001205029
588	0.053162	0.002686837	0.975	0.0235	3.6	0.908628696	0.5625	0.001373252	0.9	0.001205029
589	0.051007	0.002577922	0.975	0.0235	3.6	0.908628696	0.5625	0.001317585	0.9	0.001156181
590	0.051007	0.002577922	0.975	0.0235	3.6	0.908628696	0.5625	0.001317585	0.9	0.001156181
591	0.049744	0.00251409	0.975	0.0235	3.6	0.908628696	0.5625	0.00128496	0.9	0.001127553
592	0.049744	0.00251409	0.975	0.0235	3.6	0.908628696	0.5625	0.00128496	0.9	0.001127553
593	0.049098	0.00248144	0.975	0.0235	3.6	0.908628696	0.5625	0.001268273	0.9	0.00111291
594	0.049098	0.00248144	0.975	0.0235	3.6	0.908628696	0.5625	0.001268273	0.9	0.00111291
595	0.048847	0.002468755	0.975	0.0235	3.6	0.908628696	0.5625	0.001261789	0.9	0.00110722
596	0.048847	0.002468755	0.975	0.0235	3.6	0.908628696	0.5625	0.001261789	0.9	0.00110722

597	0.0486825	0.002460441	0.975	0.0235	3.6	0.908628696	0.5625	0.00125754	0.9	0.001103492
598	0.0486825	0.002460441	0.975	0.0235	3.6	0.908628696	0.5625	0.00125754	0.9	0.001103492
599	0.048598	0.00245617	0.975	0.0235	3.6	0.908628696	0.5625	0.001255357	0.9	0.001101576
600	0.048598	0.00245617	0.975	0.0235	3.6	0.908628696	0.5625	0.001255357	0.9	0.001101576
601	0.0485735	0.002454932	0.975	0.0235	3.6	0.908628696	0.5625	0.001254725	0.9	0.001101021
602	0.0485735	0.002454932	0.975	0.0235	3.6	0.908628696	0.5625	0.001254725	0.9	0.001101021
603	0.048731	0.002462892	0.975	0.0235	3.6	0.908628696	0.5625	0.001258793	0.9	0.001104591
604	0.048731	0.002462892	0.975	0.0235	3.6	0.908628696	0.5625	0.001258793	0.9	0.001104591
605	0.0488665	0.00246974	0.975	0.0235	3.6	0.908628696	0.5625	0.001262293	0.9	0.001107662
606	0.0488665	0.00246974	0.975	0.0235	3.6	0.908628696	0.5625	0.001262293	0.9	0.001107662
607	0.048968	0.00247487	0.975	0.0235	3.6	0.908628696	0.5625	0.001264915	0.9	0.001109963
608	0.048968	0.00247487	0.975	0.0235	3.6	0.908628696	0.5625	0.001264915	0.9	0.001109963
609	0.048994	0.002476184	0.975	0.0235	3.6	0.908628696	0.5625	0.001265587	0.9	0.001110552
610	0.048994	0.002476184	0.975	0.0235	3.6	0.908628696	0.5625	0.001265587	0.9	0.001110552
611	0.048972	0.002475072	0.975	0.0235	3.6	0.908628696	0.5625	0.001265018	0.9	0.001110054
612	0.048972	0.002475072	0.975	0.0235	3.6	0.908628696	0.5625	0.001265018	0.9	0.001110054
613	0.048857	0.00246926	0.975	0.0235	3.6	0.908628696	0.5625	0.001262048	0.9	0.001107447
614	0.048857	0.00246926	0.975	0.0235	3.6	0.908628696	0.5625	0.001262048	0.9	0.001107447
615	0.048816	0.002467188	0.975	0.0235	3.6	0.908628696	0.5625	0.001260989	0.9	0.001106518

616	0.048816	0.002467188	0.975	0.0235	3.6	0.908628696	0.5625	0.001260989	0.9	0.001106518
617	0.048887	0.002470776	0.975	0.0235	3.6	0.908628696	0.5625	0.001262823	0.9	0.001108127
618	0.048887	0.002470776	0.975	0.0235	3.6	0.908628696	0.5625	0.001262823	0.9	0.001108127
619	0.0490245	0.002477726	0.975	0.0235	3.6	0.908628696	0.5625	0.001266375	0.9	0.001111244
620	0.0490245	0.002477726	0.975	0.0235	3.6	0.908628696	0.5625	0.001266375	0.9	0.001111244
621	0.049246	0.00248892	0.975	0.0235	3.6	0.908628696	0.5625	0.001272096	0.9	0.001116264
622	0.049246	0.00248892	0.975	0.0235	3.6	0.908628696	0.5625	0.001272096	0.9	0.001116264
623	0.0495595	0.002504765	0.975	0.0235	3.6	0.908628696	0.5625	0.001280194	0.9	0.001123371
624	0.0495595	0.002504765	0.975	0.0235	3.6	0.908628696	0.5625	0.001280194	0.9	0.001123371
625	0.0498945	0.002521696	0.975	0.0235	3.6	0.908628696	0.5625	0.001288848	0.9	0.001130964
626	0.0498945	0.002521696	0.975	0.0235	3.6	0.908628696	0.5625	0.001288848	0.9	0.001130964
627	0.0499435	0.002524172	0.975	0.0235	3.6	0.908628696	0.5625	0.001290114	0.9	0.001132075
628	0.0499435	0.002524172	0.975	0.0235	3.6	0.908628696	0.5625	0.001290114	0.9	0.001132075
629	0.049804	0.002517122	0.975	0.0235	3.6	0.908628696	0.5625	0.00128651	0.9	0.001128913
630	0.049804	0.002517122	0.975	0.0235	3.6	0.908628696	0.5625	0.00128651	0.9	0.001128913
631	0.049792	0.002516515	0.975	0.0235	3.6	0.908628696	0.5625	0.0012862	0.9	0.001128641
632	0.049792	0.002516515	0.975	0.0235	3.6	0.908628696	0.5625	0.0012862	0.9	0.001128641
633	0.049887	0.002521317	0.975	0.0235	3.6	0.908628696	0.5625	0.001288654	0.9	0.001130794
634	0.049887	0.002521317	0.975	0.0235	3.6	0.908628696	0.5625	0.001288654	0.9	0.001130794

635	0.0498935	0.002521645	0.975	0.0235	3.6	0.908628696	0.5625	0.001288822	0.9	0.001130941
636	0.0498935	0.002521645	0.975	0.0235	3.6	0.908628696	0.5625	0.001288822	0.9	0.001130941
637	0.049886	0.002521266	0.975	0.0235	3.6	0.908628696	0.5625	0.001288628	0.9	0.001130771
638	0.049886	0.002521266	0.975	0.0235	3.6	0.908628696	0.5625	0.001288628	0.9	0.001130771
639	0.0499265	0.002523313	0.975	0.0235	3.6	0.908628696	0.5625	0.001289675	0.9	0.001131689
640	0.0499265	0.002523313	0.975	0.0235	3.6	0.908628696	0.5625	0.001289675	0.9	0.001131689
641	0.049961	0.002525057	0.975	0.0235	3.6	0.908628696	0.5625	0.001290566	0.9	0.001132471
642	0.049961	0.002525057	0.975	0.0235	3.6	0.908628696	0.5625	0.001290566	0.9	0.001132471
643	0.0499855	0.002526295	0.975	0.0235	3.6	0.908628696	0.5625	0.001291199	0.9	0.001133027
644	0.0499855	0.002526295	0.975	0.0235	3.6	0.908628696	0.5625	0.001291199	0.9	0.001133027
645	0.050052	0.002529656	0.975	0.0235	3.6	0.908628696	0.5625	0.001292916	0.9	0.001134534
646	0.050052	0.002529656	0.975	0.0235	3.6	0.908628696	0.5625	0.001292916	0.9	0.001134534
647	0.0500825	0.002531197	0.975	0.0235	3.6	0.908628696	0.5625	0.001293704	0.9	0.001135225
648	0.0500825	0.002531197	0.975	0.0235	3.6	0.908628696	0.5625	0.001293704	0.9	0.001135225
649	0.0499605	0.002525032	0.975	0.0235	3.6	0.908628696	0.5625	0.001290553	0.9	0.00113246
650	0.0499605	0.002525032	0.975	0.0235	3.6	0.908628696	0.5625	0.001290553	0.9	0.00113246
651	0.049888	0.002521367	0.975	0.0235	3.6	0.908628696	0.5625	0.00128868	0.9	0.001130817
652	0.049888	0.002521367	0.975	0.0235	3.6	0.908628696	0.5625	0.00128868	0.9	0.001130817
653	0.049934	0.002523692	0.975	0.0235	3.6	0.908628696	0.5625	0.001289868	0.9	0.001131859

654	0.049934	0.002523692	0.975	0.0235	3.6	0.908628696	0.5625	0.001289868	0.9	0.001131859
655	0.0499535	0.002524678	0.975	0.0235	3.6	0.908628696	0.5625	0.001290372	0.9	0.001132301
656	0.0499535	0.002524678	0.975	0.0235	3.6	0.908628696	0.5625	0.001290372	0.9	0.001132301
657	0.0498735	0.002520635	0.975	0.0235	3.6	0.908628696	0.5625	0.001288305	0.9	0.001130488
658	0.0498735	0.002520635	0.975	0.0235	3.6	0.908628696	0.5625	0.001288305	0.9	0.001130488
659	0.0498	0.00251692	0.975	0.0235	3.6	0.908628696	0.5625	0.001286407	0.9	0.001128822
660	0.0498	0.00251692	0.975	0.0235	3.6	0.908628696	0.5625	0.001286407	0.9	0.001128822
661	0.0497785	0.002515833	0.975	0.0235	3.6	0.908628696	0.5625	0.001285851	0.9	0.001128335
662	0.0497785	0.002515833	0.975	0.0235	3.6	0.908628696	0.5625	0.001285851	0.9	0.001128335
663	0.04979	0.002516414	0.975	0.0235	3.6	0.908628696	0.5625	0.001286149	0.9	0.001128595
664	0.04979	0.002516414	0.975	0.0235	3.6	0.908628696	0.5625	0.001286149	0.9	0.001128595
665	0.0497955	0.002516692	0.975	0.0235	3.6	0.908628696	0.5625	0.001286291	0.9	0.00112872
666	0.0497955	0.002516692	0.975	0.0235	3.6	0.908628696	0.5625	0.001286291	0.9	0.00112872
667	0.0497625	0.002515025	0.975	0.0235	3.6	0.908628696	0.5625	0.001285438	0.9	0.001127972
668	0.0497625	0.002515025	0.975	0.0235	3.6	0.908628696	0.5625	0.001285438	0.9	0.001127972
669	0.0497695	0.002515378	0.975	0.0235	3.6	0.908628696	0.5625	0.001285619	0.9	0.001128131
670	0.0497695	0.002515378	0.975	0.0235	3.6	0.908628696	0.5625	0.001285619	0.9	0.001128131
671	0.0497765	0.002515732	0.975	0.0235	3.6	0.908628696	0.5625	0.0012858	0.9	0.001128289
672	0.0497765	0.002515732	0.975	0.0235	3.6	0.908628696	0.5625	0.0012858	0.9	0.001128289

673	0.0497405	0.002513913	0.975	0.0235	3.6	0.908628696	0.5625	0.00128487	0.9	0.001127473
674	0.0497405	0.002513913	0.975	0.0235	3.6	0.908628696	0.5625	0.00128487	0.9	0.001127473
675	0.049696	0.002511664	0.975	0.0235	3.6	0.908628696	0.5625	0.00128372	0.9	0.001126465
676	0.049696	0.002511664	0.975	0.0235	3.6	0.908628696	0.5625	0.00128372	0.9	0.001126465
677	0.0497585	0.002514822	0.975	0.0235	3.6	0.908628696	0.5625	0.001285335	0.9	0.001127881
678	0.0497585	0.002514822	0.975	0.0235	3.6	0.908628696	0.5625	0.001285335	0.9	0.001127881
679	0.0498595	0.002519927	0.975	0.0235	3.6	0.908628696	0.5625	0.001287944	0.9	0.001130171
680	0.0498595	0.002519927	0.975	0.0235	3.6	0.908628696	0.5625	0.001287944	0.9	0.001130171
681	0.049947	0.002524349	0.975	0.0235	3.6	0.908628696	0.5625	0.001290204	0.9	0.001132154
682	0.049947	0.002524349	0.975	0.0235	3.6	0.908628696	0.5625	0.001290204	0.9	0.001132154
683	0.0499915	0.002526598	0.975	0.0235	3.6	0.908628696	0.5625	0.001291354	0.9	0.001133163
684	0.0499915	0.002526598	0.975	0.0235	3.6	0.908628696	0.5625	0.001291354	0.9	0.001133163
685	0.049959	0.002524956	0.975	0.0235	3.6	0.908628696	0.5625	0.001290514	0.9	0.001132426
686	0.049959	0.002524956	0.975	0.0235	3.6	0.908628696	0.5625	0.001290514	0.9	0.001132426
687	0.049872	0.002520559	0.975	0.0235	3.6	0.908628696	0.5625	0.001288267	0.9	0.001130454
688	0.049872	0.002520559	0.975	0.0235	3.6	0.908628696	0.5625	0.001288267	0.9	0.001130454
689	0.0497885	0.002516339	0.975	0.0235	3.6	0.908628696	0.5625	0.00128611	0.9	0.001128561
690	0.0497885	0.002516339	0.975	0.0235	3.6	0.908628696	0.5625	0.00128611	0.9	0.001128561
691	0.0497485	0.002514317	0.975	0.0235	3.6	0.908628696	0.5625	0.001285077	0.9	0.001127655

692	0.0497485	0.002514317	0.975	0.0235	3.6	0.908628696	0.5625	0.001285077	0.9	0.001127655
693	0.0496555	0.002509617	0.975	0.0235	3.6	0.908628696	0.5625	0.001282674	0.9	0.001125547
694	0.0496555	0.002509617	0.975	0.0235	3.6	0.908628696	0.5625	0.001282674	0.9	0.001125547
695	0.0495605	0.002504815	0.975	0.0235	3.6	0.908628696	0.5625	0.00128022	0.9	0.001123393
696	0.0495605	0.002504815	0.975	0.0235	3.6	0.908628696	0.5625	0.00128022	0.9	0.001123393
697	0.0494975	0.002501631	0.975	0.0235	3.6	0.908628696	0.5625	0.001278593	0.9	0.001121965
698	0.0494975	0.002501631	0.975	0.0235	3.6	0.908628696	0.5625	0.001278593	0.9	0.001121965
699	0.049444	0.002498927	0.975	0.0235	3.6	0.908628696	0.5625	0.001277211	0.9	0.001120753
700	0.049444	0.002498927	0.975	0.0235	3.6	0.908628696	0.5625	0.001277211	0.9	0.001120753
701	0.049392	0.002496299	0.975	0.0235	3.6	0.908628696	0.5625	0.001275868	0.9	0.001119574
702	0.0493105	0.00249218	0.975	0.0235	3.6	0.908628696	0.5625	0.001273762	0.9	0.001117726
703	0.049323	0.002492812	0.975	0.0235	3.6	0.908628696	0.5625	0.001274085	0.9	0.00111801
704	0.049317	0.002492509	0.975	0.0235	3.6	0.908628696	0.5625	0.00127393	0.9	0.001117874
705	0.0491895	0.002486065	0.975	0.0235	3.6	0.908628696	0.5625	0.001270637	0.9	0.001114984
706	0.0491795	0.002485559	0.975	0.0235	3.6	0.908628696	0.5625	0.001270378	0.9	0.001114757
707	0.049262	0.002489729	0.975	0.0235	3.6	0.908628696	0.5625	0.00127251	0.9	0.001116627
708	0.049339	0.002493621	0.975	0.0235	3.6	0.908628696	0.5625	0.001274499	0.9	0.001118372
709	0.0494075	0.002497083	0.975	0.0235	3.6	0.908628696	0.5625	0.001276268	0.9	0.001119925
710	0.049492	0.002501353	0.975	0.0235	3.6	0.908628696	0.5625	0.001278451	0.9	0.001121841

711	0.049451	0.002499281	0.975	0.0235	3.6	0.908628696	0.5625	0.001277392	0.9	0.001120911
712	0.049339	0.002493621	0.975	0.0235	3.6	0.908628696	0.5625	0.001274499	0.9	0.001118372
713	0.0494075	0.002497083	0.975	0.0235	3.6	0.908628696	0.5625	0.001276268	0.9	0.001119925
714	0.049492	0.002501353	0.975	0.0235	3.6	0.908628696	0.5625	0.001278451	0.9	0.001121841
715	0.049451	0.002499281	0.975	0.0235	3.6	0.908628696	0.5625	0.001277392	0.9	0.001120911
716	0.049367	0.002495036	0.975	0.0235	3.6	0.908628696	0.5625	0.001275222	0.9	0.001119007
717	0.0494075	0.002497083	0.975	0.0235	3.6	0.908628696	0.5625	0.001276268	0.9	0.001119925
718	0.049492	0.002501353	0.975	0.0235	3.6	0.908628696	0.5625	0.001278451	0.9	0.001121841
719	0.049492	0.002501353	0.975	0.0235	3.6	0.908628696	0.5625	0.001278451	0.9	0.001121841
720	0.049451	0.002499281	0.975	0.0235	3.6	0.908628696	0.5625	0.001277392	0.9	0.001120911
721	0.049451	0.002499281	0.975	0.0235	3.6	0.908628696	0.5625	0.001277392	0.9	0.001120911
722	0.049367	0.002495036	0.975	0.0235	3.6	0.908628696	0.5625	0.001275222	0.9	0.001119007
723	0.049367	0.002495036	0.975	0.0235	3.6	0.908628696	0.5625	0.001275222	0.9	0.001119007
724	0.0492575	0.002489502	0.975	0.0235	3.6	0.908628696	0.5625	0.001272393	0.9	0.001116525
725	0.0492575	0.002489502	0.975	0.0235	3.6	0.908628696	0.5625	0.001272393	0.9	0.001116525
726	0.049136	0.002483361	0.975	0.0235	3.6	0.908628696	0.5625	0.001269255	0.9	0.001113771
727	0.049136	0.002483361	0.975	0.0235	3.6	0.908628696	0.5625	0.001269255	0.9	0.001113771
728	0.0490645	0.002479747	0.975	0.0235	3.6	0.908628696	0.5625	0.001267408	0.9	0.00111215
729	0.0490645	0.002479747	0.975	0.0235	3.6	0.908628696	0.5625	0.001267408	0.9	0.00111215

730	0.049083	0.002480682	0.975	0.0235	3.6	0.908628696	0.5625	0.001267886	0.9	0.00111257
731	0.049083	0.002480682	0.975	0.0235	3.6	0.908628696	0.5625	0.001267886	0.9	0.00111257
732	0.0491125	0.002482173	0.975	0.0235	3.6	0.908628696	0.5625	0.001268648	0.9	0.001113238
733	0.0491125	0.002482173	0.975	0.0235	3.6	0.908628696	0.5625	0.001268648	0.9	0.001113238
734	0.0491085	0.002481971	0.975	0.0235	3.6	0.908628696	0.5625	0.001268544	0.9	0.001113148
735	0.0491085	0.002481971	0.975	0.0235	3.6	0.908628696	0.5625	0.001268544	0.9	0.001113148
736	0.0491675	0.002484953	0.975	0.0235	3.6	0.908628696	0.5625	0.001270068	0.9	0.001114485
737	0.0491675	0.002484953	0.975	0.0235	3.6	0.908628696	0.5625	0.001270068	0.9	0.001114485
738	0.0493215	0.002492736	0.975	0.0235	3.6	0.908628696	0.5625	0.001274047	0.9	0.001117976
739	0.0493215	0.002492736	0.975	0.0235	3.6	0.908628696	0.5625	0.001274047	0.9	0.001117976
740	0.0494485	0.002499155	0.975	0.0235	3.6	0.908628696	0.5625	0.001277327	0.9	0.001120855
741	0.0494485	0.002499155	0.975	0.0235	3.6	0.908628696	0.5625	0.001277327	0.9	0.001120855
742	0.049522	0.00250287	0.975	0.0235	3.6	0.908628696	0.5625	0.001279226	0.9	0.001122521
743	0.049522	0.00250287	0.975	0.0235	3.6	0.908628696	0.5625	0.001279226	0.9	0.001122521
744	0.049509	0.002502212	0.975	0.0235	3.6	0.908628696	0.5625	0.00127889	0.9	0.001122226
745	0.049509	0.002502212	0.975	0.0235	3.6	0.908628696	0.5625	0.00127889	0.9	0.001122226
746	0.04948	0.002500747	0.975	0.0235	3.6	0.908628696	0.5625	0.001278141	0.9	0.001121569
747	0.04948	0.002500747	0.975	0.0235	3.6	0.908628696	0.5625	0.001278141	0.9	0.001121569
748	0.0495605	0.002504815	0.975	0.0235	3.6	0.908628696	0.5625	0.00128022	0.9	0.001123393

749	0.0495605	0.002504815	0.975	0.0235	3.6	0.908628696	0.5625	0.00128022	0.9	0.001123393
750	0.049664	0.002510046	0.975	0.0235	3.6	0.908628696	0.5625	0.001282894	0.9	0.001125739
751	0.049664	0.002510046	0.975	0.0235	3.6	0.908628696	0.5625	0.001282894	0.9	0.001125739
752	0.0497205	0.002512902	0.975	0.0235	3.6	0.908628696	0.5625	0.001284353	0.9	0.00112702
753	0.0497205	0.002512902	0.975	0.0235	3.6	0.908628696	0.5625	0.001284353	0.9	0.00112702
754	0.049793	0.002516566	0.975	0.0235	3.6	0.908628696	0.5625	0.001286226	0.9	0.001128663
755	0.049793	0.002516566	0.975	0.0235	3.6	0.908628696	0.5625	0.001286226	0.9	0.001128663
756	0.0499185	0.002522909	0.975	0.0235	3.6	0.908628696	0.5625	0.001289468	0.9	0.001131508
757	0.0499185	0.002522909	0.975	0.0235	3.6	0.908628696	0.5625	0.001289468	0.9	0.001131508
758	0.050046	0.002529353	0.975	0.0235	3.6	0.908628696	0.5625	0.001292761	0.9	0.001134398
759	0.050046	0.002529353	0.975	0.0123	3.6	0.950710077	0.5625	0.001352633	0.9	0.001186936
760	0.050202	0.002537237	0.975	0.0123	3.6	0.950710077	0.5625	0.001356849	0.9	0.001190635
761	0.050202	0.002537237	0.975	0.0123	3.6	0.950710077	0.5625	0.001356849	0.9	0.001190635
762	0.0504015	0.00254732	0.975	0.0123	3.6	0.950710077	0.5625	0.001362242	0.9	0.001195367
763	0.0504015	0.00254732	0.975	0.0123	3.6	0.950710077	0.5625	0.001362242	0.9	0.001195367
764	0.050666	0.002560688	0.975	0.0123	3.6	0.950710077	0.5625	0.00136939	0.9	0.00120164
765	0.050666	0.002560688	0.975	0.0123	3.6	0.950710077	0.5625	0.00136939	0.9	0.00120164
766	0.050958	0.002575446	0.975	0.0123	3.6	0.950710077	0.5625	0.001377282	0.9	0.001208565
767	0.050958	0.002575446	0.975	0.0123	3.6	0.950710077	0.5625	0.001377282	0.9	0.001208565

768	0.0511665	0.002585983	0.975	0.0123	3.6	0.950710077	0.5625	0.001382918	0.9	0.00121351
769	0.0511665	0.002585983	0.975	0.0123	3.6	0.950710077	0.5625	0.001382918	0.9	0.00121351
770	0.0513515	0.002595333	0.975	0.0123	3.6	0.950710077	0.5625	0.001387918	0.9	0.001217898
771	0.0513515	0.002595333	0.975	0.0123	3.6	0.950710077	0.5625	0.001387918	0.9	0.001217898
772	0.0515235	0.002604026	0.975	0.0123	3.6	0.950710077	0.5625	0.001392567	0.9	0.001221977
773	0.0515235	0.002604026	0.975	0.0123	3.6	0.950710077	0.5625	0.001392567	0.9	0.001221977
774	0.0516425	0.002610041	0.975	0.0123	3.6	0.950710077	0.5625	0.001395783	0.9	0.0012248
775	0.0516425	0.002610041	0.975	0.0123	3.6	0.950710077	0.5625	0.001395783	0.9	0.0012248
776	0.0517185	0.002613882	0.975	0.0123	3.6	0.950710077	0.5625	0.001397837	0.9	0.001226602
777	0.0517185	0.002613882	0.975	0.0123	3.6	0.950710077	0.5625	0.001397837	0.9	0.001226602
778	0.0517225	0.002614084	0.975	0.0123	3.6	0.950710077	0.5625	0.001397945	0.9	0.001226697
779	0.0517225	0.002614084	0.975	0.0123	3.6	0.950710077	0.5625	0.001397945	0.9	0.001226697
780	0.0516385	0.002609839	0.975	0.0123	3.6	0.950710077	0.5625	0.001395675	0.9	0.001224705
781	0.0516385	0.002609839	0.975	0.0123	3.6	0.950710077	0.5625	0.001395675	0.9	0.001224705
782	0.051502	0.00260294	0.975	0.0123	3.6	0.950710077	0.5625	0.001391986	0.9	0.001221467
783	0.051502	0.00260294	0.975	0.0123	3.6	0.950710077	0.5625	0.001391986	0.9	0.001221467
784	0.0513945	0.002597507	0.975	0.0123	3.6	0.950710077	0.5625	0.00138908	0.9	0.001218918
785	0.0513945	0.002597507	0.975	0.0123	3.6	0.950710077	0.5625	0.00138908	0.9	0.001218918
786	0.0512415	0.002589774	0.975	0.0123	3.6	0.950710077	0.5625	0.001384945	0.9	0.001215289

787	0.0512415	0.002589774	0.975	0.0123	3.6	0.950710077	0.5625	0.001384945	0.9	0.001215289
788	0.0510245	0.002578807	0.975	0.0123	3.6	0.950710077	0.5625	0.00137908	0.9	0.001210143
789	0.0510245	0.002578807	0.975	0.0123	3.6	0.950710077	0.5625	0.00137908	0.9	0.001210143
790	0.0507435	0.002564605	0.975	0.0123	3.6	0.950710077	0.5625	0.001371485	0.9	0.001203478
791	0.0507435	0.002564605	0.975	0.0123	3.6	0.950710077	0.5625	0.001371485	0.9	0.001203478
792	0.0505095	0.002552778	0.975	0.0123	3.6	0.950710077	0.5625	0.001365161	0.9	0.001197928
793	0.0505095	0.002552778	0.975	0.0123	3.6	0.950710077	0.5625	0.001365161	0.9	0.001197928
794	0.050318	0.0025431	0.975	0.0123	3.6	0.950710077	0.5625	0.001359985	0.9	0.001193387
795	0.050318	0.0025431	0.975	0.0123	3.6	0.950710077	0.5625	0.001359985	0.9	0.001193387
796	0.050153	0.002534761	0.975	0.0123	3.6	0.950710077	0.5625	0.001355525	0.9	0.001189473
797	0.050153	0.002534761	0.975	0.0123	3.6	0.950710077	0.5625	0.001355525	0.9	0.001189473
798	0.0500585	0.002529985	0.975	0.0123	3.6	0.950710077	0.5625	0.001352971	0.9	0.001187232
799	0.0500585	0.002529985	0.975	0.0123	3.6	0.950710077	0.5625	0.001352971	0.9	0.001187232
800	0.0499815	0.002526093	0.975	0.0123	3.6	0.950710077	0.5625	0.00135089	0.9	0.001185406

A-3. Permission of copyright

Fig. 1.1 and Fig.1.2

CCC Marketplace™

This is a License Agreement between Lingjun Meng ("User") and Copyright Clearance Center, Inc. ("CCC") on behalf of the Rightsholder identified in the order details below. The license consists of the order details, the CCC Terms and Conditions below, and any Rightsholder Terms and Conditions which are included below.

All payments must be made in full to CCC in accordance with the CCC Terms and Conditions below.

Order Date	16-May-2022	Type of Use	Republish in a thesis/dissertation
Order License ID	1221969-1	Publisher	ROYAL SOCIETY OF CHEMISTRY, ETC.]
ISSN	0306-0012	Portion	Image/photo/illustration

LICENSED CONTENT

Publication Title	Chemical Society reviews	Rightsholder	Royal Society of Chemistry
Article Title	Semiconductor heterojunction photocatalysts: design, construction, and photocatalytic performances.	Publication Type	Journal
		Start Page	5234
Author/Editor	CHEMICAL SOCIETY (GREAT BRITAIN)	End Page	5244
Date	12/31/1971	Issue	15
Language	English	Volume	43
Country	United Kingdom of Great Britain and Northern Ireland		

REQUEST DETAILS

Portion Type	Image/photo/illustration	Distribution	Worldwide
Number of images / photos / illustrations	2	Translation	Original language of publication
Format (select all that apply)	Electronic	Copies for the disabled?	No
Who will republish the content?	Academic institution	Minor editing privileges?	Yes
Duration of Use	Life of current edition	Incidental promotional use?	No
Lifetime Unit Quantity	Up to 499	Currency	USD
Rights Requested	Main product		

NEW WORK DETAILS

Title	Solar Photocatalytic Treatment of Oil Sands Process Water by Bismuth Tungstate Based Semiconductor Photocatalysts	Institution name	university of alberta
		Expected presentation date	2022-06-01
Instructor name	Mohamed Gamal El-Din		

ADDITIONAL DETAILS

Order reference number	N/A	**The requesting person / organization to appear on the license**	Lingjun Meng

REUSE CONTENT DETAILS

Title, description or numeric reference of the portion(s)	ISSN: 0306-0012	**Title of the article/chapter the portion is from**	Semiconductor heterojunction photocatalysts: design, construction, and photocatalytic performances.
Editor of portion(s)	Wang, Huanli; Zhang, Lisha; Chen, Zhigang; Hu, Junqing; Li, Shijie; Wang, Zhaohui; Liu, Jianshe; Wang, Xinchen	**Author of portion(s)**	Wang, Huanli; Zhang, Lisha; Chen, Zhigang; Hu, Junqing; Li, Shijie; Wang, Zhaohui; Liu, Jianshe; Wang, Xinchen
Volume of serial or monograph	43		
Page or page range of portion	5234-5244	**Issue, if republishing an article from a serial**	15
		Publication date of portion	2014-08-06

CCC Terms and Conditions

1. Description of Service; Defined Terms. This Republication License enables the User to obtain licenses for republication of one or more copyrighted works as described in detail on the relevant Order Confirmation (the "Work(s)"). Copyright Clearance Center, Inc. ("CCC") grants licenses through the Service on behalf of the rightsholder identified on the Order Confirmation (the "Rightsholder"). "Republication", as used herein, generally means the inclusion of a Work, in whole or in part, in a new work or works, also as described on the Order Confirmation. "User", as used herein, means the person or entity making such republication.

2. The terms set forth in the relevant Order Confirmation, and any terms set by the Rightsholder with respect to a particular Work, govern the terms of use of Works in connection with the Service. By using the Service, the person transacting for a republication license on behalf of the User represents and warrants that he/she/it (a) has been duly authorized by the User to accept, and hereby does accept, all such terms and conditions on behalf of User, and (b) shall inform User of all such terms and conditions. In the event such person is a "freelancer" or other third party independent of User and CCC, such party shall be deemed jointly a "User" for purposes of these terms and conditions. In any event, User shall be deemed to have accepted and agreed to all such terms and conditions if User republishes the Work in any fashion.

3. Scope of License; Limitations and Obligations.

   3.1. All Works and all rights therein, including copyright rights, remain the sole and exclusive property of the Rightsholder. The license created by the exchange of an Order Confirmation (and/or any invoice) and payment by User of the full amount set forth on that document includes only those rights expressly set forth in the Order Confirmation and in these terms and conditions, and conveys no other rights in the Work(s) to User. All rights not expressly granted are hereby reserved.

   3.2. General Payment Terms: You may pay by credit card or through an account with us payable at the end of the month. If you and we agree that you may establish a standing account with CCC, then the following terms apply: Remit Payment to: Copyright Clearance Center, 29118 Network Place, Chicago, IL 60673-1291. Payments Due: Invoices are payable upon their delivery to you (or upon our notice to you that they are available to you for downloading). After 30 days, outstanding amounts will be subject to a service charge of 1-1/2% per month or, if less, the maximum rate allowed by applicable law. Unless otherwise specifically set forth in the Order Confirmation or in a separate written agreement signed by CCC, invoices are due and payable on "net 30" terms. While User may exercise the rights licensed immediately upon issuance of the Order Confirmation, the license is automatically revoked and is null and void, as if it had never been issued, if complete payment for the license is not received on a timely basis either from User directly or through a payment agent, such as a credit card company.

   3.3. Unless otherwise provided in the Order Confirmation, any grant of rights to User (i) is "one-time" (including the editions and product family specified in the license), (ii) is non-exclusive and non-transferable and (iii) is subject to any and all limitations and restrictions (such as, but not limited to, limitations on duration of use or circulation) included in the Order Confirmation or invoice and/or in these terms and conditions. Upon completion of the licensed use, User shall either secure a new permission for further use of the Work(s) or immediately cease any new use of the Work(s) and shall render inaccessible (such as by deleting or by removing or severing links or other locators) any further copies of the Work (except for copies printed on paper in accordance with this license and still in User's stock at the end of such period).

   3.4. In the event that the material for which a republication license is sought includes third party materials (such as photographs, illustrations, graphs, inserts and similar materials) which are identified in such material as having been used by permission, User is responsible for identifying, and seeking separate licenses (under this Service or otherwise) for, any of such third party materials; without a separate license, such third party materials may not be used.

   3.5. Use of proper copyright notice for a Work is required as a condition of any license granted under the Service. Unless otherwise provided in the Order Confirmation, a proper copyright notice will read substantially as follows: "Republished with permission of [Rightsholder's name], from [Work's title, author, volume, edition number and year of copyright]; permission conveyed through Copyright Clearance Center, Inc. " Such notice must be provided in a reasonably legible font size and must be placed either immediately adjacent to the Work as used (for example, as part of a by-line or footnote but not as a separate electronic link) or in the place where substantially all other credits or notices for the new work containing the republished Work are located. Failure to include the required notice results in loss to the Rightsholder and CCC, and the User shall be liable to pay liquidated damages for each such failure equal to twice the use fee specified in the Order Confirmation, in addition to the use fee itself and any other fees and charges specified.

   3.6. User may only make alterations to the Work if and as expressly set forth in the Order Confirmation. No Work may be used in any way that is defamatory, violates the rights of third parties (including such third parties' rights of copyright, privacy, publicity, or other tangible or intangible property), or is otherwise illegal, sexually explicit or obscene. In addition, User may not conjoin a Work with any other material that may result in damage to the reputation of the Rightsholder. User agrees to inform CCC if it becomes aware of any infringement of any rights in a Work and to cooperate with any reasonable request of CCC or the Rightsholder in connection therewith.

4. Indemnity. User hereby indemnifies and agrees to defend the Rightsholder and CCC, and their respective employees and directors, against all claims, liability, damages, costs and expenses, including legal fees and expenses, arising out of any use of a Work beyond the scope of the rights granted herein, or any use of a Work which has been altered in any unauthorized way by User, including claims of defamation or infringement of rights of copyright, publicity, privacy or other tangible or intangible property.

5. Limitation of Liability. UNDER NO CIRCUMSTANCES WILL CCC OR THE RIGHTSHOLDER BE LIABLE FOR ANY DIRECT, INDIRECT, CONSEQUENTIAL OR INCIDENTAL DAMAGES (INCLUDING WITHOUT LIMITATION DAMAGES FOR LOSS OF BUSINESS PROFITS OR INFORMATION, OR FOR BUSINESS INTERRUPTION) ARISING OUT OF THE USE OR INABILITY TO USE A WORK, EVEN IF ONE OF THEM HAS BEEN ADVISED OF THE POSSIBILITY OF SUCH DAMAGES. In any event, the total liability of the Rightsholder and CCC (including their respective employees and directors) shall not exceed the total amount actually paid by User for this license. User assumes full liability for the actions and omissions of its principals, employees, agents, affiliates, successors and assigns.

6. Limited Warranties. THE WORK(S) AND RIGHT(S) ARE PROVIDED "AS IS". CCC HAS THE RIGHT TO GRANT TO USER THE RIGHTS GRANTED IN THE ORDER CONFIRMATION DOCUMENT. CCC AND THE RIGHTSHOLDER DISCLAIM ALL OTHER WARRANTIES RELATING TO THE WORK(S) AND RIGHT(S), EITHER EXPRESS OR IMPLIED, INCLUDING WITHOUT LIMITATION IMPLIED WARRANTIES OF MERCHANTABILITY OR FITNESS FOR A PARTICULAR PURPOSE. ADDITIONAL RIGHTS MAY BE REQUIRED TO USE ILLUSTRATIONS, GRAPHS, PHOTOGRAPHS, ABSTRACTS, INSERTS OR OTHER PORTIONS OF THE WORK (AS OPPOSED TO THE ENTIRE WORK) IN A MANNER CONTEMPLATED BY USER; USER UNDERSTANDS AND AGREES THAT NEITHER CCC NOR THE RIGHTSHOLDER MAY HAVE SUCH ADDITIONAL RIGHTS TO GRANT.

7. Effect of Breach. Any failure by User to pay any amount when due, or any use by User of a Work beyond the scope of the license set forth in the Order Confirmation and/or these terms and conditions, shall be a material breach of the license created by the Order Confirmation and these terms and conditions. Any breach not cured within 30 days of written notice thereof shall result in immediate termination of such license without further notice. Any unauthorized (but licensable) use of a Work that is terminated immediately upon notice thereof may be liquidated by payment of the Rightsholder's ordinary license price therefor; any unauthorized (and unlicensable) use that is not terminated immediately for any reason (including, for example, because materials containing the Work cannot reasonably be recalled) will be subject to all remedies available at law or in equity, but in no event to a payment of less than three times the Rightsholder's ordinary license price for the most closely analogous licensable use plus Rightsholder's and/or CCC's costs and expenses incurred in collecting such payment.

8. Miscellaneous.

   8.1. User acknowledges that CCC may, from time to time, make changes or additions to the Service or to these terms and conditions, and CCC reserves the right to send notice to the User by electronic mail or otherwise for the purposes of notifying User of such changes or additions; provided that any such changes or additions shall not apply to permissions already secured and paid for.

   8.2. Use of User-related information collected through the Service is governed by CCC's privacy policy, available online here:https://marketplace.copyright.com/rs-ui-web/mp/privacy-policy

   8.3. The licensing transaction described in the Order Confirmation is personal to User. Therefore, User may not assign or transfer to any other person (whether a natural person or an organization of any kind) the license created by the Order Confirmation and these terms and conditions or any rights granted hereunder; provided, however, that User may assign such license in its entirety on written notice to CCC in the event of a transfer of all or substantially all of User's rights in the new material which includes the Work(s) licensed under this Service.

   8.4. No amendment or waiver of any terms is binding unless set forth in writing and signed by the parties. The Rightsholder and CCC hereby object to any terms contained in any writing prepared by the User or its principals, employees, agents or affiliates and purporting to govern or otherwise relate to the licensing transaction described in the Order Confirmation, which terms are in any way inconsistent with any terms set forth in the Order Confirmation and/or in these terms and conditions or CCC's standard operating procedures, whether such writing is prepared prior to, simultaneously with or subsequent to the Order Confirmation, and whether such writing appears on a copy of the Order Confirmation or in a separate instrument.

   8.5. The licensing transaction described in the Order Confirmation document shall be governed by and construed under the law of the State of New York, USA, without regard to the principles thereof of conflicts of law. Any case, controversy, suit, action, or proceeding arising out of, in connection with, or related to such licensing transaction shall be brought, at CCC's sole discretion, in any federal or state court located in the County of New York, State of New York, USA, or in any federal or state court whose geographical jurisdiction covers the location of the Rightsholder set forth in the Order Confirmation. The parties expressly submit to the personal jurisdiction and venue of each such federal or state court.If you have any comments or questions about the Service or Copyright Clearance Center, please contact us at 978-750-8400 or send an e-mail to support@copyright.com.

Fig. 1.3

CCC | RightsLink®

Home | Help | Email Support | Lingjun Meng

ACS Publications
Most Trusted. Most Cited. Most Read.

Facile Hydrothermal Synthesis of Z-Scheme Bi2Fe4O9/Bi2WO6 Heterojunction Photocatalyst with Enhanced Visible Light Photocatalytic Activity

Author: Bisheng Li, Cui Lai, Guangming Zeng, et al
Publication: Applied Materials
Publisher: American Chemical Society
Date: Jun 1, 2018

Copyright © 2018, American Chemical Society

Quick Price Estimate

This service provides permission for reuse only. If you do not have a copy of the portion you are using, you may copy and paste the content and reuse according to the terms of your agreement. Please be advised that obtaining the content you license is a separate transaction not involving RightsLink.

If credit is given to another source for the material you requested from RightsLink, permission must be obtained from that source.

Note: Individual Scheme and Structure reuse is free of charge and does not require a license. If the scheme or structure is identified as a Figure in the article, permission is required.

Permission for this particular request is granted for print and electronic formats, and translations, at no charge. Figures and tables may be modified. Appropriate credit should be given. Please print this page for your records and provide a copy to your publisher. Requests for up to 4 figures require only this record. Five or more figures will generate a printout of additional terms and conditions. Appropriate credit should read: "Reprinted with permission from {COMPLETE REFERENCE CITATION}. Copyright {YEAR} American Chemical Society." Insert appropriate information in place of the capitalized words.

I would like to...	reuse in a Thesis/Dissertation	Format	Electronic
Requestor Type	Non-profit	Select your currency	CAD - $
Portion	Table/Figure/Micrograph	Quick Price	Click Quick Price
Number of Table/Figure/Micrographs	1		

QUICK PRICE CONTINUE

PERMISSION/LICENSE IS GRANTED FOR YOUR ORDER AT NO CHARGE

This type of permission/license, instead of the standard Terms and Conditions, is sent to you because no fee is being charged for your order. Please note the following:

- Permission is granted for your request in both print and electronic formats, and translations.
- If figures and/or tables were requested, they may be adapted or used in part.
- Please print this page for your records and send a copy of it to your publisher/graduate school.
- Appropriate credit for the requested material should be given as follows: "Reprinted (adapted) with permission from {COMPLETE REFERENCE CITATION}. Copyright {YEAR} American Chemical Society." Insert appropriate information in place of the capitalized words.
- One-time permission is granted only for the use specified in your RightsLink request. No additional uses are granted (such as derivative works or other editions). For any uses, please submit a new request.

If credit is given to another source for the material you requested from RightsLink, permission must be obtained from that source.

BACK CLOSE WINDOW

Fig. 1.4

CCC Marketplace™

This is a License Agreement between Lingjun Meng ("User") and Copyright Clearance Center, Inc. ("CCC") on behalf of the Rightsholder identified in the order details below. The license consists of the order details, the CCC Terms and Conditions below, and any Rightsholder Terms and Conditions which are included below.

All payments must be made in full to CCC in accordance with the CCC Terms and Conditions below.

Order Date	16-May-2022	Type of Use	Republish in a thesis/dissertation
Order License ID	1221970-1	Publisher	ELSEVIER BV
ISSN	0926-3373	Portion	Image/photo/illustration

LICENSED CONTENT

Publication Title	Applied catalysis	Rightsholder	Elsevier Science & Technology Journals
Article Title	Construction of Bi2WO6/RGO/g-C3N4 2D/2D/2D hybrid Z-scheme heterojunctions with large interfacial contact area for efficient charge separation and high-performance photoreduction of CO2 and H2O into solar fuels	Publication Type	Journal
		Start Page	586
		End Page	598
		Volume	239
Date	12/31/1991		
Language	English		
Country	Netherlands		

REQUEST DETAILS

Portion Type	Image/photo/illustration	Distribution	Worldwide
Number of images / photos / illustrations	1	Translation	Original language of publication
Format (select all that apply)	Electronic	Copies for the disabled?	No
Who will republish the content?	Academic institution	Minor editing privileges?	Yes
Duration of Use	Life of current edition	Incidental promotional use?	No
Lifetime Unit Quantity	Up to 499	Currency	USD
Rights Requested	Main product		

NEW WORK DETAILS

Title	Solar Photocatalytic Treatment of Oil Sands Process Water by Bismuth Tungstate Based Semiconductor Photocatalysts	Institution name	university of alberta
		Expected presentation date	2022-06-01
Instructor name	Mohamed Gamal El-Din		

ADDITIONAL DETAILS

Order reference number	N/A	**The requesting person / organization to appear on the license**	Lingjun Meng

REUSE CONTENT DETAILS

Title, description or numeric reference of the portion(s)	ISSN: 0926-3373	**Title of the article/chapter the portion is from**	Construction of Bi2WO6/RGO/g-C3N4 2D/2D/2D hybrid Z-scheme heterojunctions with large interfacial contact area for efficient charge separation and high-performance photoreduction of CO2 and H2O into solar fuels
Editor of portion(s)	Tonda, Surendar; Eslava, Salvador; Kumar, Santosh; Jo, Wan-Kuen		
Volume of serial or monograph	239		
Page or page range of portion	586-598	**Author of portion(s)**	Tonda, Surendar; Eslava, Salvador; Kumar, Santosh; Jo, Wan-Kuen
		Issue, if republishing an article from a serial	N/A
		Publication date of portion	2018-12-29

RIGHTSHOLDER TERMS AND CONDITIONS

Elsevier publishes Open Access articles in both its Open Access journals and via its Open Access articles option in subscription journals, for which an author selects a user license permitting certain types of reuse without permission. Before proceeding please check if the article is Open Access on http://www.sciencedirect.com and refer to the user license for the individual article. Any reuse not included in the user license terms will require permission. You must always fully and appropriately credit the author and source. If any part of the material to be used (for example, figures) has appeared in the Elsevier publication for which you are seeking permission, with credit or acknowledgement to another source it is the responsibility of the user to ensure their reuse complies with the terms and conditions determined by the rights holder. Please contact permissions@elsevier.com with any queries.

CCC Terms and Conditions

1. Description of Service; Defined Terms. This Republication License enables the User to obtain licenses for republication of one or more copyrighted works as described in detail on the relevant Order Confirmation (the "Work(s)"). Copyright Clearance Center, Inc. ("CCC") grants licenses through the Service on behalf of the rightsholder identified on the Order Confirmation (the "Rightsholder"). "Republication", as used herein, generally means the inclusion of a Work, in whole or in part, in a new work or works, also as described on the Order Confirmation. "User", as used herein, means the person or entity making such republication.

2. The terms set forth in the relevant Order Confirmation, and any terms set by the Rightsholder with respect to a particular Work, govern the terms of use of Works in connection with the Service. By using the Service, the person transacting for a republication license on behalf of the User represents and warrants that he/she/it (a) has been duly authorized by the User to accept, and hereby does accept, all such terms and conditions on behalf of User, and (b) shall inform User of all such terms and conditions. In the event such person is a "freelancer" or other third party independent of User and CCC, such party shall be deemed jointly a "User" for purposes of these terms and conditions. In any event, User shall be deemed to have accepted and agreed to all such terms and conditions if User republishes the Work in any fashion.

3. Scope of License; Limitations and Obligations.

   3.1. All Works and all rights therein, including copyright rights, remain the sole and exclusive property of the Rightsholder. The license created by the exchange of an Order Confirmation (and/or any invoice) and payment by User of the full amount set forth on that document includes only those rights expressly set forth in the Order Confirmation and in these terms and conditions, and conveys no other rights in the Work(s) to User. All rights not expressly granted are hereby reserved.

Chapter 2

CCC Marketplace™

This is a License Agreement between Lingjun Meng ("User") and Copyright Clearance Center, Inc. ("CCC") on behalf of the Rightsholder identified in the order details below. The license consists of the order details, the CCC Terms and Conditions below, and any Rightsholder Terms and Conditions which are included below.

All payments must be made in full to CCC in accordance with the CCC Terms and Conditions below.

Order Date	16-May-2022	Type of Use	Republish in a thesis/dissertation
Order License ID	1221973-1	Publisher	ELSEVIER BV
ISSN	0304-3894	Portion	Chapter/article

LICENSED CONTENT

Publication Title	Journal of hazardous materials	Rightsholder	Elsevier Science & Technology Journals
Article Title	Solar photocatalytic treatment of model and real oil sands process water naphthenic acids by bismuth tungstate: Effect of catalyst morphology and cations on the degradation kinetics and pathways	Publication Type	Journal
		Start Page	125396
		Volume	413
Date	12/31/1974		
Language	Dutch		
Country	Netherlands		

REQUEST DETAILS

Portion Type	Chapter/article	Rights Requested	Main product
Page range(s)	1-13	Distribution	Worldwide
Total number of pages	13	Translation	Original language of publication
Format (select all that apply)	Electronic	Copies for the disabled?	No
Who will republish the content?	Academic institution	Minor editing privileges?	Yes
Duration of Use	Life of current edition	Incidental promotional use?	No
Lifetime Unit Quantity	Up to 499	Currency	USD

NEW WORK DETAILS

Title	Solar Photocatalytic Treatment of Oil Sands Process Water by Bismuth Tungstate Based Semiconductor Photocatalysts	Institution name	university of alberta
		Expected presentation date	2022-06-01
Instructor name	Mohamed Gamal El-Din		

ADDITIONAL DETAILS

Order reference number	N/A	**The requesting person / organization to appear on the license**	Lingjun Meng

REUSE CONTENT DETAILS

Title, description or numeric reference of the portion(s)	ISSN: 0304-3894	**Title of the article/chapter the portion is from**	Solar photocatalytic treatment of model and real oil sands process water naphthenic acids by bismuth tungstate: Effect of catalyst morphology and cations on the degradation kinetics and pathways
Editor of portion(s)	Meng, Lingjun; How, Zuo Tong; Ganiyu, Soliu O.; Gamal El-Din, Mohamed	**Author of portion(s)**	Meng, Lingjun; How, Zuo Tong; Ganiyu, Soliu O.; Gamal El-Din, Mohamed
Volume of serial or monograph	413	**Issue, if republishing an article from a serial**	N/A
Page or page range of portion	125396	**Publication date of portion**	2021-07-04

RIGHTSHOLDER TERMS AND CONDITIONS

Elsevier publishes Open Access articles in both its Open Access journals and via its Open Access articles option in subscription journals, for which an author selects a user license permitting certain types of reuse without permission. Before proceeding please check if the article is Open Access on http://www.sciencedirect.com and refer to the user license for the individual article. Any reuse not included in the user license terms will require permission. You must always fully and appropriately credit the author and source. If any part of the material to be used (for example, figures) has appeared in the Elsevier publication for which you are seeking permission, with credit or acknowledgement to another source it is the responsibility of the user to ensure their reuse complies with the terms and conditions determined by the rights holder. Please contact permissions@elsevier.com with any queries.

CCC Terms and Conditions

1. Description of Service; Defined Terms. This Republication License enables the User to obtain licenses for republication of one or more copyrighted works as described in detail on the relevant Order Confirmation (the "Work(s)"). Copyright Clearance Center, Inc. ("CCC") grants licenses through the Service on behalf of the rightsholder identified on the Order Confirmation (the "Rightsholder"). "Republication", as used herein, generally means the inclusion of a Work, in whole or in part, in a new work or works, also as described on the Order Confirmation. "User", as used herein, means the person or entity making such republication.

2. The terms set forth in the relevant Order Confirmation, and any terms set by the Rightsholder with respect to a particular Work, govern the terms of use of Works in connection with the Service. By using the Service, the person transacting for a republication license on behalf of the User represents and warrants that he/she/it (a) has been duly authorized by the User to accept, and hereby does accept, all such terms and conditions on behalf of User, and (b) shall inform User of all such terms and conditions. In the event such person is a "freelancer" or other third party independent of User and CCC, such party shall be deemed jointly a "User" for purposes of these terms and conditions. In any event, User shall be deemed to have accepted and agreed to all such terms and conditions if User republishes the Work in any fashion.

3. Scope of License; Limitations and Obligations.

   3.1. All Works and all rights therein, including copyright rights, remain the sole and exclusive property of the Rightsholder. The license created by the exchange of an Order Confirmation (and/or any invoice) and payment by User of the full amount set forth on that document includes only those rights expressly set forth in the Order Confirmation and in these terms and conditions, and conveys no other rights in the Work(s) to User. All rights not expressly granted are hereby reserved.

3.2. General Payment Terms: You may pay by credit card or through an account with us payable at the end of the month. If you and we agree that you may establish a standing account with CCC, then the following terms apply: Remit Payment to: Copyright Clearance Center, 29118 Network Place, Chicago, IL 60673-1291. Payments Due: Invoices are payable upon their delivery to you (or upon our notice to you that they are available to you for downloading). After 30 days, outstanding amounts will be subject to a service charge of 1-1/2% per month or, if less, the maximum rate allowed by applicable law. Unless otherwise specifically set forth in the Order Confirmation or in a separate written agreement signed by CCC, invoices are due and payable on "net 30" terms. While User may exercise the rights licensed immediately upon issuance of the Order Confirmation, the license is automatically revoked and is null and void, as if it had never been issued, if complete payment for the license is not received on a timely basis either from User directly or through a payment agent, such as a credit card company.

3.3. Unless otherwise provided in the Order Confirmation, any grant of rights to User (i) is "one-time" (including the editions and product family specified in the license), (ii) is non-exclusive and non-transferable and (iii) is subject to any and all limitations and restrictions (such as, but not limited to, limitations on duration of use or circulation) included in the Order Confirmation or invoice and/or in these terms and conditions. Upon completion of the licensed use, User shall either secure a new permission for further use of the Work(s) or immediately cease any new use of the Work(s) and shall render inaccessible (such as by deleting or by removing or severing links or other locators) any further copies of the Work (except for copies printed on paper in accordance with this license and still in User's stock at the end of such period).

3.4. In the event that the material for which a republication license is sought includes third party materials (such as photographs, illustrations, graphs, inserts and similar materials) which are identified in such material as having been used by permission, User is responsible for identifying, and seeking separate licenses (under this Service or otherwise) for, any of such third party materials; without a separate license, such third party materials may not be used.

3.5. Use of proper copyright notice for a Work is required as a condition of any license granted under the Service. Unless otherwise provided in the Order Confirmation, a proper copyright notice will read substantially as follows: "Republished with permission of [Rightsholder's name], from [Work's title, author, volume, edition number and year of copyright]; permission conveyed through Copyright Clearance Center, Inc. " Such notice must be provided in a reasonably legible font size and must be placed either immediately adjacent to the Work as used (for example, as part of a by-line or footnote but not as a separate electronic link) or in the place where substantially all other credits or notices for the new work containing the republished Work are located. Failure to include the required notice results in loss to the Rightsholder and CCC, and the User shall be liable to pay liquidated damages for each such failure equal to twice the use fee specified in the Order Confirmation, in addition to the use fee itself and any other fees and charges specified.

3.6. User may only make alterations to the Work if and as expressly set forth in the Order Confirmation. No Work may be used in any way that is defamatory, violates the rights of third parties (including such third parties' rights of copyright, privacy, publicity, or other tangible or intangible property), or is otherwise illegal, sexually explicit or obscene. In addition, User may not conjoin a Work with any other material that may result in damage to the reputation of the Rightsholder. User agrees to inform CCC if it becomes aware of any infringement of any rights in a Work and to cooperate with any reasonable request of CCC or the Rightsholder in connection therewith.

4. Indemnity. User hereby indemnifies and agrees to defend the Rightsholder and CCC, and their respective employees and directors, against all claims, liability, damages, costs and expenses, including legal fees and expenses, arising out of any use of a Work beyond the scope of the rights granted herein, or any use of a Work which has been altered in any unauthorized way by User, including claims of defamation or infringement of rights of copyright, publicity, privacy or other tangible or intangible property.

5. Limitation of Liability. UNDER NO CIRCUMSTANCES WILL CCC OR THE RIGHTSHOLDER BE LIABLE FOR ANY DIRECT, INDIRECT, CONSEQUENTIAL OR INCIDENTAL DAMAGES (INCLUDING WITHOUT LIMITATION DAMAGES FOR LOSS OF BUSINESS PROFITS OR INFORMATION, OR FOR BUSINESS INTERRUPTION) ARISING OUT OF THE USE OR INABILITY TO USE A WORK, EVEN IF ONE OF THEM HAS BEEN ADVISED OF THE POSSIBILITY OF SUCH DAMAGES. In any event, the total liability of the Rightsholder and CCC (including their respective employees and directors) shall not exceed the total amount actually paid by User for this license. User assumes full liability for the actions and omissions of its principals, employees, agents, affiliates, successors and assigns.

6. Limited Warranties. THE WORK(S) AND RIGHT(S) ARE PROVIDED "AS IS". CCC HAS THE RIGHT TO GRANT TO USER THE RIGHTS GRANTED IN THE ORDER CONFIRMATION DOCUMENT. CCC AND THE RIGHTSHOLDER DISCLAIM ALL OTHER WARRANTIES RELATING TO THE WORK(S) AND RIGHT(S), EITHER EXPRESS OR IMPLIED, INCLUDING WITHOUT LIMITATION IMPLIED WARRANTIES OF MERCHANTABILITY OR FITNESS FOR A PARTICULAR PURPOSE. ADDITIONAL RIGHTS MAY BE REQUIRED TO USE ILLUSTRATIONS, GRAPHS, PHOTOGRAPHS, ABSTRACTS, INSERTS OR OTHER PORTIONS OF THE WORK (AS OPPOSED TO THE ENTIRE WORK) IN A MANNER CONTEMPLATED BY USER; USER UNDERSTANDS AND AGREES THAT NEITHER CCC NOR THE RIGHTSHOLDER MAY HAVE SUCH ADDITIONAL RIGHTS TO GRANT.

7. Effect of Breach. Any failure by User to pay any amount when due, or any use by User of a Work beyond the scope of the license set forth in the Order Confirmation and/or these terms and conditions, shall be a material breach of the license created by the Order Confirmation and these terms and conditions. Any breach not cured within 30 days of written notice thereof shall result in immediate termination of such license without further notice. Any unauthorized (but licensable) use of a Work that is terminated immediately upon notice thereof may be liquidated by payment of the Rightsholder's ordinary license price therefor; any unauthorized (and unlicensable) use that is not terminated immediately for any reason (including, for example, because materials containing the Work cannot reasonably be recalled) will be subject to all remedies available at law or in equity, but in no event to a payment of less than three times the Rightsholder's ordinary license price for the most closely analogous licensable use plus Rightsholder's and/or CCC's costs and expenses incurred in collecting such payment.

8. Miscellaneous.

8.1. User acknowledges that CCC may, from time to time, make changes or additions to the Service or to these terms and conditions, and CCC reserves the right to send notice to the User by electronic mail or otherwise for the purposes of notifying User of such changes or additions; provided that any such changes or additions shall not apply to permissions already secured and paid for.

8.2. Use of User-related information collected through the Service is governed by CCC's privacy policy, available online here:https://marketplace.copyright.com/rs-ui-web/mp/privacy-policy

8.3. The licensing transaction described in the Order Confirmation is personal to User. Therefore, User may not assign or transfer to any other person (whether a natural person or an organization of any kind) the license created by the Order Confirmation and these terms and conditions or any rights granted hereunder; provided, however, that User may assign such license in its entirety on written notice to CCC in the event of a transfer of all or substantially all of User's rights in the new material which includes the Work(s) licensed under this Service.

8.4. No amendment or waiver of any terms is binding unless set forth in writing and signed by the parties. The Rightsholder and CCC hereby object to any terms contained in any writing prepared by the User or its principals, employees, agents or affiliates and purporting to govern or otherwise relate to the licensing transaction described in the Order Confirmation, which terms are in any way inconsistent with any terms set forth in the Order Confirmation and/or in these terms and conditions or CCC's standard operating procedures, whether such writing is prepared prior to, simultaneously with or subsequent to the Order Confirmation, and whether such writing appears on a copy of the Order Confirmation or in a separate instrument.

8.5. The licensing transaction described in the Order Confirmation document shall be governed by and construed under the law of the State of New York, USA, without regard to the principles thereof of conflicts of law. Any case, controversy, suit, action, or proceeding arising out of, in connection with, or related to such licensing transaction shall be brought, at CCC's sole discretion, in any federal or state court located in the County of New York, State of New York, USA, or in any federal or state court whose geographical jurisdiction covers the location of the Rightsholder set forth in the Order Confirmation. The parties expressly submit to the personal jurisdiction and venue of each such federal or state court.If you have any comments or questions about the Service or Copyright Clearance Center, please contact us at 978-750-8400 or send an e-mail to support@copyright.com.

APPENDIX B

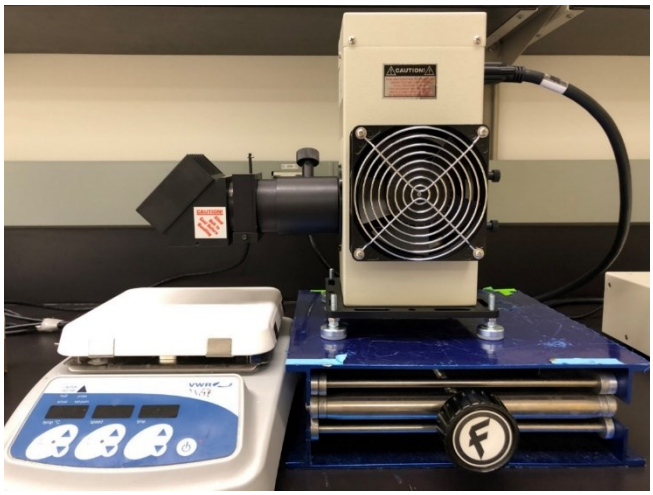

Fig. B4 Setup for the solar simulator.

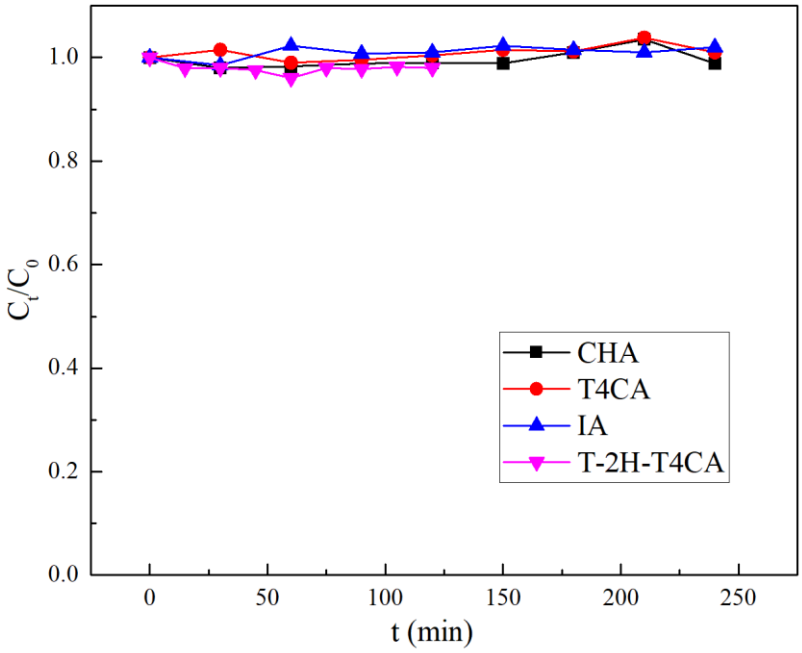

Fig. B5 Photolysis of four different NAs ([pollutants] = 25 mg/L, [HCO_3^-] = 5 mM, pH = 8.5).

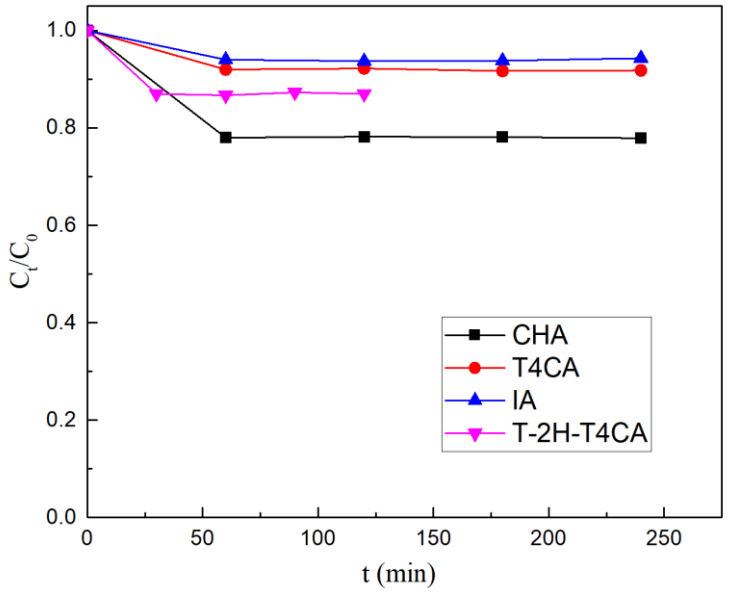

Fig. B6 Dark adsorption of four different NAs ([pollutants] = 25 mg/L, [catalysts] = 1g/L, [HCO_3^-] = 5 mM pH = 8.5).

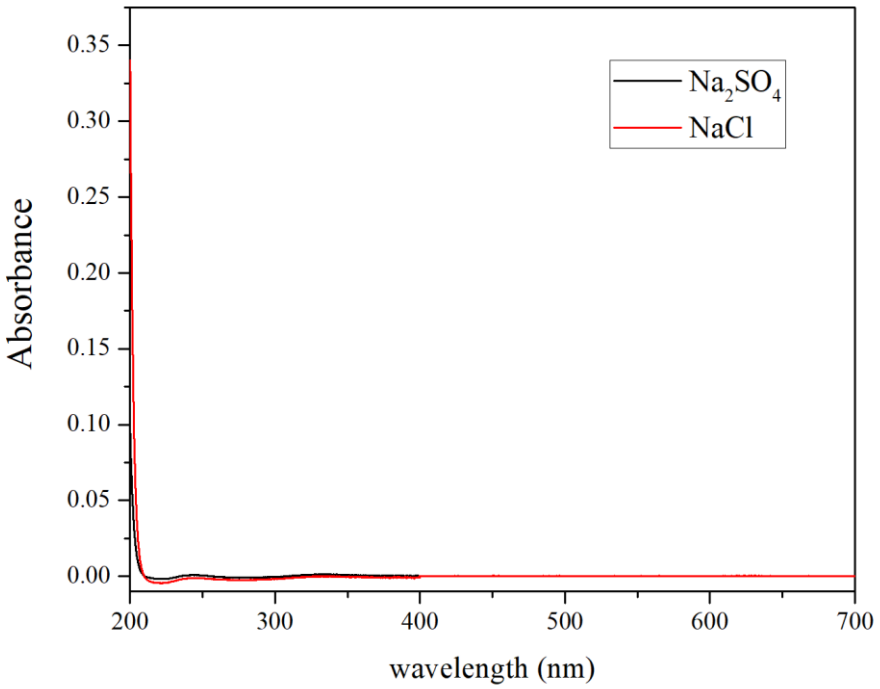

Fig. B4 UV-VIS spectra of Na_2SO_4 and NaCl.

Table B3 Identification of the degradation intermediates of NAs

	Formula [M-H]	Theoretical mass (m/z)	Measured mass (m/z)	Delta (mDa)	Molecular structure
Parent	$C_6H_9O_2S$	145.0323	145.0411	8.8	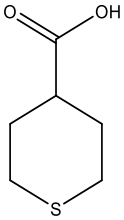
BP1	$C_6H_9O_3S$	161.0272	161.0362	9.0	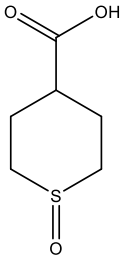
BP2	$C_6H_9O_4S$	177.0222	177.0299	7.7	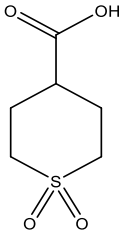
Parent	$C_{11}H_{15}O_2S$	128.0712	128.0771	5.9	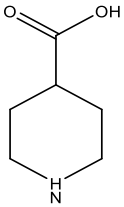
BP3	$C_6H_{10}O_3N$	144.0661	144.0732	7.1	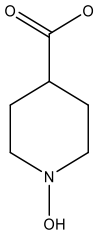
BP4	$C_6H_{10}O_3N$	144.0661	144.0732	7.1	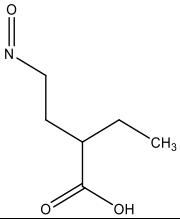

Parent	$C_{11}H_{15}O_2S$	211.0793	211.0814	2.1	
P1	$C_{11}H_{15}O_3S$	227.0742	227.0757	1.5	
P2	$C_{10}H_{13}OS$	181.0687	181.0691	0.4	
P3	$C_{11}H_{15}O_3S$	227.0742	227.0757	1.5	
P4	$C_{10}H_{15}OS$	183.0844	183.0868	2.4	
P5	$C_{10}H_{13}O_2S$	197.0636	197.0631	-0.5	
P6	$C_9H_{15}O_5S$	235.0640	235.0641	0.2	

Table B4 Identification of the degradation intermediates of ACA in different treatment systems

	Formula [M-H]	Measured mass (m/z)	Delta (mDa)	Molecular structure	Catalyst only	Nitrate only	Catalyst+nitrate
P1	$C_{11}H_{16}O_3$	195.1028	3.1	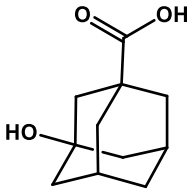	√	√	√
P2	$C_{11}H_{16}O_3$	195.1027	3.2	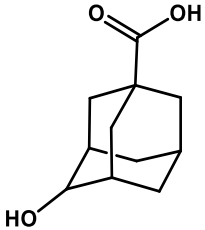	√	√	√
P3	$C_{11}H_{14}O_3$	193.0846	4.8	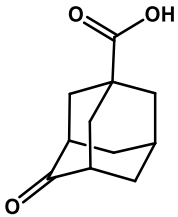	√	√	√
P4	$C_{11}H_{16}O_4$	211.0980	4.7	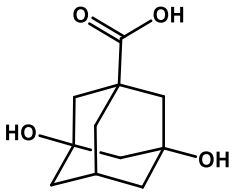	×	√	×

P5	$C_{11}H_{15}NO_5$	240.0880	3.6	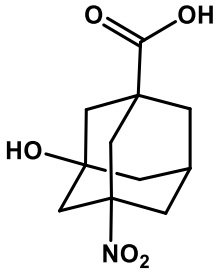	×	√	×
P6	$C_{11}H_{15}NO_5$	240.0880	3.6	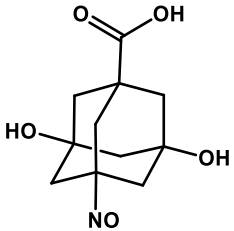	×	√	×
P7	$C_{11}H_{15}NO_6$	256.0826	2.0	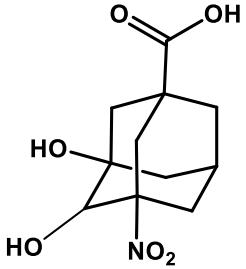	×	×	√
P8	$C_{11}H_{15}NO_6$	256.0827	2.1	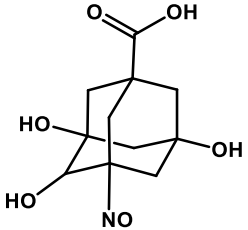	×	×	√